

University of Alberta  
Department of Civil Engineering



Structural Engineering Report No. 16

# **Analysis of Reinforced Concrete Shear Wall-Frame Structures**

by  
W.J. Clark  
and  
J.G. MacGregor

November, 1968

THE UNIVERSITY OF ALBERTA

ANALYSIS OF REINFORCED CONCRETE  
SHEAR WALL-FRAME STRUCTURES

by

WILLIAM JAMES CLARK

A THESIS

SUBMITTED TO THE FACULTY OF GRADUATE STUDIES  
IN PARTIAL FULFILMENT OF THE REQUIREMENTS FOR THE DEGREE  
OF DOCTOR OF PHILOSOPHY

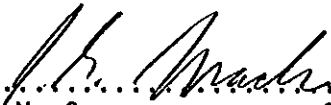
DEPARTMENT OF CIVIL ENGINEERING

EDMONTON, ALBERTA

NOVEMBER, 1968

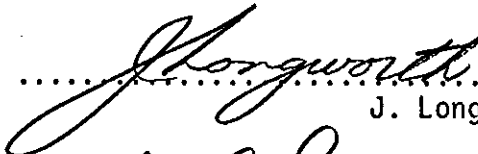
UNIVERSITY OF ALBERTA  
FACULTY OF GRADUATE STUDIES

The undersigned certify that they have read, and recommend to the Faculty of Graduate Studies for acceptance, a thesis entitled ANALYSIS OF REINFORCED CONCRETE SHEAR WALL-FRAME STRUCTURES submitted by WILLIAM JAMES CLARK in partial fulfilment of the requirements for the degree of Doctor of Philosophy.

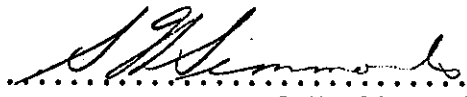
  
.....  
J.G. MacGregor Supervisor

  
.....  
P.F. Adams

  
.....  
D.G. Bellow

  
.....  
J. Longworth

  
.....  
J.R. Pounder

  
.....  
S.H. Simmonds

  
.....  
K.H. Gerstle External Examiner

Date .October 28, 1968.

## ABSTRACT

The primary objective of this thesis was the development of a method of analysis to accurately predict the behaviour of large planar reinforced concrete shear wall-frame structures.

The analysis traces the second order elastic-plastic response of planar reinforced concrete structures as loading progresses to failure. In the analysis, conditions of equilibrium are formulated on the deformed members and the deformed structure to consider the secondary axial load effects in the columns and shear walls. The analysis considers axial shortening of the columns and shear walls and includes the effects of the finite width of the shear wall elements. Time effects and shear deformations in the members and joints are neglected.

The analysis idealizes member section response as elastic-perfectly plastic moment-curvature relationships. Rationalized methods were developed to predict elastic-plastic column section moment-thrust-curvature and girder section moment-curvature relationships.

In the computer programme developed for the analysis, the solution is derived by the deformation method, using slope-deflection equations modified to consider the presence of plastic hinges in the members. The equations of equilibrium are solved by an iterative procedure.

Using the analysis, good correlation was obtained with three other analyses and with the results of tests of sway frames reported by Ferguson and Breen.

The analysis was used to investigate some aspects of the behaviour of a symmetrical, twenty storey, two bay, reinforced concrete structure. The properties of the basic structure were adjusted to isolate the effects of axial shortening, the finite width of the shear wall elements, slenderness, and the effects of varying shear wall stiffness on the behaviour of the structure.

The study indicates that a realistic analysis of a shear wall-frame structure must consider the effects of axial shortening and the finite width of the shear wall elements.

The investigation of the effects of variation of the shear wall stiffness suggests that a relatively low shear wall stiffness is required to effectively brace the structure. In this type of structure, the increasing of the shear wall stiffness was not an efficient method of increasing either the overall stiffness or the failure load of the system.

## ACKNOWLEDGEMENTS

This study forms part of a general investigation, "Behavior of Multi-Story Structures", currently in progress at the Department of Civil Engineering, University of Alberta. Dr. J.G. MacGregor and Dr. P.F. Adams are directors of the investigation. The project receives financial support from the National Research Council of Canada and the Defence Research Board.

The author wishes to express his sincere appreciation to Professor J.G. MacGregor, supervisor of the study, for his continuing encouragement and guidance throughout the course of the research and his constructive criticism during the preparation of the manuscript.

Helpful suggestions resulting from discussions with Dr. P.F. Adams and Messrs. S.N. Guhamajumdar, R.P. Nikhed, M. Suko and J.H. Wynhoven are acknowledged with thanks.

The author gratefully acknowledges the financial support of the National Research Council of Canada in providing personal financial assistance throughout his postgraduate work and in making available the computing facilities at the University of Alberta.

Miss Helen Wozniuk typed the manuscript with great care. Her co-operation is appreciated.

## TABLE OF CONTENTS

	Page
Title Page	i
Approval Sheet	ii
Abstract	iii
Acknowledgements	v
Table of Contents	vi
List of Tables	x
List of Figures	xi
List of Symbols	xvi
 CHAPTER I      INTRODUCTION	 1
 CHAPTER II     REVIEW OF PREVIOUS WORK	 9
2.1    Introduction	9
2.2    Possible Methods of Analysis	9
2.2.1   Simplification of the Analytical Model	10
2.2.2   Formulation of the Solution	12
2.3    Unbraced Structure Analyses	14
2.4    Braced Frame Analyses	19
2.5    Studies of Braced Structure Behaviour	22
2.6    Conclusions	22
 CHAPTER III    ANALYSIS OF MEMBERS	 24
3.1    Introduction	24
3.2    Analysis of a Reinforced Concrete Cross- Section	24
3.2.1   Assumptions of Rationalized Moment- Curvature Relationship	28
3.2.2   Column Section Response	29
3.2.3   Girder Section Response	41

## TABLE OF CONTENTS (Continued)

	Page
3.3 Member Properties	43
3.3.1 Plastic Hinge	43
3.3.2 Stability Functions	44
3.3.3 Assumptions of Member Analysis	45
3.3.4 Sign Conventions	45
3.3.5 Slope-Deflection Equations for Columns	47
3.3.6 Slope-Deflection Equations for Girders	54
3.3.7 Properties of a Shear Wall	61
3.3.8 Axial Shortening of Columns	61
3.3.9 Hinge Rotation Capacity	62
3.4 Summary	63
CHAPTER IV ANALYSIS OF FRAMEWORK	64
4.1 Introduction	64
4.2 Model Framework and Loading Configuration	64
4.3 Formulation of the Solution	67
4.3.1 Joint Equilibrium	69
4.3.2 Storey Sway Equilibrium	74
4.3.3 Computation of Axial Loads and Vertical Joint Displacements	76
4.4 Method of Solution	78
4.4.1 Convergence Criteria	80
4.5 Incremental Loading Procedure	80
4.5.1 Detection of Plastic Hinges	83
4.5.2 Speeding up Convergence	84
4.5.3 Detection of Instability	85
4.6 Computer Application of the Analysis	88
4.7 Limitations of the Analysis	90
4.8 Effect of Convergence Limits on Accuracy	94
CHAPTER V COMPARISON WITH OTHER ANALYSES AND TESTS	98
5.1 Introduction	98
5.2 Pfrang's Analytical Column Model	99
5.3 Parikh's Analysis for Unbraced Steel Frames	101
5.4 Reinforced Concrete Frames Tested by Ferguson and Breen	108
5.5 Approximate Braced Frame Analysis of Guhamajumdar, Nikhed et al	115



## TABLE OF CONTENTS (Continued)

	Page
CHAPTER VI DESCRIPTION OF THE INVESTIGATION OF BEHAVIOUR OF REINFORCED CONCRETE STRUCTURES	125
6.1 Introduction	125
6.2 Notation for the Structures	125
6.3 Design of the Basic Multi-Storey Frame	126
6.3.1 Section Properties	129
6.3.2 Member Section Stiffness Distributions	130
6.3.3 Verification of the Design of Frame H1	133
6.4 Scope of the Investigation	136
6.5 Details of the Analyses	136
6.6 Study of the Effects of Axial Shortening	137
6.7 Study of the Effects of Finite Shear Wall Width	138
6.8 Study of the Effects of Slenderness	139
6.9 Study of the Effects of Shear Wall Stiffness	139
CHAPTER VII PRESENTATION AND DISCUSSION OF RESULTS	142
7.1 Introduction	142
7.2 General Discussion of the Behaviour and Modes of Failure of the Structures Studied	142
7.3 The Effects of Axial Shortening	149
7.4 The Effects of Finite Shear Wall Width	158
7.5 The Effects of Slenderness	162
7.6 The Effects of Variation of Shear Wall Stiffness	165
7.6.1 The Influence of Shear Wall Stiffness on the Overall Response of the Structure	165
7.6.2 $P\Delta$ Effects in Members	173
7.7 Significance of the Consideration of Axial Shortening and the Finite Width of the Shear Wall in the Analysis	178
7.8 Limitations of the Investigation	181
CHAPTER VIII SUMMARY, CONCLUSIONS AND RECOMMENDATIONS	182
8.1 Summary	182
8.2 Conclusions	183
8.3 Recommendations for Future Research	186

## TABLE OF CONTENTS (Continued)

	Page
LIST OF REFERENCES	188
APPENDIX A Derivation of Rationalized Moment-Thrust-Curvature Parameters for the Column Cross-Section	A1
A.1 Balanced Loading Conditions	A2
A.2 Curvatures at the Yield Point of the Column Section	A3
A.2.1 Yield Curvature in Pure Flexure	A4
A.2.2 Yield Curvature under Balanced Axial Force	A5
A.3 Ultimate Curvature of a Column Section	A7
APPENDIX B Comparison of Exact and Rationalized Column and Girder Section Moment-Curvature Diagrams	B1
B.1 Column Section M-P- $\phi$ Relationship	B2
B.2 Girder Section M- $\phi$ Relationship	B3
APPENDIX C Member Behaviour	C1
C.1 Location and Magnitude of Maximum Moment in a Column	C2
C.2 Slope-Deflection Equations for Girders	C6
C.3 Evaluation of Plastic Hinge Rotation	C15
APPENDIX D Computer Programme	D1
D.1 Notation used in the Computer Programme	D2
D.2 Functions of the Subroutines	D11
D.3 Flow Diagrams for the Computer Programme	D12
D.3.1 Flow Diagram for the Main Programme	D13
D.3.2 Flow Diagram for Subroutine PCOL	D17
D.3.3 Flow Diagram for Subroutine ITER	D18
D.3.4 Flow Diagram for Subroutine HINGES	D21
D.3.5 Flow Diagram for Subroutine BMHING	D22
D.4 Listing of the Programme	D24

## LIST OF TABLES

		Page
TABLE 3.1	Variations of Basic Section Considered	27
TABLE 3.2	Coefficients for Equation (3-32)	52
TABLE 3.3	Coefficients for Equation (3-33)	53
TABLE 3.4	Coefficients for Equation (3-36)	59
TABLE 3.5	Coefficients for Equation (3-37)	60
TABLE 4.1	Effects of Iteration Convergence Accuracy on the Analysis of Structure H1	95
TABLE 4.2	Effects of Iteration Convergence Accuracy on the Analysis of Structure H50	96
TABLE 5.1	Ultimate Loads for Ferguson and Breen Frames	114
TABLE 5.2	Results of the Exact and Approximate Analyses	118
TABLE 6.1	Working Load Values for Frame H1	127
TABLE 7.1	Failure Conditions of Basic Series H and J Structures	146
TABLE 7.2	Failure Conditions of Structures Used to Study the Effects of Variables	147

## LIST OF FIGURES

	Page
FIGURE 1.1 Elevation View of a Shear Wall-Frame Structure	2
FIGURE 1.2 Effects of Lateral Bracing on Load-Deflection Response	4
FIGURE 1.3 Effects of Lateral Bracing on Column Elastic Critical Load	6
FIGURE 2.1 Possible Assumptions for Section Response	11
FIGURE 2.2 Considerations of a Second Order Analysis	11
FIGURE 2.3 Effects of Simplifications of Analytical Model Behaviour on Computed Load-Deflection Response	13
FIGURE 2.4 Simplified Braced Structure Configurations Considered by Previous Analyses	20
FIGURE 3.1 Assumed Material Stress-Strain Properties for Exact Analysis	26
FIGURE 3.2 Column Cross-Section and Properties of the Basic Section Investigated	27
FIGURE 3.3 Column Section M-P- $\phi$ Relationship	31
FIGURE 3.4 Column Section Ultimate Interaction Diagram	31
FIGURE 3.5 Relationship Between Column Section Yield Curvature and Axial Load Value	35
FIGURE 3.6 Relationship Between Column Section Ultimate Curvature and Axial Load Value	39
FIGURE 3.7 Girder Cross-Section	42

## LIST OF FIGURES (Continued)

	Page
FIGURE 3.8 Idealized Girder Section Moment-Curvature Relationship	42
FIGURE 3.9 Sign Conventions for Member Analysis	46
FIGURE 3.10 Typical Deflected Column Configuration	48
FIGURE 3.11 Sequence of Hinge Formation in Columns	49
FIGURE 3.12 Typical Girder Configuration	55
FIGURE 3.13 Adjustment of Girder Plastic Moment Capacities	55
FIGURE 3.14 Sequence of Hinge Formation in Girders	57
FIGURE 4.1 Model Framework and Loading Configuration	65
FIGURE 4.2 Nomenclature for a Typical Joint	68
FIGURE 4.3 Forces at a Joint	70
FIGURE 4.4 Operator for Moment Equilibrium at a Joint	73
FIGURE 4.5 Free-Body Diagram of a Typical Storey	75
FIGURE 4.6 Free-Body Diagram of a Typical Column	75
FIGURE 4.7 Operator for $B_U + B_L + P\Delta$ for a Typical Column	77
FIGURE 4.8 Typical Load-Deformation Response Curve	82
FIGURE 4.9 Storey Sway Mechanism	86
FIGURE 4.10 Joint Mechanism	86
FIGURE 4.11 Complete Load-Deformation Response History of a Structure	92
FIGURE 5.1 Pfrang's Idealized Column Model	100
FIGURE 5.2 Comparison with Pfrang's Figure 4 Column	102
FIGURE 5.3 Comparisons with Two of Pfrang's Figure 8 Columns	103

## LIST OF FIGURES (Continued)

	Page
FIGURE 5.4 Comparisons with Two of Pfrang's Figure 11 Columns	104
FIGURE 5.5 Parikh's Three Storey Two Bay Steel Frame	105
FIGURE 5.6 Load-Deformation Curves for Parikh's Frame	106
FIGURE 5.7 Location of Plastic Hinges in Parikh's Frame	107
FIGURE 5.8 Ferguson and Breen Test Frame	109
FIGURE 5.9 Column Behaviour of Ferguson and Breen Frames L1 and L2	111
FIGURE 5.10 Column Behaviour of Ferguson and Breen Frames L3 and L5	112
FIGURE 5.11 Column Behaviour of Ferguson and Breen Frames L6 and L7	113
FIGURE 5.12 Twenty Storey Structure for Comparison of Exact and Approximate Analyses	116
FIGURE 5.13 Load-Deflection Curves for Exact and Approximate Analyses	119
FIGURE 5.14 Hinge Configurations by Exact and Approximate Analyses at $\lambda = 4.00$	121
FIGURE 5.15 Hinge Configurations by Exact and Approximate Analyses at $\lambda = 5.00$	122
FIGURE 5.16 Hinge Configurations by Exact and Approximate Analyses at Last Load Stages	123
FIGURE 6.1 Elevation of Frame H1	128
FIGURE 6.2 Column and Shear Wall Section Properties in Structures Studied	131

## LIST OF FIGURES (Continued)

	Page
FIGURE 6.3 Girder Section Properties in Structures Studied	131
FIGURE 6.4 Distribution of Column and Shear Wall Stiffnesses in Frame H1	132
FIGURE 6.5 Distribution of Girder Stiffness in Frame H1	132
FIGURE 6.6 Load-Deformation Relationship for H1	134
FIGURE 6.7 Propagation of Plastic Hinges in H1	135
FIGURE 6.8 Method of Increasing Shear Wall Section Stiffness in Series H and J Structures	141
FIGURE 7.1 Hinge Propagation in Structures H1 and J1	144
FIGURE 7.2 Hinge Propagation in Structures H50 and J50	145
FIGURE 7.3 Types of Differential Axial Shortening in Multi- Storey Structures	150
FIGURE 7.4 Effects of Axial Shortening in Structure H1	152
FIGURE 7.5 Effects of Axial Shortening in Structure H50	153
FIGURE 7.6 Hinge Propagation in H50 with Different Wall Areas	157
FIGURE 7.7 Effects of Finite Wall Width in Structure H1	159
FIGURE 7.8 Effects of Finite Wall Width in Structure H50	160
FIGURE 7.9 Effects of Slenderness on Load-Deflection Relation- ships	163
FIGURE 7.10 Load-Deflection Relationships for Series H Structures	166
FIGURE 7.11 Load-Deflection Relationships for Series J Structures	167
FIGURE 7.12 Bending Moment Diagrams for the Shear Walls in Structures H1 and H50 at Working Loads	169

## LIST OF FIGURES (Continued)

	Page
FIGURE 7.13 Lateral Loads Supported by the Shear Walls in Structures H1 and H50 at Working Loads	170
FIGURE 7.14 Effect of Relative Shear Wall Stiffness on the Column Moment Magnifier in Series H and J Structures	174
FIGURE 7.15 Distribution of Moment Magnifiers in Leeward Column Stack at Working Loads	176
FIGURE 7.16 Significance of the Neglect of Axial Shortening in the Analysis of H1 and H50	179
FIGURE 7.17 Significance of the Neglect of Shear Wall Finite Width in the Analysis of H1 and H50	180



## LIST OF SYMBOLS

### Subscripts

- A = subscript referring to conditions at the left end of a girder
- B = subscript referring to conditions at the right end of a girder
- b = subscript referring to balanced loading conditions in a column or shear wall
- L = subscript referring to conditions at the lower end of a column or a shear wall
- U = subscript referring to conditions at the upper end of a column or a shear wall

### Variables

- $A_s$  = area of tension reinforcement
- B = bending moment in columns or shear walls, in general
- b = width of compression face of a flexural member
- C,S = stability functions
- D,L,W = working values of dead, live and wind loads
- d = distance from extreme compression fibre to centroid of tension reinforcement
- d' = distance from extreme compression fibre to centroid of compression reinforcement
- $E_s$  = modulus of elasticity of reinforcement

## LIST OF SYMBOLS (Continued)

$EI$	= flexural rigidity of a flexural member section
$e_b$	= balanced eccentricity of a column or shear wall section
$f_c$	= concrete stress
$f'_c$	= compressive strength of concrete as determined by test of 6 x 12 in cylinder cured for 28 days
$f_y$	= yield stress of reinforcement
$f_s$	= reinforcement stress
$h$	= length of a column or shear wall member
$K_c$	= sum of $\frac{EI}{h}$ values for all columns in any storey of a structure
$K_w$	= sum of $\frac{EI}{h}$ values for all shear wall elements in any storey of a structure
$k$	= $\sqrt{\frac{P}{EI}}$ , when used in conjunction with $h$ = ratio of distance from extreme compression fibre to neutral axis to effective depth $d$ , when used in conjunction with $d$
$k_y d$	= $kd$ in a girder or column section at yield of the moment- curvature diagram
$k_{yb} d$	= $k_y d$ in column or wall section subjected to balanced axial force $P_b$
$k_{y0} d$	= $k_y d$ in column or wall section in pure flexure
$k_u d$	= $kd$ in a girder or column section at ultimate rotational capacity in pure flexure
$L$	= span of a girder

## LIST OF SYMBOLS (Continued)

$M$	= bending moment in a girder, in general
$M_o$	= ultimate moment capacity of a column in pure flexure
$M_{pc}$	= ultimate moment capacity of a column under combined axial load and flexure
$M_{pl}$	= plastic moment capacity of a girder
$n$	= modular ratio = $\frac{E_s}{E_c}$
$P$	= axial force in columns, in general
$P_{cr}$	= critical column buckling load, based on an effective column length
$P_e$	= Euler column buckling load, based on a column of length $h$ with pinned ends
$P_o$	= axial load capacity of a centrally loaded column
$p$	= longitudinal reinforcement ratio = $\frac{A_s}{bd}$
$p_t$	= total longitudinal reinforcement ratio in a column = $\frac{2A_s}{bt}$
$T_L$	= resisting bending moment at a plastic hinge at the left end of a girder
$T_R$	= resisting bending moment at a plastic hinge at the right end of a girder
$t$	= total depth of a section
$WW_L$	= width of the shear wall element at the left end of a girder
$WW_R$	= width of the shear wall element at the right end of a girder
$w$	= total uniformly distributed load acting on a girder

## LIST OF SYMBOLS (Continued)

$\delta$	= displacement in general
$\Delta$	= displacement in general
$\Delta h$	= change in length of a column or shear wall member resulting from axial shortening
$\epsilon_c$	= concrete strain in general
$\epsilon_s$	= reinforcement strain in general
$\epsilon_o$	= compressive strain in concrete corresponding to maximum stress
$\epsilon_u$	= ultimate concrete strain in flexure
$\theta$	= rotation in general
$\theta_D$	= rotational discontinuity at a plastic hinge
$\theta_{Dall}$	= total permissible rotation at a plastic hinge, beyond which excessive hinge rotation is assumed
$\lambda$	= load factor or load parameter in general
$\rho$	= chord rotation in a girder $(\frac{\delta_B - \delta_A}{L})$ or a column $(\frac{\delta_U - \delta_L}{h})$
$\phi$	= curvature at a cross-section in general
$\phi_b$	= curvature at balanced failure of a column cross-section
$\phi_{pc}$	= ultimate curvature in a column section under combined axial load and flexure
$\phi_y$	= curvature of a column or girder section at yield of the moment-curvature diagram
$\phi_{yb}$	= $\phi_y$ in a column section subjected to balanced axial force $P_b$

## LIST OF SYMBOLS (Continued)

- $\phi_{y0}$  =  $\phi_y$  in a column section subjected to pure flexure
- $\phi_u$  = ultimate curvature in a girder or column section  
subjected to pure flexure

Computer Programme Notation

A complete listing of the notation used in the computer programme is presented in SECTION D.1 of APPENDIX D.

## CHAPTER I

### INTRODUCTION

In the latter part of the nineteenth century when multi-storey construction had its beginning, heavy bearing walls provided adequate resistance to lateral loads. Today, however, the increasing height of structures, the quest for as much column-free interior space as possible and the replacement of the bearing walls by light precast curtain walls have resulted in the development of the shear wall-frame type of construction for multi-storey structures.

As the name implies, the shear wall is a stiff element incorporated into a structure primarily to provide resistance to lateral load. In addition to carrying vertical and lateral loads, shear walls also serve, when required by planning, to divide and enclose space. Consequently a shear wall may function as a service core wall, elevator shaft, stairwell or partition wall, and may assume a great variety of shapes. The analysis of a shear wall-frame structure is sufficiently complex that consideration of the third dimension and the effects of torsion becomes quite unmanageable in terms of the treatment considered in this thesis. Hence, this thesis will examine the system represented by the plane structure shown in FIGURE 1.1. Shear walls will be treated as members of finite width possessing relatively high stiffness properties.

The adoption of the shear wall type of construction and changes in design procedures have left unanswered a number of questions regarding

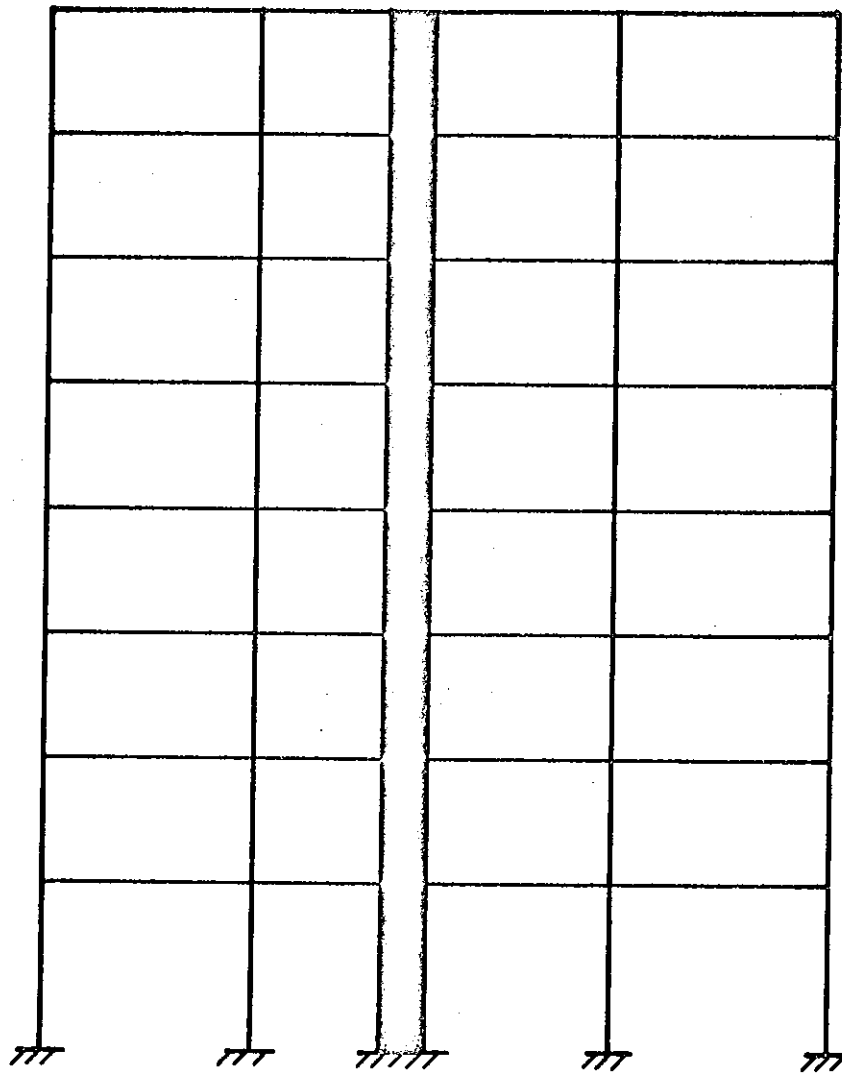


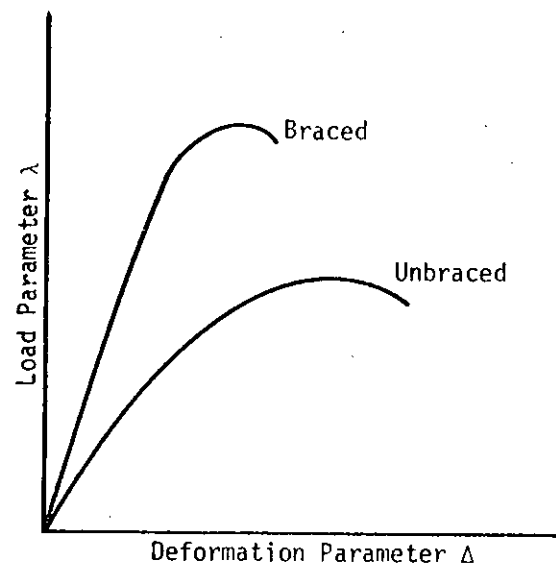
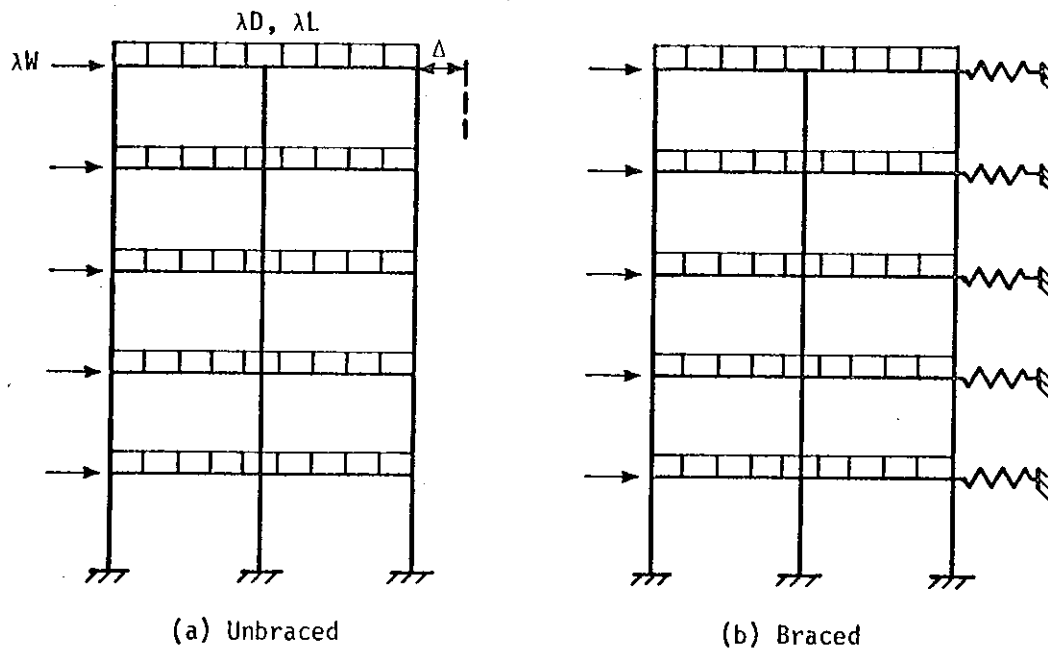
FIGURE 1.1  
ELEVATION VIEW OF A  
SHEAR WALL-FRAME STRUCTURE

the design and behaviour of shear wall-frame structures. The current trend in structural design is to replace the working stress design method by limit design procedures, dealing with the limiting strength of the structure. Most analyses presently available for shear wall-frame structures, discussed in CHAPTER II, are limited to the consideration of elastic behaviour. Consequently, little is known as yet regarding the complete response history of these structures.

Limit design of engineering structures considers three basic criteria of structural damage. First of these is the strength criterion which is the primary consideration in proportioning mild steel structures by the plastic design method. The serviceability criterion of limited deformations and limited cracking may also control the design. The third criterion of the limit design process is that of buckling strength or the inception of instability. The stability limit of a structure may be defined as the loading condition at which an increase in deformation may occur with no corresponding increase in load. In recent years it has become evident that in most cases it is not possible to separate the strength and stability failure criteria.

Shear wall bracing will significantly influence the response of a structure to loads. If an unbraced structure under generalized loading as shown in FIGURE 1.2(a) were tested, it would demonstrate a load-deflection response as shown in FIGURE 1.2(c). The non-linearity of the relationship is caused by secondary  $P\Delta$  effects and by softening of the structure as inelastic action progresses. If the members are sufficiently slender, it is conceivable that failure could be initiated by elastic instability before any portion of the structure reached the inelastic behaviour range. If the





(c) Generalized Load-Deformation Diagram

FIGURE 1.2  
EFFECTS OF LATERAL BRACING ON  
LOAD-DEFORMATION RESPONSE

structure were braced laterally as shown in FIGURE 1.2(b), it would be stiffened and possibly strengthened. Because of the increased lateral rigidity, the  $P\Delta$  effects would be reduced, reducing the danger of frame instability so that failure would result primarily from the progress of inelastic action. The efficiency of a shear wall in providing bracing stiffness to alter the overall response of a shear wall-frame structure has not been investigated previously. Methods have been developed for the plastic design of unbraced and heavily braced steel structures<sup>(1)\*</sup>, but little is known regarding the limit design of structures with intermediate degrees of bracing.

The effects of lateral bracing are also considered in the design of discrete members of the structure. In the current ACI Building Code<sup>(2)</sup>, when dealing with the design of long columns, different effective length criteria are applied to cases of columns in which "relative lateral displacement of the ends of the member is prevented" and "is not prevented". Thus, the code considers the effective length of a column to be a function of the lateral bracing stiffness. However, no method is suggested for differentiating between the braced and unbraced structures.

In his study of the elastic buckling behaviour of columns Goldberg<sup>(3)</sup> has expressed the problem in a simple form. In the structure depicted in FIGURE 1.3, the columns can buckle in either a symmetrical or a lurching mode, depending upon the bracing stiffness and the degree of end restraint provided by the girders. Goldberg's elastic analysis of the system yielded a relationship similar to that shown in FIGURE 1.3. In the area ABCD of this plot, the critical column load is a function of the degree

---

\*Numbers in parentheses denote references listed at the end of the thesis.

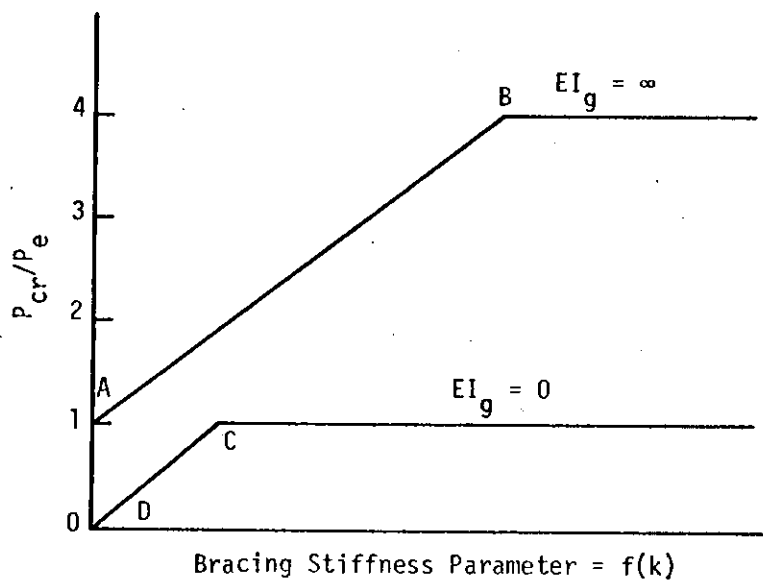
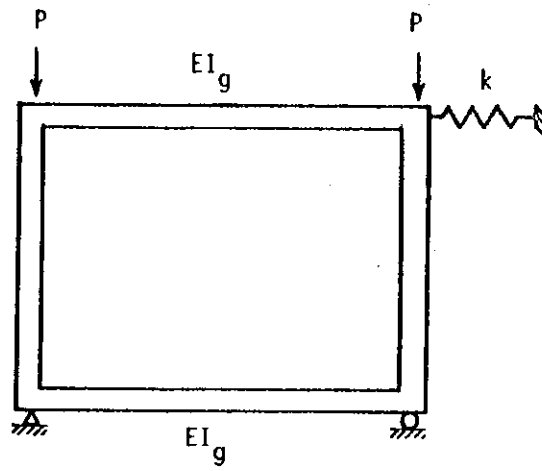


FIGURE 1.3  
EFFECTS OF LATERAL BRACING ON  
COLUMN ELASTIC CRITICAL LOAD

of lateral bracing provided, and can vary over a wide range as the degree of lateral bracing is changed.

Due to the predominance of the relatively stiff shear wall element in a braced structure, the deformation response characteristics of the shear walls in any storey are strongly influenced by the response of those in other storeys of the structure. For this reason, in a braced structure, it is not possible to isolate a particular storey or group of members to derive a simplified model like that of Goldberg. Information regarding the effects of bracing stiffness must be obtained from an analysis of the entire structure.

The interaction behaviour in a shear wall-frame system which results in sharing of the lateral loads by the shear wall and frame also merits some investigation. A realistic assessment of the load-sharing character of interaction is necessary for a rational and economical design of the structure. Often shear walls are designed to resist all lateral forces while the frame is assumed to carry only vertical loads. A number of authors have shown that if the wall is tall and slender or if the frame itself possesses some degree of lateral stiffness, a safer and more economical design could be achieved by taking the shear wall-frame interaction into account. Neglect of the lateral load carrying ability of the frame could result in overdesign of the shear wall and underdesign of the frame members. Any redistribution of this lateral force resistance resulting from inelastic action would influence the limit design of these structures.

In view of these apparent gaps in the current state of knowledge of shear wall-frame systems, the object of this thesis is to develop an accurate analysis to trace the behaviour of a reinforced concrete shear wall-

frame structure as it progresses through the elastic and inelastic ranges to failure.

The methods currently available for the analysis of braced and unbraced structures are discussed in CHAPTER II. In CHAPTER III, methods are developed to express the section response characteristics of reinforced concrete members as elastic-perfectly plastic moment-curvature relationships. This type of section response leads to consideration of plastic hinges. Slope-deflection equations are derived to treat members with varying numbers of plastic hinges. These slope-deflection equations are employed in CHAPTER IV to derive a second order elastic-plastic analysis for shear wall-frame systems. The analysis, formulated using displacement method principles, employs an iterative method of solution. A computer programme is developed to perform the analysis and provide information regarding the behavioural history of the structure. The applicability of the analysis is demonstrated in CHAPTER V by comparison with the results of laboratory tests and other methods of analysis.

CHAPTER VI and VII are devoted to an investigation of the effects of axial shortening, finite wall width, slenderness, and relative shear wall stiffness on the behaviour of a shear wall-frame structure. A twenty storey, two bay reinforced concrete structure, designed by ultimate strength procedures, is taken as a basis for the study. Since the study is limited to this one structure, it is not complete or definitive. However, the study does illustrate the applicability of the analysis and shows trends which must be considered in the design of multi-storey reinforced concrete structures.

## CHAPTER II

### REVIEW OF PREVIOUS WORK

#### 2.1 Introduction

For the investigation of the problems discussed in CHAPTER I, it is necessary to employ a method of analysis which will accurately trace the response of a plane shear wall-frame structure as loading progresses to failure.

A review of the current state of knowledge regarding the analysis of unbraced frames and braced structures is presented in this chapter. To permit comparison of the analyses currently available, the variety of possible approaches and the relative merits of each are mentioned.

On the basis of this review, the considerations leading to the development of the method of analysis derived in this thesis are discussed.

At the moment, little is known about the behaviour of shear wall-frame structures. However, a brief discussion of the extent of the information presented by other investigators is included in this chapter.

#### 2.2 Possible Methods of Analysis

In formulating an analysis, it is necessary to simplify the problem by idealizing the configuration of the structural model and the behavioural characteristics of the member cross-sections, individual members and the overall structure. The type and extent of simplification used to develop the analytical model can significantly influence the accuracy and

validity of the results.

Once the form of the simplified analytical model has been chosen, several alternate methods can be used to arrive at a solution.

### 2.2.1 Simplification of the Analytical Model

Assuming that the geometry and loading configuration of the analytical model have been defined, an engineering analysis is derived by making some of the following assumptions:

1. The cross-section behaviour is
  - (a) purely elastic
  - (b) rigid-plastic neglecting axial thrust
  - (c) rigid-plastic considering axial thrust
  - (d) elastic-plastic
  - (e) elastic-inelastic considering gradual plastification, residual stresses, strain-hardening or any combination of these.

These are illustrated in FIGURE 2.1.

2. The member behaviour is
  - (a) first order, meaning that equilibrium is formulated on the undeformed member
  - (b) second order, meaning that equilibrium is formulated on the deformed member, considering beam-column action.
3. The structure behaviour is
  - (a) first order, meaning that equilibrium is formulated on the undeformed structure
  - (b) second order, meaning that equilibrium is formulated on the deformed structure, considering  $P\Delta$  effects.

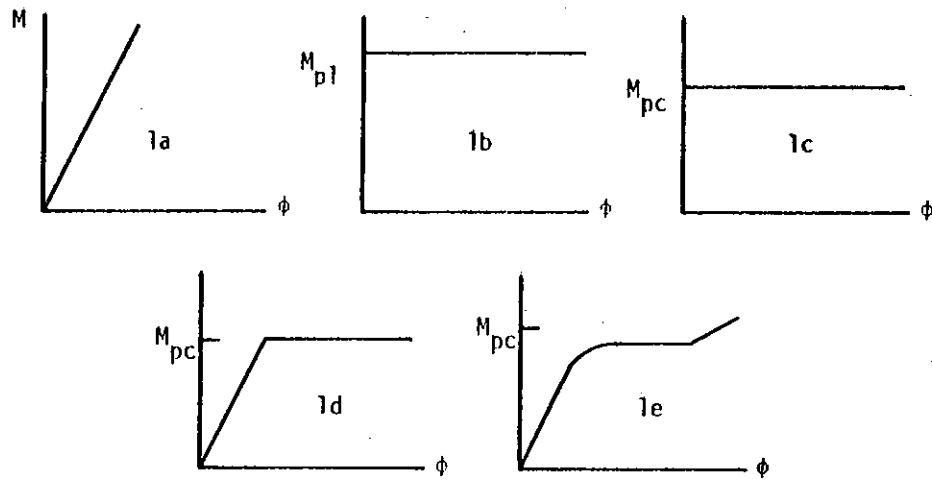


FIGURE 2.1  
POSSIBLE ASSUMPTIONS FOR SECTION RESPONSE

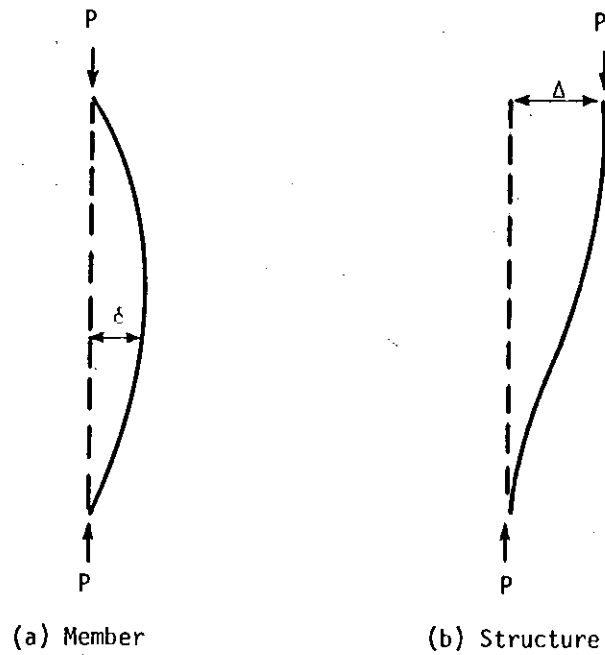


FIGURE 2.2  
CONSIDERATIONS OF A SECOND ORDER ANALYSIS



FIGURE 2.2 indicates the axial load effects in the member and the overall structure which are considered by a second order analysis.

A qualitative representation of the effects of these assumptions on the load-deflection relationship for a portal frame is presented in FIGURE 2.3. The true behaviour is shown by the continuous heavy line. The numbers denoting the other relationships refer to the assumptions involved in their derivation. It will be noted that the second order elastic-plastic and second order elastic-inelastic analyses most closely approximate the true behaviour.

To complete the analytical model, decisions must also be made regarding the consideration or neglect of axial shortening, shear deformations, finite member widths, "large deflection" effects and imperfections in the actual structure.

### 2.2.2 Formulation of the Solution

Essentially three different approaches have been adopted by investigators for the solution of this type of problem. These are the analytical methods, the convergence methods and the energy methods. The analytical methods of solution, which might better be termed matrix methods, involve the derivation of sufficient linear simultaneous equations to provide a unique solution. The equations are established by classical force or displacement methods, also known as flexibility or stiffness methods, or by some variation of these methods. The convergence methods involve a series of successive approximations of deformations to achieve force compatibility. The energy methods utilize the techniques of variational calculus applied to the total potential energy of the system. There are, of

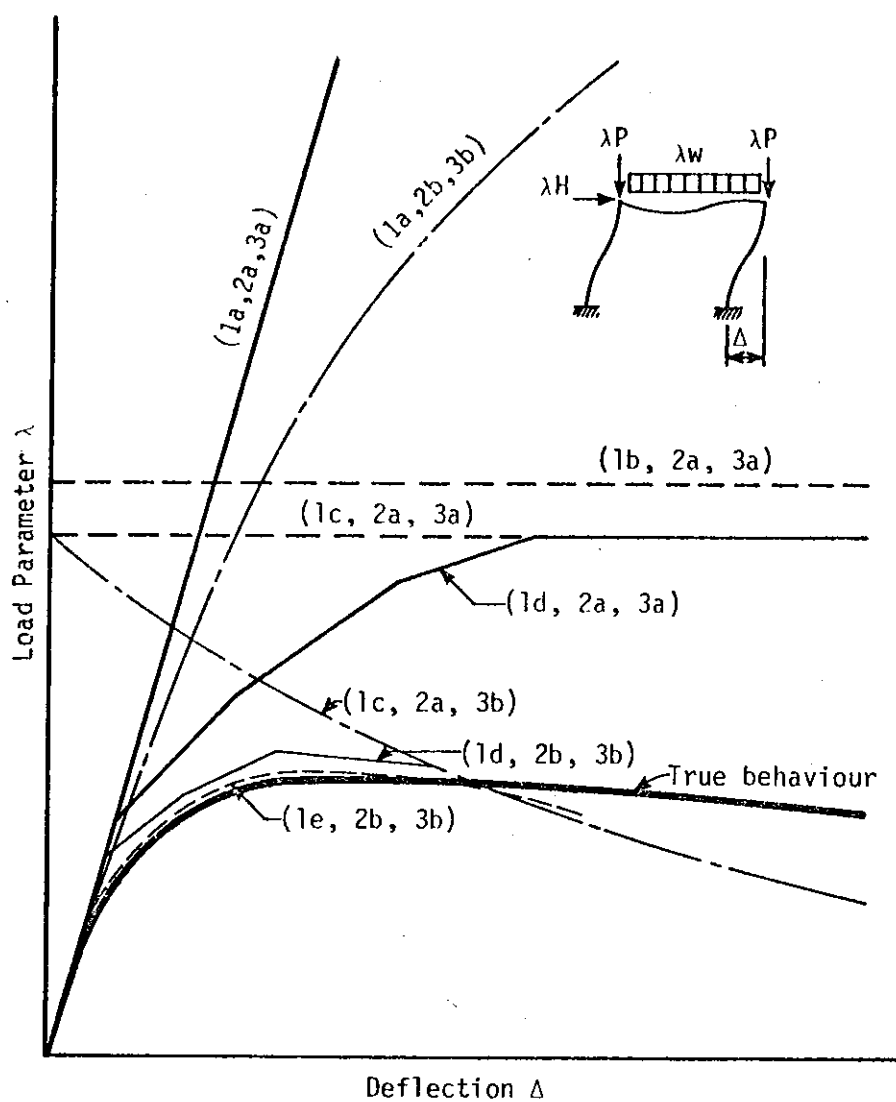


FIGURE 2.3  
EFFECTS OF SIMPLIFICATIONS OF ANALYTICAL  
MODEL BEHAVIOUR ON COMPUTED  
LOAD-DEFLECTION RESPONSE  
[after Ostapenko<sup>(4)</sup>]

course, many variations of each of these general methods.

Each of these methods can be shown to be advantageous in particular cases. With a large structure, none of the techniques are easily executed in the elastic range of stresses, and consideration of inelastic behaviour complicates the problem even more.

### 2.3 Unbraced Frame Analyses

The advent of plastic methods for the design of mild steel structures has provided impetus to the investigation of the limiting load-carrying capacity of structures. The initially proposed simple plastic method proportioned members on the basis of the loading configuration which produced a failure mechanism. This first order rigid-plastic method effectively established strength as the sole failure criterion, neglecting the possibility of instability occurring prior to the formation of the critical failure mechanism. The question of the validity of such an approach in tall slender structures naturally focussed attention on the effects of instability.

The well known methods for evaluating the elastic critical load of frameworks consisting of centrically-loaded columns are summarized by Bleich<sup>(5)</sup>. A great deal of work<sup>(6)</sup> has also been done in deriving elastic and inelastic solutions for the buckling load of symmetrical structures subjected to symmetrically distributed gravity loads. Unfortunately, the concept of elastic stability finds limited application in multi-storey frames of usual dimensions, since the frames are usually strained into the inelastic range before critical or buckling loads are reached. Moreover, the solutions for symmetrical structures, even with primary bending moments due to distributed gravity loads, treat the bifurcation type of failure. The case

where lateral loads are applied, leading to translational instability of the structure, is by far the most practical engineering problem.

In view of the apparent complexity of an exact solution under conditions of inelastic instability, British investigators turned their attention to the approximation of critical loads in multi-storey unbraced frames. Merchant<sup>(7)</sup> proposed the use of a Rankine formula  $\frac{1}{\lambda_F} = \frac{1}{\lambda_P} + \frac{1}{\lambda_C}$  which enables evaluation of the maximum capacity of the structure  $\lambda_F$  as a function of the rigid-plastic collapse load  $\lambda_P$  and the elastic critical load  $\lambda_C$ . Horne<sup>(8)</sup> has provided a justification for the formula, and its range of validity has been experimentally verified for certain cases<sup>(9)</sup>.

Wood<sup>(10)</sup>, employing what he termed the "deteriorated" structure, derived a method to establish upper and lower bounds to the carrying capacity. Reasoning that a fully plastic hinge contributes no more to the stiffness of the structure than does a real hinge, Wood replaced the plastic hinge by a pin joint and computed the "deteriorated" critical load of the structure. As the load increases and more plastic hinges form, the deteriorated critical load decreases until it corresponds to the applied load, at which time the structure becomes unstable. However, the prediction of the deteriorated structure implies prior knowledge of the order of hinge formation.

While these two approximate methods have helped to clarify the significance of instability effects in reducing failure loads below the values predicted by the strength criterion, neither is simple to apply to large structures. The essential weakness of Wood's method in requiring knowledge of the order of hinge formation points out the fact that methods for accurately predicting failure loads must be historical in nature.

Accurate methods must trace the response of the structure as loading progresses, detecting and making allowances for all inelastic action as it occurs.

A number of very sophisticated second order analyses<sup>(4)</sup> have been developed to provide the complete load-deflection relationship for simple laterally loaded structures throughout the elastic and inelastic ranges. These "exact" solutions were derived using compatibility methods. In place of the elastic-perfectly plastic relationship which results in the consideration of point plastic hinges, more realistic moment-curvature relationships were employed to treat inelastic behaviour. Since the performance of an accurate compatibility analysis is quite complex, these theoretical studies were limited to portal frames, with the hope that the knowledge gained would provide some insight into the behavior of larger structures. It seems safe to say that extension of these rigorous analyses to multi-bay multi-storey structures would severely tax computer capacity.

Recently, computerized methods have been developed to carry out a complete elastic-plastic analysis of large unbraced planar frames. However, to formulate these solutions it has been necessary to relax the rigorous requirements of strain compatibility by assuming point plastic hinges consistent with elastic-perfectly plastic section behaviour.

Jennings and Majid<sup>(11)</sup>, extending the displacement method of analysis to the inelastic range, developed an iterative procedure to perform an elastic-plastic analysis of unbraced structures loaded by static, proportional, concentrated loads. The solution is derived by matrix techniques with joint displacements as the unknowns. As each successive plastic hinge forms, the hinge rotation becomes an additional unknown, and

the augmented stiffness matrix for the deteriorated structure must be reconstructed. This revised stiffness matrix is used to perform an elastic analysis for prediction of conditions when the next hinge forms. Instability is assumed when the determinant of the stiffness matrix changes sign. Secondary axial load effects in all members and the overall structure are considered by incorporating stability functions<sup>(12)</sup>. The Jennings and Majid analysis provides the complete load-deflection history for the structure and directly yields information regarding the order of plastic hinge formation.

Davies<sup>(13)</sup> has since extended the Jennings and Majid analysis to study the behaviour of frames subjected to cyclic loading. His analysis is capable of considering the effects of hinge reversals by replacing the closing hinge by a "locked" hinge with a rotational discontinuity. This is the only analysis yet formulated which considers the possibility of strain reversals.

Parikh<sup>(14)</sup>, also using the displacement method, has formulated a second order elastic-plastic analysis for unbraced planar frames. The method employs slope-deflection equations which are modified to consider members in different stages of plastic hinge formation. P $\Delta$  effects are considered in satisfying equilibrium conditions and columns are treated as beam-columns by the use of stability functions. In this analysis, hinge rotations need not be considered as additional unknowns, and the requirement of performing a separate elastic analysis to detect each successive hinge is removed. Loading is incremental and at any stage of loading, the analysis procedure is continued until the plastic hinge pattern converges. Thus, the

solution does not yield the exact order of hinge formation but does detect the total number of new hinges which form in a particular increment. Classical matrix methods are replaced by an iteration procedure for the solution of the simultaneous equations resulting from equilibrium conditions. Instability is detected by non-convergence of the iterative procedure.

Parikh's approach offers several advantages over that of Jennings and Majid. The use of slope-deflection equations removes the limitation of concentrated loads, and uniformly distributed loads can be considered. Of greater significance is the fact that Parikh's analysis makes more efficient use of computer storage capacity than does the Jennings and Majid analysis. Using the iteration procedure for a solution, it is not necessary to set up a formal stiffness matrix. This saving of computer capacity should permit study of larger structures.

Korn<sup>(15)</sup>, combining features of the Jennings and Majid and Parikh analyses, has also formulated a second order elastic-plastic analysis for unbraced planar structures subjected to static, proportional concentrated loads. Korn used modified slope-deflection equations similar to Parikh's to formulate a solution satisfying second order equilibrium conditions. However, in place of the iterative method of solution used by Parikh, Korn used matrix techniques, with a determinant sign change signifying failure of the structure. Korn also employed a procedure similar to that of Jennings and Majid to establish the order of formation of successive plastic hinges.

Thus, three different methods are currently available for the accurate analysis of large unbraced planar frames. These analyses require no simplification of frame geometry. All consider only bending and axial deformations, neglecting shear deformations. Inelastic action is represented

by point plastic hinges in all three methods. The hinges at member ends are considered to form in the joint at the intersection of the centrelines of all members framing into the joint. No provision is made for consideration of the finite width of the members.

## 2.4 Braced Structure Analyses

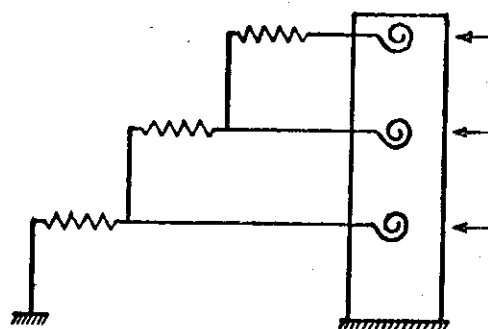
The basic difference between the braced structure and unbraced frame is the presence of a relatively stiff element which possesses significant finite width. In this thesis, the stiff element is represented by the reinforced concrete shear wall.

The concept of limit design of reinforced concrete structures is a relatively recent development. The primary concern of most previous investigators of shear wall-frame structures has been the partitioning of lateral forces between the frame and the shear wall at the working load. Consequently, most analyses have been limited to the consideration of elastic behaviour of braced structures subjected only to lateral forces. They were intended to serve primarily as quick office design tools, and must be considered quite approximate compared to the analyses discussed in SECTION 2.3.

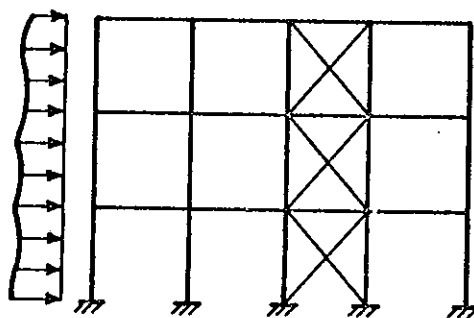
In most cases, the analysts have reduced the structure to an equivalent system and solved the resulting indeterminate structure in a variety of manners. Typical simplified configurations are shown in FIGURE 2.4.

Gould<sup>(16)</sup> replaced the frame by a system of rotational and translational springs linked by rigid bars, as shown in FIGURE 2.4(a). Using a finite difference approach, Gould proportioned the lateral load to satisfy

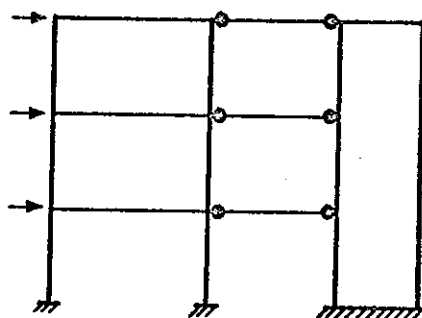




(a) Gould's Model



(b) Bandel's Model



(c) Khan and Sbarounis Model

FIGURE 2.4  
SIMPLIFIED BRACED STRUCTURE CONFIGURATIONS  
CONSIDERED BY PREVIOUS ANALYSES

conditions of deformational compatibility.

Bandel<sup>(17)</sup> replaced the shear wall by an equivalent truss to derive the configuration shown in FIGURE 2.4(b). With deformation relationships expressed in power series form, principles of virtual work were used to derive the solution.

Khan and Sbarounis<sup>(18)</sup> considered a model consisting of a shear wall and a simplified lumped frame system as shown in FIGURE 2.4(c). The solution was accomplished by an iterative procedure of force-fitting until deformational compatibility was achieved.

In addition to these, numerous other analyses<sup>(19,20,21,22,23)</sup> have been formulated. However, because they are all first order elastic solutions of simplified structures, they are not suitable for use in the investigation described in this thesis. Moreover, the methods of analysis employed by these investigators are difficult to extend to inelastic structures.

Clough, King and Wilson<sup>(24)</sup> have developed a computerized first order elastic analysis for multi-storey braced structures subjected to lateral loads. The only simplification of the frame required for the analysis is that of constant shear wall finite width, though the stiffness may vary. The analysis is accomplished by the deformation method using matrix techniques. Axial deformations of the columns and shear wall are considered in the analysis.

Guhmajumdar, Nikhed, MacGregor and Adams<sup>(25)</sup> have derived an elastic-plastic analysis for braced structures subjected to concentrated lateral and gravity loads applied only at the joints. The shear wall-frame

model considered is similar to that of Khan and Sbarounis, with a simplified substitute frame derived by a lumping procedure. The effects of shear wall finite width and  $P\Delta$  are considered, but axial shortening and beam-column behaviour are neglected. The analysis is performed by the convergence method. Loading is proportional and incremental, with failure signified by non-convergence of the force-fitting procedure.

## 2.5 Studies of Braced Structure Behaviour

Few authors of the articles discussed in SECTION 2.4 have applied their analyses to anything but a sample calculation of a specific design problem. However, both Khan and Sbarounis and Parme, using first order elastic analyses, produced sets of charts showing the distribution of storey shear forces in the shear wall and frame for a variety of member stiffness distributions and loading configurations. These were intended to provide guidance in the preliminary sizing of braced structures. In addition, Khan and Sbarounis carried out a limited study of the effects on elastic behaviour of foundation rotation, plasticity in the shear wall, wall shear deformations and axial shortening of columns.

Guhamajumdar, Nikhed et al applied their elastic-plastic analysis to investigate the behaviour of a twenty-four storey two bay braced structure. The study considered the effect of neglecting secondary  $P\Delta$  moments and the finite width of the shear wall on the overall load-deflection history. The flexural stiffness of the shear wall in the structure was varied to study the effects on overall elastic-plastic behaviour.

## 2.6 Conclusions

Previous studies of braced frame behaviour have been quite limited,

and a number of questions remain unanswered. To accomplish the behavioural investigation proposed in CHAPTER I, the inelastic analysis must be accurate and should involve as few idealizations of the analytical model geometry and behaviour as possible.

Only the analysis of Guhamajumdar, Nikhed, MacGregor and Adams is capable of considering the second order elastic-plastic behaviour of braced structures. However, in the formulation of this analysis, a simplified substitute frame system is assumed. The validity of the lumping procedure used in establishing this substitute frame has yet to be demonstrated for a partially inelastic structure.

Since the use of the "exact" compatibility analyses discussed in SECTION 2.3 is clearly impracticable for large structures, it is necessary to assume elastic-plastic section response characteristics. All three second-order elastic-plastic solutions for unbraced structures employ essentially the same analytical model. However, the iterative procedure of Parikh appears to have greater capabilities in analyzing large structures because of its more efficient use of computer storage capacity. For this reason, the braced frame analysis developed in this thesis is modelled after the Parikh analysis. The finite width of the shear wall element will be accommodated in the analysis.

The extension of this type of elastic-plastic analysis to consider reinforced concrete structures introduces a significant problem. Parikh and the other investigators considered mild steel structures for which elastic-plastic section moment-thrust-curvature relationships have been defined. Similar relationships for reinforced concrete members must be established to permit the application of an elastic-plastic analysis.

## CHAPTER III

### ANALYSIS OF MEMBERS

#### 3.1 Introduction

In this chapter, the methods used to define the behaviour of reinforced concrete members are described, and the related assumptions are discussed. The method of analysis applied to the structure itself is presented in CHAPTER IV. It is based on the member properties described in this chapter.

The basic assumption made in the analysis is that the behaviour of any cross-section can be defined in terms of an elastic-perfectly plastic moment-thrust-curvature relationship. Accordingly, elastic-perfectly plastic section response relationships for girders and columns are presented in this chapter. These relationships are compared with those derived using other assumptions.

The response of the entire member to applied forces is expressed in slope-deflection equation form. A series of these equations, modified to consider the presence of plastic hinges at any point in a member, the effects of axial loads, and the finite width of the shear wall element, is also presented in this chapter.

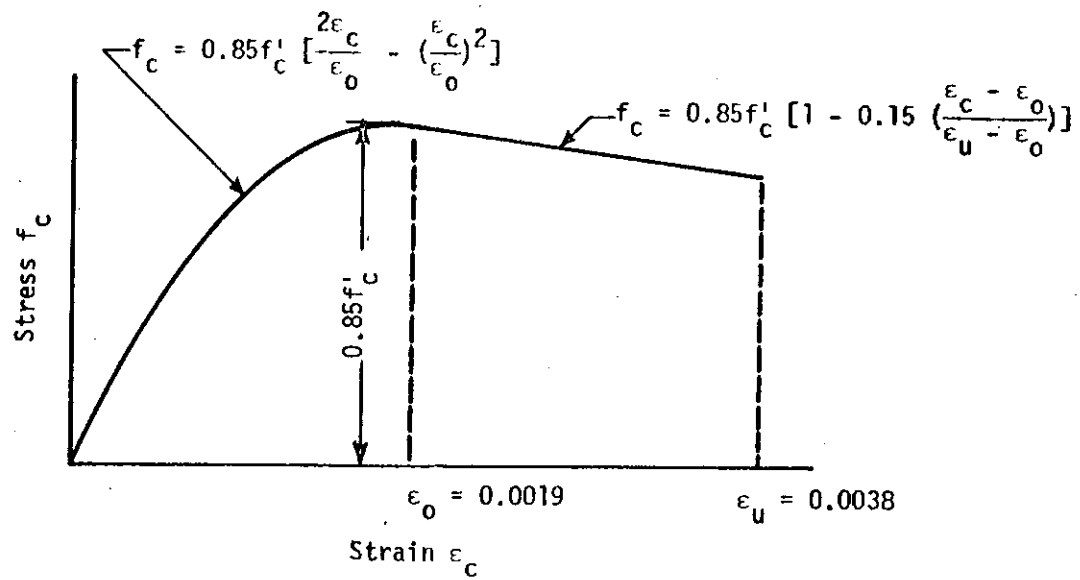
#### 3.2 Analysis of a Reinforced Concrete Cross-Section

For any section subjected to constant axial force, curvature is a function of the applied moment. This moment-curvature relationship for the section must be known to establish the deflected shape of the member.

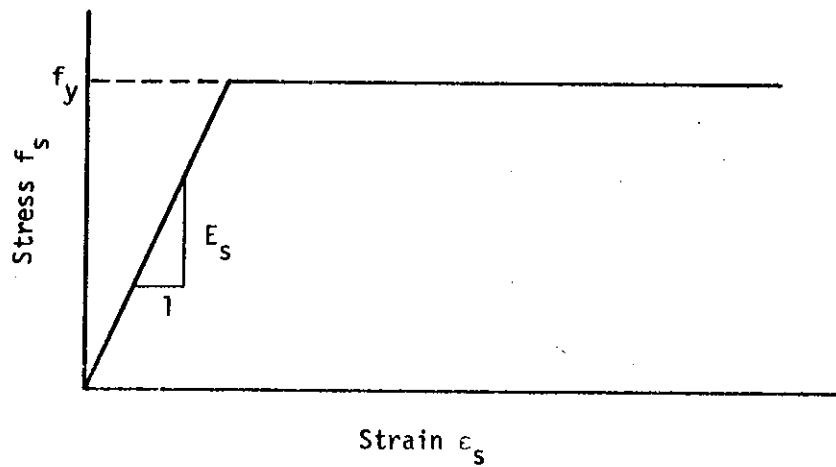
In dealing with materials having simple stress-strain relationships, it is generally possible to formulate a closed form of solution relating bending moment, axial load, and curvature ( $M-P-\phi$ ). However, to consider the complex stress-strain relationships encountered in dealing with the inelastic response of a reinforced concrete section, it is necessary to resort to numerical methods<sup>(26)</sup> or a set of analytical expressions<sup>(27)</sup>. In the simplest case of a girder section, where axial load can be neglected, a unique  $M-\phi$  curve can be generated without much difficulty if creep of the concrete is ignored. The derivation of the same relationship for a column section is complicated by the presence of axial load.

To gain some understanding of the response of a column section to load, a computer programme was prepared using the procedures developed by Pfrang et al<sup>(28)</sup>. For clarity, this will be termed the "exact" analysis. In this analysis, the concrete is assumed to exhibit the stress-strain curve defined by Hognestad<sup>(29)</sup> modified as shown in FIGURE 3.1(a) and the steel is considered to be elastic-plastic as shown in FIGURE 3.1(b). This analysis was applied to the symmetrically reinforced column section shown in FIGURE 3.2, the basic properties of which are also presented. To separate the effects of the several section parameters, eight variations of this basic cross-section were investigated, as listed in TABLE 3.1.

In an effort to derive an elastic-plastic  $M-P-\phi$  relationship, several unsuccessful attempts were made to non-dimensionalize the values generated by the exact analysis for the range of variables considered. Recourse was then made to a "rationalized" approach, basing the response characteristics on the section geometry and material properties. This rationalized relationship, used throughout the thesis, is presented in



(a) Concrete in Compression



(b) Steel

FIGURE 3.1  
 ASSUMED MATERIAL STRESS-STRAIN  
 PROPERTIES FOR EXACT ANALYSIS

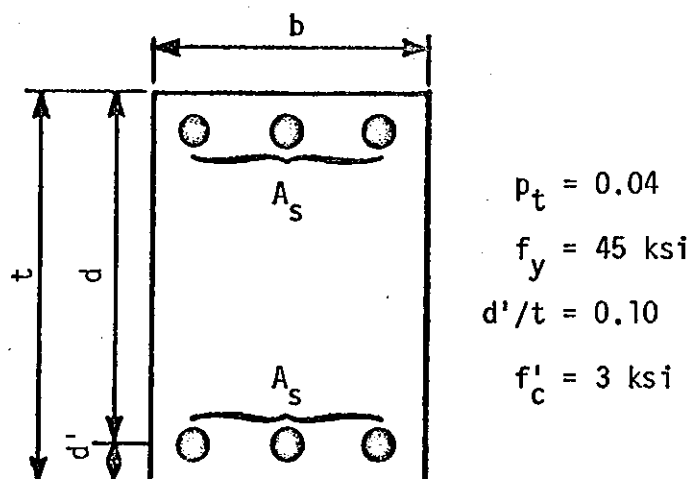


FIGURE 3.2  
COLUMN CROSS-SECTION AND PROPERTIES  
OF THE BASIC SECTION INVESTIGATED

CASE	PARAMETER VARIED
1	$p_t = 0.02$
2	$p_t = 0.06$
3	$f_y = 30 \text{ ksi}$
4	$f_y = 60 \text{ ksi}$
5	$d'/t = 0.05$
6	$d'/t = 0.15$
7	$f'_c = 2 \text{ ksi}$
8	$f'_c = 4 \text{ ksi}$

TABLE 3.1  
VARIATIONS OF BASIC SECTION CONSIDERED



the balance of SECTION 3.2.

### 3.2.1 Assumptions of Rationalized Moment-Curvature Relationship

In deriving the rationalized section response characteristics, the following assumptions were made.

1. The maximum stress developed in concrete in a column or a girder is 0.85 times the standard 28 day compressive strength. This value of the concrete strength reduction factor has been verified by numerous tests.
2. No consistent assumption is made regarding the concrete stress-strain relationship. When ultimate section response characteristics are considered, the complete stress-strain relationship shown in FIGURE 3.1(a) is used. When conditions at the "yield point" of the section are considered, a linear stress-strain relationship, representing the initial portion of the complete stress-strain diagram, is employed. The assumptions will be presented as they arise in the derivations.
3. Creep and shrinkage deformations can be neglected in the analysis. This assumption leads to an underestimation of the reinforcement strains, particularly in lightly reinforced columns, and an underestimation of the secondary deflections, particularly at high stress levels. On the other hand, the relative stiffness of the columns tends to be overestimated if time effects are ignored. Consequently, in indeterminate structures, the errors resulting from the neglect of creep are compensating to some extent. This problem has been studied extensively by Manuel and MacGregor<sup>(30)</sup>.

4. The tensile load-carrying capacity of concrete, small relative to the compressive strength, can be neglected.
5. The ultimate capacity of the section is based on a limiting concrete strain criterion. The useful limit of concrete strain used here is 0.0038. Test results<sup>(29)</sup> indicate that this is a realistic value of the useful strain limit for unconfined concrete.
6. The column section is assumed to have sufficient transverse reinforcement to make the axial load capacity of the core equal to that of the gross section.
7. The reinforcement exhibits a linear elastic-plastic stress-strain relationship with no strain-hardening. This assumption is not entirely realistic for high strength steel.
8. At all load levels, plane sections remain plane. Shear deformations and localized disturbances at cracks are neglected.
9. The axial load and bending moment increase continuously to failure. Hence, strain reversals can be ignored.

### 3.2.2 Column Section Response

The column section considered throughout this thesis is a rectangular symmetrically reinforced section as depicted in FIGURE 3.2. The essential column features are described by the geometry of the section and the material properties  $f'_c$ ,  $f_y$  and  $E_s$ .

To permit the formulation of the method of member analysis described in SECTION 3.3, the response of a column section to applied moment in the presence of axial load must be described by a rationalized elastic-plastic

M- $\phi$  diagram. A typical M- $\phi$  relationship is that shown in FIGURE 3.3. The dashed line represents the moment-curvature relationship derived by the "exact" analysis discussed previously. The solid line represents the "rationalized" relationship derived in this section. Throughout the initial stage of the M- $\phi$  diagram, the column section is assumed to behave elastically. When the "yield point" of the cross-section is reached, the section behaves plastically with constant resisting moment until the useful limit of strain is reached in the compressed concrete.

If the three co-ordinate values,  $M_{pc}$ ,  $\phi_y$  and  $\phi_{pc}$  can be expressed as functions of the axial load P, it is possible to derive M- $\phi$  curves for any value of P, and obtain the complete M-P- $\phi$  relationship for the section.

(a) Interaction Diagram Relating P and  $M_{pc}$

The ultimate strength interaction diagram, essentially an envelope of all possible combinations of axial load and moment which do not lead to material failure of the cross-section, provides a relationship between P and  $M_{pc}$ . The rationalized interaction diagram shown in FIGURE 3.4, was derived by simplification of the exact solution.

The capacity of a section subjected to pure axial load can be expressed simply as the summation of the ultimate capacities of the steel and concrete.

$$P_0 = 0.85 f'_c b(t - 2pd) + 2pbdf_y \quad (3-1)$$

The ultimate moment capacity of a column section in pure flexure is a rather complex quantity to evaluate by the exact analytical equations.

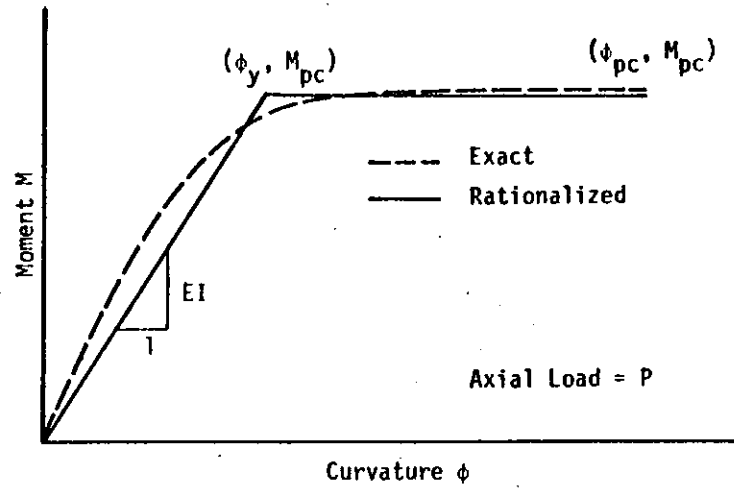


FIGURE 3.3

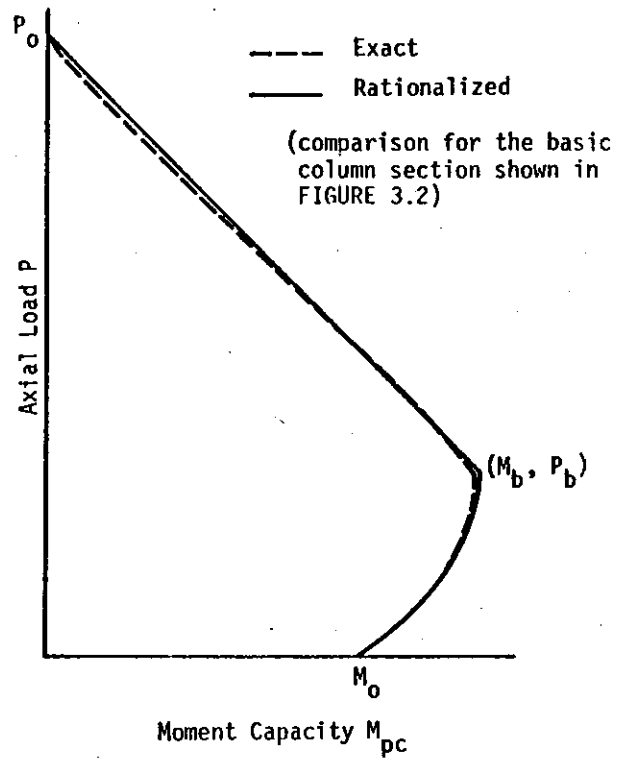
COLUMN SECTION M-P- $\phi$  RELATIONSHIP

FIGURE 3.4

## COLUMN SECTION ULTIMATE INTERACTION DIAGRAM

A rationalized  $M_o$ , based on the couple of the yielded steel sections, compared very favourably with the exact values over the range of variables considered.

$$M_o = A_s f_y (d - d') \quad (3-2)$$

The balance point of the interaction diagram represents the combination of axial load and moment which leads to simultaneous initial tension steel yield and the attainment of the ultimate compressive strain in the extreme concrete fibre. By definition, then:

$$\phi_b = \frac{\epsilon_u + \frac{f_y}{E_s}}{d} \quad (3-3)$$

A simplification of an exact analytical expression makes it possible to express the balanced axial load value as:

$$P_b = \frac{0.00257 f'_c b}{\phi_b} \quad (3-4)$$

An approximate expression for the evaluation of the balanced eccentricity has been presented<sup>(31)</sup>. While this simplified approach is more suitable for slide-rule operations, it was found to be insensitive to variations in  $f_y$  and  $\frac{d'}{t}$ . The exact equations were used to derive the expression which follows.

$$e_b = t \left[ 0.5 - \frac{1.542 \times 10^{-3}}{\phi_b t} + 195 (d - d') \phi_b \frac{p_t f_y}{f'_c} \right] \quad (3-5)$$

The derivations of EQUATIONS (3-4) and (3-5) appear in APPENDIX

A.

Finally, by definition:

$$M_b = P_b e_b \quad (3-6)$$

With these points established on the interaction diagram, it is necessary to complete the locus of bounding points by joining them in a suitable manner. For the tension failure portion of the interaction curve boundary below  $P = P_b$ , a parabola was fitted such that  $\frac{dM_{pc}}{dP} = 0$  at  $P = P_b$  and  $M_{pc} = M_o$  at  $P = 0$ . A similar relationship was developed independently by Quast<sup>(32)</sup>. A linear relationship was assumed for the compression failure portion of the boundary. Thus, the following relationships provide a value of  $M_{pc}$  for any axial load value.

If  $0 \leq P < P_b$ :

$$M_{pc} = M_o + (M_b - M_o) \left( \frac{P}{P_b} \right) \left( 2 - \frac{P}{P_b} \right) \quad (3-7)$$

If  $P_b \leq P \leq P_o$ :

$$M_{pc} = \left( \frac{P_o - P}{P_o - P_b} \right) M_b \quad (3-8)$$

Values from this rationalized relationship compared favourably with the exact values in most regions of the interaction curve.

(b) The Yield Curvature  $\phi_y$  as a Function of P

In general, the "yield point" of a column cross-section is the point at which the slope of the M- $\phi$  curve decreases considerably. In the absence of axial load, the yield point of the column section considered here is well defined. The application of axial load results in a progressive onset of inelastic action in the section, masking the yield point as shown in FIGURE 3.3. However, to derive the elastic-plastic M-P- $\phi$  relationship, it is necessary that a  $\phi_y$  value be defined.

M-P- $\phi$  curves were plotted using the results of the exact analysis. From these plots, best fit elastic-plastic M- $\phi$  parameters were chosen. Plots of the graphically-derived "exact"  $\phi_y$  as a function of P yielded a family of curves similar to that illustrated by the dashed line in FIGURE 3.5. Starting from  $\phi_{y0}$  for pure flexure, the  $\phi_y$  value increases to a peak value at a value of P somewhat lower than  $P_b$ , and naturally drops to zero at  $P_0$ .

The rationalized  $\phi_y$  - P relationship adopted here is shown by the solid line in FIGURE 3.5. The essential co-ordinates are defined by  $\phi_{y0}$ ,  $\phi_{yb}$  and  $P_b$ .

The apparent yield in the M- $\phi$  diagram could be attributed to several occurrences:

1. yield of the tension reinforcement
2. yield of the compression reinforcement
3. strain-softening of the concrete in compression
4. a combination of these.

The relative significance of these varies according to the section properties and the axial load value. Consequently, it is difficult to formulate an ex-

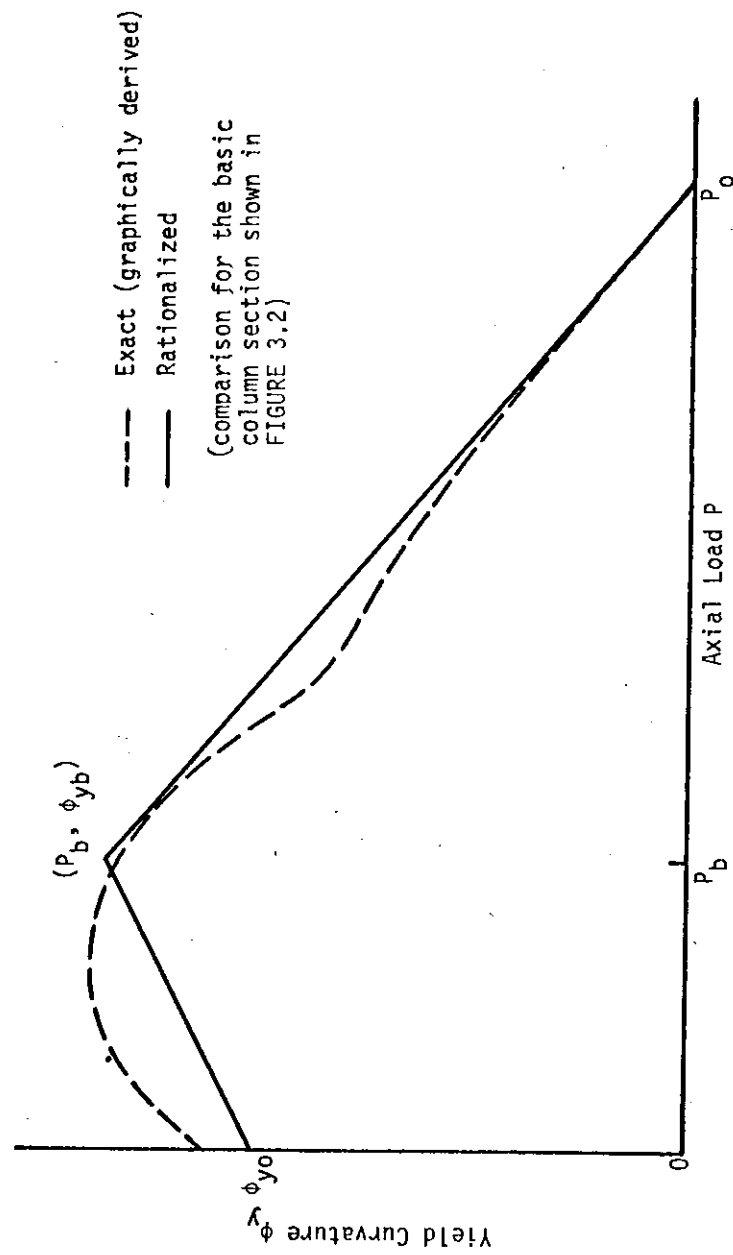


FIGURE 3.5  
RELATIONSHIP BETWEEN COLUMN SECTION  
YIELD CURVATURE AND AXIAL LOAD VALUE



pression for  $\phi_y$  which is applicable in all cases.

In this thesis, the derivation of a value of  $\phi_{y0}$  assumes that the yield of the M- $\phi$  diagram is brought about by the yielding of the tension steel. A detailed derivation of EQUATIONS (3-9) and (3-10) with the related assumptions is presented in APPENDIX A.

$$k_{y0} = -2pn + \sqrt{4(pn)^2 + 2pn(1 + \frac{d'}{d})} \quad (3-9)$$

where  $n = \frac{500}{\sqrt{f'_c}}$

$$\phi_{y0} = \frac{f_y}{E_s d (1 - k_{y0})} \quad (3-10)$$

Similarly, the derivation of  $\phi_{yb}$ , also presented in APPENDIX A, assumes initial tension steel yield as the yield criterion.

$$k_{yb} = \frac{-y + \sqrt{y^2 - 4xz}}{2x} \quad (3-11)$$

where  $x = \frac{1}{2n}$

$$y = 2p + \frac{P_b}{f_y b d}$$

$$z = -p(1 + \frac{d'}{d}) - \frac{P_b}{f_y b d}$$

$$\phi_{yb} = \frac{f_y}{E_s d (1 - k_{yb})} \quad (3-12)$$

In deriving the rationalized  $\phi_{yb}$  value, several other possibilities were considered. Most notably, a similar solution was formulated using initial compression steel yield as the yield criterion. Within the range of variables considered, this assumption yielded excessively conservative values of  $\phi_{yb}$ .

Since  $\phi_{y0}$  and  $\phi_{yb}$  values were based on the same yield criterion, it is apparent that EQUATION (3-12) is applicable for any  $0 \leq P \leq P_b$  if that value of  $P$  were used in evaluating EQUATION (3-11). A study of the  $\phi_y - P$  relationship so calculated yields virtually a straight line, with no intermediate peak value as indicated by the exact analysis. Hence, for any value of  $P$ , the corresponding value of  $\phi_y$  can be computed using EQUATIONS (3-13) and (3-14). These are plotted in FIGURE 3.5.

If  $0 \leq P < P_b$ :

$$\phi_y = \phi_{y0} + (\phi_{yb} - \phi_{y0}) \frac{P}{P_b} \quad (3-13)$$

If  $P_b \leq P \leq P_o$ :

$$\phi_y = \frac{P_o - P}{P_o - P_b} \phi_{yb} \quad (3-14)$$

### (c) The Ultimate Curvature $\phi_{pc}$ as a Function of $P$

The last component required to define the rationalized column M- $\phi$  relationship is the ultimate curvature  $\phi_{pc}$ .

Again, using the exact analysis, plots of  $\phi_{pc}$  versus  $P$  were prepared for the range of section properties considered. The general shape

of these plots is illustrated by the dashed line in FIGURE 3.6. The sharp break noted in the range  $0 < P < P_b$  can be attributed to the inception of compression steel yield as  $P$  increases.

The relationship between  $\phi_{pc}$  and  $P$  assumed in this analysis is shown by the solid line in FIGURE 3.6. The value of  $\phi_u$ , the ultimate curvature of the section in pure flexure, can be derived in a rationalized manner. The derivation and assumptions leading to the formulas which follow appear in APPENDIX A.

$$k_u = \frac{-y + \sqrt{y^2 - 4xz}}{2x} \quad (3-15)$$

where

$$\begin{aligned} x &= 0.7 f'_c \\ y &= p (E_s \epsilon_u - f_y) \\ z &= -p E_s \epsilon_u \frac{d'}{d} \end{aligned}$$

$$\phi_u = \frac{\epsilon_u}{k_u d} \quad (3-16)$$

With  $\phi_u$  defined, equations for the  $\phi_{pc} - P$  relationship, broken into four segments, were developed empirically from the plots of the exact analysis.

If  $0 \leq P \leq P_b$ :

$$\begin{aligned} \phi_{pc} &= \frac{P_b}{P} \phi_b \\ &\times \phi_u \left(1 - 0.6 \frac{P}{P_b}\right) \end{aligned} \quad (3-17)$$

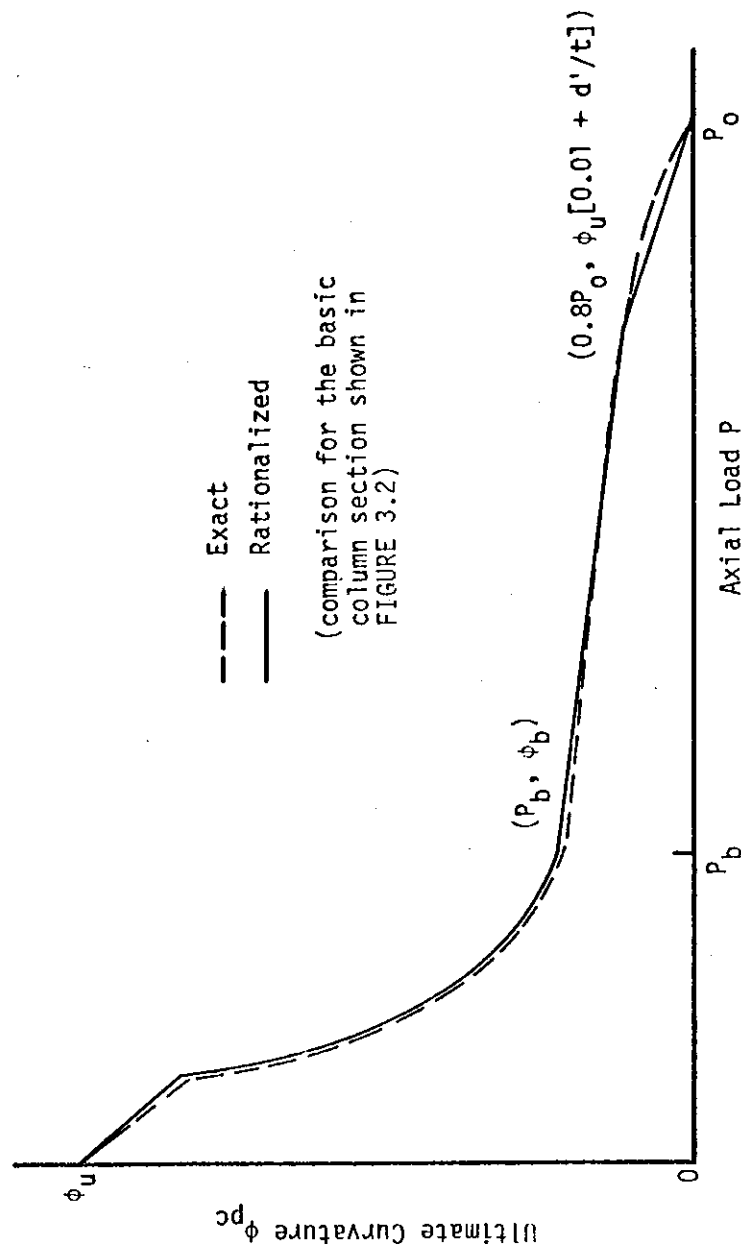


FIGURE 3.6

RELATIONSHIP BETWEEN COLUMN SECTION  
 ULTIMATE CURVATURE AND AXIAL LOAD VALUE

If  $P_b < P < 0.8 P_o$ :

$$\phi_{pc} = \phi_b + \left[ \left( \frac{d'}{t} + 0.01 \right) \phi_u - \phi_b \right] \frac{P - P_b}{0.8 P_o - P} \quad (3-18)$$

If  $0.8 P_o \leq P \leq P_o$ :

$$\phi_{pc} = 5\phi_u \left( \frac{d'}{t} + 0.01 \right) \left( 1 - \frac{P}{P_o} \right) \quad (3-19)$$

(d) Comparison of Rationalized and Exact M-P- $\phi$  Relationships

At this stage, all values necessary to define rationalized elastic-perfectly plastic M- $\phi$  diagrams for any column section subjected to an axial load  $0 \leq P \leq P_o$  have been derived. In the course of the derivations, these rationalized parameters were compared with values provided by the exact analysis and were found to yield good comparisons. To check the overall effect of combined errors in values, the rationalized M-P- $\phi$  curves were compared with those generated by the exact analysis for all sections considered in the investigation. A sample comparison for a typical section is provided in APPENDIX B. In conducting the analyses discussed in CHAPTERS V and VI, the accuracy of the method was checked for sections with other properties.

It was found that, within the limitations of an elastic-plastic relationship, the rationalized method described here provides good quantitative representation of section response and adequately accounts for the effects of variation of the several section parameters. As will be noted in the sample plots, the idealization of the response as an elastic-plastic relationship does yield conservative section stiffness values throughout

much of the "elastic" range of behaviour of a section subjected to axial loads. It does, however, provide quite reliable section stiffness values as the "yield point" of the section is approached.

### 3.2.3 Girder Section Response

Unless otherwise stipulated, the girder section considered throughout this thesis is a rectangular section reinforced only in tension as shown in FIGURE 3.7. Other authors<sup>(33)</sup> have succeeded in expressing the girder section response in an elastic-plastic manner as illustrated in FIGURE 3.8. The derivations and related assumptions are provided in the reference.

$$k_y = \sqrt{(pn)^2 + 2pn} - pn \quad (3-20)$$

$$\phi_y = \frac{f_y}{E_s d (1 - k_y)} \quad (3-21)$$

$$k_u = \frac{pf_y}{0.7 f'_c} \quad (3-22)$$

$$\phi_u = \frac{\epsilon_u}{k_u d} \quad (3-23)$$

$$M_{pl} = A_s f_y d (1 - 0.4 k_u) \quad (3-24)$$

An exact analysis, similar to that applied to the column section was prepared for the girder section. The results were compared to the rationalized  $M-\phi$  curves over the same range of variation of  $f'_c$ ,  $f_y$  and  $\frac{d'}{t}$  of the section, with reinforcement ratios varied from  $0.25p_b$  to  $p_b$  as de-

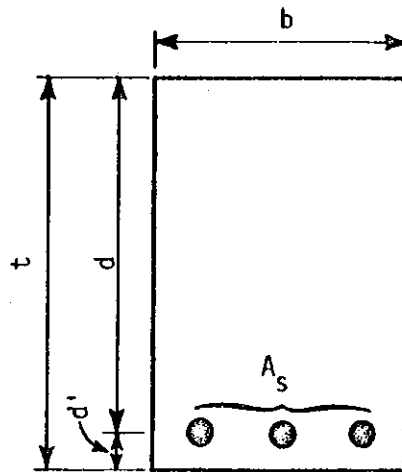


FIGURE 3.7  
GIRDER CROSS-SECTION

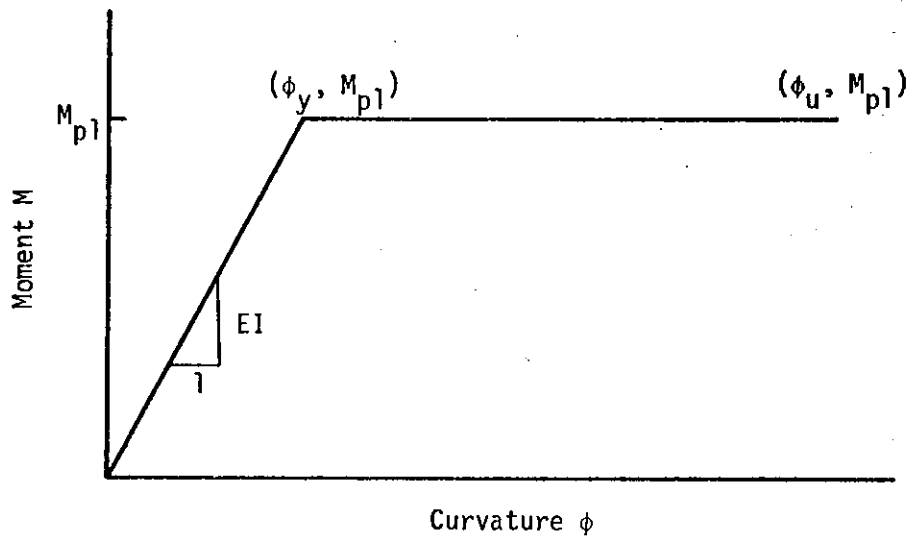


FIGURE 3.8  
IDEALIZED GIRDER SECTION  
MOMENT-CURVATURE RELATIONSHIP

defined in the ACI Building Code. A sample comparison is presented in APPENDIX B. Inspection of this comparison indicates that the rationalized  $M-\phi$  relationship, while yielding slightly unconservative girder stiffness values, provides good quantitative representation of the effects of variation of section properties.

### 3.3 Member Properties

With the section response characteristics defined, it is possible to establish the deflection response of the entire member to the application of external forces. In this analysis, member behaviour is described by slope-deflection equations. This method, frequently used for first order elastic analysis, has been extended by the incorporation of stability functions<sup>(5)</sup> to consider the non-linear behaviour of a member under variable axial load. To consider elastic-plastic section behaviour, Parikh<sup>(14)</sup> has modified the equations for elastic members to apply to members in different states of plastic hinge formation. Before proceeding with the presentation of these slope-deflection equations, the concept and implications of a plastic hinge and stability functions will be discussed.

#### 3.3.1 Plastic Hinge

The formation of "point" plastic hinges in members is the only possibility consistent with the assumption of elastic-perfectly plastic section behaviour. The neglect of gradual yielding of the section leads to plastic hinges of zero width at points of maximum moment. All inelastic rotation takes place at the hinge, the remainder of the member continuing to behave elastically.



In this analysis, the unloading branch of the moment-curvature relationship is not considered. Consequently, it must be assumed that a plastic hinge, once formed, is maintained, and further, that it remains stationary at the point where it first formed during the loading cycle.

### 3.3.2 Stability Functions

In the analysis of an elastic beam-column, the effective stiffness of the member is found to be a function of the axial force. Softening and stiffening of the member result from axial compressive and tensile forces respectively. To include these effects in the analysis, stability functions  $S$  and  $C$  are used in the slope-deflection equations for columns.

The basic slope-deflection equation for a beam-column, subjected to end forces only, can be written as:

$$M_A = \frac{EI}{h} [C\theta_A + S\theta_B - (C + S)\rho] \quad (3-25)$$

For zero axial force,  $C$  and  $S$  have values of 4.0 and 2.0 respectively, and EQUATION (3-25) reverts to the traditional slope-deflection equation. For other values of compressive axial load,  $S$  and  $C$  assume the values given by EQUATIONS (3-26) and (3-27).

$$S = kh \left( \frac{kh - \sin kh}{2 - 2 \cos kh - kh \sin kh} \right) \quad (3-26)$$

$$C = kh \left( \frac{\sin kh - kh \cos kh}{2 - 2 \cos kh - kh \sin kh} \right) \quad (3-27)$$

where  $kh = \sqrt{\frac{P}{EI}} h$

The possible stiffening effect of tensile forces in columns is neglected in the analysis as is the effect of axial loads in the girders.

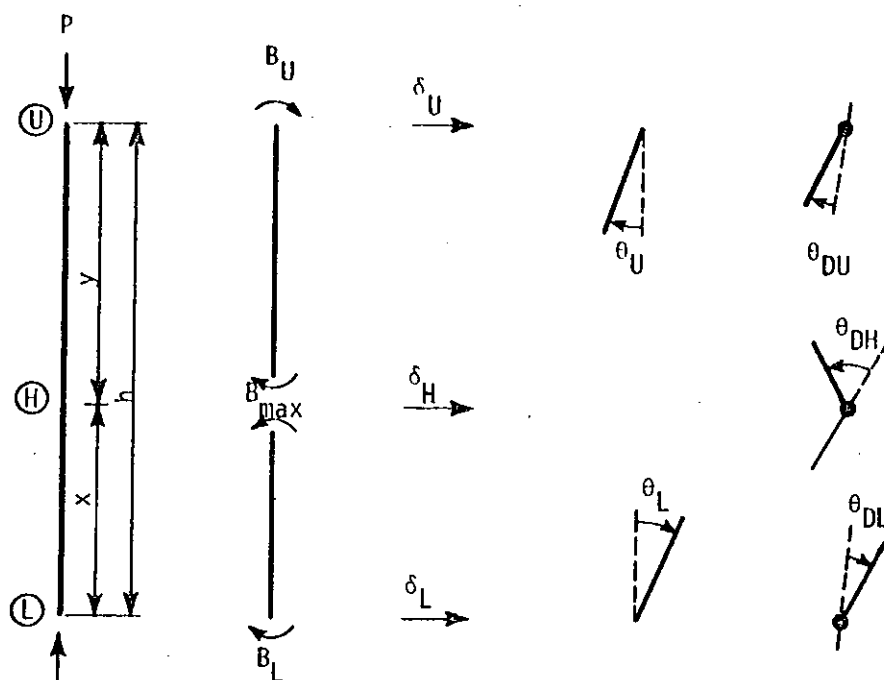
### 3.3.3 Assumptions of Member Analysis

The following assumptions were made in the analysis of members.

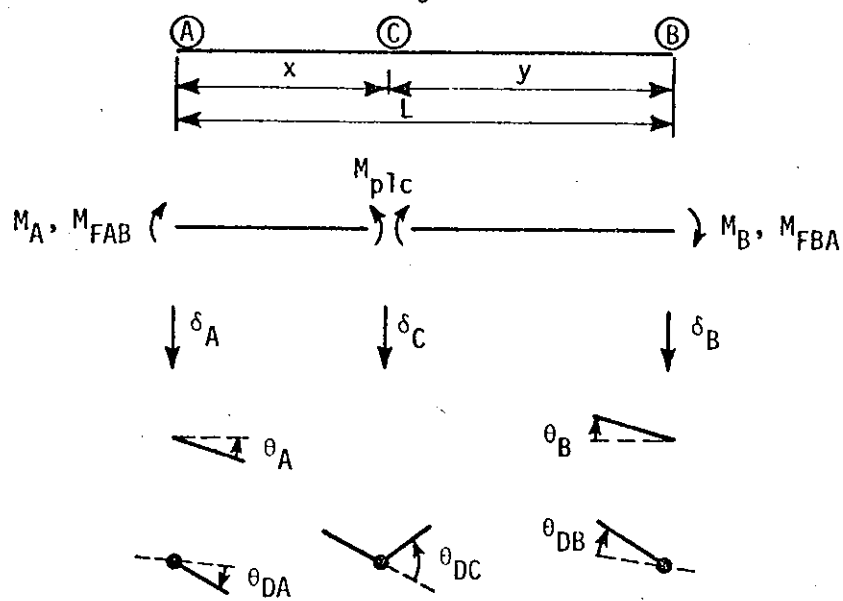
1. "Small deflection theory" is applicable to the elastic portion of a member. This is a necessary condition for the validity of the slope-deflection equations and implies that the effects of curvature shortening are neglected.
2. All members are initially straight and exhibit a constant flexural stiffness,  $EI$ , throughout their length, except at points where plastic hinges have formed.
3. Members are subjected to uniaxial flexure and out-of-plane instability is prevented.
4. The possibility of shear or diagonal tension failure is neglected.
5. Member sections exhibit elastic-plastic  $M-\phi$  response. Thus, "point plastic hinges" may form at points of maximum moment in a member. Once formed, the hinges remain stationary and are maintained, with no hinge reversals.
6. Shearing deformations are neglected.

### 3.3.4 Sign Conventions

The sign conventions adopted in formulating the slope-deflection equations for columns and girders are shown in FIGURES 3.9(a) and 3.9(b)



(a) Column Sign Conventions



(b) Girder Sign Conventions

FIGURE 3.9  
SIGN CONVENTIONS FOR MEMBER ANALYSIS

respectively. All directions indicated are in the positive sense.

### 3.3.5 Slope-Deflection Equations for Columns

An individual column in a structure, in maintaining deformational compatibility with the rest of the structure, behaves as a beam-column subjected to end moments. A typical column in its initial and deflected state is shown in FIGURE 3.10. Initially the entire member responds elastically, and the slope-deflection equations modified for axial load can be applied.

$$B_U = \frac{EI}{h} [C\theta_U + S\theta_L - (C + S) \frac{\delta_U - \delta_L}{h}] \quad (3-28)$$

$$B_L = \frac{EI}{h} [C\theta_L + S\theta_U - (C + S) \frac{\delta_U - \delta_L}{h}] \quad (3-29)$$

As the load on the structure increases, the bending moment magnitude at any point in the column may reach  $M_{pc}$ , and a plastic hinge will form. The possible column hinging configurations considered in this analysis are shown in FIGURE 3.11, in conjunction with the sequences of hinge formation considered possible. It should be noted that, because of the symmetry of the column reinforcement, plastic hinges may open in either direction.

Three possibilities of first hinge formation must be considered. Usually in a laterally loaded structure, the maximum moment in an elastic column (case 1) occurs at either the top or bottom of the column. This can lead to either a case 2 or case 3 hinge configuration. However, in certain cases, it is possible that the maximum moment value occurs between the ends

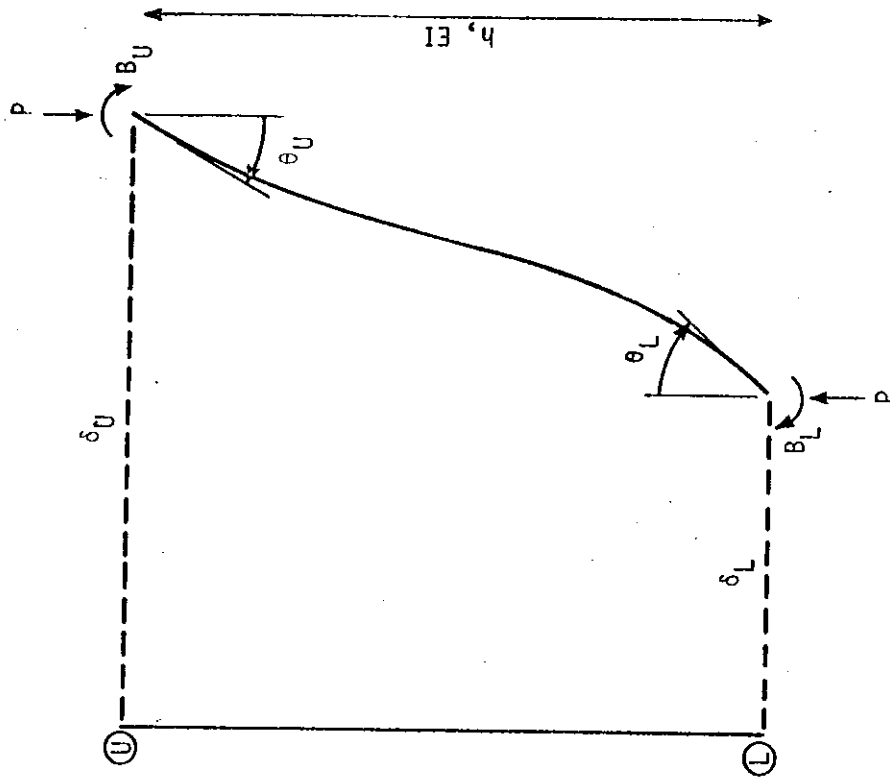


FIGURE 3.10  
TYPICAL DEFLECTED COLUMN CONFIGURATION

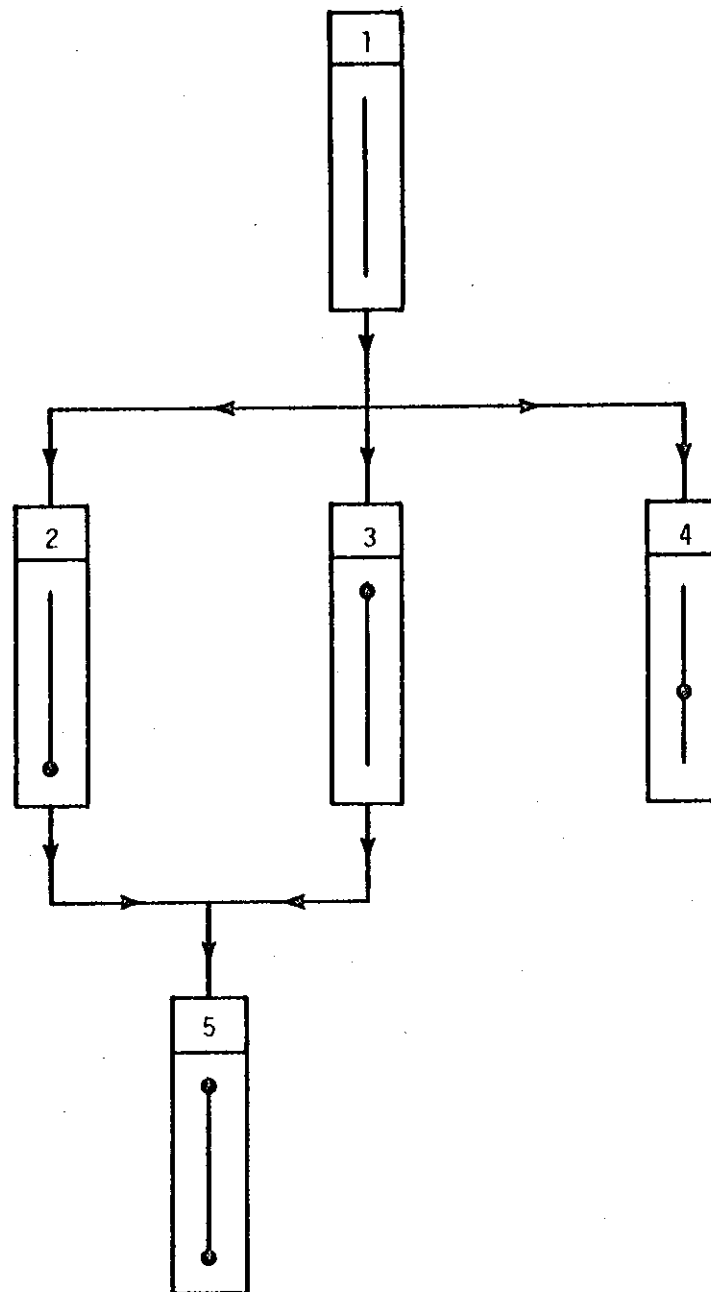


FIGURE 3.11  
SEQUENCE OF HINGE FORMATION IN  
COLUMNS

of the column. The possibility of this occurrence is dependent upon the level of the axial load, the slenderness ratio, and the end moment magnitudes and directions. The best example, of course, is in a column bent in single curvature when the secondary effects of axial force amplify the interior column moment value. EQUATION (3-30) can be used to determine the position of the point of maximum moment.

$$kx = \tan^{-1} \left[ - \frac{B_U + B_L \cos kh}{B_L \sin kh} \right] \quad (3-30)$$

where  $k = \sqrt{\frac{P}{EI}}$

If  $0 < kx < kh$ , the point of maximum moment is between L and U. If not, it is at a fictitious point outside the length of the column. Assuming that the condition is satisfied, the value of the maximum moment is computed as:

$$M_{\max} = \frac{\sqrt{B_L^2 + B_U^2 + 2 B_U B_L \cos kh}}{\sin kh} \quad (3-31)$$

If  $|M_{\max}| > M_{p1}$ , the column moves from a case 1 to a case 4 hinge configuration. The derivations for EQUATIONS (3-30) and (3-31) appear in APPENDIX C.

Assuming that the column was initially straight, it is difficult to visualize a case where an end hinge could form after the case 4 hinging configuration is reached. Consequently, the case 4 hinging configuration is considered a final condition for a column. However, a check is incorporated in the computer programme to detect any violation of this assumption.

If an end hinge condition is detected in a case 4 column, the occurrence is noted in computer output, but the column continues to be treated as a case 4 column in the analysis.

Similarly, the possibility seems remote that an interior hinge could form after the development of an initial end hinge. Consequently cases 2 and 3 may progress to a case 5 hinging configuration, at which point all member stiffness is exhausted.

It is possible to alter the slope-deflection equations for the elastic column, EQUATIONS (3-28) and (3-29), to formulate slope-deflection equations of the form of EQUATIONS (3-32) and (3-33) for each column hinging configuration considered.

$$B_U = C_{1U}\theta_U + C_{2U}\theta_L + C_{3U}\frac{\delta_U - \delta_L}{h} + C_{4U} \quad (3-32)$$

$$B_L = C_{1L}\theta_U + C_{2L}\theta_L + C_{3L}\frac{\delta_U - \delta_L}{h} + C_{4L} \quad (3-33)$$

Coefficients for these equations are presented in TABLES 3.2 and 3.3. The equations were originally derived by Parikh<sup>(14)</sup>.

It should be noted that the resisting moment at a column plastic hinge,  $M_{pc}$ , is a function of  $P$ , and consequently is not likely to be a constant value. As is shown in FIGURE 3.4, should the  $P$  value increase, but still remain below  $P_b$ , the resisting moment at a hinge will actually increase. If a column hinge has formed, it is assumed to remain active with the value of  $M_{pc}$  corresponding to the current axial load.



Hinging Case	$C_{1U}$	$C_{2U}$	$C_{3U}$	$C_{4U}$
1	$\frac{CEI}{h}$	$\frac{SEI}{h}$	$-(C+S)\frac{EI}{h^2}$	0
2	$\frac{C^2 - S^2}{C} \frac{EI}{h}$	0	$-(\frac{C^2 - S^2}{C}) \frac{EI}{h^2}$	$\pm \frac{S}{C} M_{pc}$
3	0	0	0	$\pm M_{pc}$
4	$-\frac{PY}{F}$ <div style="border: 1px solid black; padding: 5px; margin-top: 5px;"> <math display="block">D = \frac{Y}{h} - \frac{PX^2}{EI} \frac{C_x}{C_x^2 - S_x^2}</math> <math display="block">F = -\frac{P}{EI} \left[ \frac{X^3}{hD} \frac{C_x}{C_x^2 - S_x^2} + Y^2 \frac{C_y}{C_y^2 - S_y^2} \right]</math> </div>	$-\frac{PXY}{hFD}$	$\frac{PY}{hF} (1 + \frac{X}{hD})$	$\pm \frac{P}{EIF} (-Y^2 \frac{S_y}{C_y^2 - S_y^2})$ $+ \frac{X^2}{D} \frac{C_x}{C_x^2 - S_x^2}$ $+ \frac{X^2 Y}{hD} \frac{S_x}{C_x^2 - S_x^2}$
5	0	0	0	$\pm M_{pc}$

TABLE 3.2  
COEFFICIENTS FOR EQUATION (3-32)

Hinging Case	$C_{1L}$	$C_{2L}$	$C_{3L}$	$C_{4L}$
1	$\frac{SEI}{h}$	$\frac{CEI}{h}$	$-(C+S)\frac{EI}{h^2}$	0
2	0	0	0	$\pm M_{pc}$
3	0	$\frac{C^2 - S^2}{C} \frac{EI}{h}$	$-(\frac{C^2 - S^2}{C}) \frac{EI}{h^2}$	$\pm \frac{S}{C} M_{pc}$
4	$-\frac{Pxy}{hAB}$	$-\frac{Px}{A}$	$\frac{Px}{hA} (1 + \frac{y}{hB})$	$\pm \frac{P}{EIA} (x^2 \frac{S_x}{C_x^2 - S_x^2} - \frac{y^2}{B} \frac{C_y}{C_y^2 - S_y^2} - \frac{xy^2}{hB} \frac{S_y}{C_y^2 - S_y^2})$
5	0	0	0	$\pm M_{pc}$

TABLE 3.3

COEFFICIENTS FOR EQUATION (3-33)

### 3.3.6 Slope-Deflection Equations for Girders

The girder configuration considered in this analysis is shown in FIGURE 3.12. The girder, spanning between points A and B on the face of shear walls with finite widths  $WW_L$  and  $WW_R$  respectively, supports a uniformly distributed load  $w$  which represents the girder self-weight and superimposed dead and live load. When a column is considered in place of a shear wall, the finite width reverts to zero and centre-line dimensions are employed.

In the analysis of girder behaviour, finite shear wall width has two effects. In the first instance, the wall width reduces the effective span,  $L$ , of the girder. Moreover, rotation of joints A' and B' causes a vertical translation of points A and B respectively, either increasing or decreasing the effective differential column axial shortening deformation to which the girder is subjected.

The inhomogeneous nature of a reinforced concrete girder complicates the analysis of its behaviour. A steel girder is usually of uniform section throughout its span, providing constant values of  $M_{pl}$  and  $EI$ , regardless of the sense of the moment. It is also realistic to assume that a symmetrically reinforced column is a homogeneous member throughout a storey height. In proportioning a reinforced concrete girder, however, the designer will normally provide different reinforcement areas at various points along the length of the girder. This design procedure produces a member in which both  $EI$  and  $M_{pl}$  vary. To consider this possibility in the analysis of a real structure, provision is made to adjust the plastic moment capacities as shown in FIGURE 3.13. The girder section at an interior support is used for the derivation of  $M_{pl}$  and  $EI$  values for the member. By

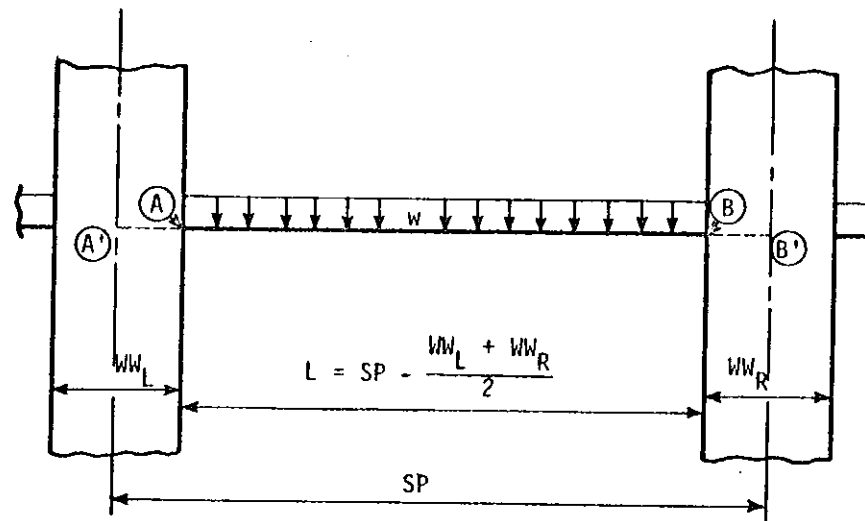
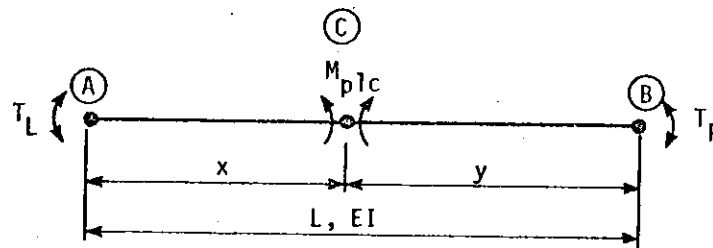


FIGURE 3.12  
TYPICAL GIRDER CONFIGURATION



$$M_{p1c} = TPRATMx M_{p1}$$

At Interior Support:

$$T_L = M_{p1}$$

$$T_R = M_{p1}$$

At Exterior Support:

$$T_L = TPRATE \times M_{p1}$$

$$T_R = TPRATE \times M_{p1}$$

FIGURE 3.13  
ADJUSTMENT OF GIRDER PLASTIC MOMENT CAPACITIES

reading in values of TPRATE and TPRATM, each girder can be assigned adjusted plastic moment capacities at exterior supports and interior points. No alteration in the girder EI value is considered, however. This leads to unconservative results if the interior support is stiffer.

Moreover, since the girder is assumed to be reinforced on one side only, it is possible that cases will arise where the end moments are in a direction opposite to that of the reinforcement resistance. In the computer programme, violations of this sort can be detected and recorded. In this case, the analysis of the structure continues, neglecting the incompatibility and assuming that the girder possesses equal moment capacities in both directions.

As the loads on a structure increase, a girder may develop plastic hinges in much the same manner as a column. Again, it is possible that hinges can form at three different locations. However, because of the different nature of the external loading, plastic hinges can occur at both an end point and an interior point. Consequently, it is necessary to consider the seven possible girder hinge configurations shown in FIGURE 3.14.

To detect a possible interior hinge, EQUATIONS (3-34) and (3-35) can be employed.

$$x = \frac{L}{2} - \frac{M_A + M_B}{wL} \quad (3-34)$$

If  $0 < x < L$ :

$$M_{\max} = M_A + \frac{wL^2}{8} - \frac{M_A + M_B}{2} + \frac{(M_A + M_B)^2}{2wL^2} \quad (3-35)$$

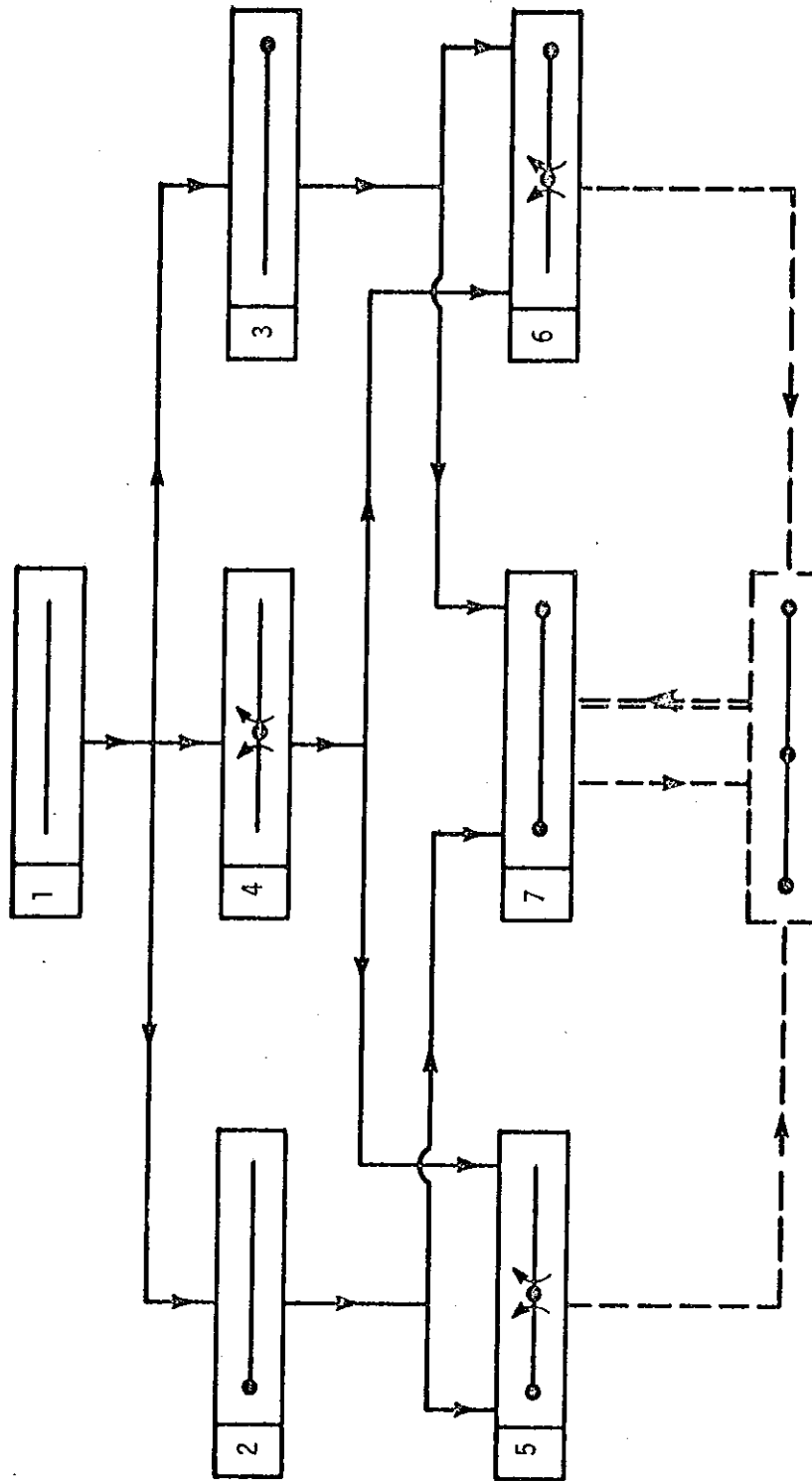


FIGURE 3.14  
SEQUENCE OF HINGE FORMATION IN GIRDERS

Only positive moment hinges are considered in the interior portion of a girder.

For each combination of girder plastic hinges, the slope-deflection equations originally derived by Parikh have been extended to incorporate finite wall width effects. The equations have also been generalized to consider the variable plastic moment capacity of a reinforced concrete girder. The general form of these equations is as follows:

$$M_A = C_{1A} \theta_A + C_{2A} \theta_B + C_{3A} \delta_B' + C_{4A} \delta_A' + C_{5A} \quad (3-36)$$

$$M_B = C_{1B} \theta_A + C_{2B} \theta_B + C_{3B} \delta_B' + C_{4B} \delta_A' + C_{5B} \quad (3-37)$$

The coefficient values for these equations are presented in TABLES 3.4 and 3.5, and the derivations appear in APPENDIX C.

In the formulation of simple plastic theory methods, the formation of three hinges in any girder produces a beam mechanism which is considered to constitute a failure mechanism for the entire structure. While it is true that a girder hinged in this manner can not support additional gravity loading by flexure, the remainder of the system may still be stiff enough to resist additional load. In this analysis, the formation of a beam mechanism will not be considered to represent the attainment of the maximum load for the entire structure. It will be treated simply as a localized failure. Conditions of serviceability will be overlooked. Should a beam mechanism be detected at any stage of loading, the occurrence will be recorded. And, as shown by the dotted line portion of FIGURE 3.14, the system can continue to be analyzed by reverting from a beam

Hinging Case	C <sub>1A</sub>	C <sub>2A</sub>	C <sub>3A</sub>	C <sub>4A</sub>	C <sub>5A</sub>
1	$(4 + \frac{3wL}{L}) \frac{EI}{L}$	$(2 + \frac{3wL}{L}) \frac{EI}{L}$	$-\frac{6EI}{L^2}$	$+\frac{6EI}{L^2}$	$+ M_{FAB}$
2	0	0	0	0	$\pm T_L$
3	$\frac{3EI}{L} (1 + \frac{wL}{2L})$	$\frac{3EI}{2L^2} wL$	$-\frac{3EI}{L^2}$	$+\frac{3EI}{L^2}$	$\pm \frac{T_R}{2} - \frac{M_{FBA}}{2} + M_{FAB}$
4	$\frac{3EI}{x} [(1 + \frac{wL}{2x})$ $(1 - \frac{f_{xy}}{x})]$	$\frac{3EI}{y} [\frac{f_{xy}}{y}$ $(1 + \frac{wL}{2y})]$	$-\frac{3EI}{y^2} \frac{f_{xy}}{y}$	$+\frac{3EI}{x^2} (1 - \frac{f_{xy}}{x})$	$+ (1 - \frac{f_{xy}}{x}) (M_{FAC} - \frac{M_{FCA}}{2})$ $+ \frac{f_{xy}}{y} (M_{FBC} - \frac{M_{FCB}}{2})$ $- \frac{M_{p1c}}{2} [1 - 3 f_{xy} (\frac{1}{x} + \frac{1}{y})]$ $- \frac{f_{xy} wL}{2}$
5	0	0	0	0	$\pm T_L$
6	0	0	0	0	$\pm T_R \frac{x}{y} + M_{p1c} \frac{L}{y} - \frac{wL}{2}$
7	0	0	0	0	$\pm T_L$

TABLE 3.4

COEFFICIENTS FOR EQUATION (3-36)



Hinging Case	$C_{1B}$	$C_{2B}$	$C_{3B}$	$C_{4B}$	$C_{5B}$
1	$(2 + \frac{3W}{L}) \frac{EI}{L}$	$(4 + \frac{3W}{L}) \frac{EI}{L}$	$-\frac{6EI}{L^2}$	$+\frac{6EI}{L^2}$	$+ M_{FBA}$
2	$\frac{3EI}{2L^2} \frac{W}{L}$	$\frac{3EI}{L} (1 + \frac{W}{2L})$	$-\frac{3EI}{L^2}$	$+\frac{3EI}{L^2}$	$\pm \frac{T_L}{2} - \frac{M_{FAB}}{2} + M_{FBA}$
3	0	0	0	0	$\pm T_R$
4	$\frac{3EI}{x} \frac{f_{yx}}{x}$ $(1 + \frac{W}{2x})$ $f_{yx} = \frac{1}{y^2} (\frac{1}{3} + \frac{1}{y})$	$\frac{3EI}{y} [(1 + \frac{W}{2y}) (1 - \frac{f_{yx}}{y})]$	$-\frac{3EI}{y^2} (1 - \frac{f_{yx}}{y})$	$+\frac{3EI}{x^2} \frac{f_{yx}}{x}$	$+ (1 - \frac{f_{yx}}{y}) (M_{FBC} - \frac{M_{FCB}}{2})$ $+ \frac{f_{yx}}{x} (M_{FAC} - \frac{M_{FCA}}{2})$ $+ \frac{M_{plc}}{2} [1 - 3 f_{yx} (\frac{1}{x} + \frac{1}{y})]$ $+ \frac{f_{yx} W}{2}$
5	0	0	0	0	$\pm T_L \frac{y}{x} - M_{plc} \frac{L}{x} + \frac{wyL}{2}$
6	0	0	0	0	$\pm T_R$
7	0	0	0	0	$\pm T_R$

TABLE 3.5  
COEFFICIENTS FOR EQUATION (3-37)

mechanism configuration to a case 7 hinging configuration with appropriate end hinge moment values. These resisting moments and the accompanying end reaction values represent the effect of the deteriorated girder on the rest of the structure.

### 3.3.7 Properties of a Shear Wall

Throughout this thesis, the shear wall section is assumed to be that of a solid symmetrically reinforced tied column. In this case, the wall can be considered to behave exactly like a column with finite width. Shear deformations of the wall are neglected.

While the assumption of a solid wall section may not be considered consistent with the variety of wall section shapes possible, the analysis can easily be adapted to consider any shear wall section if the section response can be expressed by an elastic-perfectly plastic  $M-\phi$  relationship.

### 3.3.8 Axial Shortening of Columns

In a multi-storey frame, relative axial column shortening may induce significant bending moments, particularly in the upper floors where the cumulative effect is imposed. The effects of these deformations are discussed in CHAPTER VII.

The axial shortening of any column under axial load  $P$  is computed using EQUATION (3-38), which is based on the composite action of elastic reinforcement and concrete behaving according to Hognestad's stress-strain relationship.

$$\Delta h = \left( \frac{-y - \sqrt{y^2 - 4xz}}{2x} \right) h \quad (3-38)$$

where

$$x = \frac{0.85 f'_c (bt - 2A_s)}{\epsilon_o^2}$$

$$y = \frac{1.7 f'_c (2A_s - bt)}{\epsilon_o} - 2A_s E_s$$

$$z = P$$

To be consistent with the assumption of small deflection theory, curvature shortening has been neglected. Korn<sup>(15)</sup> has already shown that its effects are minimal.

### 3.3.9 Hinge Rotation Capacity

Compared to mild steel, reinforced concrete is a material of limited ductility. Proponents of limit design of reinforced concrete structures have noted this problem. One limitation of limit design methods is that at any hinge location each member must possess sufficient rotation capacity to permit the redistribution of bending moments necessary for the formation of a collapse mechanism.

Experimental studies<sup>(34,35)</sup> indicate that a conservative value of girder rotation capacity is obtained by considering that the inelastic hinging region extends for a distance  $0.5d$  on either side of the idealized "point" plastic hinge. It will be assumed that the same is true in columns. Hence, for a girder, the permissible hinge rotation  $\theta_{Dall} = 0.5 \phi_u d$  and for a column,  $\theta_{Dall} = 0.5 \phi_{pc} d$  for an end hinge. The values are doubled at interior hinges. Actually, the laboratory tests indicated that  $\theta_{Dall} = 0.5 (\phi_u - \phi_y) d$ , but a less restrictive estimate was used in this study.

By manipulation of the member slope-deflection equations presented

earlier, it is possible to compute the finite inelastic rotation developed at any plastic hinge. Formulas for these are presented in APPENDIX C. In the analysis, any occurrences of excessive hinge rotation are recorded. Such a violation is not considered to constitute failure of the structure, and the analysis is continued assuming that the resisting moment at the hinge remains unchanged.

### 3.4 Summary

Methods have been presented to describe the behaviour of reinforced concrete members throughout the entire range of loading of a structure. The major assumptions made are those related to the idealized elastic-plastic section behaviour.

The elastic-plastic section response characteristics defined in this chapter are used throughout the thesis. However, they can be altered for any future elastic-plastic analysis and need not limit the applicability of the method of analysis.

## CHAPTER IV

### ANALYSIS OF FRAMEWORK

#### 4.1 Introduction

In the previous chapter, methods were presented to define the behaviour of individual girders, columns and shear walls with given loading and end constraints. In a framework, the end constraints provided for any member are functions of the stiffness of the rest of the structure, and an individual frame member cannot be analyzed separately.

This chapter will deal with the formulation of a solution for a plane framework consisting of an assemblage of girders, columns and shear walls. A computer programme is developed to trace the second order elastic-plastic response history for the framework as loading progresses to failure. The limitations and possible errors of the analysis are discussed.

#### 4.2 Model Framework and Loading Configuration

The model framework and loading configuration considered in the formulation of the solution is that shown in FIGURE 4.1. The structure is a rigid-jointed, plane, rectangular multi-storey, multi-bay frame with complete base fixity. The size of the frame which can be considered is limited only by computer capacity. The structure must be a regular frame with no missing members and no staggered spacing of members.

The model may be either an unbraced frame with no shear walls or a braced structure with shear walls in any or all of the column lines.

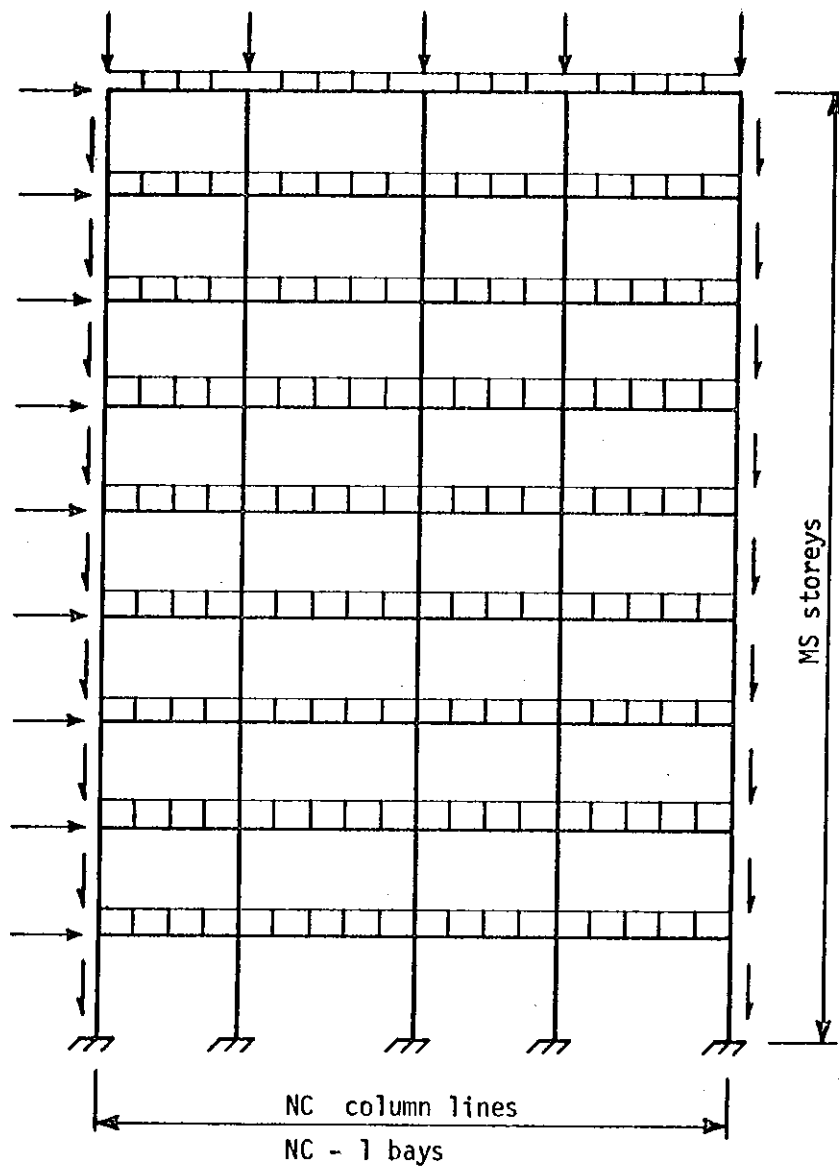


FIGURE 4.1  
MODEL FRAMEWORK AND LOADING  
CONFIGURATION

When a shear wall is present, it must be treated as such throughout the entire height of the structure, although its stiffness and width may approach that of a column.

The joints are assumed to be completely rigid at the points of intersection of the centre-lines of the members. The effect of the overlapping of columns and girders in this region is neglected, and computations are based on centre-line dimensions except where finite shear wall widths are considered. Thus, all hinges at the ends of members form in a joint or at the face of a shear wall. This assumption results in conservative estimates of framework strength and stiffness.

Member properties may vary from bay to bay and storey to storey, subject only to the limitations in cross-section discussed in CHAPTER III. Similarly, bay widths and storey heights may vary in any desired manner.

Only static loads have been considered and all loads are assumed to act only in the plane of the frame. The gravity loading cases which can be considered are:

1. uniformly distributed loads on girders representing dead load, live load and member self-weight,
2. exterior loads at the top of all column stacks,
3. exterior wall weights acting on the exterior column lines.

As is normal practice, lateral loads are assumed to act only at windward joints.

To systematize the solution for computer adaptation, a co-ordinate system was used for numbering individual joints and members in the framework. For a typical joint (M,N), M refers to the floor number and N the column line working from the top left corner joint as (1,1) for reference. The

nomenclature for the members framing into a typical interior joint (M,N) is shown in FIGURE 4.2.

#### 4.3 Formulation of the Solution

To obtain a solution for a stable structure subjected to static loads, three fundamental conditions must be satisfied simultaneously.

1. Geometrical compatibility must be maintained. Stated simply, this means that no matter how the structure deforms the component members must fit together and continue to satisfy any boundary conditions.
2. Statical equilibrium must be maintained. The external applied forces must be balanced by internal reactive forces in the structure. This applies equally for the entire structure, any combination of members, any member or any portion of any member.
3. The relationship between force and displacement must be satisfied. In this particular case, since deformation is assumed to occur only as a result of bending and axial shortening, if the curvature of each portion of the structure satisfies the appropriate  $M-P-\phi$  relationship and the relationship between column axial load and axial shortening is satisfied, material behaviour is adequately considered.

The third condition has already been satisfied in the derivation of the slope-deflection equations and the relationship for axial shortening of the columns.

To simultaneously satisfy the other conditions in an indeterminate structure, two different approaches could be adopted. The force or flexibility methods initially satisfy the equilibrium condition and solve for



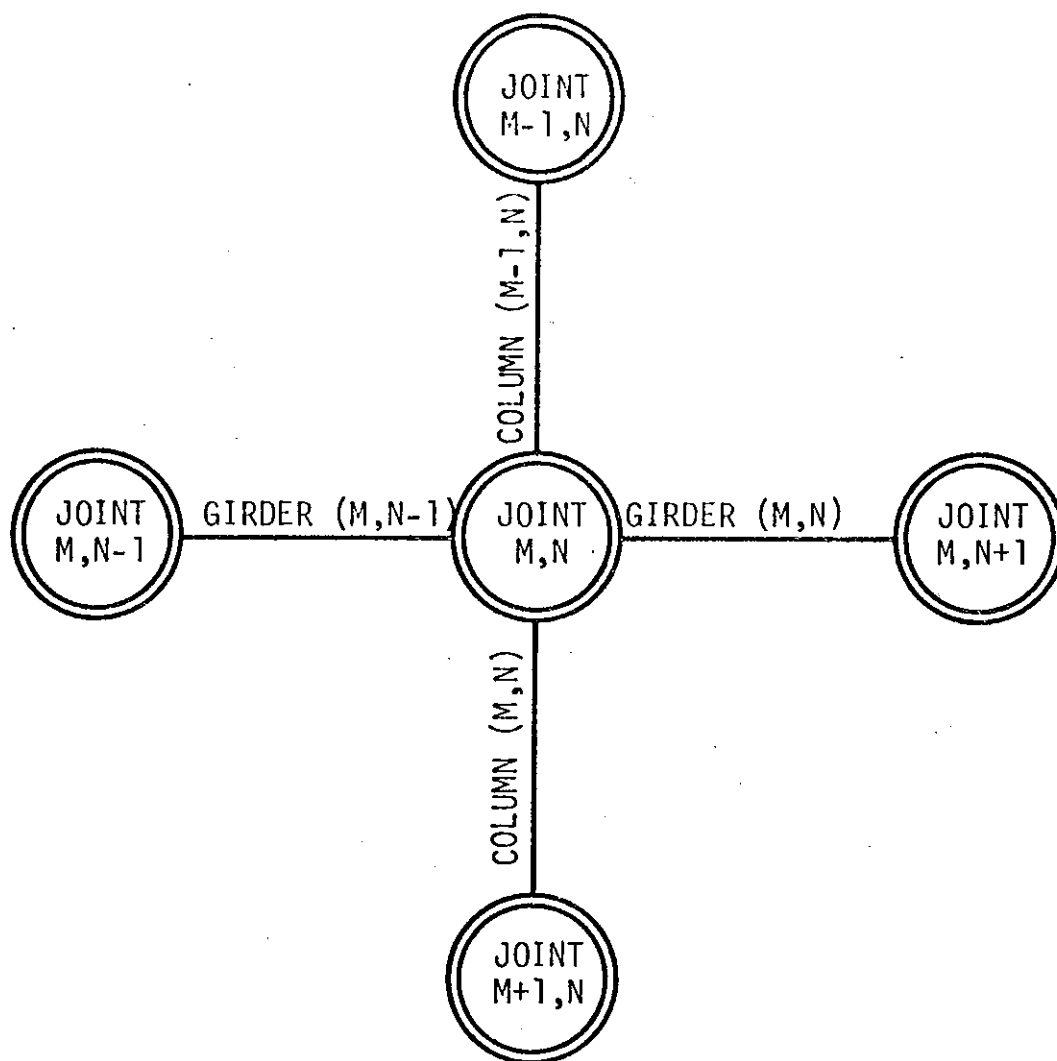


FIGURE 4.2

NOMENCLATURE FOR A TYPICAL JOINT

redundant forces as the unknowns by satisfying the compatibility condition. In contrast, the displacement or stiffness methods are formulated by initially satisfying compatibility conditions and solving for displacements as the unknowns necessary to satisfy equilibrium.

The slope-deflection equation formulation of the problem is suited for a displacement method of analysis. To satisfy the compatibility condition, it is necessary only to assume that the joint displacements, rotation and translations, are the same for all members framing into a particular joint. The boundary conditions at the base of the frame must be satisfied. The problem then reduces to one of satisfying statical equilibrium conditions.

Equilibrium of the overall frame under gravity loads can be achieved if the columns can support these loads and conduct the loads to the foundation. The equilibrium condition for any girder or any portion of any girder can be satisfied if the restraining end moment and end reaction values can be imparted through the joint by the rest of the structure. This amounts essentially to satisfaction of the conditions of joint equilibrium. To satisfy equilibrium of the structure under lateral loads, it is necessary to consider the conditions for storey sway equilibrium.

Thus, the satisfaction of the conditions of joint and storey sway equilibrium constitutes simultaneous fulfilment of all three conditions necessary for a solution.

#### 4.3.1 Joint Equilibrium

FIGURE 4.3 illustrates the forces acting on the ends of all members framing into a typical interior joint (M,N). All forces are shown in the

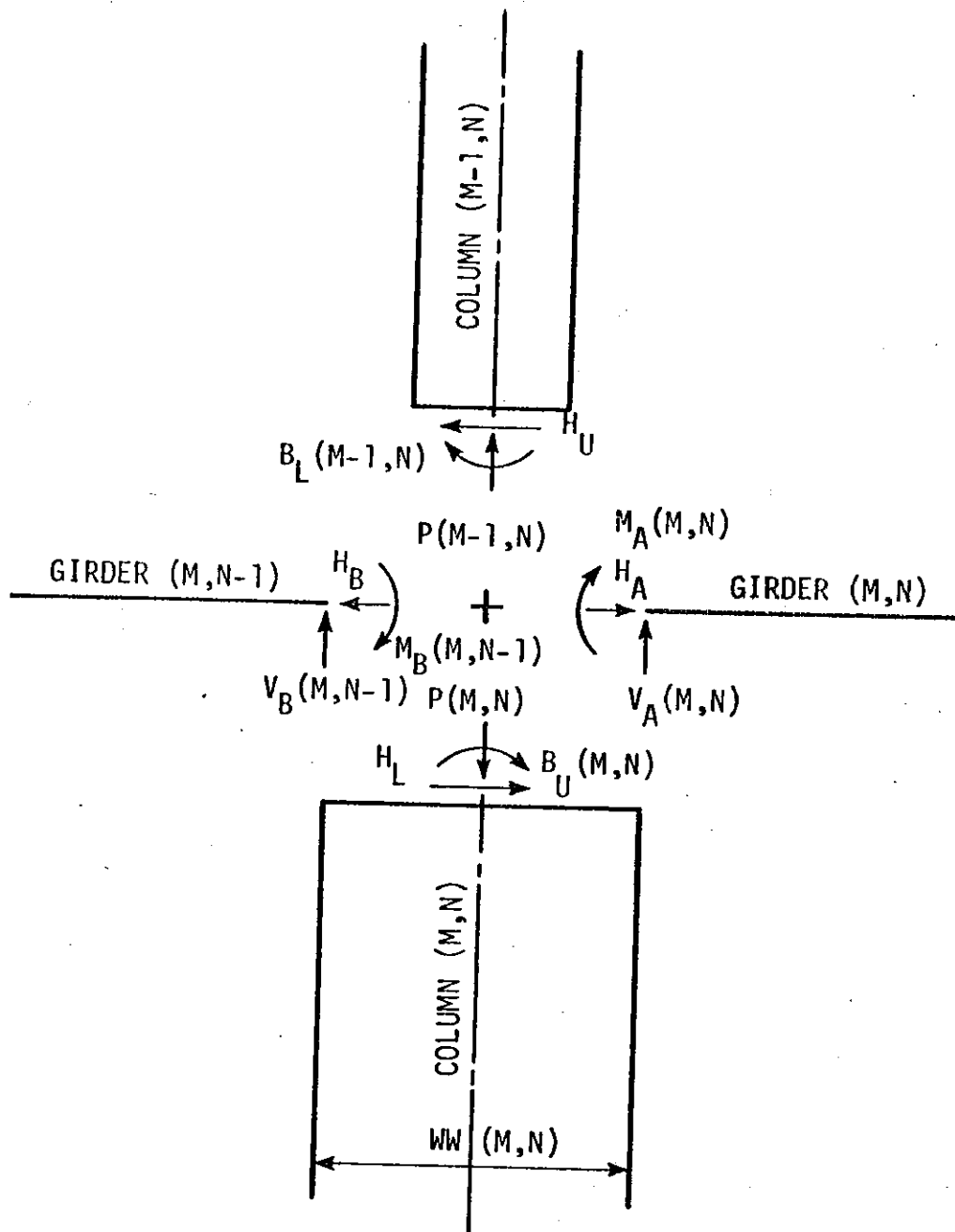


FIGURE 4.3  
FORCES AT A JOINT

positive sense. The constraining forces in the members are opposed by reactions equal in magnitude and opposite in direction acting on the joint, though these are not shown.

To maintain statical rotational equilibrium of the joint:

$$M_A(M,N) + M_B(M,N-1) + B_U(M,N) + B_L(M-1,N) \\ + [V_B(M,N-1) - V_A(M,N)] \frac{WW(M,N)}{2} = 0 \quad (4-1)$$

The last term of the equation results from consideration of the finite shear wall width, with shear transfer at the face of the shear wall providing the required girder end reaction values.

Consideration of equilibrium of the girders provides values of the end reactions.

In girder (M,N):

$$V_A = \frac{wL}{2} - \frac{M_A + M_B}{L} \quad (4-2)$$

In girder (M,N-1):

$$V_B = \frac{wL}{2} + \frac{M_A + M_B}{L} \quad (4-3)$$

Moreover, for translational equilibrium of the joint:

$$H_U + H_B - H_L - H_A = 0 \quad (4-4)$$

$$P(M,N) - P(M-1,N) - V_A(M,N) - V_B(M,N-1) = 0 \quad (4-5)$$

EQUATION (4-4) will be satisfied in the consideration of storey sway equilibrium in the next section. EQUATION (4-5) will be considered in computing the column axial load values.

By combining EQUATIONS (4-1), (4-2) and (4-3) it is possible to express the joint moment equilibrium condition in terms of member end moment values and known girder distributed load values. Substitution of the appropriate slope-deflection equations derived in CHAPTER III for each of these member end moment values and grouping of the coefficients provided in TABLES 3.2, 3.3, 3.4 and 3.5 produces a joint "operator" which can be represented graphically as shown in FIGURE 4.4. Each coefficient in a girder (i.e. GR) can take on seven different values, the choice of the appropriate value being determined by the current hinge configuration in the girder to which it applies. Similarly in columns, five different values of coefficients are provided.

Thus, EQUATION (4-1) can be rewritten as:

$$\begin{aligned} \theta(M,N)[AL + AR + AA + AB] + GL + GR + GA + GB \\ + CC + DD + EE + FF = 0 \end{aligned} \quad (4-6)$$

This equation can be applied at any typical interior joint to satisfy moment equilibrium at the joint with the framing members in any stage of hinging. Naturally, adjustments must be made at exterior joints where

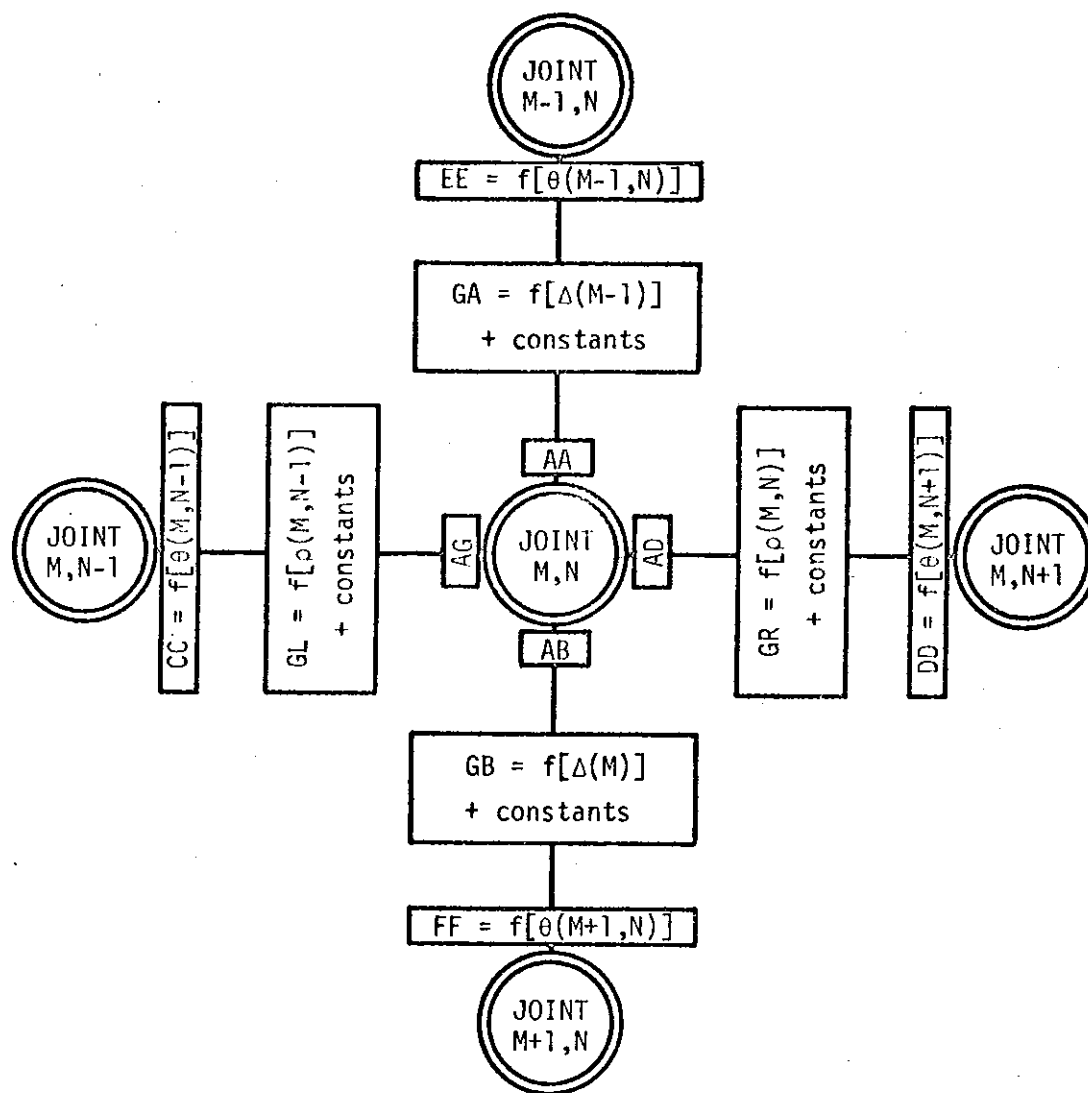


FIGURE 4.4

OPERATOR FOR MOMENT EQUILIBRIUM  
AT A JOINT

members are non-existent. The boundary conditions of base fixity are satisfied by setting FF at zero for all first floor joints.

#### 4.3.2 Storey Sway Equilibrium

As was mentioned previously, to achieve the condition of equilibrium of lateral forces, storey sway equilibrium must be maintained. FIGURE 4.5 shows a free-body diagram of the columns or shear walls in a typical storey in their initial and deflected positions. Since axial shortening of girders is neglected, all columns in a storey are subjected to the same storey sway deflection value  $\Delta$ . The total externally applied lateral force  $\Sigma W$  acting on the storey is the sum of all lateral forces acting above that storey. To maintain equilibrium of the storey, this external lateral force must be balanced by the horizontal reactions developed by the columns, which are provided by the end moments in the columns.

Moreover, it was decided that this analysis was to be a second order analysis. The secondary axial load effects in the columns and shear walls themselves have already been considered by the incorporation of stability functions in the slope-deflection equations. But to satisfy the requirements of a second order solution in the structure, equilibrium must be formulated on the deformed structure. Consequently, the  $P\Delta$  moment must also be balanced by the column end moments developed.

FIGURE 4.6 shows a free-body diagram of a typical column. For equilibrium of this column:

$$Hh = - (B_U + B_L + P\Delta) \quad (4-7)$$

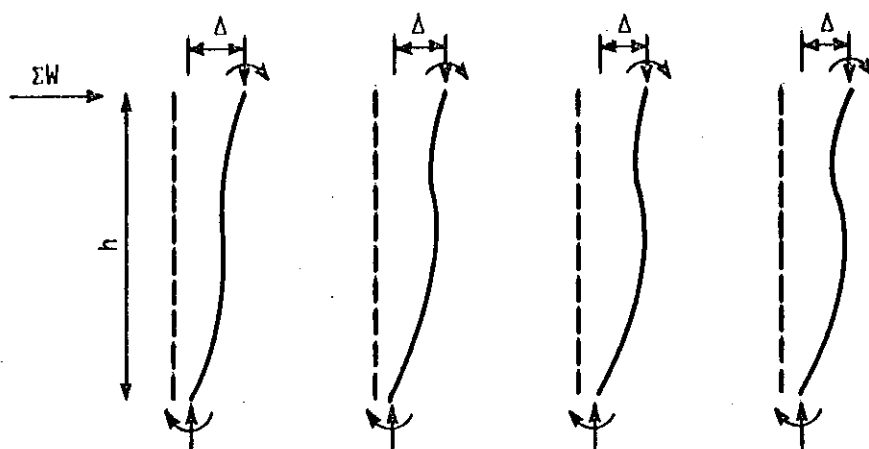


FIGURE 4.5  
FREE-BODY DIAGRAM OF A TYPICAL STOREY

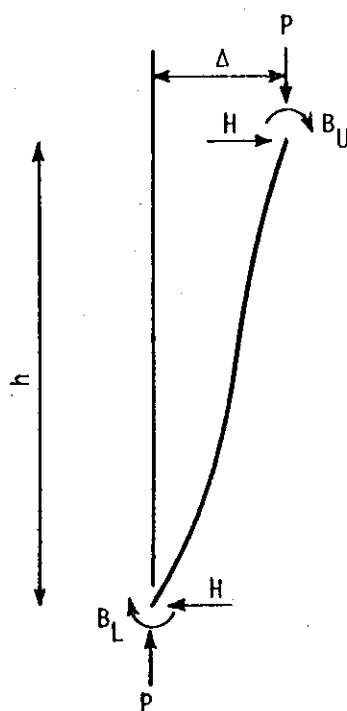


FIGURE 4.6  
FREE-BODY DIAGRAM OF A TYPICAL COLUMN



The relationship  $B_U + B_L + P\Delta$  for a typical column (M,N) can be expressed in "operator" form as shown in FIGURE 4.7. This operator is similar to that derived in the previous section. Using the terms shown in FIGURE 4.7, EQUATION (4-7) can be rewritten as:

$$Hh = - (V + T + U + Z\Delta) \quad (4-8)$$

For equilibrium of the entire storey:

$$\Sigma H = \Sigma W \quad (4-9)$$

Therefore, for an entire storey consisting of NC columns or walls:

$$(\Sigma W)h = - \sum_{N=1}^{N=NC} (V + T + U) - \Delta \sum_{N=1}^{N=NC} Z \quad (4-10)$$

The satisfaction of EQUATION (4-10) for every storey in a structure indicates fulfilment of the condition of statical equilibrium of lateral forces.

#### 4.3.3 Computation of Axial Loads and Vertical Joint Displacements

In EQUATIONS (4-6) and (4-10), derived to satisfy the conditions of joint and storey sway equilibrium respectively, values of column axial loads  $P$ , vertical joint displacements  $\delta'_A$  and  $\delta'_B$ , and stability functions  $C$  and  $S$  appear. The terms  $\delta'_A$ ,  $\delta'_B$ ,  $C$  and  $S$  are all functions of the column axial load values  $P$ , which are, in turn, functions of the deformed shape of the indeterminate structure.

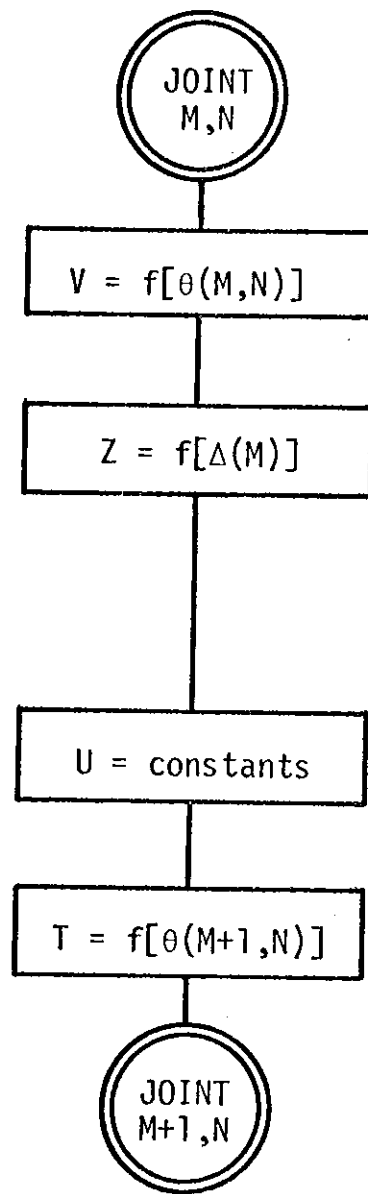


FIGURE 4.7  
OPERATOR FOR  $B_U + B_L + P\Delta$  FOR  
A TYPICAL COLUMN

The object of the displacement method of analysis is to set up a system of simultaneous linear equations which can be solved for the unknown displacements. In EQUATION (4-10), however, the  $P\Delta$  terms is non-linear since  $P = f(\theta, \Delta, \delta, C, S)$ . Thus, to derive a system of linear equations in terms of the unknowns  $\theta$  and  $\Delta$ , it is necessary to perform a separate solution for values of  $P$ ,  $\delta'_A$ ,  $\delta'_B$ ,  $C$  and  $S$ , and treat these values as constants in solving EQUATIONS (4-6) and (4-10).

The column axial load  $P$  is computed using the relationships expressed in EQUATIONS (4-5), (4-2) and (4-3). A recurrence relationship or "operator" similar to those derived in the previous sections can be formulated for this operation.

With  $P$  values known, the vertical joint displacements are computed by using EQUATION (3-38), and are cumulative from the base of any column stack since no foundation settlement is considered.

#### 4.4 Method of Solution

At this stage, a solution for the model framework has been formulated which simultaneously satisfies all three necessary conditions discussed in SECTION 4.3. The solution is expressed in terms of EQUATIONS (4-6) and (4-10). Temporary linearization of these equations, accomplished by the separate computation of column axial load values  $P$  and  $\delta'_A$ ,  $\delta'_B$ ,  $C$  and  $S$ , leaves the values of joint rotations  $\theta$  and the storey sway displacements  $\Delta$  as the unknowns. If all values of  $\theta$  and  $\Delta$  can be computed, the deformed shape of the structure under any stable loading configuration is known. By applying the slope-deflection equations, the bending moment distribution in all members of the framework can be determined.

For each joint in the framework, EQUATION (4-6), depicted graphically by the recurrence relationship in FIGURE 4.4, can be applied. For each storey, EQUATION (4-10) can be applied. This produces a series of simultaneous linear equations, one per unknown, with joint rotations and storey sway displacements as the unknowns.

The question then is how to solve this system of linear equations. Several investigators<sup>(11,13,15,24)</sup> have formulated solutions by setting up a formal stiffness matrix. Others<sup>(14)</sup> have chosen to solve the equations by an iteration procedure. The advantage of the iteration procedure is that no formal matrix need be set up and computer storage space is saved. The disadvantage, of course, is that the iteration procedure yields an approximate solution rather than the exact solution which is provided by matrix operation. The implications of this inaccuracy will be discussed in SECTION 4.8.

The method of solution used in this analysis is the Gauss-Seidel procedure<sup>(36)</sup> of iteration by single steps.

EQUATIONS (4-6) and (4-10) can be rearranged to express joint and storey sway equilibrium conditions explicitly in terms of the unknown displacement values.

$$\theta(M,N) = - \frac{GL + GR + GA + GB + CC + DD + EE + FF}{AL + AR + AA + AB} \quad (4-11)$$

$$\Delta(M) = - \frac{\sum_{N=1}^{N=NC} (V + T + U)] + h(\Sigma W)}{\sum_{N=1}^{N=NC} Z} \quad (4-12)$$

Using these equations, the iteration procedure can be continued until successive values of deformation have converged to the desired degree of accuracy. These deformation values represent the statically admissible and geometrically compatible solution for the response of the structure to the applied loads.

#### 4.4.1 Convergence Criteria

Since this is an iterative method of solution, it is necessary that some criterion be used to define adequate convergence. Moreover, since it is necessary to separate the solutions for column axial loads  $P$  on the one hand, and joint rotations and storey sway deflections on the other, it is necessary for a correct solution that convergence of both  $P$  values and deformations be achieved.

In setting up the iteration procedure for a solution, the convergence check used is that of comparing successive values of the unknowns. Values of ACCURP and ACCURD are chosen to represent the desired degree of accuracy. If at the end of a cycle of iteration, the ratio of successive  $P$  values in all columns fits within the range of  $1 \pm \text{ACCURP}$ , the  $P$  values are assumed to have converged sufficiently close to the exact values. A similar check is employed to signify adequate convergence of the deformation values. When both have converged, the solution is assumed to be correct. The inaccuracies inherent in this convergence check are discussed in SECTION 4.8.

#### 4.5 Incremental Loading Procedure

In the computer programme, the behaviour of the frame is analyzed at various load factors  $\lambda$  as loads increase to the failure load. The loading

is incremental and may be, but need not be, proportional. A load-deflection plot, typifying the response history of the structure as traced by the programme, appears in FIGURE 4.8.

To set up the incremental loading procedure, three different sets of data must be fed into the computer. Working load values, corresponding to the case  $\lambda = \lambda_w = 1.0$ , are assigned to all loads on the structure. The initial loads applied to the structure correspond to the case where  $\lambda = \lambda_i$ . In the programme, these initial loads are set by providing values of FAUGE, FAUGL, FAUGLL, and FAUGDL which denote load factors for exterior column loads, lateral loads, live loads and dead loads respectively. Thus, the loading conditions at  $\lambda = \lambda_i$  are assigned by multiplying the working load values of exterior column loads by FAUGE, and so on. Moreover, the size of the increments are set by values of AUGL, AUGLL and AUGDL, again expressed as a portion of the working load value. After the analysis is completed at  $\lambda_i$ , the second loading condition analyzed,  $\lambda_2$ , is represented by  $\text{FAUGL} = \text{FAUGL} + \text{AUGL}$ , and so on.

This incrementing procedure continues until plastic hinging progresses to the point where the structure has lost a significant portion of its initial stiffness. At this stage, it becomes advantageous to reduce the size of the increments. This is accomplished by multiplying the original load factor increments AUGL, AUGLL and AUGDL by a "deterioration factor" DETF, which is computed as a function of the ratio of the total number of plastic hinges present to the degree of indeterminacy of the structure.

At some stage, the application of a load factor  $\lambda_{F1}$  will result in indications of frame instability as discussed in SECTION 4.5.3. This

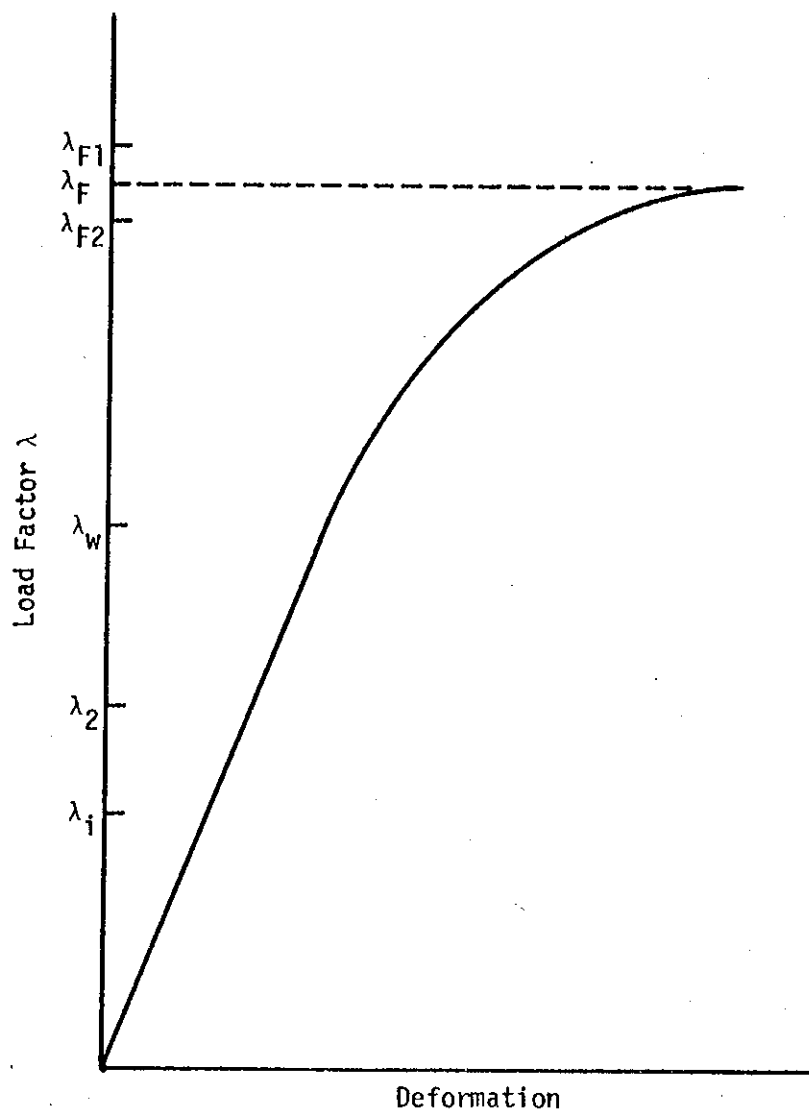


FIGURE 4.8  
TYPICAL LOAD-DEFORMATION RESPONSE  
CURVE

$\lambda_{F1}$  value is equal to or greater than the load causing failure of the structure. To converge closer to the actual failure load, the size of the last load increment is halved and the structure reanalyzed at  $\lambda_{F2}$ . If  $\lambda_{F2}$  yields instability, the increment is again halved. If a stable configuration is found at  $\lambda_{F2}$ , the true failure load lies between  $\lambda_{F2}$  and  $\lambda_{F1}$ . After the first detection of instability at  $\lambda_{F1}$ , the increment is subdivided four times by choosing the midpoint between the last stable and the last unstable  $\lambda$  values. After these four adjustments, it is assumed that the last load factor is sufficiently close to the true failure load factor  $\lambda_F$ .

As was mentioned previously, the loading procedure need not be proportional. For instance, by initially setting FAUGDL = 1.0 and AUGDL = 0, full working dead load will be on the structure initially and will never be incremented in the analysis. Caution must be exercised in applying non-proportional loading, however, since the plastic hinge reversals which might occur are not considered in the analysis.

#### 4.5.1 Detection of Plastic Hinges

The formation of a plastic hinge at any point in any member is detected using the slope-deflection equations and the procedures discussed in CHAPTER III. If a hinge is detected, the member hinge configuration is adjusted accordingly.

In tracing the response of the structure to incremental loading, the analysis detects the occurrence and location of all new plastic hinges which form in any load increment. In this way it differs from analyses<sup>(11,13,15)</sup> which are set up to provide the order of formation of plastic hinges directly.

The deflected shape at the end of an increment is computed using



the hinge configuration existing at the end of the increment. Several iterations may be required to satisfy the yield condition by detecting all the hinges which develop in the increment. The load-deformation relationship is assumed to be linear throughout the increment.

#### 4.5.2 Speeding up Convergence

Initially all deformation values are set at zero. Thus, in iterating for convergence at the first load stage  $\lambda_1$ , the iteration procedure must alter the deformations from the zero values to the statically admissible values. Thereafter the final deformation values obtained for one cycle of analysis could be used as initial values for the next cycle. To speed convergence, however, the known deformation values were extrapolated to predict approximate starting values for the new load stage.

To avoid storing all previous deformation values, the extrapolation procedure used in this analysis considers that the relationship between FAUGL and the total sway deflection at the top of the frame is representative of all load-deformation relationships in the structure. In the initial load stages, a linear extrapolation procedure is applied to this relationship to establish a value of  $RATIO$ . All values of joint rotations  $\theta$  and storey sway deflections  $\Delta$  from the previous load stage are multiplied by  $RATIO$  to provide approximate values of deformations for the start of the convergence procedure at the new load stage. After at least three points of the load-deformation relationship have been determined, Lagrange's procedure<sup>(37)</sup> is used to fit a second degree equation to the last three points to derive a value of  $RATIO$  for the extrapolation operation.

### 4.5.3 Detection of Instability

As the loads on the frame are increased, the applied loads will eventually exceed the maximum load-carrying capacity of the frame. In formulating the computer programme, it is necessary to incorporate checks to indicate that instability conditions have been reached in the structure. The load is considered to be at or beyond the frame instability load if any one of the following conditions arises.

1. A storey sway mechanism, as shown in FIGURE 4.9, is detected. This hinging condition is a recognized collapse mechanism condition in simple plastic theory. In applying EQUATION (4-12) to this hinge configuration, it will be found that the numerator equals  $2\sum M_{pc}$  and the denominator equals  $\sum P$  in all storey columns.
2. A joint mechanism, as shown in FIGURE 4.10, is detected. Again this is a valid collapse mechanism condition in simple plastic theory. Since the denominator in EQUATION (4-11) would be zero with this hinge condition, it is not possible to derive a unique value of the joint rotation.
3. The storey sway deflection value computed by EQUATION (4-12) shows a reversal in one or more storeys. EQUATION (4-12) computes the equilibrium value of the storey sway deflection under the current load values. If at some load stage, this equilibrium deformation value drops below that for the previous load stage, it indicates that the columns in the storey in question are able to support the incremented loads only at a reduced sway deflection value because of the reduced column

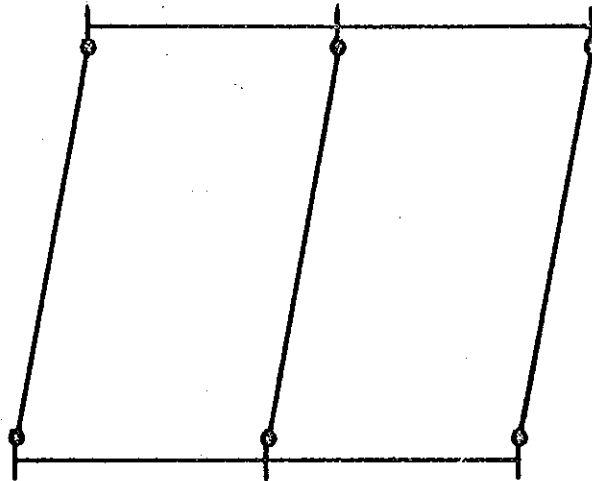


FIGURE 4.9  
STOREY SWAY MECHANISM

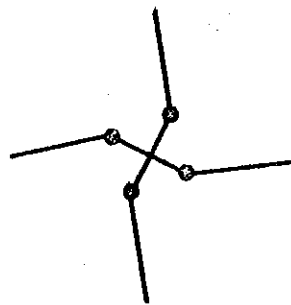


FIGURE 4.10  
JOINT MECHANISM

stiffness. This serves to indicate that the structure is unstable in that storey.

4. The iteration procedure fails to converge after a limiting number of cycles. In a formal matrix solution of the problem, instability is signified by a change of sign of the stiffness matrix determinant. In an iteration procedure, however, instability will be detected by non-convergence of the iteration procedure. Some sufficient, but not necessary, conditions for convergence of a matrix have been suggested<sup>(36)</sup>, but the question of where the borderline between convergence and non-convergence lies has not been answered. Thus, in the programme, it is necessary to set some realistic limits on the number of cycles of iteration required to bring about convergence of values of column axial loads and deformations in a stable structure. And beyond these limits, defined as LIMITP and LIMITD in conjunction with ACCURP and ACCURD, the structure will be assumed to be unstable. The problems involved in assigning realistic values to LIMITP and LIMITD are discussed in SECTION 4.8.

The first two conditions for instability are usual criteria for a failure mechanism in simple plastic analysis. As was noted in SECTION 3.3.6, the formation of a beam mechanism is not considered to represent instability of the structure in this analysis. A combined collapse mechanism will obviously be detected by one of the last two conditions. But these last two conditions will also detect instability of the structure should it occur prior to the formation of a collapse mechanism as a result of softening

of the structure by hinging and secondary axial load effects.

#### 4.6 Computer Application of the Analysis

A computer programme was prepared to carry out the incremental analysis described in this chapter. The programme was written in IBM System/360 Fortran IV language. The programme nomenclature, flow diagrams and a listing of the programme are presented in APPENDIX D.

The basic steps in the programme can be summarized as follows:

1. Read frame geometry, material properties and section properties. Set convergence limits. Initialize all deformations as zero, and all hinge configurations as elastic.
2. Compute all girder section properties. These remain unchanged as loads on the structure are increased.
3. Read working load values, initial load factors and initial load factor increments, and use these to compute the initial loads on the structure.
4. Compute axial loads in all columns. Compute vertical joint deformations, column section properties and stability functions under these current axial load values.
5. Compute joint rotations and storey sway translations by iteration until sufficient convergence is achieved. This involves the use of the "operator" relationships shown in FIGURES 4.4 and 4.7. If instability is detected due to inability to converge, a joint mechanism, or reversal of a storey sway deflection value, skip to step 10.
6. With these current deformation values, check for the emergence

of new hinges in the frame. If a storey sway mechanism is detected, skip to step 10.

7. Check for convergence of column axial load values and the frame hinging configuration. If axial load values have not converged to the specified degree, or new hinges were detected in step 6, revert to step 4 and try again for convergence to a proper solution. If instability is detected due to insufficient convergence of column axial load values, skip to step 10.
8. If all values of deformations and column axial loads have converged and no new hinges were detected in the last pass through step 6, the current solution satisfies all conditions of equilibrium and compatibility under the current external loads. Print out all pertinent information, including cases of excessive rotation at plastic hinges.
9. Increment the load factors, extrapolate deformation values, and return to step 4. However, if four load factor adjustments have been made since the initial detection of instability, skip to step 11.
10. Record the source of instability. Reduce the load factors as described in SECTION 4.5 and return to step 4. However, if four load factor adjustments have been made since the initial detection of instability, proceed to step 11.
11. Stop the analysis, and take the last stable loading configuration as indicative of the true failure load of the structure.

With slight modifications, the computer programme can be used for

first order elastic-plastic or first order elastic analysis.

#### 4.7 Limitations of the Analysis

Simplifications introduced in both the framework model and the analysis of member behaviour impose limitations on the use of the computer programme presented in this thesis.

In the model, all shearwalls are considered to be continuous throughout the height of the structure, and all columns must have fixed foundations. These conditions do not represent limitations of the method of analysis, but do restrict the use of the present programme. The programme could easily be revised to consider shear walls terminated below the top of the structure and any conditions of base fixity. In addition, the model is assumed to be a regular rectangular frame with no missing members. For the analysis, new conditions of equilibrium could be formulated to consider the boundary conditions imposed by missing frame members or irregular member spacing.

Although it is a limitation of the present analysis, the assumption of point joints is not essential since the finite widths of all members framing into a joint could be considered in the same manner as was the finite shear wall width.

Of the assumptions of member behaviour, perhaps the most significant is that regarding the maintenance of all plastic hinges once they have formed. The possibility of plastic hinges ceasing to rotate during proportional loading has been discussed by Neal<sup>(38)</sup> and Davies<sup>(13)</sup> who illustrated the occurrence in the analysis of simple structures. Neglect of the presence of unloaded plastic hinges may lead to erroneous estimates

of deflection values. In his analysis, designed to consider variable repeated loading, Davies takes into account the reversibility of plastic hinging. In the course of loading, if cessation of plastic rotation is detected at any hinge, the plastic hinge is replaced by an elastic "passive" hinge locked with a permanent deformation. The formation of passive hinges could be detected by this method of analysis. To consider the permanent rotational discontinuities at the closed hinge, it would be necessary to revise the slope-deflection equations to consider "kinked" elastic members instead of the straight members considered in the present analysis. However, Davies' investigations indicate that, in a structure subjected to proportional loading, hinge reversals are unlikely to occur before instability is detected. In view of this, it was felt that the sophistication required to consider hinge reversals was not warranted in this analysis.

The analysis as presently constituted will yield only the stable equilibrium configuration denoted by the portion OA of the load-deformation plot shown in FIGURE 4.11, stopping where instability is detected at A. When the  $P\Delta$  effect is considered in the formulation of equilibrium, two distorted configurations of the structure can be in equilibrium with a given set of loads. The second configuration, represented by the dotted line AB in FIGURE 4.11, is a post-instability or unloading case.

To extend this type of analysis to consider the post-instability behaviour, a number of modifications would be required. As was noted in SECTION 4.5.3, EQUATION (4-11) becomes inoperative for a joint mechanism and failure of the structure is assumed. Similarly, in formal stiffness matrix formulations<sup>(11,13,15)</sup> of an analysis, the formation of a joint



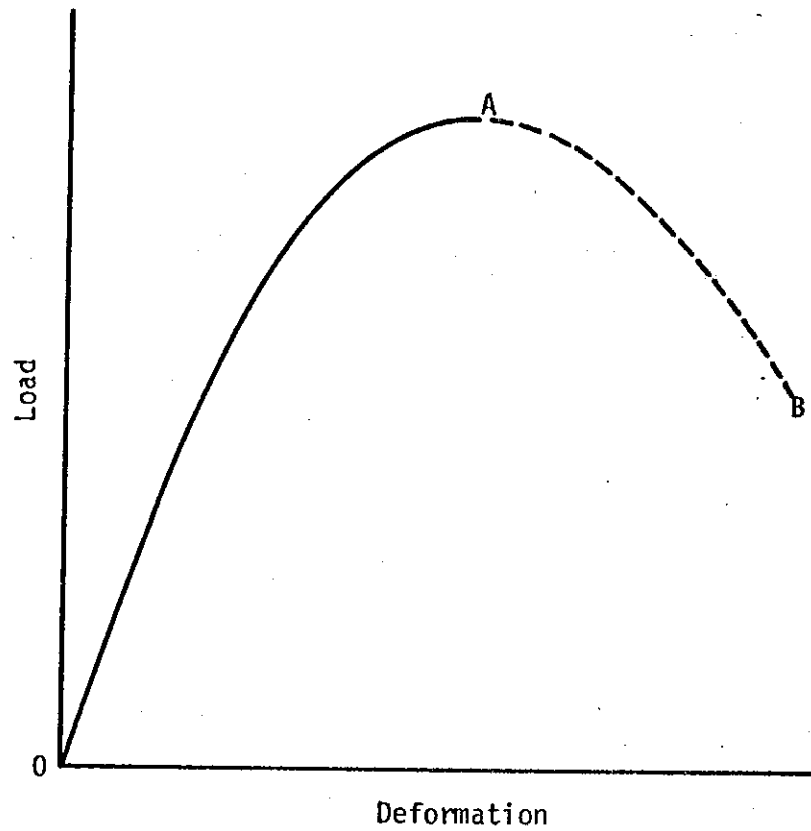


FIGURE 4.11  
COMPLETE LOAD-DEFORMATION RESPONSE  
HISTORY OF A STRUCTURE

mechanism leads to a breakdown of the solution because the inoperative equation results in a zero stiffness matrix determinant, which signifies failure. To permit extension of this analysis to consider post-instability behaviour, some method must be found to treat the joint mechanism condition. Fortunately, the formation of a joint mechanism need not lead to a mathematical breakdown of the solution. If a joint mechanism occurs, the behaviour of all members framing into the joint is found to be independent of the rotation of the joint itself, and the members can continue to be analyzed neglecting the rotation of the joint. By simply skipping the evaluation of the joint rotation in the analysis, the inoperative equation can be eliminated, and the evaluation of the response of the rest of the structure can be continued. This, of course, implies that the maintenance of serviceability at an isolated joint is not a serious consideration, or that remedial design procedures can be employed to minimize the loss of serviceability. No such problem arises in the event of occurrence of a storey sway mechanism since EQUATION (4-12) remains operative, treating the hinged columns essentially as rigid bodies.

In addition, provision would have to be made for decreasing the load factors after instability is detected, and for predicting the initial trial values of the increased deformations. Davies' work indicates that the closing of plastic hinges should also be considered in the post-instability range.

In this manner, it would be possible to express the equilibrium equations for the structure on the unloading branch much as was done before. Wright and Gaylord<sup>(39)</sup>, using a compatibility analysis, indicate that post-instability behaviour is non-convergent. To permit derivation of the

unloading branch, the structure was modified by providing fictitious lateral spring supports. The adoption of such an approach in this analysis would require a number of major assumptions and modifications. Moreover, there is no apparent reason why the equations satisfying equilibrium on the unloading branch should be ill-conditioned for a solution.

#### 4.8 Effect of Convergence Limits on Accuracy

To solve the system of linear equations, an iteration procedure is used instead of a formal matrix solution. Consequently, the solution must be regarded as approximate, the departure from the exact solution being a function of the degree of accuracy specified for the convergence of deformations and column axial loads. In the computer programme these are denoted by ACCURD and ACCURP respectively.

To illustrate the significance of this error in convergence, two structures discussed in CHAPTER VI were analyzed with three different values of ACCURD and ACCURP. The results of these analyses appear in TABLES 4.1 and 4.2. Because the loads and deformations are progressively increasing in the analysis, it might be expected that the lower specified value of convergence accuracy would produce unconservative values of overall frame stiffness. However, a comparison of the deflection values indicates that no such consistent result can be observed while the structures remain elastic. This inconsistency is probably caused by the interrelationship between  $P$ ,  $C$ ,  $S$ ,  $M_{pc}$  and  $EI$ . When a low degree of accuracy is specified, there is a definite tendency to overestimate the stiffness of the structure as the structure becomes inelastic and the behaviour becomes more sensitive to errors. In the inelastic frame, this leads to an underestimation of the

ACCURD and ACCURP		0.02		0.005		0.002	
$\lambda$		Plastic Hinges Detected	Sway $\Delta$ at Roof (in)	Plastic Hinges Detected	Sway $\Delta$ at Roof (in)	Plastic Hinges Detected	Sway $\Delta$ at Roof (in)
		0	4.2197	0	4.2201	0	4.2201
0.50		0	5.1776	0	5.1780	0	5.1782
0.60		0	6.1748	0	6.1729	0	6.1727
0.70		0	7.2116	0	7.2110	0	7.2112
0.80		0	8.2993	0	8.2981	0	8.2983
0.90		0	9.4442	0	9.4412	0	9.4414
1.00		0	10.652	0	10.649	0	10.649
1.10		12	12.163	12	12.410	12	12.499
1.20		25	16.355	27	17.442	27	17.722
1.30		31	18.384	32	19.941	32	20.182
1.325		33	20.662	34	21.525	34	21.778
1.3375		37	22.164				
1.34375							
Failure $\lambda$ Interval		1.34375 - 1.350		1.3375 - 1.34375		1.3375 - 1.34375	
Total Iterations for Convergence of:	P Values	39		54		72	
	Deformations	213		390		597	
Execution Time		0.83 minutes		1.05 minutes		1.31 minutes	

TABLE 4.1

EFFECTS OF ITERATION CONVERGENCE ACCURACY ON THE ANALYSIS OF STRUCTURE H1

ACCURD and ACCURP		0.02		0.005		0.002	
$\lambda$		Plastic Hinges Detected	Sway $\Delta$ at Roof (in)	Plastic Hinges Detected	Sway $\Delta$ at Roof (in)	Plastic Hinges Detected	Sway $\Delta$ at Roof (in)
0.50		0	2.7278	0	2.8073	0	2.8073
0.60		0	3.3243	0	3.3901	0	3.4284
0.70		0	3.9611	0	4.0451	0	4.0662
0.80		0	4.6559	0	4.7361	0	4.7313
0.90		0	5.4056	0	5.4231	0	5.4193
1.00		0	6.2046	0	6.1495	0	6.1362
1.10		0	7.0323	0	6.9294	0	6.8996
1.20		0	7.8631	0	7.7446	0	7.7071
1.30		12	8.7068	12	8.6384	12	8.6523
1.40		22	10.104	24	10.627	26	10.742
1.4125							
1.41875							
1.425							
1.44375							
1.45		30	11.526	28	10.930	30	11.889
1.45625		31	12.772	28	11.134	31	12.819
Failure $\lambda$ Interval		1.45625 - 1.4625		1.41875 - 1.425		1.44375 - 1.45	
Total Iterations for Convergence of:	P Values	38		54		76	
	Deformations	698		1271		2607	
Execution Time		1.36 minutes		1.97 minutes		3.58 minutes	

TABLE 4.2

EFFECTS OF ITERATION CONVERGENCE ACCURACY ON THE ANALYSIS OF STRUCTURE H50

number of plastic hinges present and an overestimation of the failure load. It is important to note, however, that the inaccuracies are not cumulative in their effects, since the frame is reanalyzed at each load stage to the same specified degree of accuracy.

In setting up the programme, it was necessary to set limits on the number of cycles of iteration required for a solution. These limits are specified by LIMITD and LIMITP in the computer input. As was noted in SECTION 4.5.3, instability is assumed if these values are exceeded in iteration for a solution at any load stage. Unfortunately, the rate of convergence of a solution to any desired degree of accuracy is a property of the system under consideration. Comparison of the execution time and total number of cycles of iteration of H1 and H50 serves to indicate this. H1 is a structure with a relatively weak shear wall compared to that in H50. In keeping with the condition that a matrix in which the diagonal elements predominate is more amenable to solution by the Gauss-Seidel iteration procedure<sup>(37)</sup>, the solution for H1 should be obtained more rapidly than that for H50. Thus, it can be said that LIMITD and LIMITP must be considered as functions of the system under analysis, the size of load increment and the degree of accuracy required. As such, the assignment of values to LIMITD and LIMITP is a matter of judgment. Perhaps the best test of the applicability of the values chosen is to check that the load-deformation plot flattens adequately with the onset of instability. In all cases shown in TABLES 4.1 and 4.2, the frames failed by the formation of a joint mechanism and LIMITD and LIMITP exerted no effect on the failure loads.

## CHAPTER V

### COMPARISONS WITH OTHER ANALYSES AND TESTS

#### 5.1 Introduction

To illustrate the validity and applicability of the method of analysis described in CHAPTERS III and IV, results derived using the analysis are compared with available information provided by other investigators. Certainly the most desirable information for comparison is that derived either from full scale field tests or from laboratory tests. Unfortunately such tests on reinforced concrete frames are both expensive and complicated, and most investigators have chosen to test analytical models by computer. Consequently only one group of the comparisons made in this chapter is based on actual laboratory test results.

In this chapter, the tests chosen for comparison include:

1. the analytical reinforced concrete column study performed by Pfrang<sup>(40)</sup>, to check the applicability of the rationalized M-P- $\phi$  relationship and the slope-deflection equations derived in CHAPTER III,
2. the unbraced multi-storey steel frames analyzed by Parikh<sup>(14)</sup>, to check the performance of the computer programme developed in CHAPTER IV,
3. the laterally loaded reinforced concrete frames tested by Ferguson and Breen<sup>(41)</sup>, to provide a check on the overall effects of the assumptions made in formulating the analysis

for reinforced concrete structures,

4. the approximate braced frame analysis of Guhamajumdar, Nikhed et al<sup>(25)</sup>, to check the applicability of the analysis in braced structures.

## 5.2 Pfrang's Analytical Column Model

Pfrang investigated the behaviour and capacity of a reinforced concrete column in a structural framework subjected to vertical loads and relative lateral joint displacements. To approximate the system in an actual frame, Pfrang represented the column and its restraining members by the equivalent model shown in FIGURE 5.1. The rectangular column section was symmetrically reinforced and possessed section and material properties identical to those used for the sample M-P- $\phi$  computations in APPENDIX B.

In his study of column behaviour, Pfrang analyzed many of these individual systems, varying the several parameters  $h/t$ ,  $e_2/e_1$ ,  $e_2/t$ ,  $\alpha$ ,  $\beta$  and  $\theta_y$  known to influence the behaviour and capacity of this type of structural system. The analysis used by Pfrang was an incremental analysis employing a convergence procedure to achieve compatibility at a number of stations along the column. Non-linearity of the reinforced concrete column M- $\phi$  relationship was considered in using M-P- $\phi$  curves based on the exact analysis<sup>(28)</sup> described in CHAPTER III.

Using the rationalized bilinear M-P- $\phi$  relationship and the resultant constant EI condition throughout the column length, an analysis was formulated for Pfrang's model column. This analysis was applied to several of Pfrang's column cases, and the resulting comparisons appear



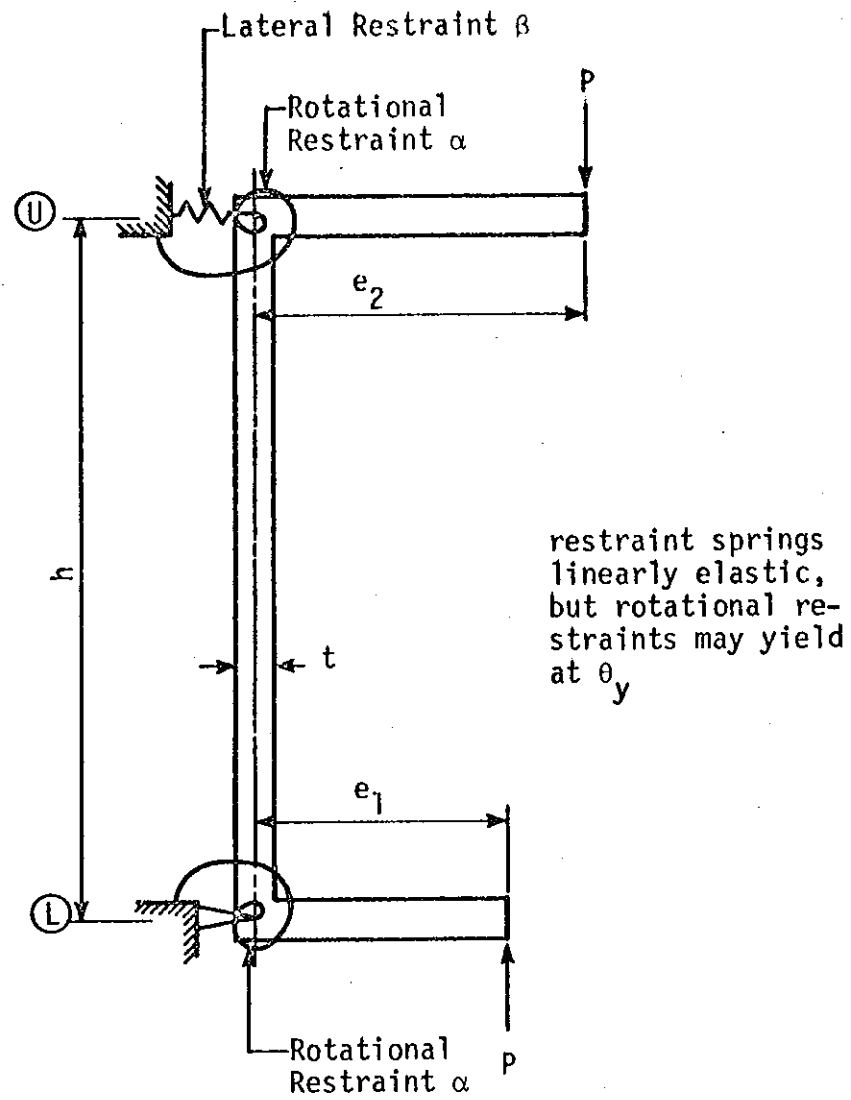


FIGURE 5.1

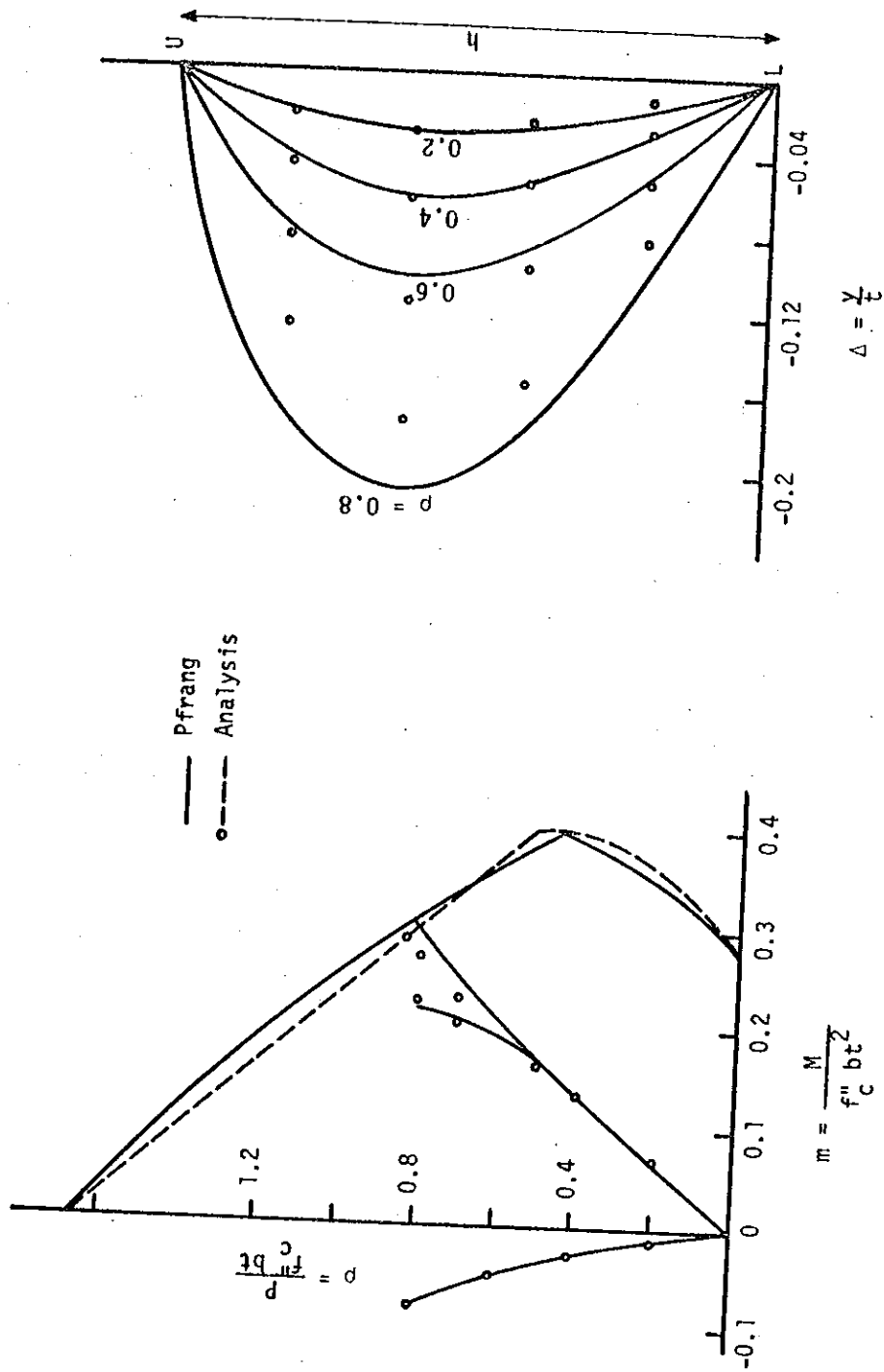
PFRANG'S IDEALIZED COLUMN MODEL

in FIGURES 5.2, 5.3 and 5.4. It should be noted that the results shown for Pfrang's analysis were scaled from his figures. The rationalized and exact M-P- $\phi$  diagrams showed satisfactory agreement.

The comparison justifies the applicability of the rationalized M-P- $\phi$  relationship to this column section. The validity of the slope-deflection equations for unhinged members, which assume a constant EI value throughout the length of the member, is also demonstrated. The departures of the exact M- $\phi$  relationship from the idealized elastic-plastic relationship are shown in APPENDIX B. Despite these departures, the analysis predicts the behaviour of the member quite accurately. As is shown in FIGURE 5.2(b), the analysis somewhat underestimates the deformation values at high load levels approaching the failure condition. This, of course, could be expected in view of the excessive stiffness values considered by the bilinear M- $\phi$  relationship in the yielding portion of the M- $\phi$  diagram. The failure loads, however, do agree very well with those derived by Pfrang's more sophisticated analysis.

### 5.3 Parikh's Analysis for Unbraced Steel Frames

To check the formulation of the computer programme for frame analysis described in CHAPTER IV, an attempt was made to duplicate the results of an unbraced steel frame analyzed by Parikh. The structure chosen for study was Parikh's three storey, two bay steel frame loaded as shown in FIGURE 5.5. The computer programme was modified to use the M-P- $\phi$  relationships for steel members derived by Parikh. A comparison of the load-deformation characteristics of all three floors appears in FIGURE 5.6, and a comparison of the order of plastic hinge formation is

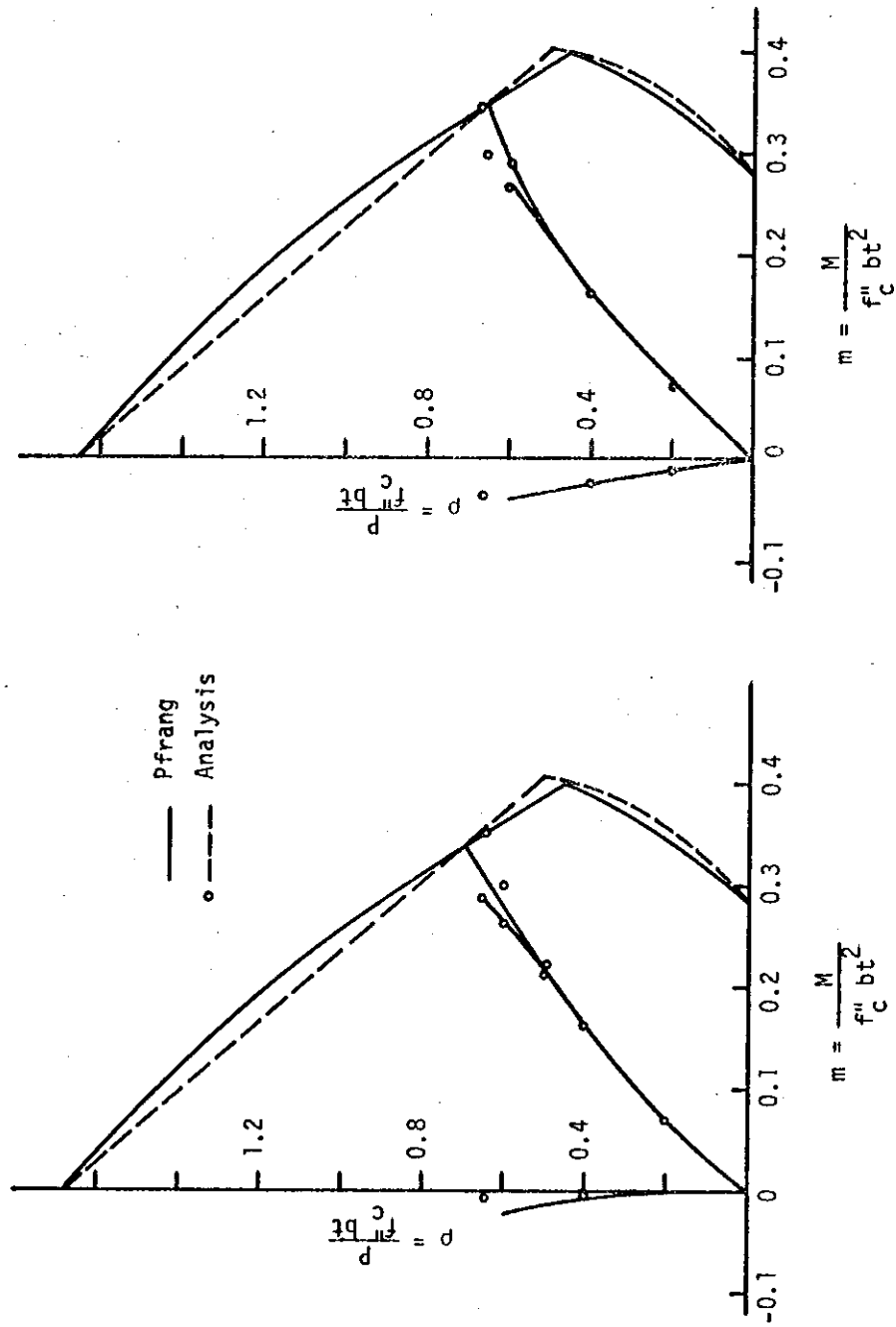


(a). Interaction Diagram

(b) Deflection Profile

FIGURE 5.2

COMPARISON WITH PFRANG'S FIGURE 4 COLUMN

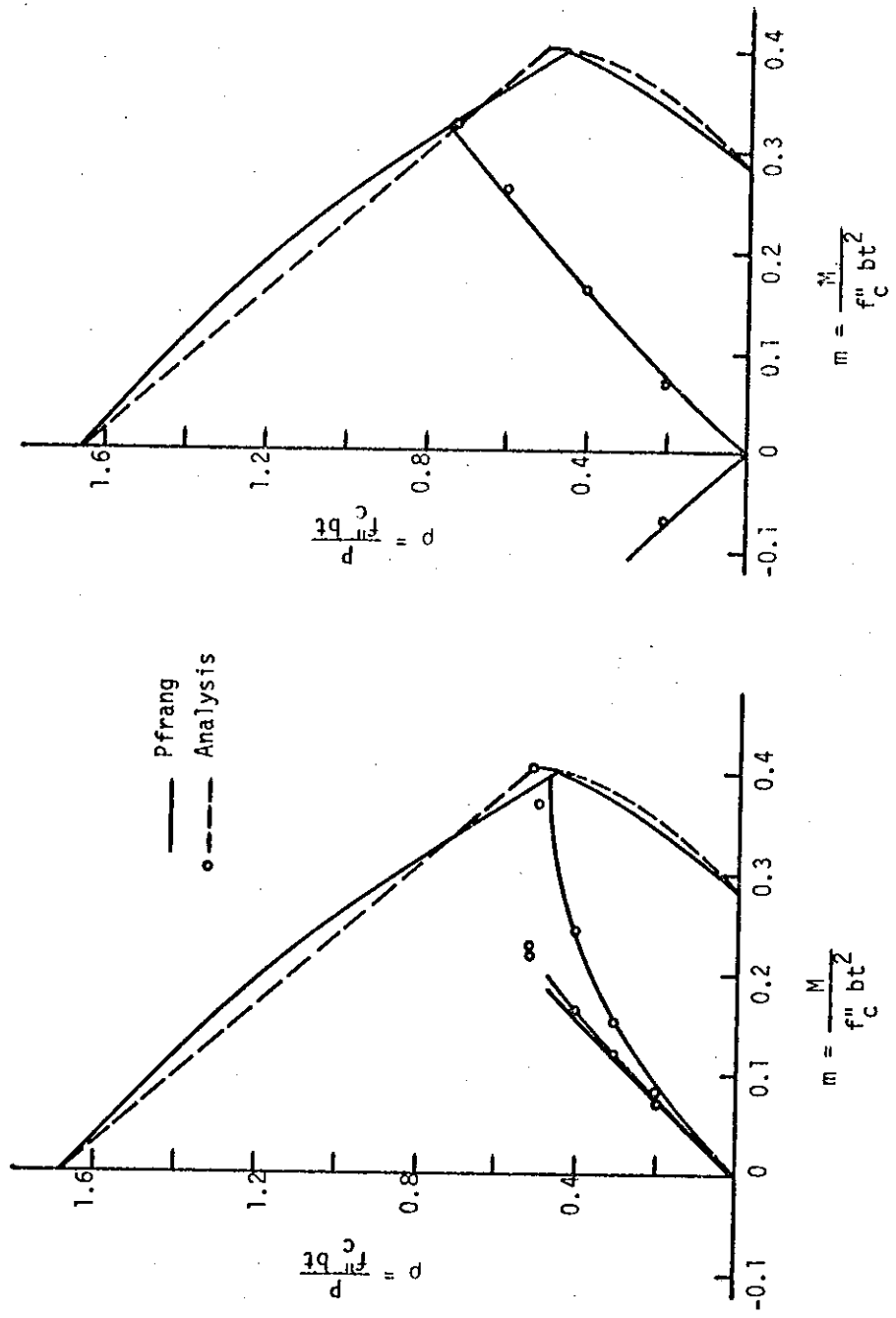


(a) Figure 8(c) column

(b) Figure 8(d) column

FIGURE 5.3

COMPARISONS WITH TWO OR PFRANG'S FIGURE 8 COLUMNS



(a) Figure 11(c) column (b) Figure 11(d) column

FIGURE 5.4  
COMPARISONS WITH TWO OF PFRANG'S FIGURE 11 COLUMNS

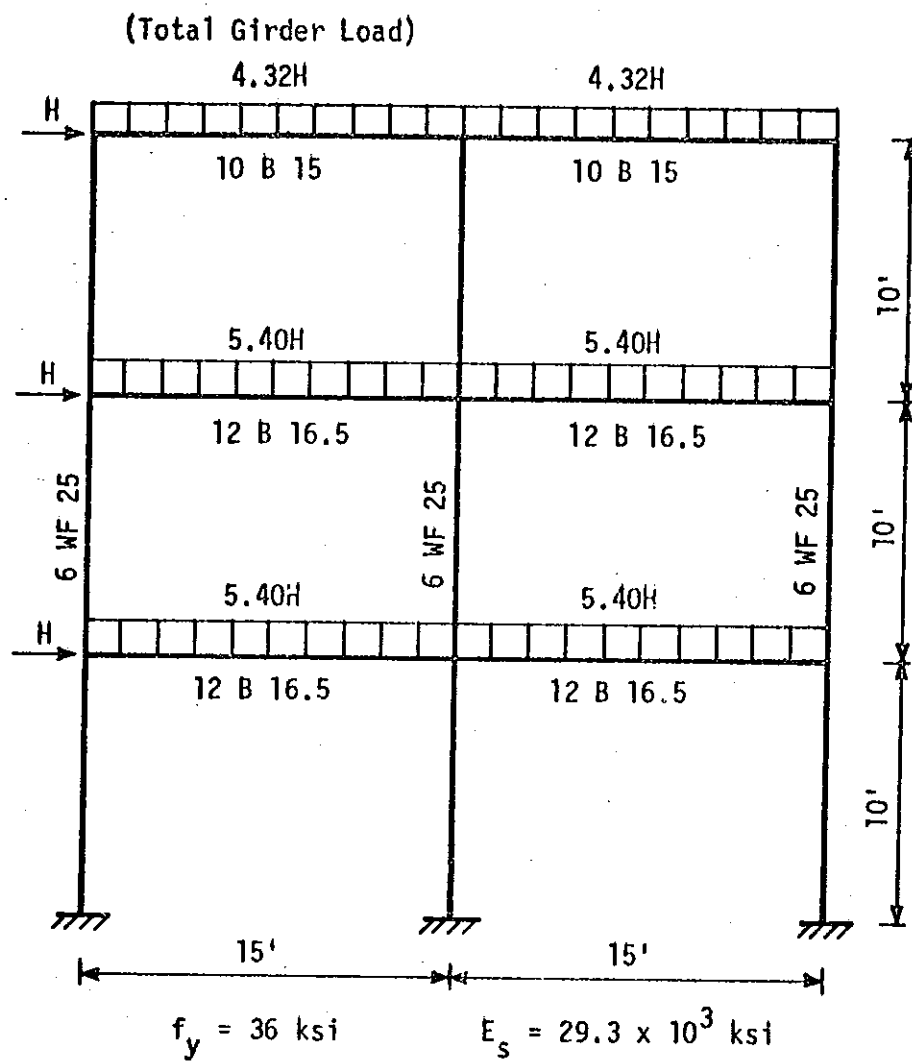


FIGURE 5.5  
 PARIKH'S THREE STOREY TWO BAY  
 STEEL FRAME

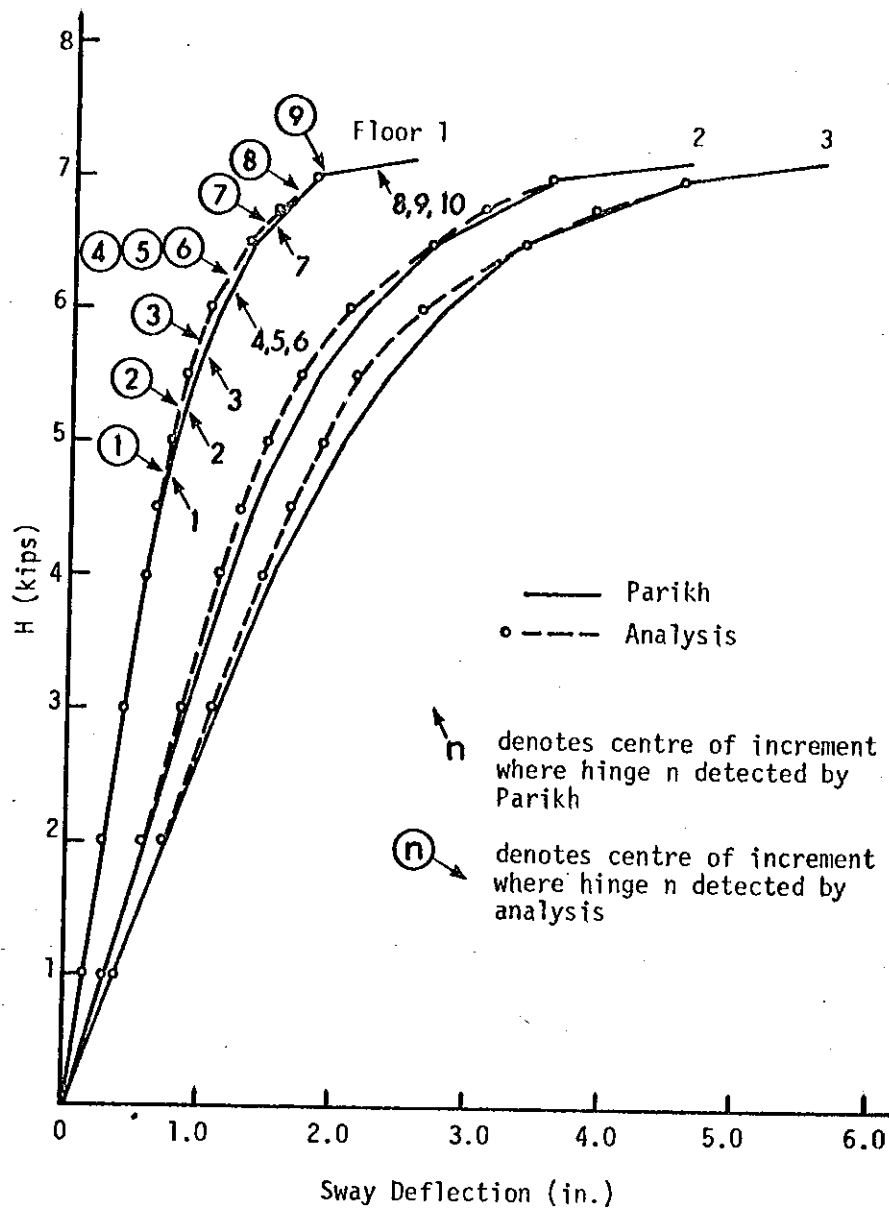


FIGURE 5.6  
LOAD-DEFORMATION CURVES FOR  
PARIKH'S FRAME

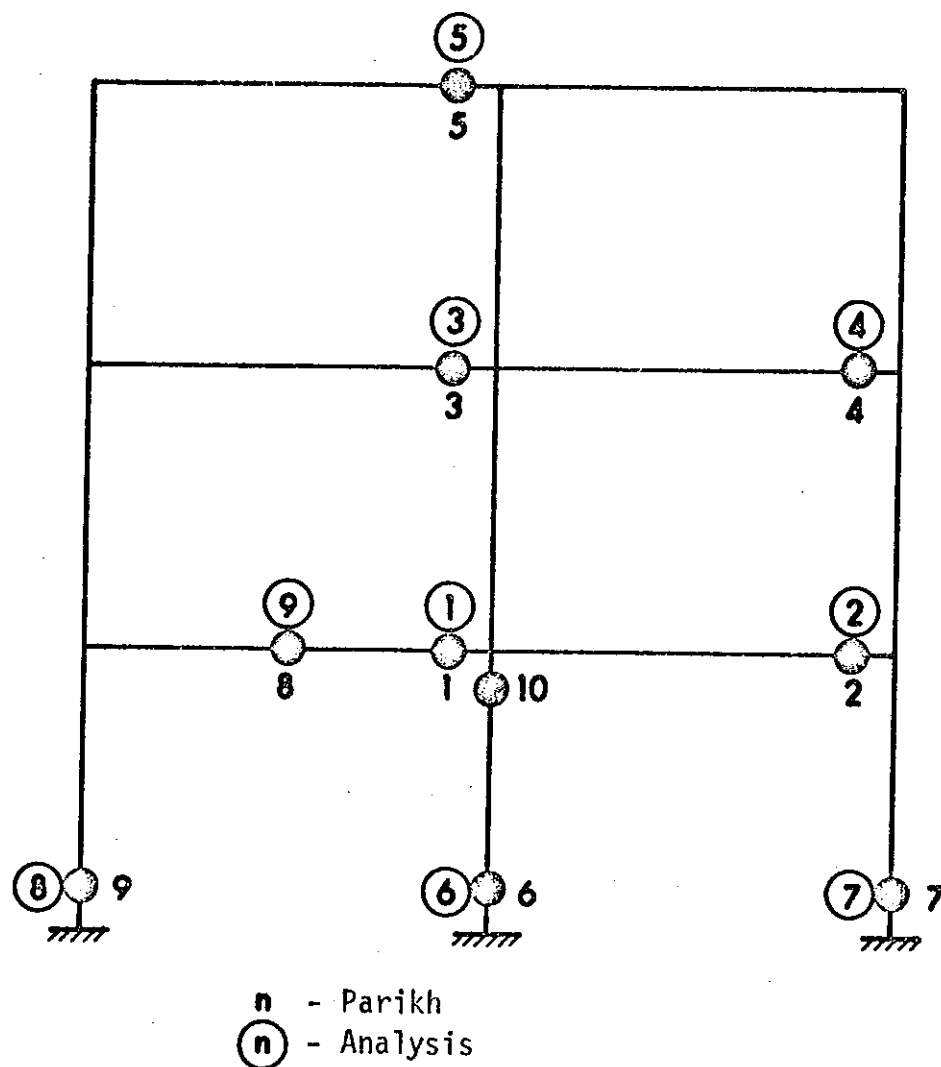


FIGURE 5.7  
LOCATION OF PLASTIC HINGES  
IN PARIKH'S FRAME



shown in FIGURE 5.7.

The results generally indicate a good comparison of the two analyses. In view of the similarity of the methods, however, one might expect duplication of results. Both analyses detected failure by instability prior to the formation of a collapse mechanism. The analysis in CHAPTER IV, with  $ACCURD = 0.005$  and  $ACCURP = 0.01$ , detected instability in the interval  $6.96875 < H < 6.98375$  kips when the ninth hinge formed. Instability was indicated by a significant drop in the equilibrium sway deflection value of the second storey. Parikh notes simply that his analysis indicated failure by instability with ten plastic hinges at what appears to be  $H = 7.125$  kips. Unfortunately, Parikh does not give details regarding his accuracy of convergence or his criteria for detecting instability.

Despite the differences in the results, it would appear that this check adequately establishes the validity of performance of the programme formulated in CHAPTER IV.

#### 5.4 Reinforced Concrete Frames Tested by Ferguson and Breen

To study the interaction between long columns and other frame members in a framing system, Ferguson and Breen tested a series of reinforced concrete frames of the type shown in FIGURE 5.8. All columns were symmetrically reinforced with  $p_t \approx 0.02$ , and all beams reinforced similarly with a higher percentage of reinforcement to induce column failure. In all, eight such frames were tested with different values of  $e/t$ ,  $h/t$  and column to girder stiffness ratio. Six of these could be considered adequate short term tests for comparison with the analysis.

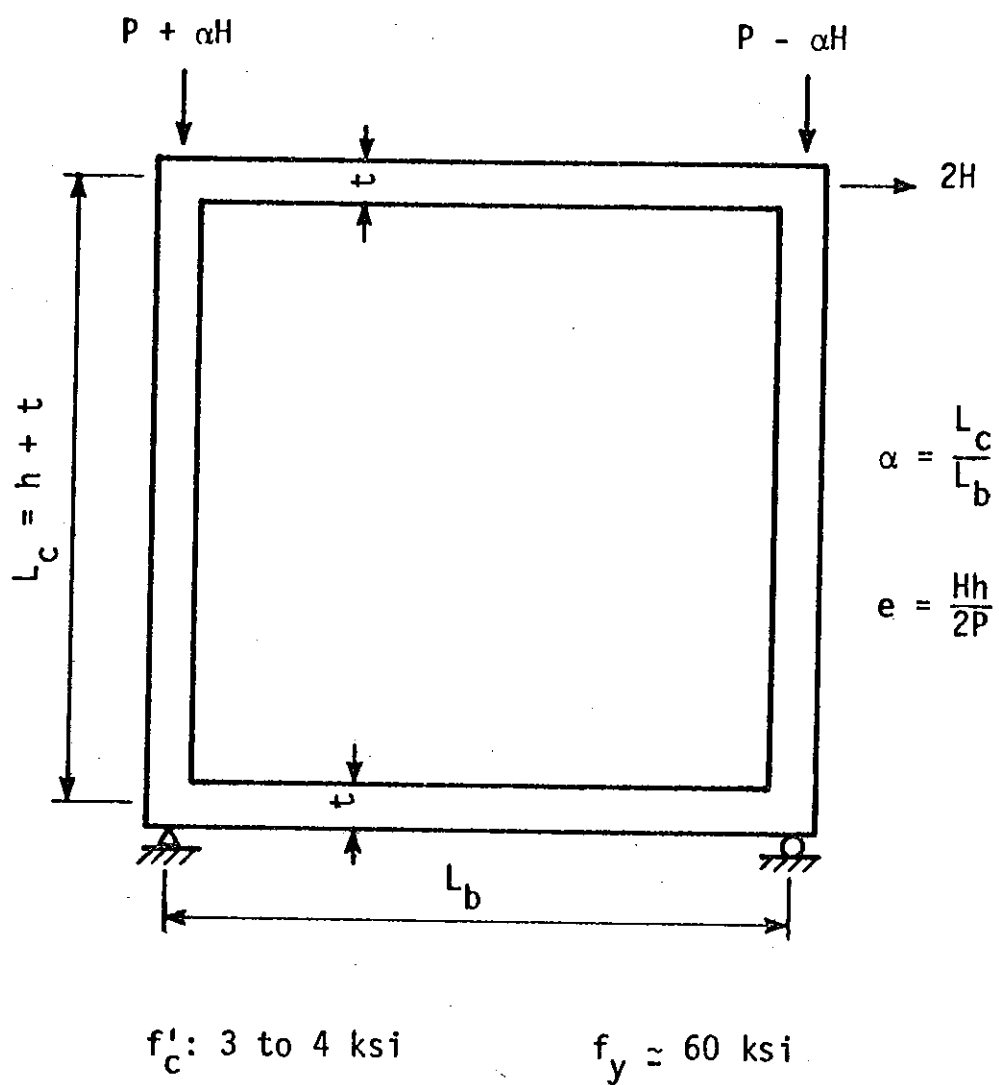


FIGURE 5.8

FERGUSON AND BREEN TEST FRAME

An analysis similar to that presented in CHAPTER IV was prepared to analyze these frames considering all variations in frame geometry and material and section properties. The results of this analysis are compared to the test results in FIGURES 5.9, 5.10 and 5.11. These figures show the interaction diagram for the column section and a record of load and moment at the failure section. Two values of indicated moment were provided by Ferguson and Breen, one derived from measured deflections using the known external load values, the other from curvature measurements using exact M-P- $\phi$  curves.

As will be seen from the interaction diagrams, in the early stages of loading, the computed column moments from this analysis were generally higher than the measured moments, indicating a softer structure than was found in the tests. The fact that the analysis neglected the finite width of the members and considered centre-line member dimensions may account for some of this discrepancy in overall stiffness. At higher loads, the analysis failed to detect the progressive softening of the structure as the ultimate load was approached. Two probable explanations for this discrepancy could be advanced. First, it is evident that the discrepancies at both low and high load levels are similar to the discrepancies between the exact M-P- $\phi$  and the rationalized M-P- $\phi$ . The rationalized M- $\phi$  relationship tends to be too soft initially, especially if the section has not yet cracked in flexure, and tends to be too stiff in the final stages before the yield moment is reached. Moreover, one of the major problems encountered in comparing the analysis to tests is that of considering time effects. The analysis is formulated using M-P- $\phi$  curves

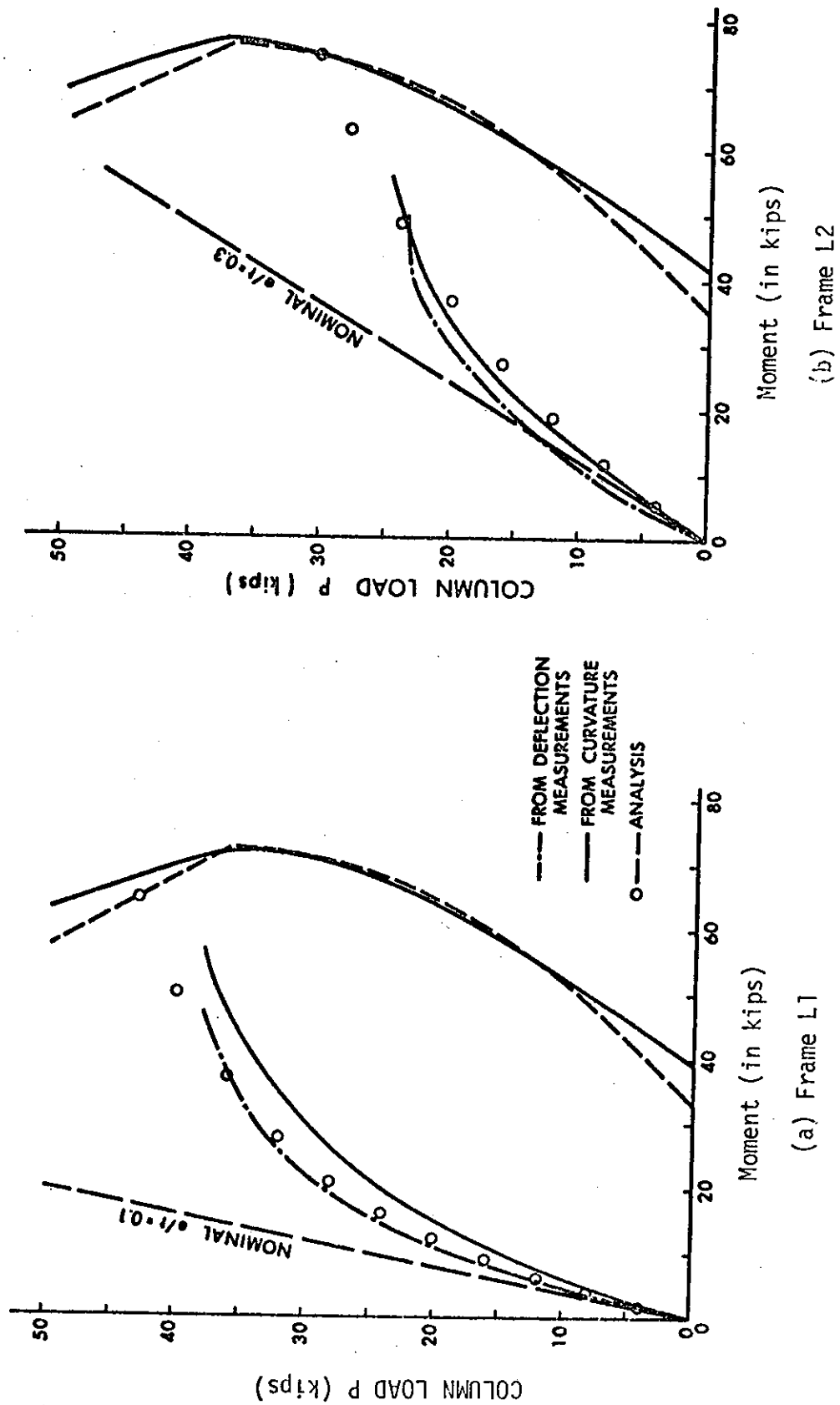
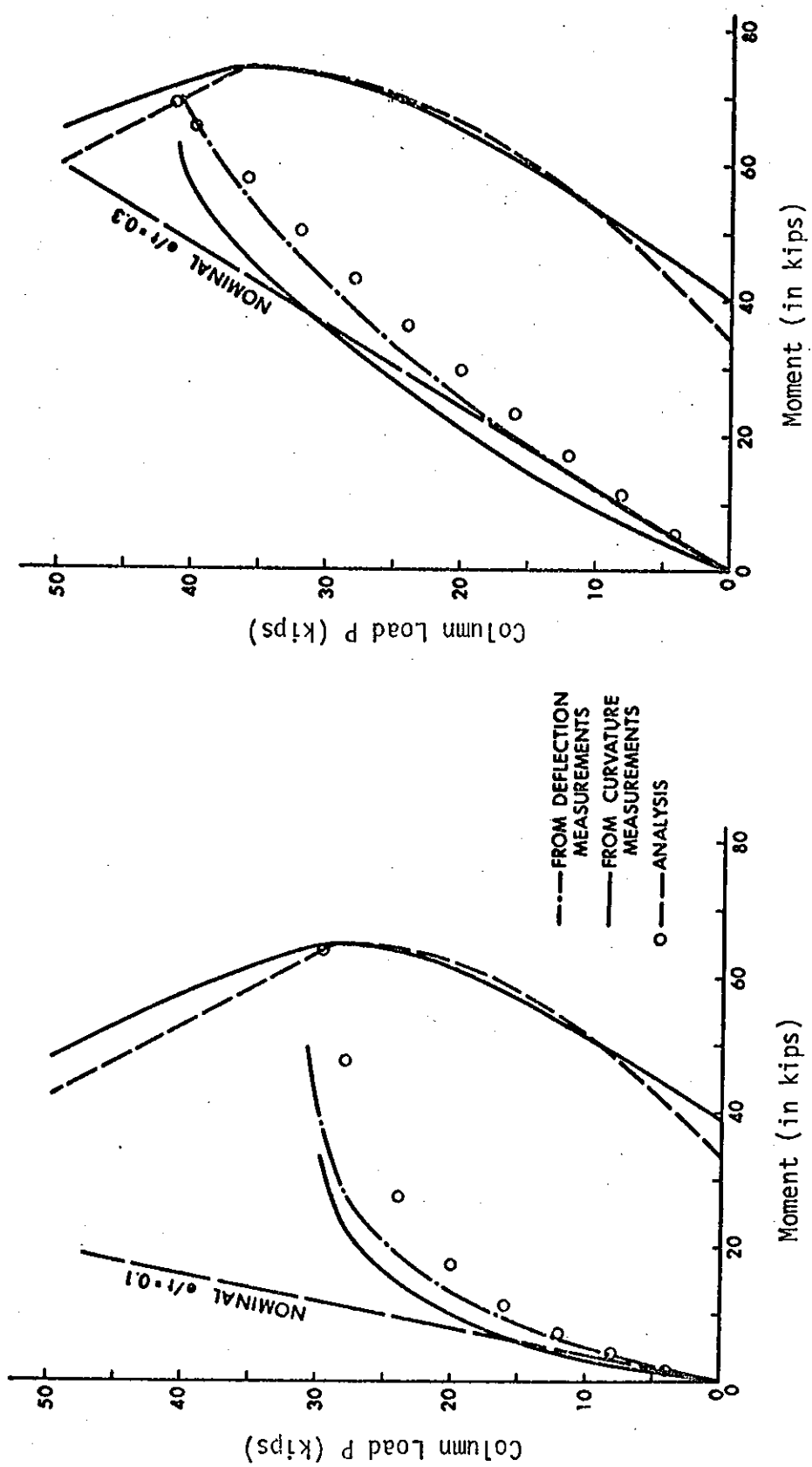


FIGURE 5.9

COLUMN BEHAVIOUR OF FERGUSON AND BREEN FRAMES L1 AND L2



(b) Frame L5

(a) Frame L3

FIGURE 5.10

COLUMN BEHAVIOUR OF FERGUSON AND BREEN FRAMES L3 AND L5

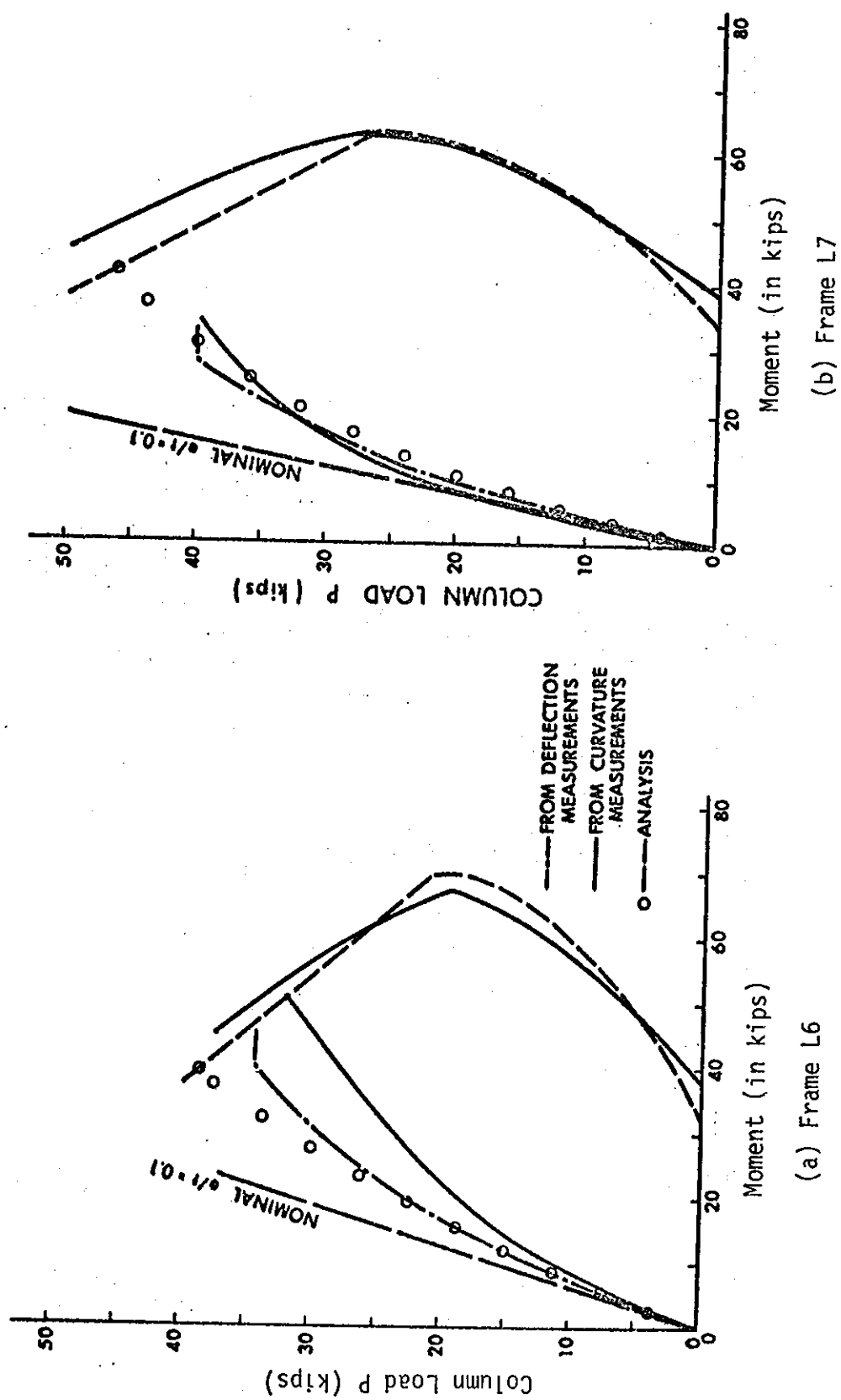


FIGURE 5.11

COLUMN BEHAVIOUR OF FERGUSON AND BREEN FRAMES L6 AND L7

which do not consider concrete creep effects. Each of these frames was tested to failure in a period of a few hours. Even in that length of time, however, concrete creep effects at high stress levels could substantially alter the observed deformation values<sup>(42)</sup>.

Despite these differences between true and idealized behaviour, the computer prediction of failure loads appear adequate. A comparison of computed and observed failure loads is presented in TABLE 5.1. Parme<sup>(43)</sup>, using a more sophisticated analysis than that employed here reported ratios of measured to computed failure loads ranging from 0.81 to 1.02 with a mean value of 0.92.

Frame	P <sub>ult</sub> Analysis (kips)	P <sub>ult</sub> Test (kips)	<u>Test</u> Analysis
L1	43.03	37.5	0.87
L2	30.47	25.0	0.82
L3	29.66	31.0	1.04
L5	41.53	42.5	1.02
L6	61.97	55.0	0.89
L7	46.28	40.0	0.87
		Mean	0.92

TABLE 5.1

ULTIMATE LOADS FOR FERGUSON AND BREEN FRAMES

The results indicate that the method of analysis yields results which compare with test results as well as could be expected in view of

the idealizations of the analytical model. Tests on more complex reinforced concrete structures are required to establish the reliability of the analysis when applied to multi-storey structures.

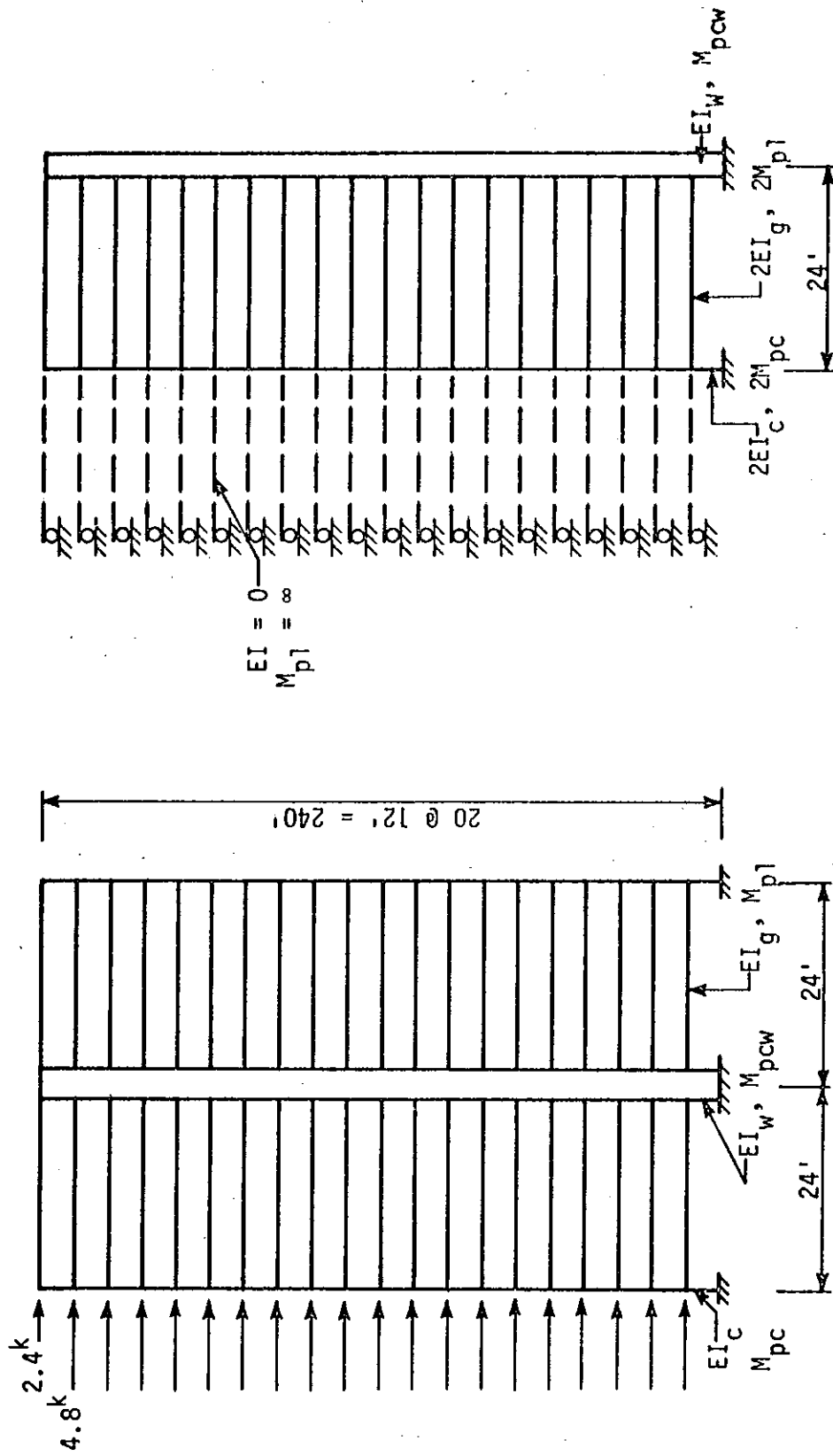
#### 5.5 Approximate Braced Frame Analysis of Guhamajumdar, Nikhed et al

Guhamajumdar, Nikhed, MacGregor and Adams have formulated an "approximate" elastic-plastic analysis for multi-storey shear wall-frame structures. Compared to the "exact" analysis presented here, their analysis is approximate in that it deals with an idealized lumped model rather than the actual structure.

To compare the two analyses, the symmetrical, twenty-storey two-bay braced reinforced concrete frame shown in FIGURE 5.12(a) was used. The section properties of the exterior columns and the girders are varied throughout the height of the structure to provide stiffness distributions as shown in FIGURES 6.4 and 6.5 respectively. The shear wall with a finite width of 25.7 inches is prismatic throughout the twenty-storeys with an  $EI_w$  value of  $11.95 \times 10^{12}$  lb in<sup>2</sup>. The lumped model used in the approximate analysis is shown in FIGURE 5.12(b).

To provide as meaningful a comparison as possible, the structure was subjected only to lateral loads, the working values of which appear in FIGURE 5.12(a). Since the exact analysis considers column  $M_{pc}$  and  $EI$  values as functions of  $P$  while the approximate analysis considers  $M_{pc}$  and  $EI$  as constant values, it was desirable to minimize the column axial load values in any comparison. Consequently external gravity loading was not considered, and the  $M_{pc}$  and  $EI$  values for columns in the approximate model are those corresponding to zero column axial load. At all stages of loading,





(a) Exact Analysis Model

(b) Approximate Analysis Model

FIGURE 5.12

TWENTY STOREY STRUCTURE FOR COMPARISON OF EXACT  
AND APPROXIMATE ANALYSES

however, the exact analysis considers the self-weight of the girders, columns and shear wall although the axial shortening of columns and walls are neglected in the exact analysis, in keeping with the approximate analysis assumptions.

Both analyses were performed using incremental lateral loading. A numerical comparison of the results at various load factors  $\lambda$  is presented in TABLE 5.2. The working load case corresponds to  $\lambda$  equal to one. Load-deformation plots appear in FIGURE 5.13. In the analyses, a convergence accuracy  $\text{ACCURD} = 0.003$  was used for the exact analysis, and the convergence limit in the approximate analysis was set at 0.005.

While the structure remains elastic, the results compare very well. The approximate analysis has been shown<sup>(25)</sup> to compare well with the Khan and Sbarounis analysis<sup>(18)</sup> in the elastic range of behaviour. In the exact analysis, the  $P\Delta$  effect due to self-weight may account for the initially more rapid detection of plastic hinges by the exact analysis. The delay in detection of hinges by the approximate analysis may also be the result of the lumping of girder plastic moment capacities, creating the condition that girder hinges cannot form singly, but rather in pairs in the complete structure.

The approximate analysis did, however, indicate earlier softening of the structure than the exact analysis. A comparison of the plastic hinge configurations at  $\lambda = 4.00$  appears in FIGURE 5.14. Although the exact analysis structure contains more plastic hinges, the approximate analysis indicates a softer structure at that stage of loading.

On the other hand, the exact analysis does not indicate significant

$\lambda$	Exact		Approximate	
	Sway $\Delta$ at roof (in)	Plastic hinges detected	Sway $\Delta$ at roof (in)	Plastic hinges* detected
0.50	1.9944	0	2.0382	0
0.75	2.9943	0	3.0572	0
1.00	4.0029	0	4.0764	0
1.25	5.0227	0	5.0954	0
1.50	6.0553	0	6.1146	0
1.75	7.1012	0	7.1337	0
2.00	8.1589	0	8.1528	0
2.25	9.2255	0	9.1718	0
2.50	10.296	0	10.191	0
2.75	11.363	0	11.210	0
3.00	12.419	0	12.229	0
3.25	13.458	0	13.248	0
3.50	14.473	8	14.267	4
3.75	15.466	14	15.402	12
4.00	16.449	21	16.976	18
4.25	17.447	26	18.797	30
4.50	18.492	30	21.195	42
4.625	19.071	33		
4.75	19.730	37	24.317	50
4.875	20.555	40		
5.00	21.634	44	27.818	66
5.125	23.050	46		
5.25	28.206	62	32.70	88
5.3125	32.181	76		
5.375	37.027	84		
5.4375	42.634	85		
5.50			39.58	92
5.75			45.79	92

\*Number of hinges shown here is double the number detected in the lumped members

TABLE 5.2  
RESULTS OF THE EXACT AND APPROXIMATE ANALYSES

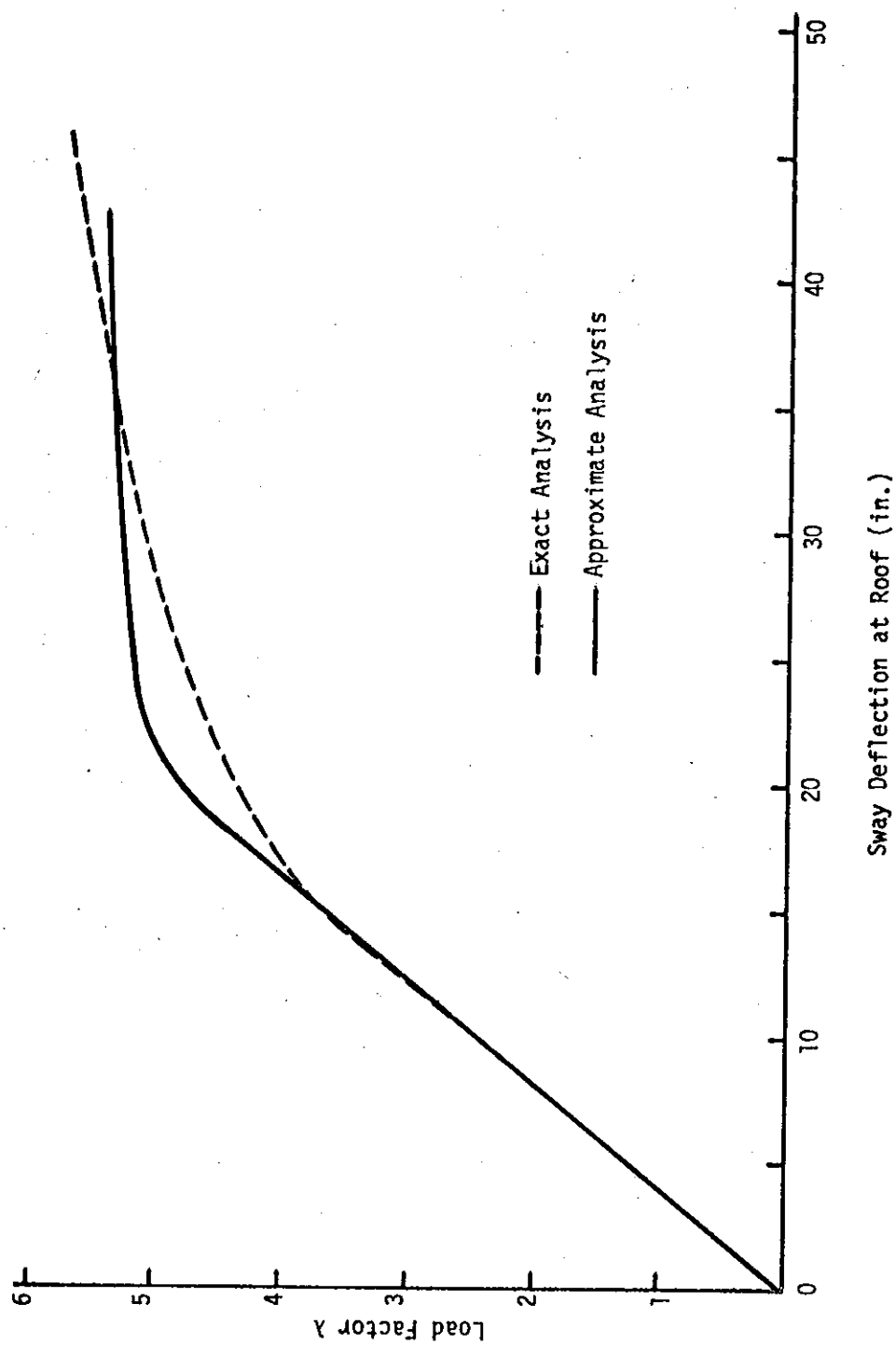


FIGURE 5.13  
LOAD-DEFLECTION CURVES FOR EXACT AND APPROXIMATE  
ANALYSES

softening of the overall structure until  $\lambda \approx 5$ , when the hinging of the girders is much more extensive. A comparison of the hinge configurations from the two analyses is presented in FIGURE 5.15. It will be noted that the approximate analysis has detected more extensive hinging at this load stage than has the exact analysis.

Neither analysis was carried to failure of the structure. The exact analysis was carried to  $\lambda = 5.4375$  and the approximate analysis to  $\lambda = 5.75$ . The hinge configurations at these load factors are shown in FIGURE 5.16. The exact analysis first detected cases of excessive plastic hinge rotation at  $\lambda = 5.25$ , and the locations of hinges where over-rotation was noted at  $\lambda = 5.375$  are shown in FIGURE 5.16(a). Reference to FIGURE 5.16 indicates that, at the stage of loading considered, plastic hinging has progressed to the point where the shear wall and columns are acting essentially as free-standing cantilevers. At  $\lambda = 5.50$ , the equilibrium roof sway deflection, assuming that the shear wall carries the entire lateral load as a cantilever, is about 130 inches. The load-deflection relationship shown in FIGURE 5.13 shows a transition from frame action to cantilever action as the frame stiffness deteriorates. The computed deflection is less than 130 inches because the structure has not yet been entirely converted into a single cantilever system.

The load-deformation relationship shown in FIGURE 5.13 indicates that the exact analysis detects a much more sudden and complete degeneration of the overall stiffness of the structure than does the approximate analysis. Apart from differences due to the lumping procedure used in the approximate analysis and the presence of self-weight in the exact analysis, the only

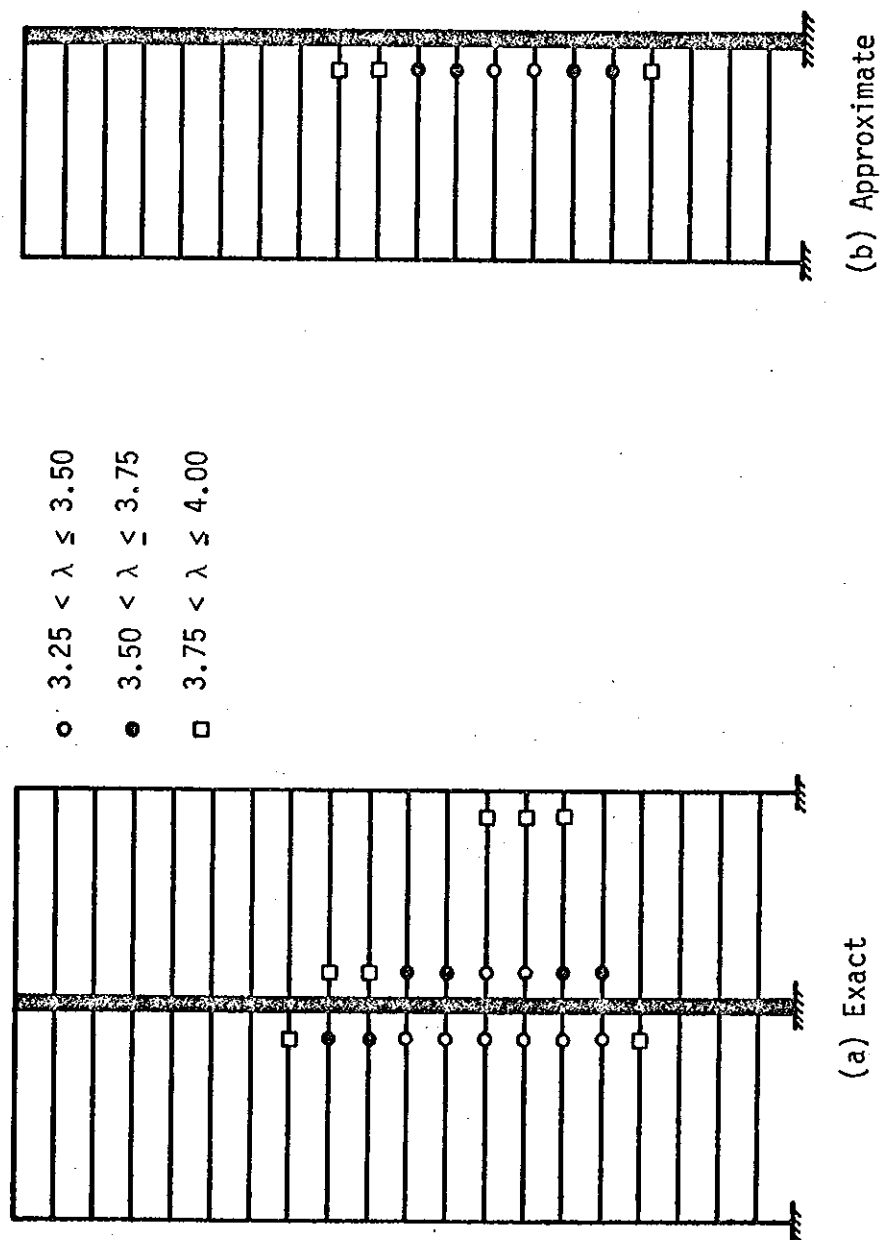


FIGURE 5.14  
 HINGE CONFIGURATIONS BY EXACT AND APPROXIMATE  
 ANALYSES AT  $\lambda = 4.00$

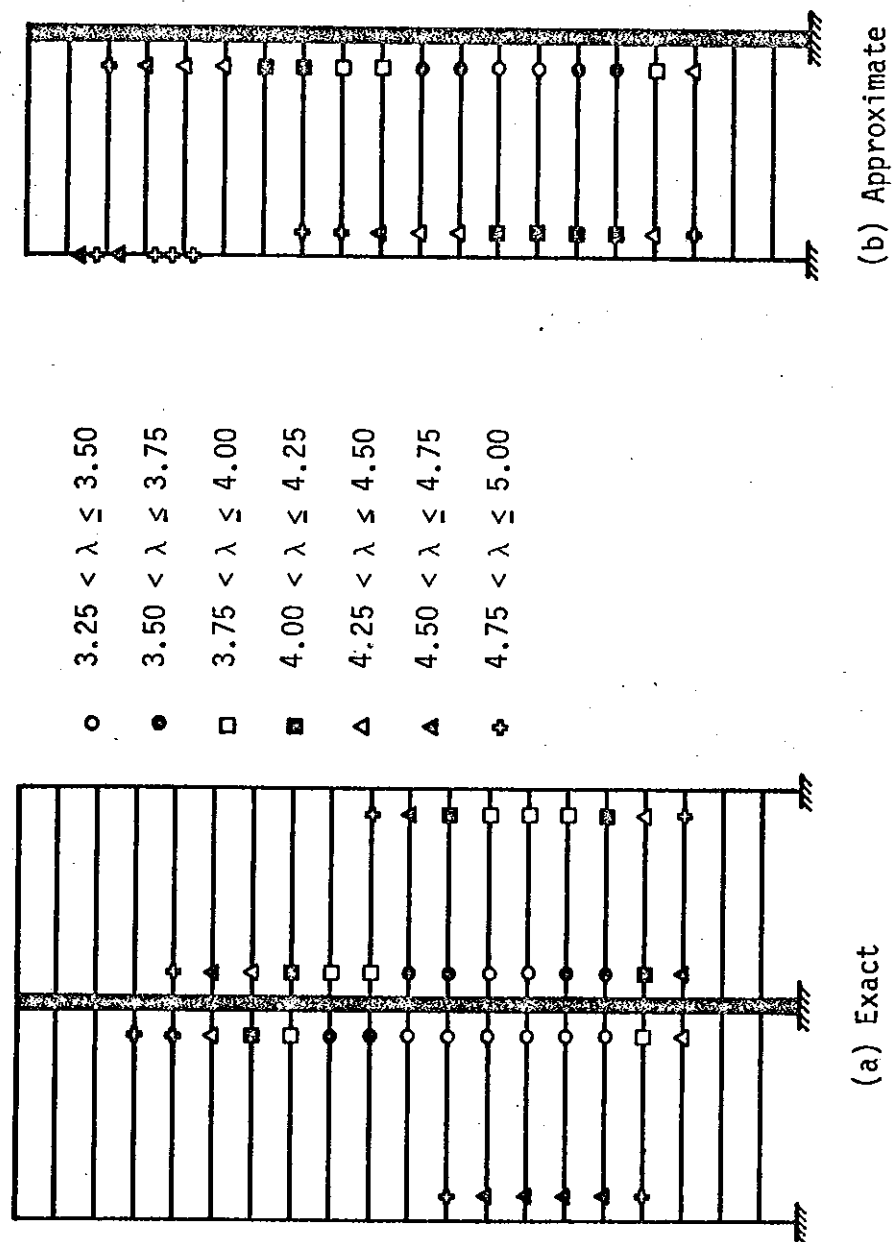


FIGURE 5.15  
HINGE CONFIGURATIONS BY EXACT AND APPROXIMATE  
ANALYSES AT  $\lambda = 5.00$

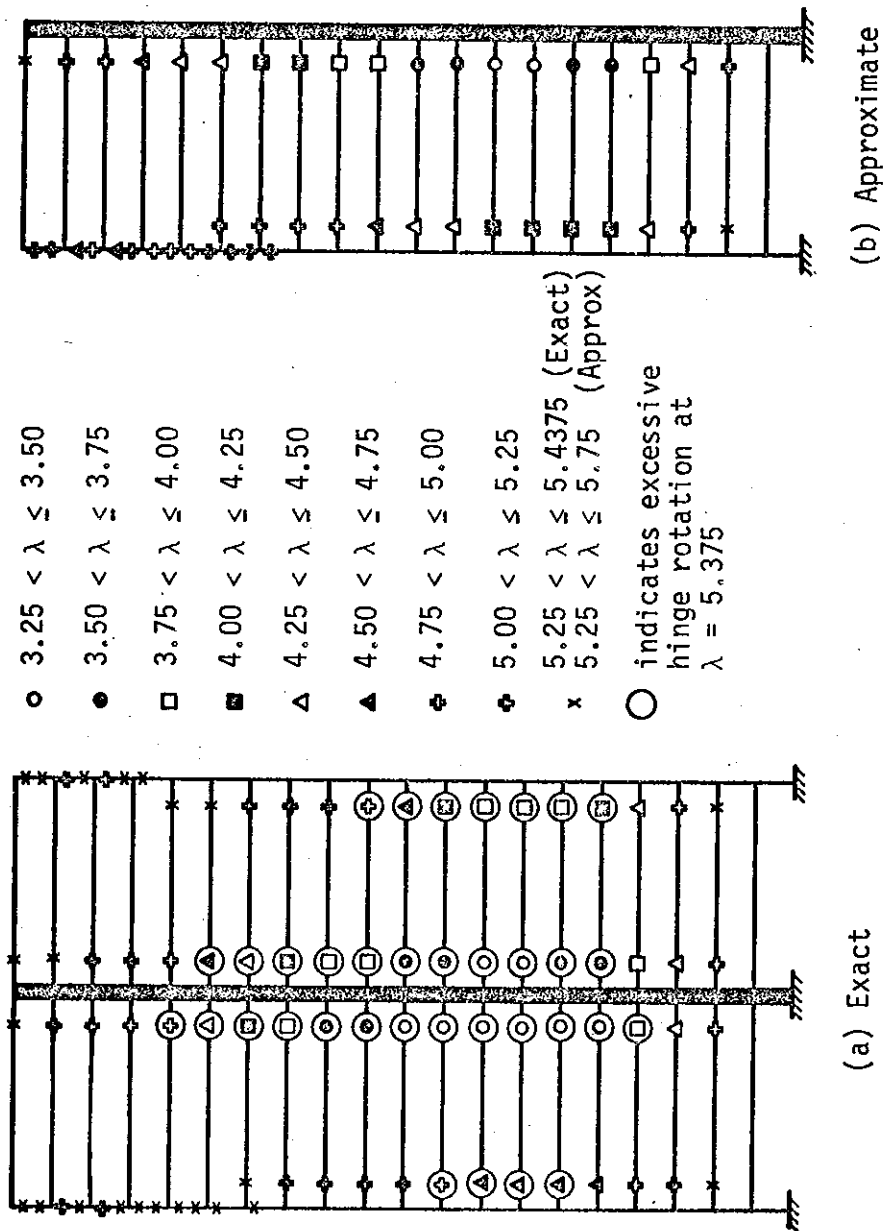


FIGURE 5.16  
 HINGE CONFIGURATIONS BY EXACT AND APPROXIMATE  
 ANALYSES AT LAST LOAD STAGES



difference between the two analyses is that due to axial compressive loads in the leeward column of the exact frame as a result of the lateral load. In accordance with the behavioural properties of the column sections discussed in CHAPTER III, the presence of this axial force increases the plastic moment capacity and the stiffness of the leeward columns somewhat. At a load level of  $\lambda = 5.00$ , the leeward column stiffnesses are increased by 10 to 15 percent. In the windward column, where column axial loads are tensile, the exact analysis assumes the same values of  $M_{pc}$  and  $EI$  as are used in the approximate analysis. It is unlikely that this slight increase in the stiffness of the leeward column could account for the difference in response in the inelastic range.

The more rapid reduction in stiffness predicted by the exact analysis may be partially caused by the  $P\Delta$  effect of the self-weight of the structure. However, with the deflected configuration predicted by the exact analysis at  $\lambda = 5.25$ , the  $P\Delta$  moment at the base of the structure is only 14,000 inch-kips compared to the applied lateral load moment of 727,000 inch-kips, assuming cantilever behaviour. This slight  $P\Delta$  effect is unlikely to account for the difference in the stiffness characteristics of the inelastic structures observed in the analyses.

Thus, the only explanation for the differences in inelastic response is the lumping procedure used in the approximate analysis. The validity of this lumping procedure has not yet been demonstrated for inelastic structures.

## CHAPTER VI

### DESCRIPTION OF THE INVESTIGATION OF BEHAVIOUR OF REINFORCED CONCRETE STRUCTURES

#### 6.1 Introduction

A twenty storey two bay reinforced concrete structure was chosen as the basis for the study of the behaviour of multi-storey reinforced concrete structures. The properties of this basic structure were adjusted to permit assessment of the effects of several variables on the behaviour of the structure. The variables considered in the study are:

1. axial shortening of columns and shear wall,
2. shear wall width,
3. column slenderness ratio,
4. shear wall stiffness.

In this chapter, the design and proportioning of the basic structure are described and the methods used to vary the parameters considered in the investigation are discussed. The results of the study will be presented in CHAPTER VII.

#### 6.2 Notation for the Structures

The behaviour of two series of structures, H and J, are examined in the study. To distinguish these structures, they will be referred to by means of a letter denoting the series and a number denoting the ratio  $\frac{K_w}{K_c}$ , of the EI of the shear wall to the sum of the EI values of the columns

in each storey of the structure. For example, H1 refers to a series H structure with  $\frac{K_w}{K_c} = 1$ . H1 is the basic structure for the study, and its properties are altered to produce other structures considered in the study. The difference between series H and J structures is detailed in SECTION 6.8, and the methods used to alter  $\frac{K_w}{K_c}$  are discussed in SECTION 6.9. Additional notation used to distinguish the structures considered in the studies of axial shortening and shear wall width effects is presented in SECTIONS 6.6 and 6.7.

### 6.3 Design of the Basic Multi-Storey Frame

Several authors have studied the effects of different member stiffness proportions on the behaviour of braced<sup>(18)</sup> and unbraced<sup>(33)</sup> multi-storey structures. However, since these investigations were limited to the elastic range of behaviour, strength was not considered in the proportioning. Hence, the structures used in the studies are of little value to this investigation of elastic-plastic behaviour where proper proportions for both strength and stiffness are necessary.

At the outset, it was intended that this investigation should compare the behaviour of braced and unbraced structures. A comparison of the braced and unbraced steel structures presented in a recent publication<sup>(1)</sup> indicates that there is a difference in the proportioning of braced and unbraced frames, particularly as regards the distribution of girder stiffness and strength throughout the height of the structure. A braced frame requires almost constant girder sizes in all floors whereas the unbraced frame requires stiffer girders in the lower floors than in the upper floors. Since one object of the investigation was to study the transition from un-

braced to braced structures, the basic structure was designed as an unbraced frame. To simulate the transition to the braced structure, the stiffness of the shear wall was increased with no alterations being made in the frame portion of the structure. The alternative procedure to conduct a comparative study, of course, would have been to design the basic structure as a braced frame and to simulate the unbraced structure by decreasing the shear wall stiffness. However, studies of the behaviour indicated that the unbraced structure was sensitive to departures from the ideal member proportioning while the braced structure was relatively insensitive. Subsequent analyses indicated that the use of unbraced frame proportions in the braced structure did not lead to unusual or early distress in the structure.

A symmetrical twenty storey two bay reinforced concrete frame was proportioned by ultimate strength design methods. The geometry, loading configuration and material properties of this basic structure are shown in FIGURE 6.1. The values of working loads presented in TABLE 6.1 represent reasonable values of design loads assuming a twenty foot spacing of bents in the type of structure considered. Member sizes were estimated, and  $\frac{K_w}{K_c}$  was assumed to be 1.0 in all storeys of the structure.

	Roof	Other Floors
Wind	2.4 kips	4.8 kips
Dead*	1.6 k/ft	2.0 k/ft
Live	0.6 k/ft	2.0 k/ft
D(exterior wall)	12 kips/storey	

\*Does not include member self-weight, also considered as dead load

TABLE 6.1  
WORKING LOAD VALUES FOR FRAME H1

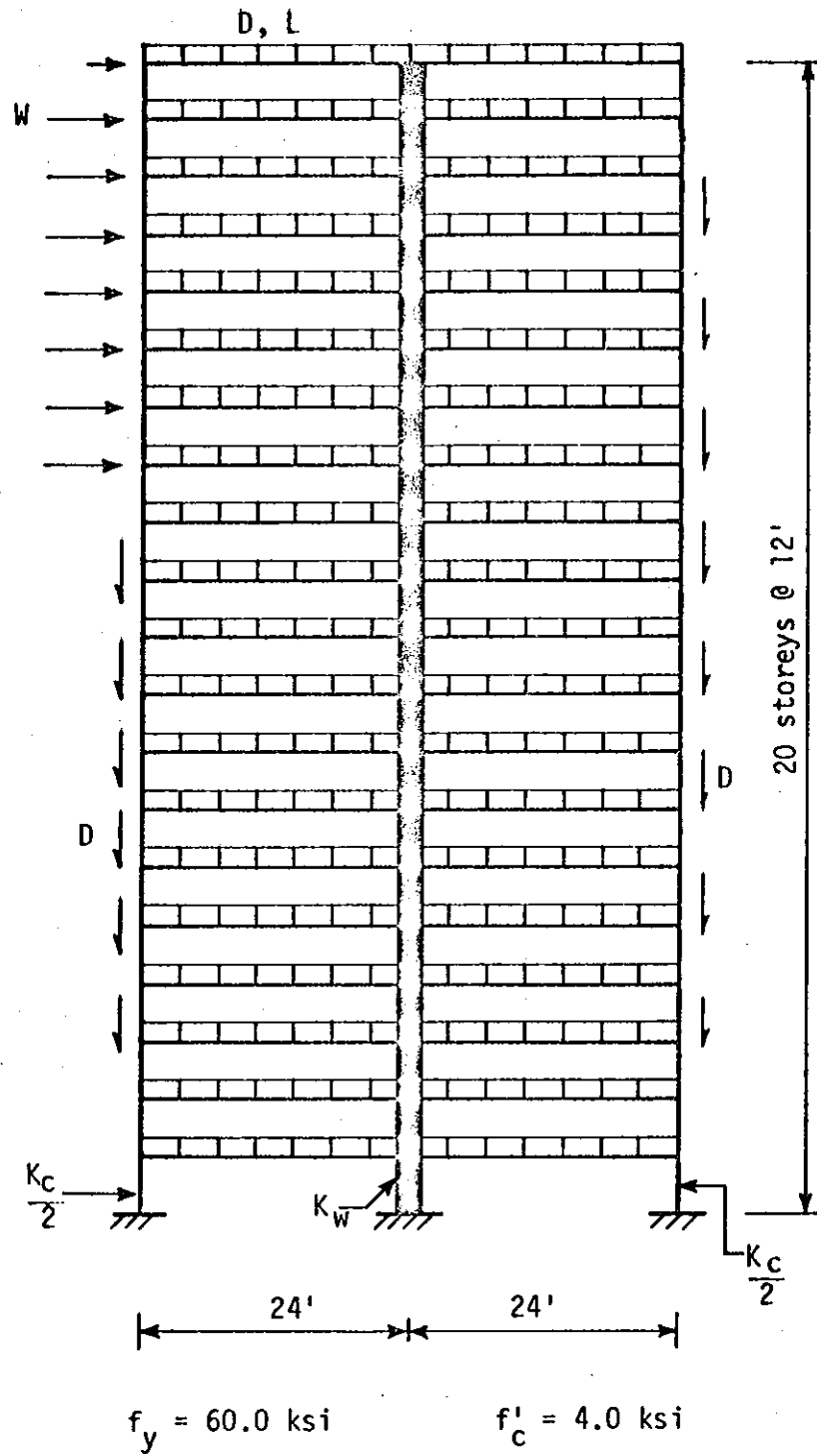


FIGURE 6.1

ELEVATION OF FRAME H1

Following normal design practice, the axial loads used in the design of the columns were derived by a simple gravity load analysis based on a tributary area concept. Bending moment distribution, performed on the equivalent frame model described in Section 905 of the ACI Building Code, furnished maximum column and girder moment values. The portal method was used to derive values of wind load moments. In accordance with the ACI Building Code requirements for ultimate strength design, the forces derived from the elastic analysis were factored to  $1.25 (D + L + W)$  and  $1.5D + 1.8L$ , where D, L and W represent working values for dead, live and wind loads respectively. With these factored values of ultimate load capacities, the member sections were proportioned using ACI ultimate strength design handbooks<sup>(44,45)</sup>, assuming material understrength factors  $\phi$  equal to 1.0 in all members. Since the EI values for these sections differed from the initial estimates, the process was repeated to obtain a final "office" design.

This design procedure was selected because it is reasonably similar to the normal building design procedure. The structure designed in this manner was altered somewhat, as described in SECTIONS 6.3.1 and 6.3.2, to derive the final H1 structure considered in the study.

#### 6.3.1 Section Properties

In the design of the structure, member section properties were chosen to fit within the bounds prescribed by the ACI Building Code. However, it was found that the range of choice of properties in any member permitted significant variations in EI, resulting in noticeable irregularities in the member EI distributions in the structure. For consistency and to

eliminate possible relative weak spots in the structure, all members were designed with similar non-dimensionalized section properties. All column and shear wall sections were designed in accordance with the requirements shown in FIGURE 6.2, and all girder sections have properties similar to those shown in FIGURE 6.3.

No attempt was made to consider the variation in plastic moment capacity along the length of the girders, and the values of TPRATE and TPRATM were set at 1.00. Moreover, details of girder reinforcement placement were neglected, and all girder sections were considered to be capable of developing  $M_p$  regardless of the sense of the bending moment.

#### 6.3.2 Member Section Stiffness Distribution

Again for the sake of regularity in the structure, the EI distributions resulting from the design described in SECTION 6.2 were smoothed to fit the distributions shown in FIGURES 6.4 and 6.5. The girder stiffness distribution was found to be essentially linear. The column stiffness distribution, however, was idealized as a two stage linear relationship.

Employing the section properties discussed in SECTION 6.2.1 to fit these stiffness distributions, the resultant girder sizes varied from 9.76 inches wide by 21.52 inches deep at the roof to 13.80 by 29.60 inches at the ground floor. The exterior columns varied in size from 8.37 inches square in the top storey to 21.64 inches square in the bottom storey. The "shear wall" at the centre of the unbraced structure H1 had an EI value twice that of the exterior column and varied in size from 9.54 inches square in the top storey to 25.70 inches square at the base.

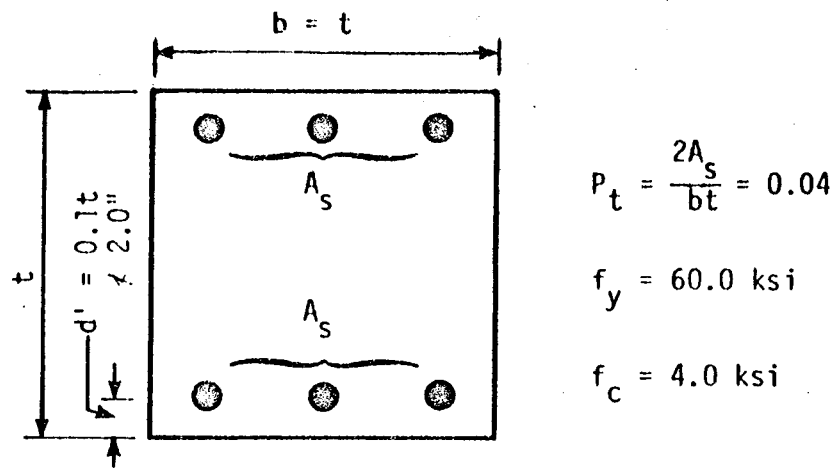


FIGURE 6.2

COLUMN AND SHEAR WALL SECTION  
PROPERTIES IN STRUCTURES STUDIED

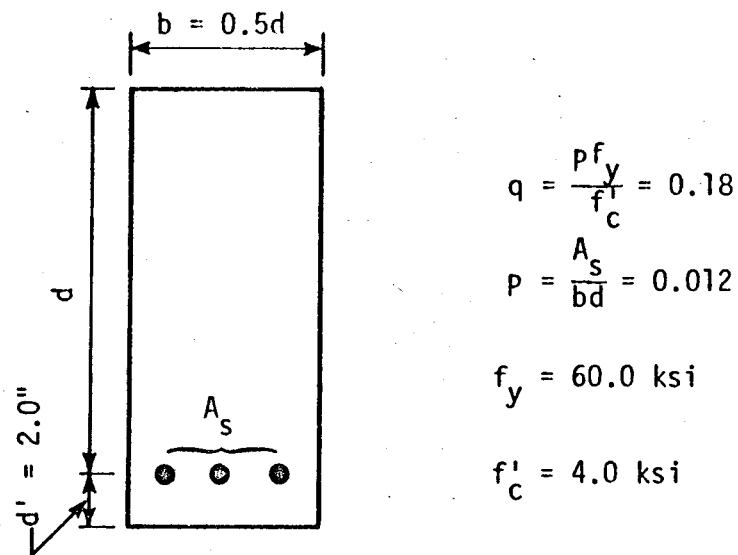


FIGURE 6.3

GIRDER SECTION PROPERTIES  
IN STRUCTURES STUDIED



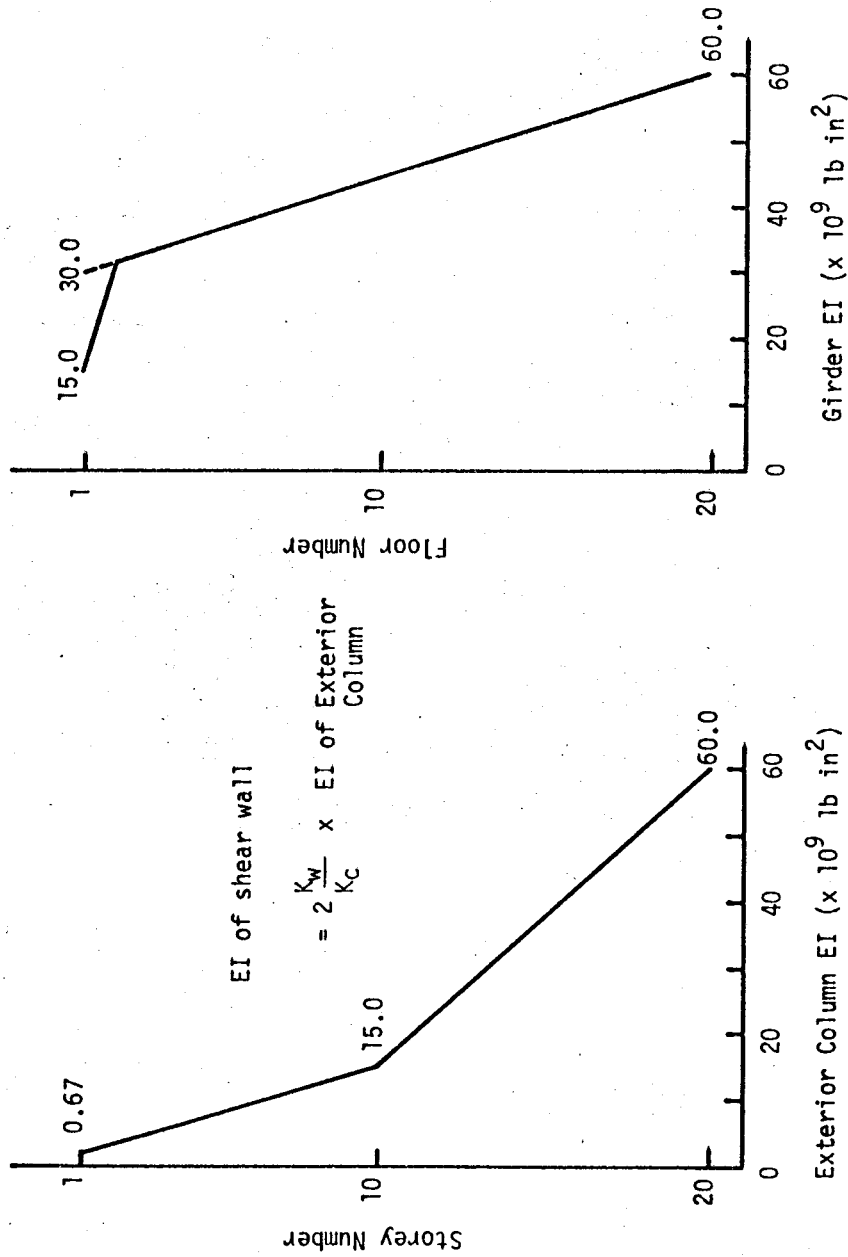


FIGURE 6.4

DISTRIBUTION OF COLUMN AND  
SHEAR WALL STIFFNESSES IN  
FRAME H1

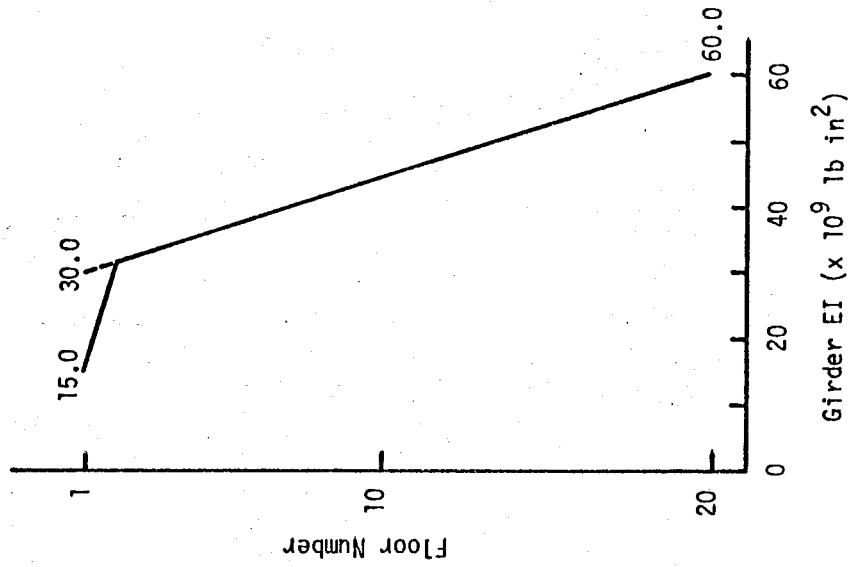


FIGURE 6.5

DISTRIBUTION OF GIRDER  
STIFFNESS VALUES IN  
FRAME H1

### 6.3.3 Verification of the Design of Frame H1

Since the structure designed by ultimate strength methods as described in SECTION 6.3 was revised somewhat to fit the section properties and predetermined stiffness distributions discussed in SECTIONS 6.3.1 and 6.3.2, it was necessary to check that the revised structure H1 continued to satisfy the combined strength and stiffness requirements. Second order elastic-plastic analyses were conducted using two different cases of proportional loading.

With loading according to  $\lambda(D + L + W)$ , the analysis yielded a load-deformation plot as shown in FIGURE 6.6. The order of plastic hinge formation appears in FIGURE 6.7. The first plastic hinges formed in the girders in the lower floors of the structure at  $1.10 < \lambda \leq 1.20$ . The structure failed by the formation of a joint mechanism on the leeward side of the frame at  $1.3375 < \lambda \leq 1.34375$ . For this loading case, the ACI Building Code would require a load factor  $\lambda = 1.25$ .

The ratio of total sway deflection at the roof to the total height of the structure was  $1/300$  at  $\lambda = 1.0$ . The first order analysis conducted later indicated a ratio of working load sway deflection to height of  $1/350$ . A recent ACI Committee report<sup>(46)</sup> suggested that this value should be limited to  $1/500$ . In designing this structure, the ACI material understrength factors,  $\phi$ , were set at  $1.0$ . If these factors had been used, the deflections of the structure would have been reduced.

With loading according to  $\lambda_G(1.5D + 1.8L + 0.1W)$ , the structure failed at  $1.019 < \lambda_G \leq 1.025$  by instability of several storeys. Crushing of the shear wall at the base was also noted at this stage of loading.

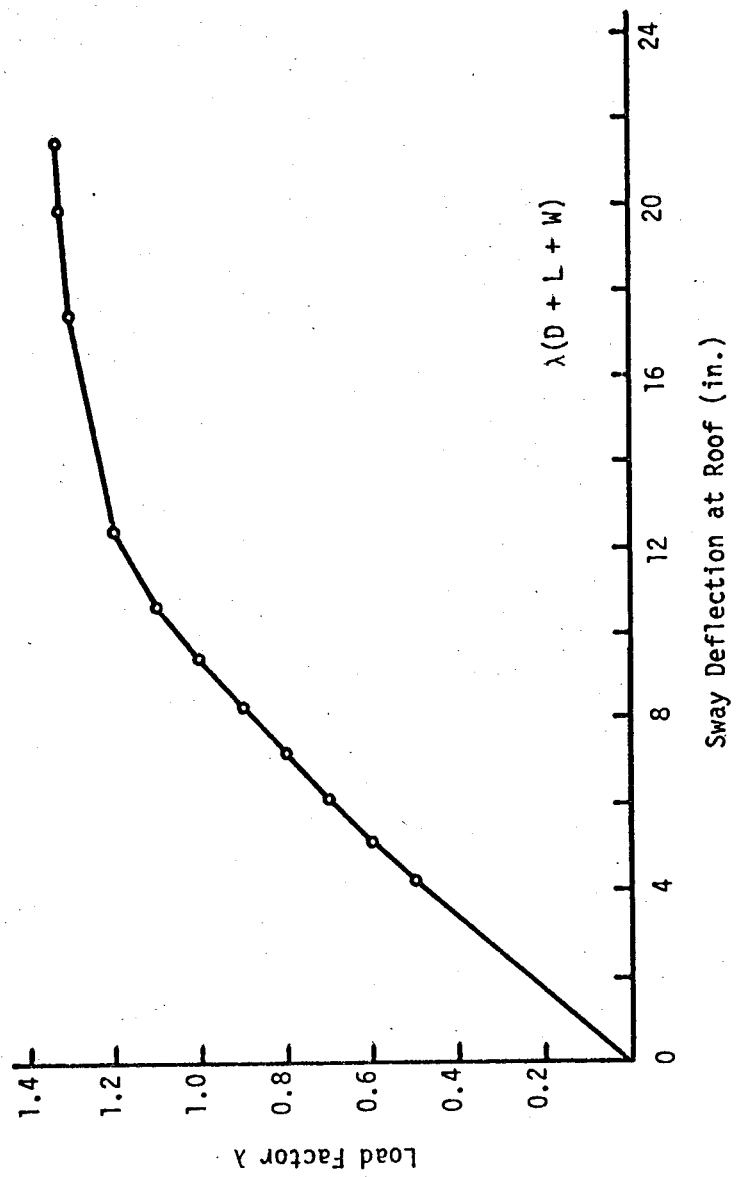


FIGURE 6.6  
LOAD-DEFORMATION RELATIONSHIP FOR H1

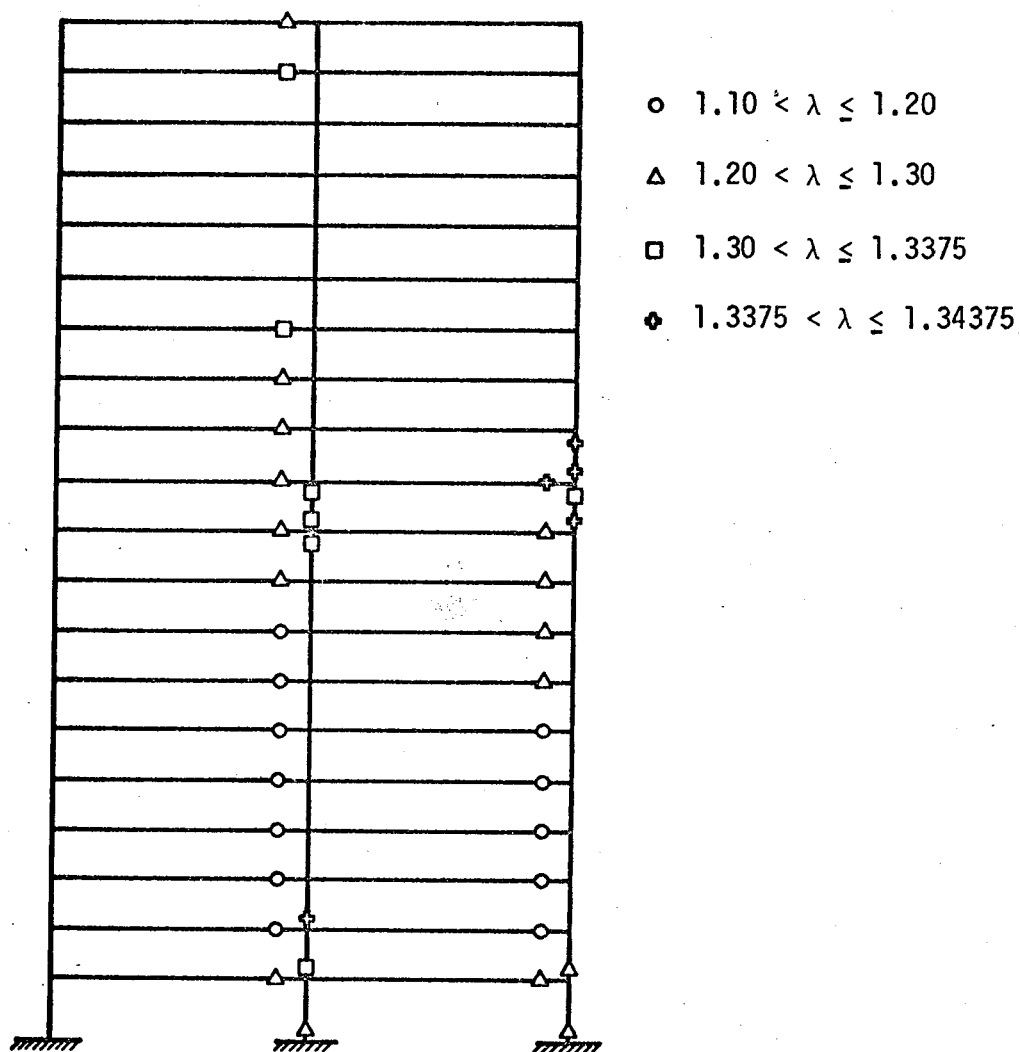


FIGURE 6.7

PROPAGATION OF PLASTIC HINGES IN H1

The first plastic hinges formed at  $0.8 < \lambda_G \leq 0.9$  in the girders at the top of the structure. Fourteen girder hinges had formed at  $\lambda_G = 1.025$ .

Thus, the analyses indicate that frame H1 is a "weak girder-strong column" structure which satisfies the building code requirements for adequate strength and stiffness except that the lateral deflections are on the large side.

#### 6.4 Scope of the Investigation

The investigation reported in this thesis is a study of the effects of several variables on the behaviour of braced and unbraced multi-storey structures. These variables include:

1. axial shortening of columns and shear wall,
2. shear wall width,
3. column slenderness ratio,
4. shear wall stiffness.

To study the effects of these variables, appropriate adjustments were made to the basic frame H1. Early in the investigation, it became obvious that it would be necessary to separate the effects of these variables for a meaningful comparison of results. The methods used to isolate these variables and the approaches adopted for the study are discussed in the remaining sections of this chapter.

#### 6.5 Details of the Analyses

In all analyses the loading was proportionally increased until failure occurred. Results will be reported in terms of the load factor  $\lambda$  in the expression  $\lambda(D + L + W)$  where D, L and W represent the working load

values of dead, live and wind loads presented in TABLE 6.1. Since the primary purpose of a shear wall is to resist lateral loads, gravity loading in the absence of wind loads was not considered.

For all analyses, the initial value of  $\lambda$  was set at 0.50 and the initial size of the increment at 0.10. The convergence limits ACCURD and ACCURP were set at 0.005 and LIMITD and LIMITP at 500 and 200 cycles respectively. The effects of these limits on the solution have been discussed in SECTION 4.8.

Unless otherwise specified, all analyses considered the axial shortening of the shear wall and columns and the effects of finite shear wall width.

Second order elastic-plastic analyses were performed using the computer programme presented in APPENDIX D. In these analyses, the effects of axial loads were considered by incorporating the  $P\Delta$  effect, the stability functions C and S in the shear wall and columns, and the M-P- $\phi$  relationship for shear wall and column sections.

The computer programme was revised to perform a first order elastic analysis which, of course, neglected the development of plastic hinges. In this analysis, the effects of axial loads on the M-P- $\phi$  relationships for the wall and column sections was included, but  $P\Delta$  effects were neglected and C and S were set at 4.0 and 2.0 respectively.

## 6.6 Study of the Effects of Axial Shortening

Two structures, H1 and H50, were analyzed to study the effects of relative column to shear wall axial shortening. Second order elastic-plastic analyses were conducted on both structures considering the effects

of axial shortening based on the shear wall area in the basic H1 structure. Both structures were also analyzed neglecting axial shortening completely. The structures in which axial shortening is neglected are referred to as H1-NA and H50-NA.

In addition, H1 was analyzed with an artificially doubled shear wall area. This structure is referred to as H1-2A. The wall area was doubled in computing self-weight and axial shortening, but the stiffness and moment capacity of the wall remained unchanged. Essentially, this resulted in a halving of the vertical deformations of all shear wall joints. In a similar manner, H50-4A was considered with the shear wall area artificially quadrupled.

In all cases, the finite width of the shear wall was kept constant at the value in the basic H1 structure.

#### 6.7 Study of the Effects of Finite Shear Wall Width

To examine the significance of the finite shear wall width on the behaviour, the properties of H1 and H50 were again adjusted. In addition to the normal analyses of H1 and H50 considering unit shear wall width, analyses were performed on both H1-0W and H50-0W neglecting finite shear wall width completely. Both structures were also considered assuming artificially incremented shear wall widths. In these analyses, the finite wall width alone was changed, and no other properties of the structure were altered. Since the girder loads are uniformly distributed, the total gravity load acting on the structure is a function of the finite shear wall width. To isolate the effects of finite wall width and minimize the difference in  $P\Delta$  effects in the structure resulting from differences in  $P$ , the

uniformly distributed load values were adjusted to provide the same total girder load regardless of the finite shear wall width considered. Using this approach, H1-2W was analyzed with an artificially doubled shear wall width and H50-4W with an artificially quadrupled shear wall width.

#### 6.8 Study of the Effects of Slenderness

To assess the effects of slenderness on the behaviour of multi-storey structures, the series J structures were studied. The only difference between the structures of the H and J series is the storey height. As is shown in FIGURE 6.1, series H structures have a 12 foot storey height. In series J structures, the storey height is increased to 18 feet. The section properties of all members are identical in both series of structures. The applied gravity loads are the same, but in keeping with the  $\frac{3}{2}$  ratio of storey heights, the working lateral load values for series J structures are reduced to  $\frac{2}{3}$  of those shown in TABLE 6.1 for series H structures.

#### 6.9 Study of the Effects of Shear Wall Stiffness

The study of the effects of relative shear wall stiffness  $\frac{K_w}{K_c}$  on the behaviour of series H and J structures involved increasing the shear wall stiffness in the unbraced frames H1 and J1 to simulate braced structures.

Studies of the effects of axial shortening and finite wall width indicated that changes in either could significantly influence the behaviour of the structure. Hence, to isolate the effects of variation of shear wall stiffness, the wall stiffness was assumed to increase without changing either the shear wall area or finite width. To augment the shear wall



stiffness, the plastic moment capacity and EI of the shear wall section were increased by the appropriate value of  $\frac{K_W}{K_C}$ , as shown in FIGURE 6.8. Physically this could be accomplished simply by increasing the shear wall section breadth  $b$  by a factor of  $\frac{K_W}{K_C}$ . No changes were made in the basic frame portion of H1 or J1, and the analysis was carried out assuming no increase in shear wall area or finite width.

The only difference between H1 and H50 is that the plastic moment capacity and EI value of any shear wall section in H50 are fifty times those at a comparable section in H1. Thus, the braced structure H50 consists of a frame originally designed as an unbraced frame and a shear wall with the same finite width and area as the "shear wall" in the unbraced structure H1 but EI and  $M_{pc}$  values fifty times as high.

The reasons for using the same frame throughout the study were discussed in SECTION 6.3. While the assumptions regarding shear wall properties may not be consistent with the variety of wall section shapes possible in a braced structure, no clearcut guidelines for estimating the rate of increase of shear wall area and finite width as stiffness increases are available. Since it was desired to isolate the effects of the variables in comparing the behaviour of braced and unbraced structures, the assumptions are justifiable.

For the investigation, series H and J structures with values of  $\frac{K_W}{K_C}$  equal to 1, 2, 6, 12, 20 and 50 were studied. H50 is considered to be essentially a braced structure, with other values of  $\frac{K_W}{K_C}$  representing intermediate wall stiffnesses. First order elastic and second order elastic-plastic analyses were conducted on each of these structures.

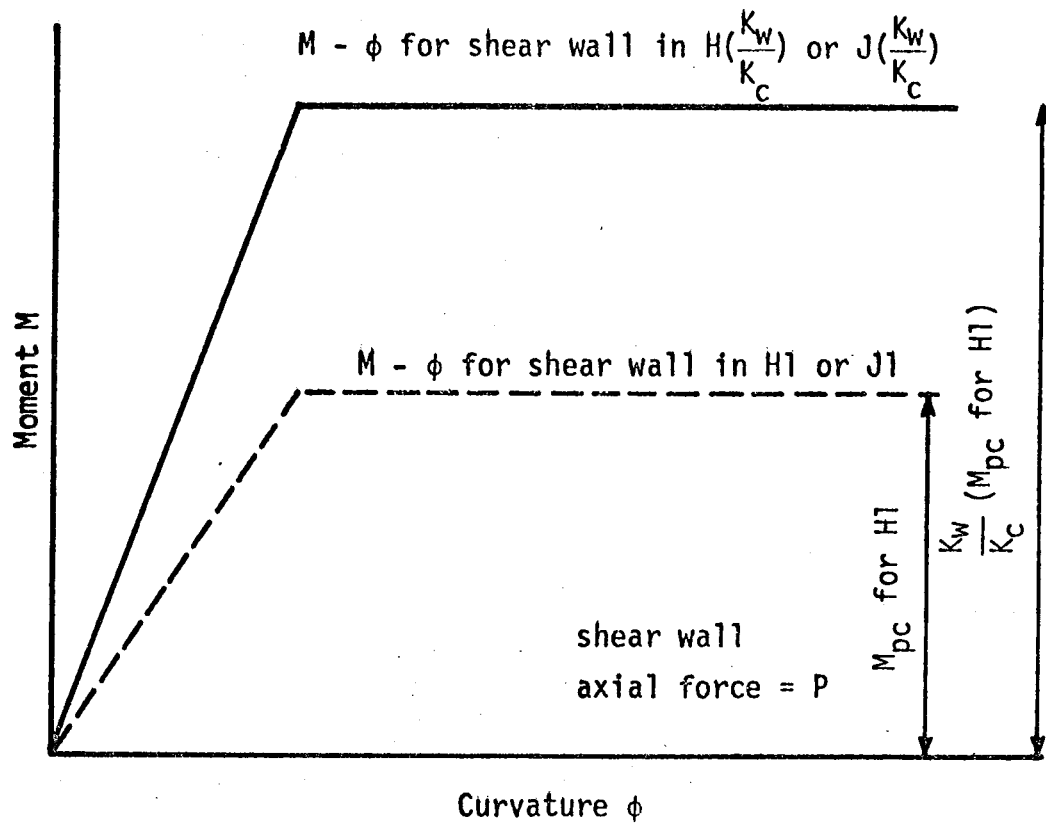


FIGURE 6.8  
METHOD OF INCREASING SHEAR WALL  
SECTION STIFFNESS IN SERIES H AND J  
STRUCTURES

## CHAPTER VII

### PRESENTATION AND DISCUSSION OF RESULTS

#### 7.1 Introduction

The results of the investigation of the two series of reinforced concrete structures described in CHAPTER VI are presented in this chapter. The implications of these results in the design and analysis of reinforced concrete shear wall-frame structures are discussed.

Because of the copious quantity of behavioural data derived from the computer analyses, it is impossible to include all the results in this thesis. For each structure analyzed, the computer programme provides information regarding the load-deformation relationship, failure load, mode of failure, plastic hinge locations, the nature of load-sharing resulting from interaction of the shear wall and frame, the occurrence of excessive rotations at plastic hinges, and the distribution of internal forces in the structure. Only those results pertinent to the discussion are presented here, and of necessity, much is presented in graphical form.

#### 7.2 General Discussion of the Behaviour and Modes of Failure of the Structures Studied

Since it is impossible to present the complete results of the analyses, the behaviour predicted by the analyses will be described briefly as an introduction to the discussion of the effects of variables presented in succeeding sections.

The structures, even in the more slender J series, behaved con-

sistently as weak girder, strong column structures. Before failure occurred, plastic hinges formed in the leeward column of all structures except the slender, lightly braced J1 and J2 structures. H1 was the only structure to form plastic hinges in the "shear wall" before failure. FIGURES 7.1 and 7.2 indicate the location of plastic hinges in the limiting series H and J structures at various stages of loading. Details of failure conditions in all the structures studied are summarized in TABLES 7.1 and 7.2 for the loading case  $\lambda(D + L + W)$ .

Since the ACI material understrength safety parameters,  $\phi$ , were taken equal to 1.0 in proportioning the frame, actual structures should statistically have failure load factors in excess of those reported here.

As might be expected, excessive plastic hinge rotations were detected in the structures which displayed significant deformation capacity at failure. Excessive rotations were first detected at loads close to the failure loading condition, generally at plastic hinges which formed early in the loading history. The hinges which experienced excessive rotation in H1 and J1 are shown in FIGURE 7.1. The first evidence of excessive hinge rotation in H1 occurred at  $\lambda = 1.30$  and in J1 at  $\lambda = 1.1375$ . As the wall stiffness was increased, failure deformations were reduced and the number of incidents of excessive hinge rotation decreased. At failure, J20 showed two cases of excessive rotation and H6 only one. No excessive hinge rotations were found in H50 or J50.

As is shown in TABLE 7.1, the majority of these structures failed by the formation of a joint mechanism. The location of this critical joint was consistently in the leeward column near the mid-height of the structure, as shown in FIGURE 7.1(a). It is quite probable that this weak spot in the

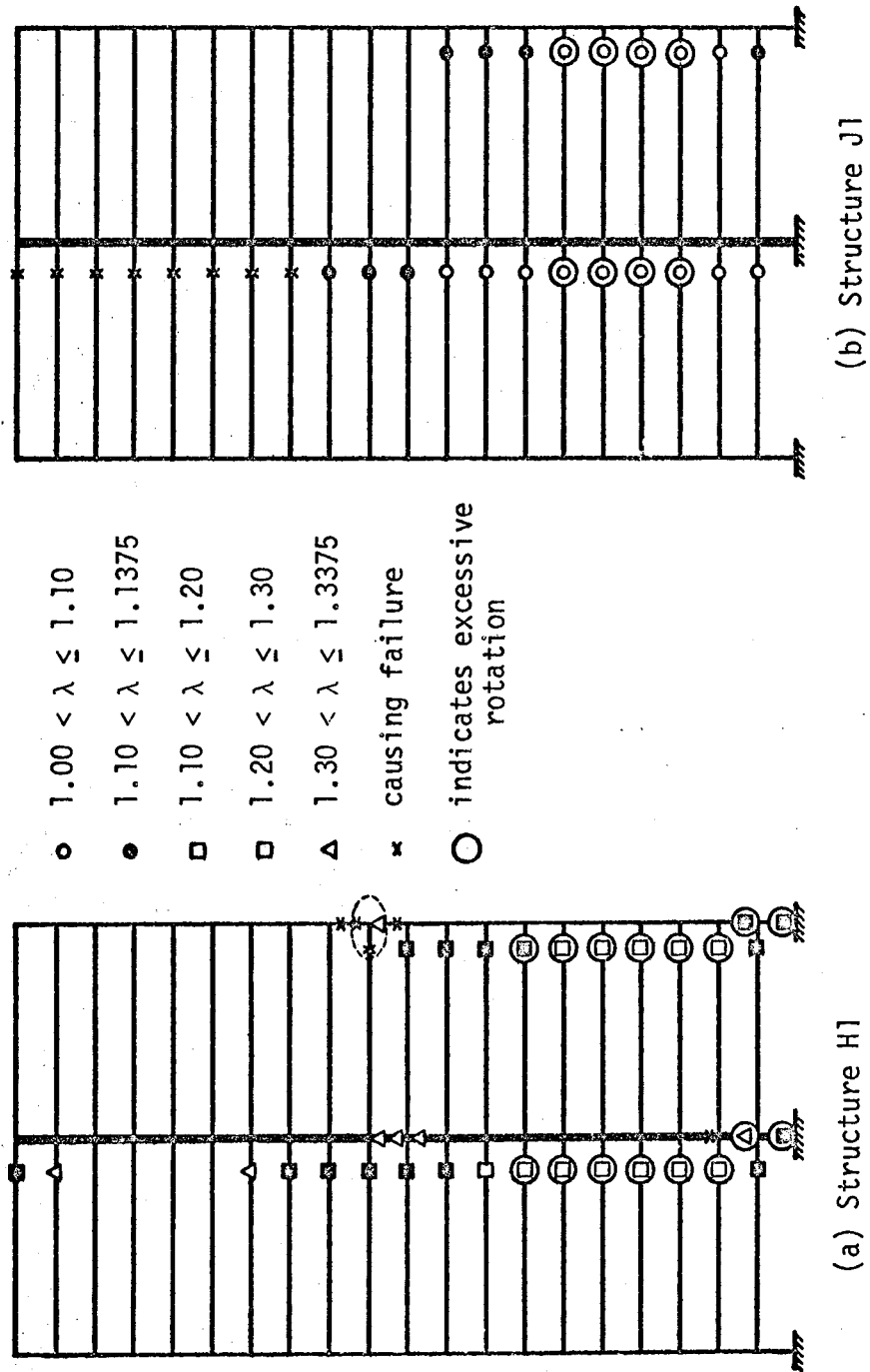


FIGURE 7.1

HINGE PROPAGATION IN STRUCTURES H1 AND J1

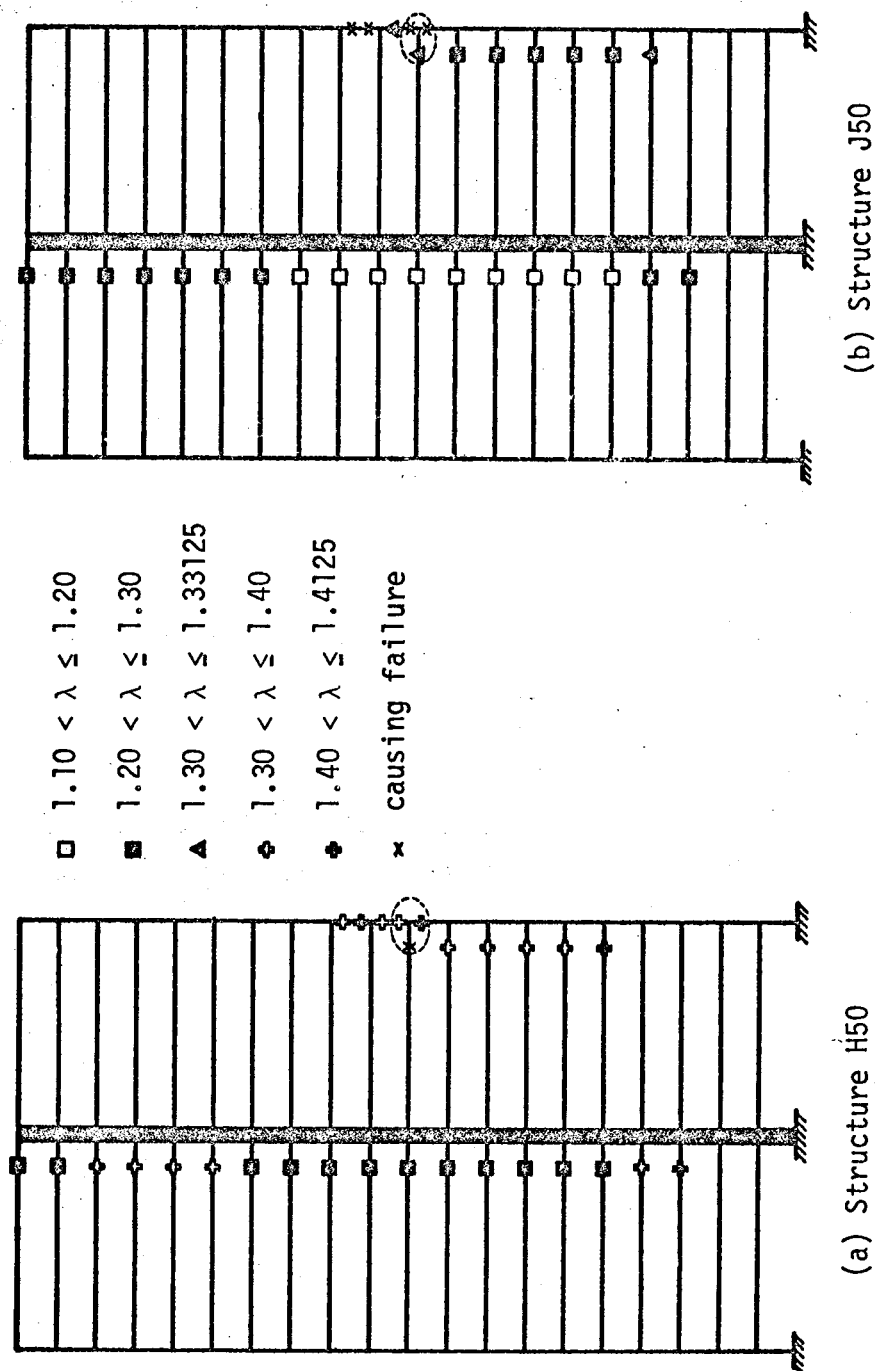


FIGURE 7.2

HINGE PROPAGATION IN STRUCTURES H50 AND J50

Structure	Failure load $\lambda$ interval	Number of plastic hinges detected at these $\lambda$ values	Roof sway deflection at last stable $\lambda$ value (in.)	$\lambda$ value at which excessive hinge rotation first noted	Mode of failure*
H1	1.3375-1.34375	34 - 38	21.53	1.30	joint mechanism at (10,3)
H2	1.36875-1.375	36 - 38	19.47	1.35	joint mechanism at (10,3)
H6	1.375-1.38125	35-36	16.11	1.375	joint mechanism at (11,3)
H12	1.375-1.38125	31 - 33	13.23	None	joint mechanism at (11,3)
H20	1.38125-1.3875	30 - 32	12.16	None	joint mechanism at (11,3)
H50	1.41875-1.425	28 - 29	11.13	None	joint mechanism at (11,3)
J1	1.14375-1.15	21 - 29	34.34	1.1375	drop in equilibrium sway deflection of top 7 storeys
J2	1.14375-1.15	18 - 28	24.59	None	drop in equilibrium sway deflection of storeys 2 to 8
J6	1.25-1.25625	28 - 32	32.19	1.25	drop in equilibrium sway deflection of storeys 1 to 4 and 17 to 20
J12	1.28125-1.2875	31 - 34	30.71	1.275	joint mechanism at (10,3)
J20	1.30313-1.30625	31 - 34	26.96	1.30	joint mechanism at (11,3)
J50	1.325-1.3375	27 - 31	23.00	None	joint mechanism at (11,3)

\*Storeys are numbered from the roof. Coordinates refer to storey and column number, respectively, column 3 being on the leeward side.

TABLE 7.1

Structure	Failure load $\lambda$ interval	Number of plastic hinges detected at these $\lambda$ values	Roof sway deflection at last stable $\lambda$ value (in.)	$\lambda$ value at which excessive hinge rotation first noted	Mode of failure*
<u>Effects of Axial Shortening</u>					
H1-NA	1.3625-1.3656	44 - 50	20.51	1.35	deformations would not converge after 500 cycles
H1-2A	1.3219-1.325	36 - 48	23.61	1.30	drop in equilibrium sway de- flections of storeys 9 to 19
H50-NA	1.375-1.38125	24 - 24	9.13	None	drop in equilibrium sway de- flections of storeys 18 and 19
H50-4A	1.525-1.5375	32 - 37	21.00	1.20	joint mechanism at (12,3)
<u>Effects of Finite Width of Shear Wall</u>					
H1-0W	1.275-1.28125	33 - 41	24.34	1.25	deformations would not converge after 500 cycles
H1-2W	1.3875-1.39375	36 - 54	18.49	1.3875	sway mechanism in storey 10
H50-0W	1.35-1.35625	28 - 29	11.57	None	joint mechanism at (11,3)
H50-4W	1.50-1.50624	29 - 35	9.20	1.50	joint mechanism at (15,3)

\*Storeys are numbered from the roof.

TABLE 7.2

FAILURE CONDITIONS OF STRUCTURES USED TO STUDY THE EFFECTS OF VARIABLES



structure was the result of the abrupt change in the distribution of the column stiffness shown in FIGURE 6.4.

The frequency of joint mechanism failures in these structures suggests that this type of failure should be studied more fully. The formation of a joint mechanism is a mathematical possibility in this analysis because of the elastic-plastic section response characteristics assumed. Joint mechanisms resulted from reductions in the column  $M_{pc}$  value due to changes in axial load after the end of the girder had hinged. While the assumption of elastic-plastic section response is realistic for girders and lightly loaded columns, it is not as good for heavily loaded columns in which "yielding" is a much less sudden occurrence. For this reason, the actual behaviour of a joint, where a joint mechanism is indicated, would be quite different from that considered in the analysis.

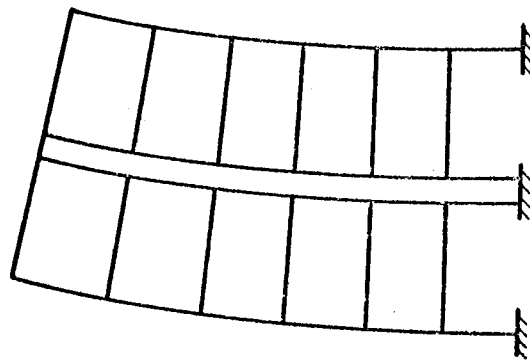
If a joint mechanism were to form in an actual structure, the condition would probably be replaced by indications of rotational distress at the joint, or the hinge would stiffen due to strain-hardening in the girders. With the advent of limit design procedures for reinforced concrete, a good deal of work has been done to develop methods of increasing the rotation capacity of a member while retaining the essential strength properties. If joints can be designed to have the required ductility, conditions of serviceability could be neglected in the inelastic analysis of strength and stiffness properties, and the formation of an isolated joint mechanism in a structure should not be deemed to constitute failure of the entire structure provided the rest of the structure has not formed a mechanism. As was mentioned in SECTION 4.7, the formation of a joint mechanism

need not lead to a breakdown of the solution, and appropriate adjustments could be made in the computer programme presented in APPENDIX D to accommodate a joint mechanism condition. With these considerations in mind, it would be advisable to eliminate the formation of a joint mechanism as a primary mode of failure in future applications of this analysis. As with beam mechanisms, the occurrence of a joint mechanism could be recorded in the course of the analysis and appropriate remedial action taken in the design of the structure.

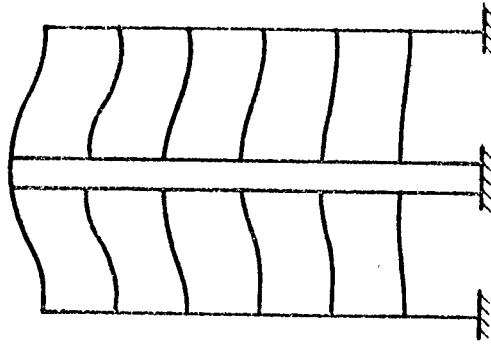
For similar reasons, excessive hinge rotations of the magnitudes recorded by the computer programme need not impair the strength properties of the structure if the structure is detailed correctly. In the load-deflection curves presented in this chapter, the portion of the curve following the initial detection of excessive hinge rotations is shown by dashed lines to indicate the need for remedial detailing of the structure to permit attainment of the ultimate load-carrying capacity of the structure.

### 7.3 The Effects of Axial Shortening

The relative axial shortening of the columns and shear wall in a structure can influence its behaviour in two principal manners. These are indicated in exaggerated form in FIGURE 7.3. FIGURE 7.3(a) illustrates the effects of axial shortening of the leeward column stack relative to the windward column stack, resulting in significant sway deflections when the geometrical compatibility conditions are imposed in the solution. The relative column shortening, of course, results from the application of lateral loads, the overturning effects of which produce higher axial forces in the leeward column than in the windward column. The configuration in



(a) Differential Shortening of  
Windward and Leeward Columns



(b) Differential Shortening of  
Shear Wall and Columns

FIGURE 7.3

TYPES OF DIFFERENTIAL AXIAL SHORTENING IN  
MULTI-STOREY STRUCTURES

FIGURE 7.3(b) illustrates the axial shortening effects in a structure where the area of the shear wall is significantly larger relative to its axial load than are the columns. Under gravity loading, the columns shorten significantly more than the shear wall leading to settlement moments in beams at the top of the structure.

The effects of these two variations of axial shortening cannot be separated completely in this study. However, the investigation discussed in SECTION 6.6 was set up to permit some differentiation between the effects. The basic structure was designed to minimize the effects of axial shortening of the type shown in FIGURE 7.3(b). Consequently, comparison of the case where axial shortening effects were neglected with the case where axial shortening was considered will permit some assessment of the effects of axial shortening of the type depicted in FIGURE 7.3(a). Moreover, a comparison of the behaviour of the structure with normal shear wall area with the case where the wall area was artificially increased will provide some indication of the effects of the type of axial shortening shown in FIGURE 7.3(b).

The load-deflection results from the second order elastic-plastic analyses discussed in SECTION 6.6 are presented in FIGURES 7.4 and 7.5.

In the case of the unbraced frame H1, when axial shortening of the wall and columns was neglected, the lateral deflection at the top of the frame at working load values was underestimated by 18 percent and the failure load was overestimated by about 2 percent. On the other hand, when the wall area was artificially doubled in computing axial shortening and self-weight, the stiffness of the structure remained essentially unchanged

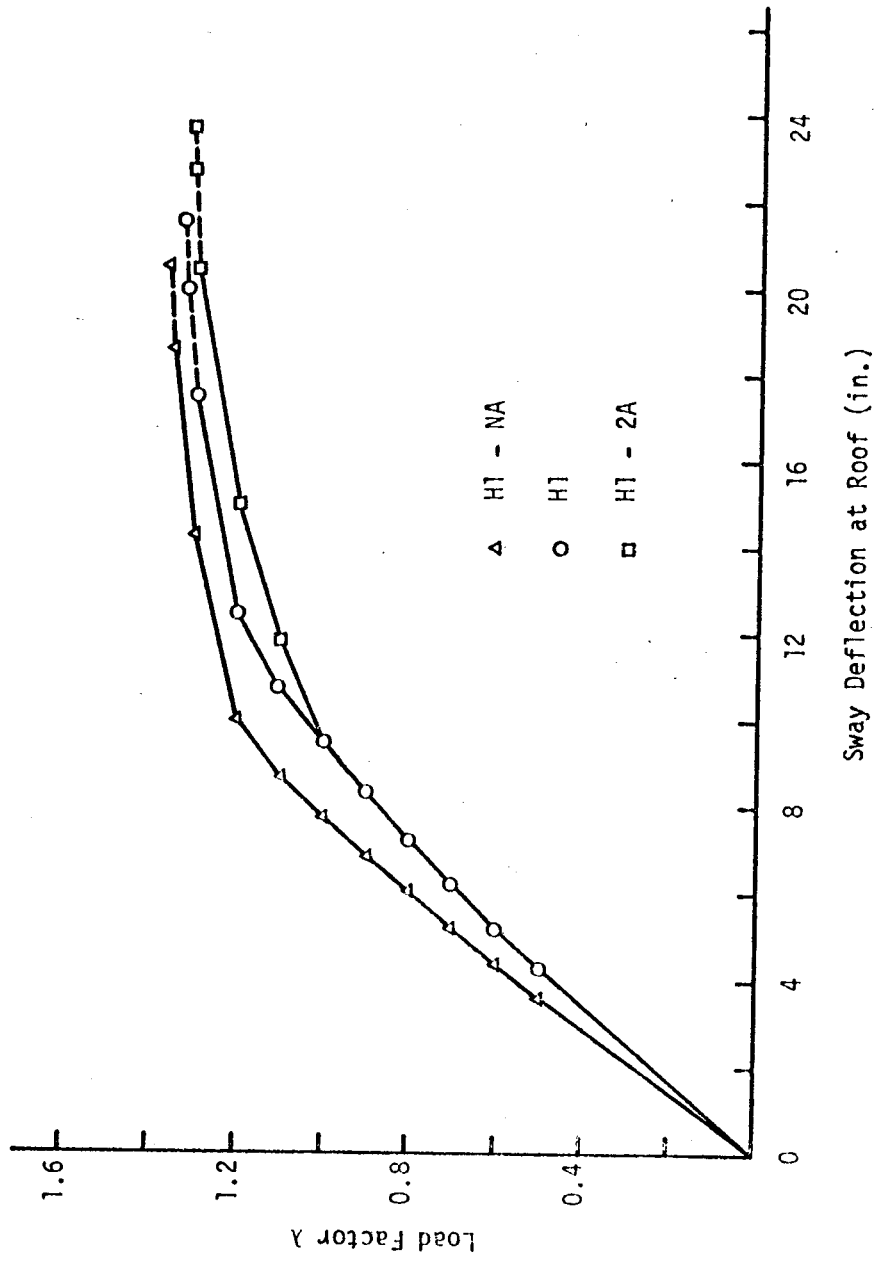


FIGURE 7.4  
EFFECTS OF AXIAL SHORTENING IN STRUCTURE H1

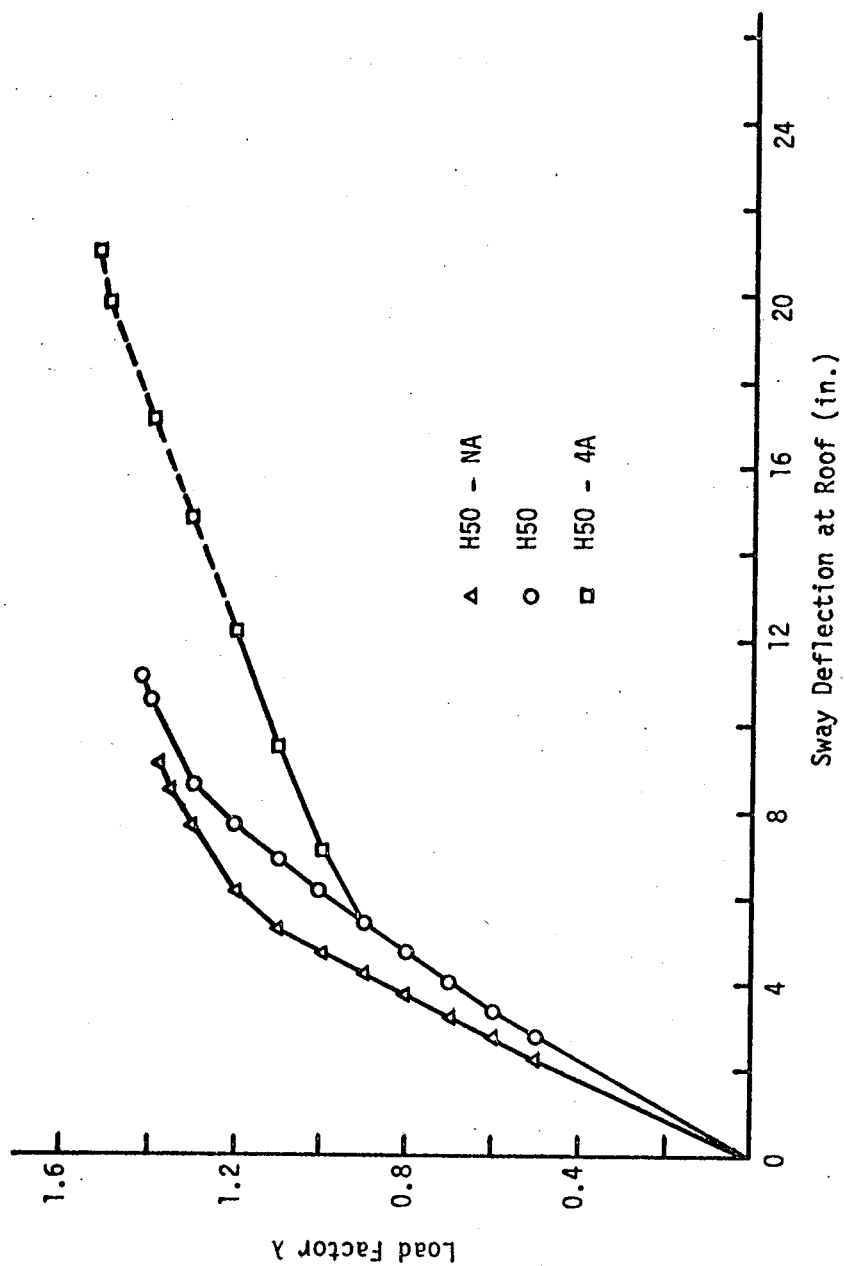


FIGURE 7.5  
EFFECTS OF AXIAL SHORTENING IN STRUCTURE H50

at low load values. However, the reduction in axial shortening of the wall resulted in greater relative column to wall deflections, particularly in the upper floors of the structure, which caused earlier plastic hinging in the girders in the windward bay of the frame. At working loads the vertical deformations at the top of the windward column stack, the shear wall, and the leeward column stack were 1.191, 1.644 and 1.616 inches respectively for the normal H1 structure, compared with 1.039, 0.857 and 1.449 inches in H1-2A. In H1-2A, four girder plastic hinges formed in the interval  $0.9 < \lambda \leq 1.00$  and an additional fifteen hinges formed in the interval  $1.00 < \lambda \leq 1.10$ . The first girder hinges in H1 formed in the interval  $1.10 < \lambda \leq 1.20$ . As is shown in FIGURE 7.4, this earlier plastic hinging resulted in a loss of stiffness of the structure, though the loss in ultimate carrying capacity was less than 2 percent. At failure, the plastic hinge configurations in all three variations of H1 were quite similar, and the failure deformations were only slightly different, although all three failed in different ways as shown in TABLES 7.1 and 7.2.

Korn<sup>(15)</sup>, in his study of unbraced frames, reported similar axial shortening effects. In unbraced frames, he found that the axial shortening had a negligible effect on the collapse load capacities, but could substantially alter the sway deflections at working loads. At working loads, axial deformations can effectively alter the sway deflection response of the structure since, as is shown in FIGURE 7.3(a), larger lateral deflections are required to meet conditions of geometrical compatibility. With the formation of plastic hinges in the girders, however, the effects of geometrical compatibility conditions are reduced and axial shortening deformations become much less significant. Reference to TABLES 3.4 and 3.5 indicates that the

sway coefficients  $C_3$  and  $C_4$  in the slope-deflections for a girder rapidly diminish as progressive hinging of a girder occurs. This explains why the collapse loads and deformations are much the same for all three variations of H1, since the hinge patterns at failure are very similar. It should, however, be noted that the unbraced structures considered by Korn and those considered in this study were all "weak girder, strong column" systems in which collapse occurred after the formation of a large number of girder plastic hinges. It is conceivable that, in structures where fewer girder hinges formed at failure, axial shortening effects could influence the collapse loads and deformations of the structure.

The effects of axial shortening in the braced structure H50, shown in FIGURE 7.5 were quite similar to those in H1 in the early loading stages. The failure loads and deformations of the braced structure were influenced by axial deformations, however. In this case, neglect of axial shortening resulted in the roof sway deflection at working load being underestimated by 22 percent, and the failure load being underestimated by 3 percent. When the shear wall area was artificially quadrupled, the overall stiffness of the structure remained basically unchanged at low load levels, as was the case in the unbraced frame H1. However, the loss of stiffness brought about by earlier girder hinging in the structure with increased wall area was somewhat more dramatic in H50 than in H1. Despite this earlier loss of stiffness, H50-4A exhibited increased deformation capacity at failure, and was able to support about 8 percent more load at failure than H50.

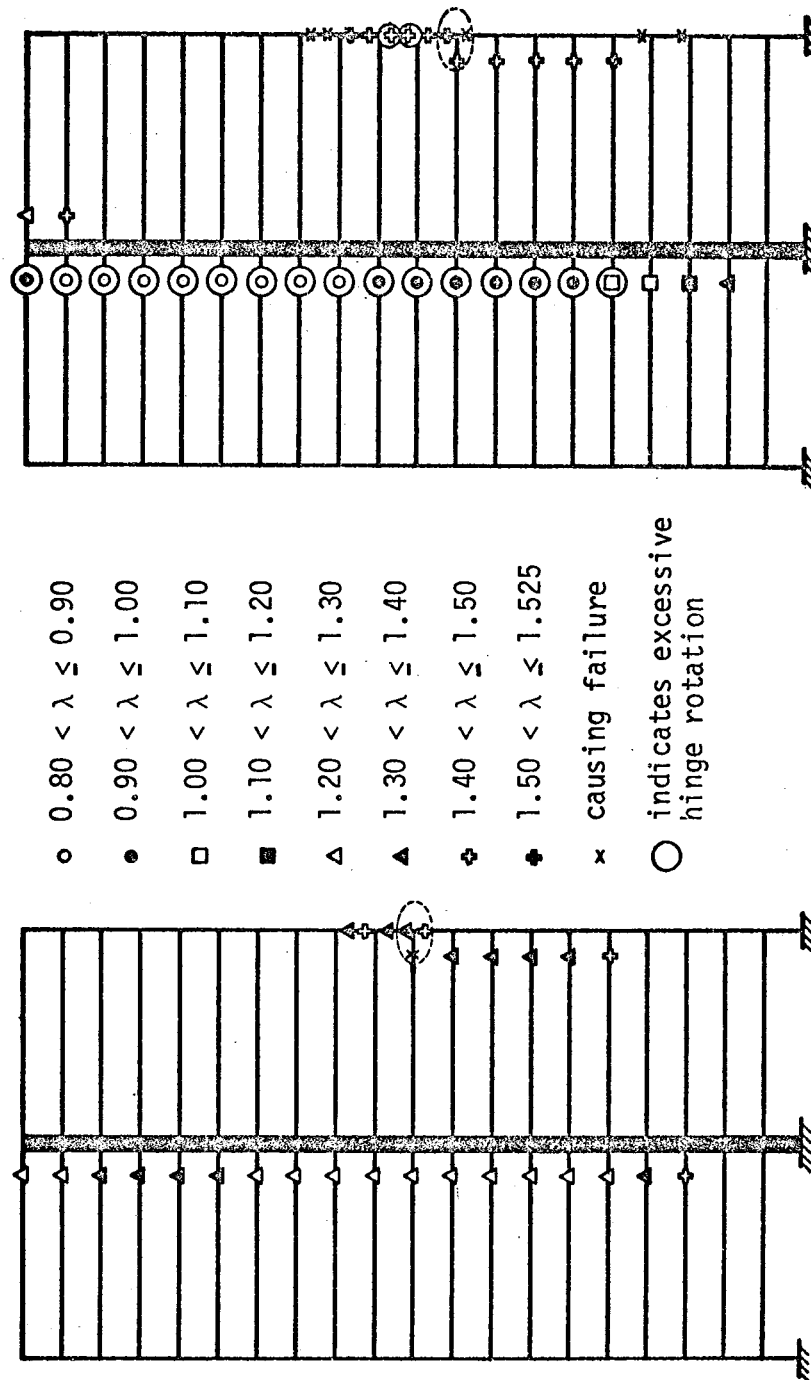
All three variations of the H50 structure failed by the formation of a joint mechanism at the leeward side of the structure. A comparison of the hinge disposition at various stages of loading of the basic structure



H50 and H50-4A is shown in FIGURE 7.6. The hinge pattern at failure when axial shortening was neglected was similar to that shown in FIGURE 7.6(a). Comparison of the hinge patterns demonstrates the earlier plastic hinge formation in the windward girders of H50-4A, the first hinges forming before  $\lambda = 0.90$ . At the same time, however, it will be noted that plastic hinging progressed further in this structure before the joint mechanism was produced. Reference to the configuration shown in FIGURE 7.3(b) indicates that the augmented shear wall area of H50-4A would tend to reduce the bending moments at the right end of the leeward girder and reduce the leeward column stack axial loads, thus retarding the formation of the joint mechanism.

It is significant that seven cases of excessive girder hinge rotation were detected at  $\lambda = 1.20$  in H50-4A, whereas no excessive rotations were detected in the other two structures. The locations of hinges at which excessive rotation was detected just prior to failure are shown in FIGURE 7.6(b). Thus, the increase in load-carrying capacity was obtained at the expense of a possible serious loss of serviceability.

The results indicate that any realistic analysis of a braced or unbraced multi-storey structure should consider the effects of axial shortening because of its effect on the sway deflections at working loads. The alterations in the initial lateral stiffness of the structures resulting from axial shortening are compared with the effects of alteration in shear wall stiffness in SECTION 7.7. The results also suggest that the relative axial shortening of walls and columns under gravity loads should be considered in the design of multi-storey structures to eliminate possible premature plastic hinging of the girders. In the cases investi-



(b) H50 - 4A

FIGURE 7.6

HINGE PROPAGATION IN H50 WITH DIFFERENT WALL AREAS

gated here, significant differences in the stress level in the shear wall and columns induced sufficiently high girder moments due to relative axial shortening to produce girder plastic hinges at load levels below the working load values.

#### 7.4 The Effects of Finite Shear Wall Width

In the analysis of frames comprised of girders and columns, the finite width of the members is generally neglected. In braced structures containing shear walls, the finite width of the wall elements is generally considered, although it complicates the analysis. The effects of the shear wall width were studied by analyzing three variations of H1 and H50 as described in SECTION 6.7. It should be noted that these structures, particularly the braced H50 structures, were highly idealized. In each case, the "normal" width wall had the same width as the interior column in the unbraced frame, varying from 9.8 inches wide at the roof to 25.7 inches wide in the bottom storey.

The load-deflection relationships for the six structures studied appear in FIGURES 7.7 and 7.8.

In the unbraced frame H1, neglect of the finite width of the "shear wall" resulted in an 8 percent overestimation of the roof sway deflection at working loads and an underestimation of the failure load by 5 percent. Doubling the finite wall width accomplished similar increases in stiffness and strength. As the width of the wall was increased, the formation of plastic hinges was retarded. At failure, the hinge configurations in all three structures were quite similar, although each structure failed in a different manner as indicated in TABLE 7.2.

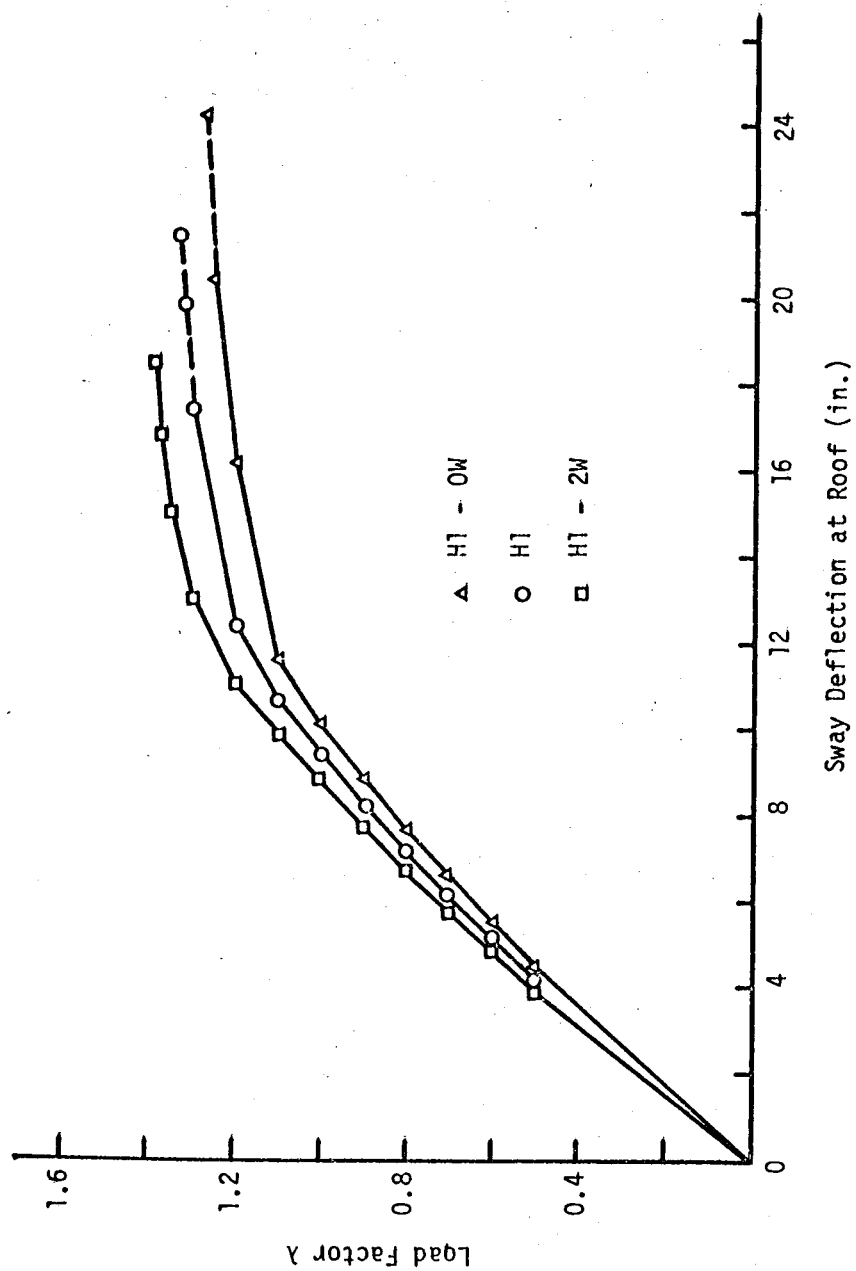


FIGURE 7.7

EFFECTS OF FINTE WALL WIDTH IN STRUCTURE H1

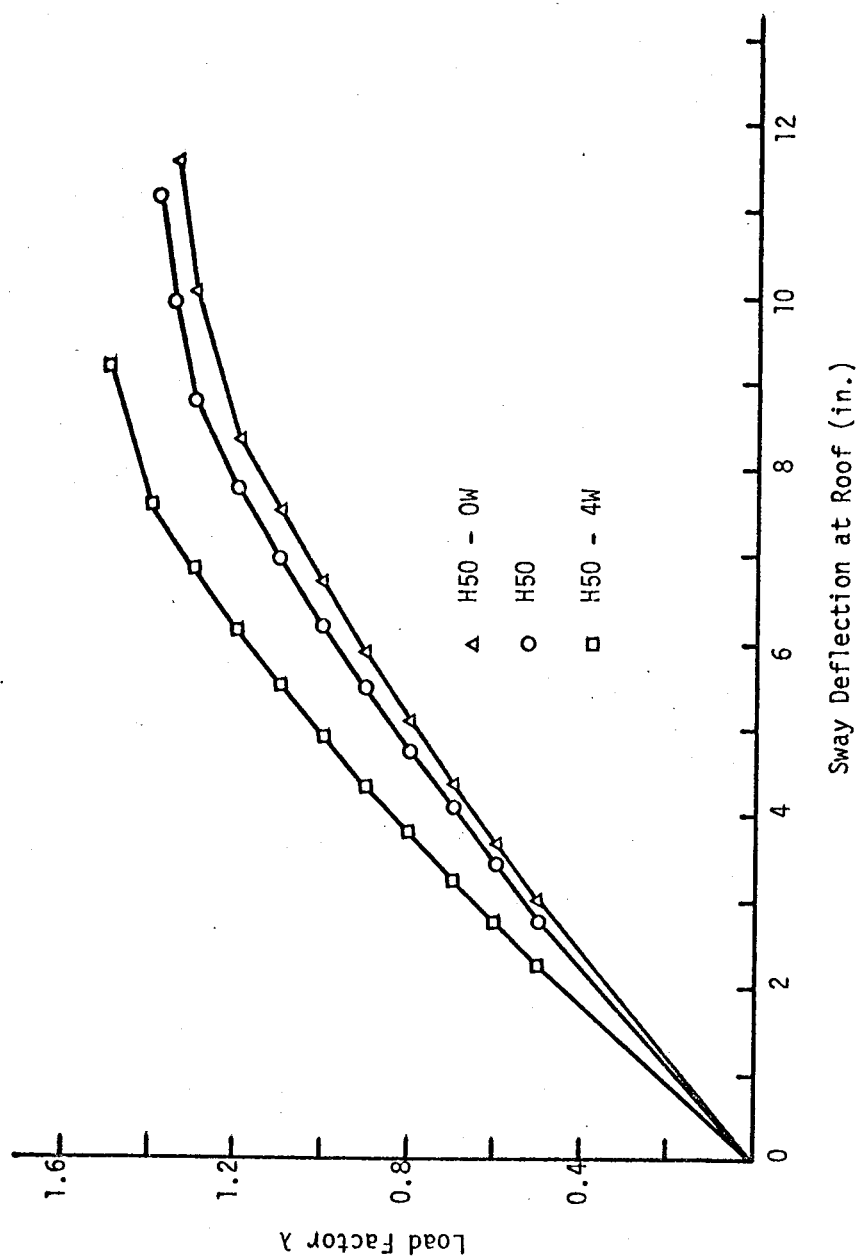


FIGURE 7.8

EFFECTS OF FINITE WALL WIDTH IN STRUCTURE H50

The effects of shear wall finite width are much the same in the braced structure H50. Again the hinge configurations at failure were almost identical although H50 failed by a drop of equilibrium sway deflections in the lower storeys while in the other two cases a joint mechanism developed.

These results indicate that the consideration of finite wall width both initially stiffens and ultimately strengthens both unbraced and braced structures of the type studied here. The significance of the increase in stiffness resulting from consideration of the width of the shear wall will be compared to the increases in stiffness resulting from changes in the flexural stiffness of the shear wall in SECTION 7.7.

The consideration of finite width effectively increases the stiffness of the girders which play a major part in the resistance to sway deflections. Moreover, the results of the analyses indicated that finite width effects slightly increased the percentage of lateral load carried by the shear wall and reduced the bending moments in the girders. This redistribution of internal forces retarded the formation of plastic hinges.

Inspection of FIGURES 7.7 and 7.8 indicates that shear wall finite width effects increased the ultimate strength of the structure and decreased the failure deformations in spite of the basically unaltered hinge configurations at failure. Mathematically this can be explained by the fact that, as plastic hinging progresses, the finite width terms in the slope-deflection equations retain more significance in the analysis than do the axial shortening terms mentioned in SECTION 7.3.

### 7.5 The Effects of Slenderness

Two different storey heights were considered to study the effect of slenderness in reinforced concrete structures. The properties of the series H and J structures, which were identical in all respects except the storey heights and the working values of lateral loads, were varied in the investigation as described in SECTION 6.8.

Comparisons of the second order elastic-plastic load-deflection properties of unbraced and braced structures of the H and J series appear in FIGURE 7.9. FIGURES 7.1 and 7.2 detail the progress of plastic hinging in the unbraced and braced structures respectively. Details of failure conditions in all series H and J structures are summarized in TABLE 7.1.

The more slender series J structures were less stiff initially and exhibited considerably less deformation capacity before failure than the series H structures. Moreover, the series J structures failed at lower loads than the series H structures despite the reduction in lateral loads. Perhaps the most notable difference between the behaviour of the structures was the mode of failure. All series H structures failed by the formation of a joint mechanism. The series J structures with high shear wall stiffness also failed in this manner with essentially the same number of plastic hinges as the comparable series H structures. Though plastic hinging in all cases had progressed significantly, these joint mechanism failures are essentially localized in nature. By comparison, the lightly braced slender structures J1, J2 and J6 failed by overall frame instability extending over seven or eight storeys. At the time instability was detected, the number of hinges present was significantly less than in the case of the corresponding H structure. This reversion from localized

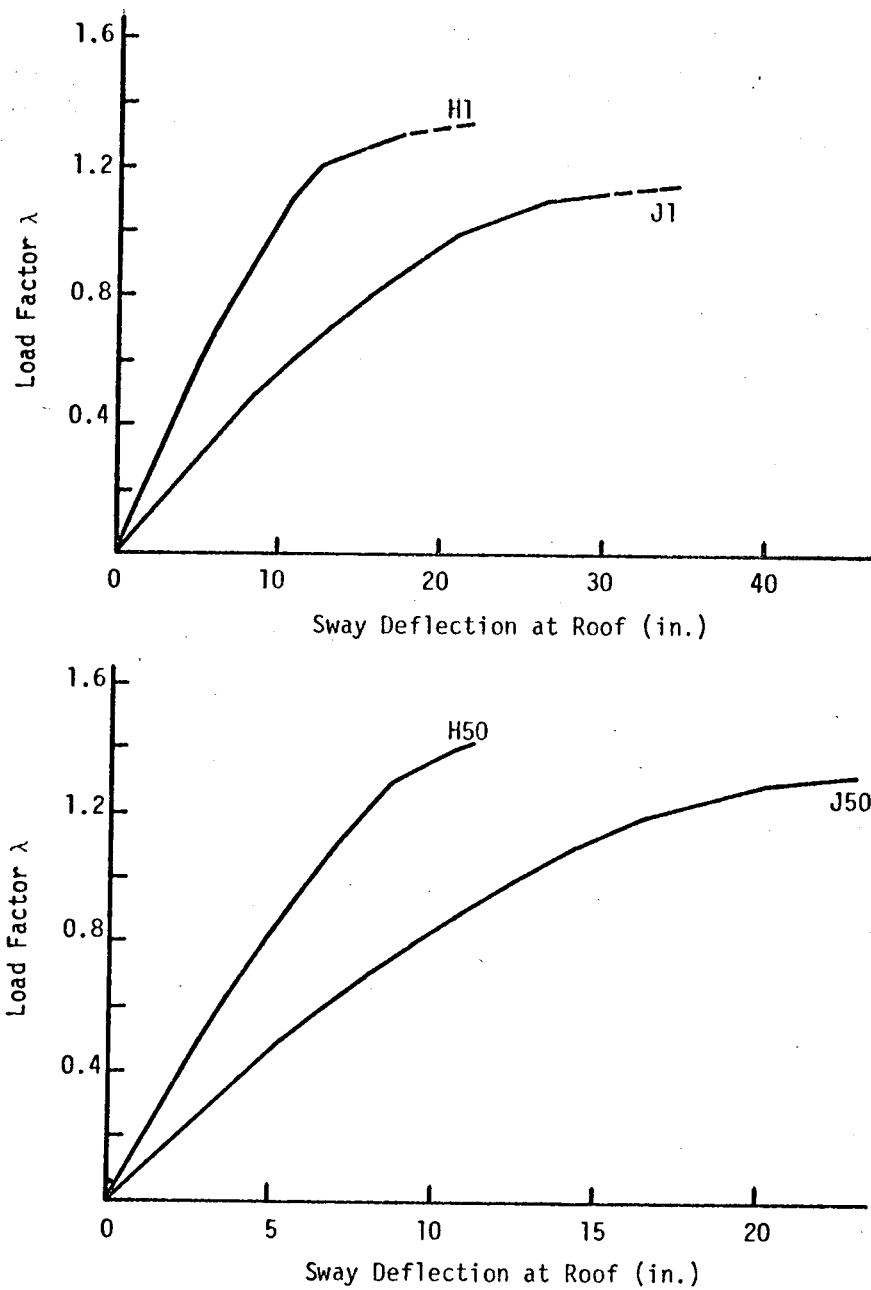


FIGURE 7.9  
EFFECTS OF SLENDERNESS ON  
LOAD-DEFLECTION RELATIONSHIPS



to overall instability is reflected in the sudden drop of failure load factor in the series J structures as they approach the unbraced frame condition.

While this study is much too brief to adequately define the effects of slenderness, a few general comments can be made.

The columns in the frames studied had  $\frac{h}{t}$  values ranging from 17 in the top storey to 6.7 in the bottom storey of the series H structures. In the series J structures,  $\frac{h}{t}$  values ranged from 26 to 10. A study<sup>(47)</sup> of the practical values of  $\frac{h}{t}$  indicated that 98 percent of all columns in braced structures had  $\frac{h}{t}$  less than 12.5 and 50 percent less than 5.75. In unbraced structures, 98 percent of all columns had  $\frac{h}{t}$  less than 18 and 50 percent less than 5.0. This indicates that the series H frames are quite realistic, whereas the series J frames are a good deal more slender than a normal frame.

These slenderness ratios correspond to column  $\frac{kh}{r}$  values ranging from 29 to 21 in the H frames and from 41 to 30 in the J frames, if the frames were considered to be braced. If the frames were assumed to be unbraced,  $\frac{kh}{r}$  values range from 50 to 46 in the H structures and 73 to 60 in the J structures.

Proposed revisions to the ACI Building Code<sup>(51)</sup> suggest that slenderness effects can be ignored in sway frames if  $\frac{kh}{r} < 22$ , and in braced frames if  $\frac{kh}{r}$  is less than about 43 for the type of structure studied here. All the braced frames studied satisfied the limiting  $\frac{kh}{r}$  value, and no serious slenderness effects were noted. However, according to the proposed rule, slenderness effects should have been noticed in the

lightly braced series H structures, not only in the lightly braced series J structures. The fact that the lightly braced H structures were not subject to noticeable slenderness effects suggests that the proposed limiting  $\frac{kh}{r}$  value for unbraced structures is excessively conservative for the type of structure considered. However, a far more extensive study is needed to clarify this point.

## 7.6 The Effects of Variation of Shear Wall Stiffness

In what follows, the effects of variation of shear wall stiffness will be dealt with in terms of the response of the overall structure and the response of individual members in the structure. The effects of the shear wall stiffness on the modes of failure of the structure were discussed in connection with the effects of the slenderness of the frame in the previous section. SECTION 7.6.1 is devoted to a discussion of the effects of the variation of wall stiffness on the load-deflection response of the structure and the interaction between the shear wall and the frame. SECTION 7.6.2 deals with the significance of secondary  $P\Delta$  effects in isolated members in the structure.

### 7.6.1 The Influence of Shear Wall Stiffness on the Overall Response of the Structure

Second order elastic-plastic analyses were carried out on series H and J structures with  $\frac{K_w}{K_c}$  values of 1, 2, 6, 12, 20 and 50. The load-deflection diagrams resulting from these analyses appear in FIGURES 7.10 and 7.11. From these plots, it is apparent that stiffening of the shear wall is not an efficient method of increasing the stiffness of the overall

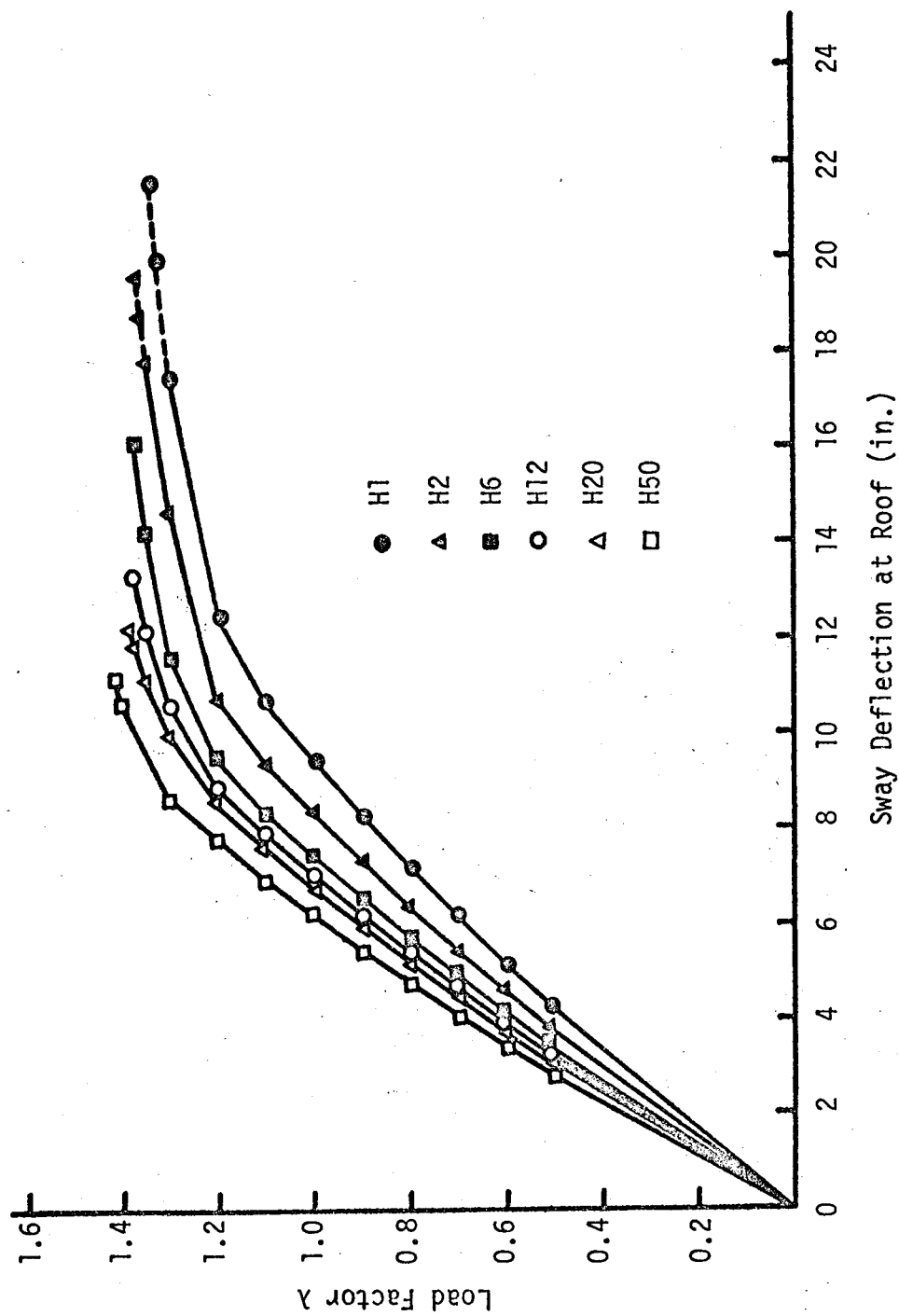


FIGURE 7.10

LOAD-DEFLECTION RELATIONSHIPS FOR SERIES H STRUCTURES

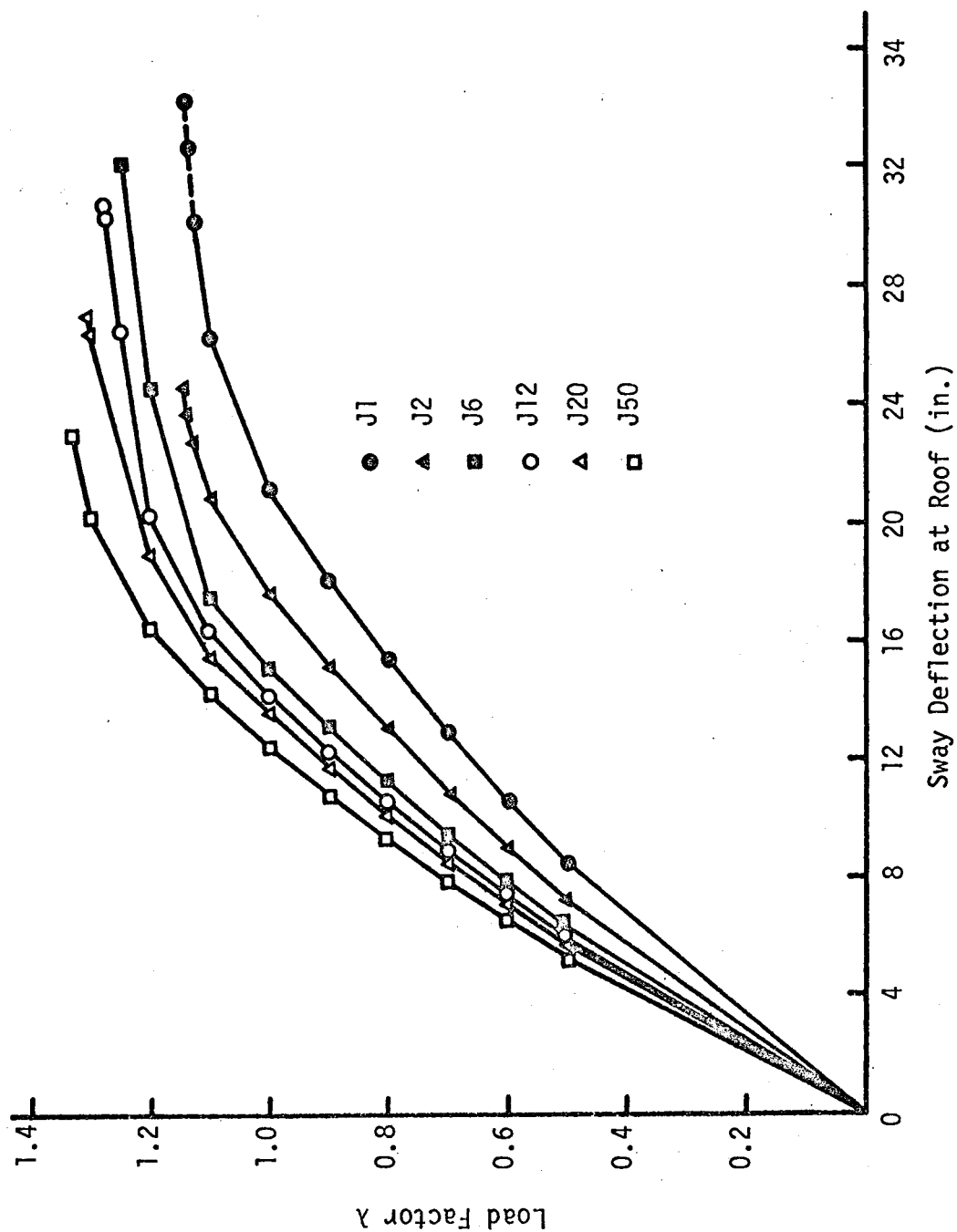


FIGURE 7.11

LOAD-DEFLECTION RELATIONSHIPS FOR SERIES J STRUCTURES

structure. Although the wall and columns of H50 possess a total lateral stiffness of 25.5 times those in the unbraced frame H1, the overall stiffness of the structure increases only by a factor of 1.5. The same effect was observed in series J structures.

This inefficient utilization of increased lateral stiffness capacity can be explained by the basic difference in behaviour of a portal frame and a cantilever wall. FIGURE 7.12 shows bending moment diagrams for the shear walls in H1 and H50 at  $\lambda = 1.00$ , prior to the formation of any plastic hinges in the structures. Inspection of these indicates that the stiffening function of the wall is diminished as the structure reverts to cantilever behaviour at the base of the wall, as indicated by a gradual shift of the initial point of contraflexure up the wall as wall stiffness increases. Thus, it appears that stiffening of the structure might better be accomplished by stiffening the network linking the frame to the wall then by increasing the wall stiffness.

In considering the effects of wall stiffness on the proportion of total lateral load carried by the shear wall in these structures, it was also evident that the loads carried by the shear wall did not increase in direct proportion to the increase in relative stiffness of the wall. FIGURE 7.13 shows the distribution of total lateral load carried by the shear wall in all storeys of H1 and H50 at working loads. In the unbraced structure H1, the "shear wall" consistently carries about one-half of the total lateral load, as might be expected from a portal method analysis. Increasing the shear wall stiffness does little to alter the interaction in the upper storeys of the structure, but does result in greater total shear carrying properties of the base of the shear wall.

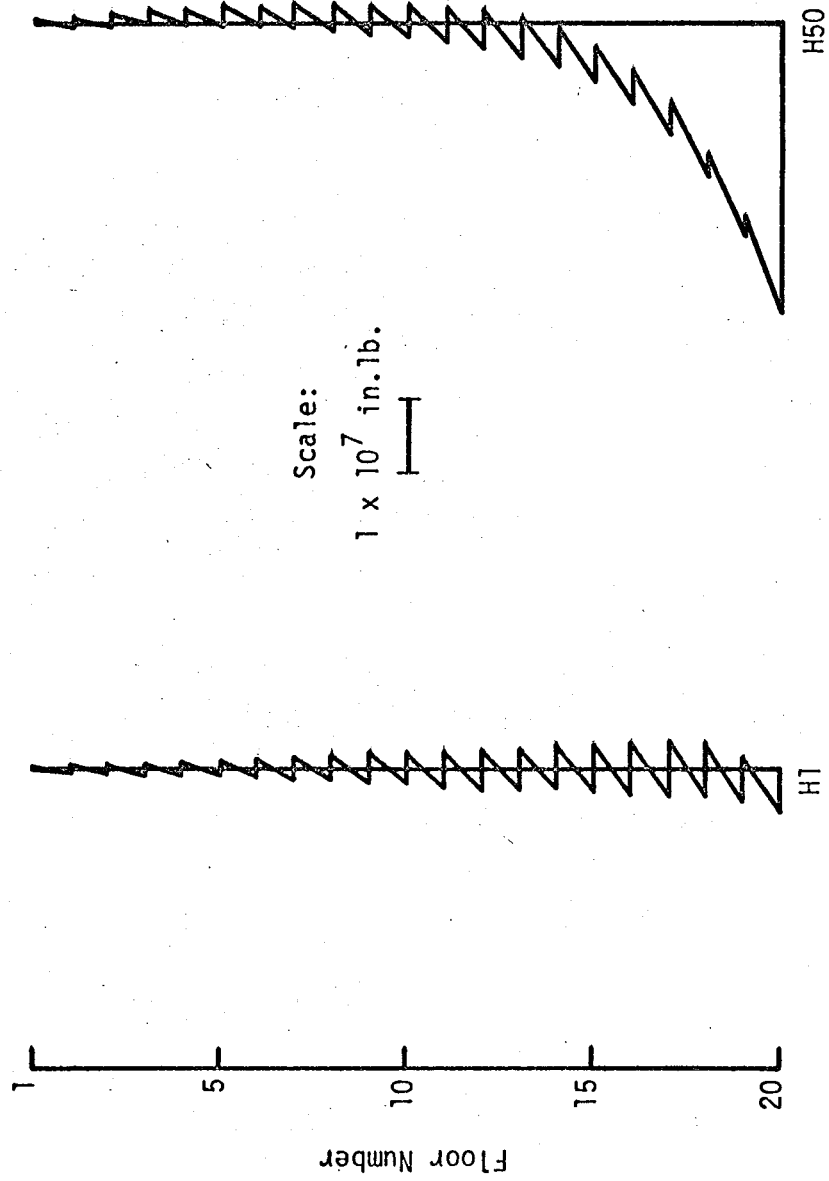


FIGURE 7.12  
BENDING MOMENT DIAGRAMS FOR THE SHEAR WALLS  
IN STRUCTURES H1 AND H50 AT WORKING LOADS

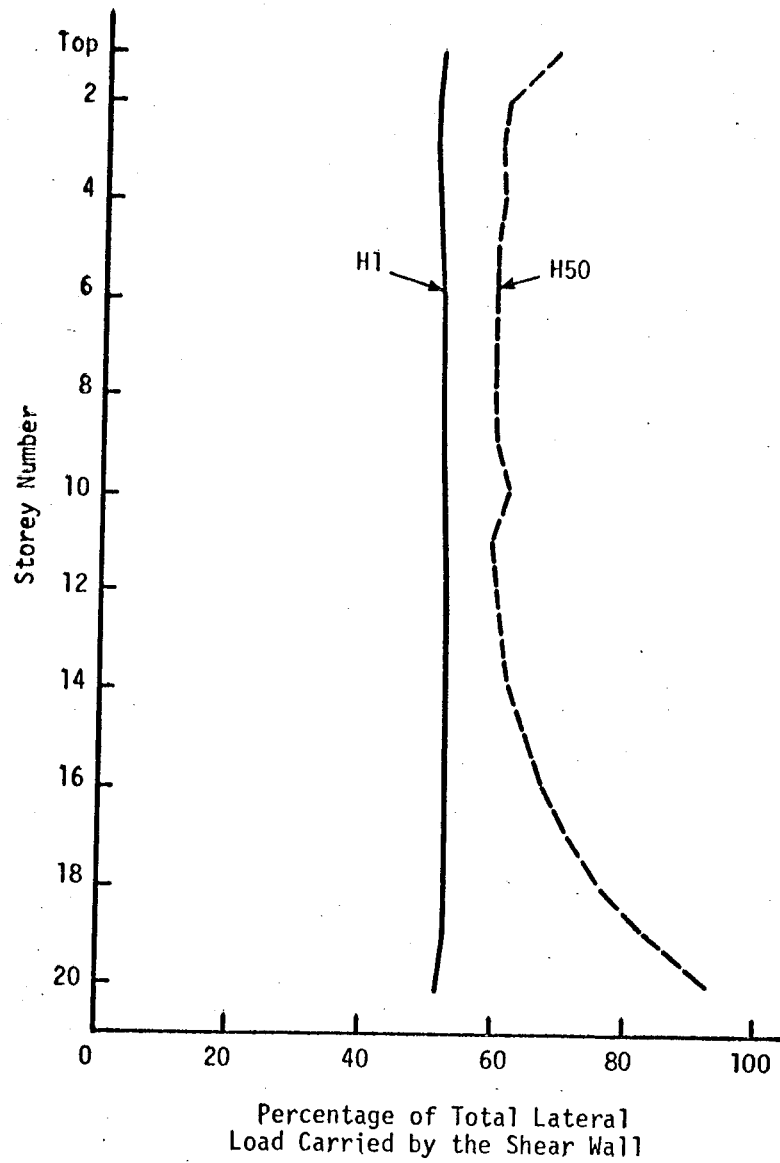


FIGURE 7.13  
LATERAL LOADS SUPPORTED BY THE  
SHEAR WALLS IN STRUCTURES  
H1 AND H50 AT WORKING LOADS

The implication of this is that, except for structures with extremely stiff walls, the frame members may be underdesigned if the interaction of the shear wall and frame are neglected and the wall is assumed to carry the entire lateral load.

Khan and Sbarounis<sup>(18)</sup> have suggested that the enforcement of the compatibility condition on the free deflected shapes of a shear wall and a frame could result in a significant decrease in the proportion of the applied shear load carried by the wall at the top of the structure. In their study of the elastic behaviour of shear wall-frame structures, they found cases where the shear wall was actually pulling on the frame rather than supporting it in the top storeys of the structure. Guhamajumdar, Nikhed et al<sup>(25)</sup>, investigating the elastic-plastic response of a twenty four storey structure, found that the shear force developed in the frame in the top storey of the structure exceeded the applied lateral force, the effect worsening as inelastic action progressed.

In this study, no such effects were noted. In all cases the shear wall supported some percentage of the lateral load and continued to carry roughly the same proportion at all load stages up to failure. However, this behaviour should not be considered to be representative of all shear wall-frame structures. There are significant differences between the model and loading procedure used by Guhamajumdar, Nikhed et al and those used in this study. The approximate analysis model consisted of a steel frame which was proportioned as a braced frame. As was mentioned in SECTION 6.3, the strength and stiffness proportions of a braced frame differ considerably from those of the unbraced frame considered here. Khan and Sbarounis have indicated the significance of model proportions on the out-



come of an analysis. Moreover, in the loading procedure for the approximate analysis study, full column axial loads were applied initially, and only the lateral loads were incremented until failure occurred. In the study comparing the Guhamajumdar and Nikhed analysis with that used here, detailed in SECTION 5.5, the load-sharing characteristics compared very well. In that case, with a stiff prismatic shear wall, there was no evidence of negative shear wall loads in either analysis, although as loading progressed there was a tendency for the proportion of lateral load carried by the shear wall in the upper storeys to diminish.

FIGURES 7.10 and 7.11 indicate that increasing shear wall stiffness accomplishes some increase in loading capacity, and at the same time causes a decrease in the deformation capacity at failure. The results also show that stiffening of the shear wall retards the formation of plastic hinges in these structures. In considering the failure conditions of these structures, it should be remembered that all the structures except J1, J2 and J6 failed by the formation of a joint mechanism. The validity of the joint mechanism as a mode of failure was discussed in SECTION 7.2.

The study conducted using the approximate analysis of Guhamajumdar, Nikhed et al indicated that increased shear wall stiffness substantially increased the loading and deformation capacity at failure. The differences between the loading history and model proportions of the approximate analysis structure and those considered here, discussed earlier in this section, may influence the load-deflection characteristics. More important, however, was the fact that when joint mechanisms were detected in this analysis,

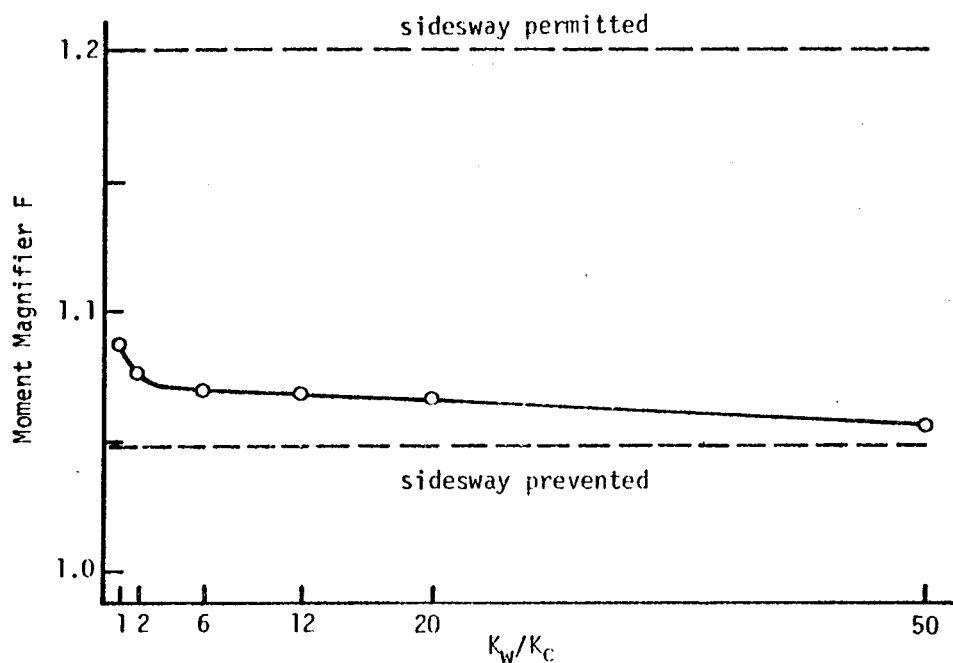
they constituted failure, while the joint mechanism condition was bypassed in the approximate analysis. Undoubtedly this fact, more than any other, led to the differences in the ultimate load-deflection behaviour predicted by the two analyses.

#### 7.6.2 P $\Delta$ Effects in Members

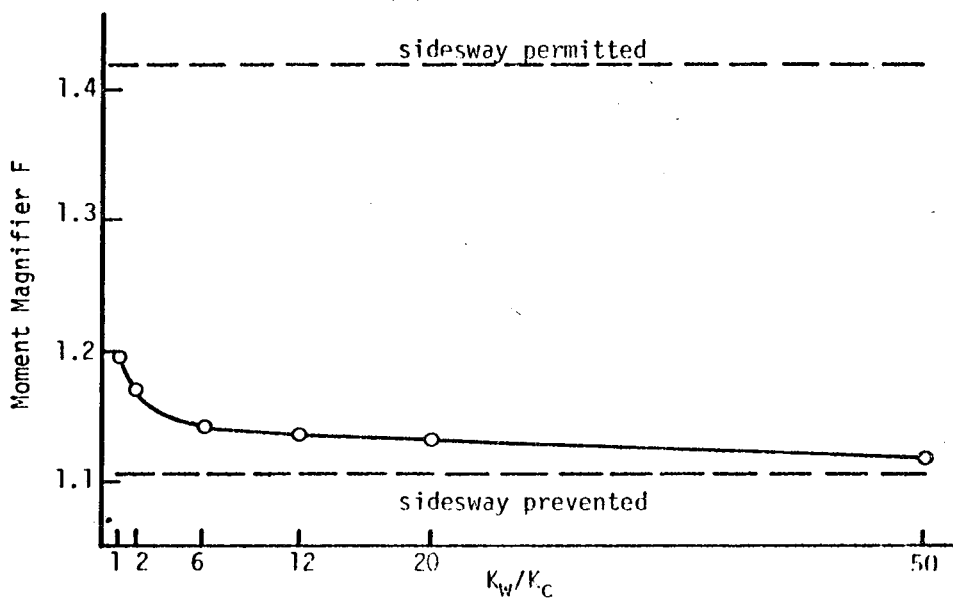
In conjunction with the second order elastic-plastic analyses discussed in SECTION 7.6.1, first order elastic analyses were performed on all basic H and J structures. The difference between the two analyses, apart from the neglect of plastic hinging in the elastic analysis, is the consideration of P $\Delta$  effects in the wall and columns resulting from the changes in the value of the stability functions C and S due to the axial load P, and P $\Delta$  effects in the overall structure by formulating equilibrium conditions on the deformed structure. The resulting bending moment values were compared to observe the significance of the secondary P $\Delta$  moments in these various structures. This effect is expressed in terms of a moment magnifier, F, equal to the value of the maximum column moment from the second order analysis divided by the corresponding moment from the first order analysis.

The values of the moment magnifier, F, at working loads ( $\lambda = 1.00$ ) in the leeward column of the twelfth storey of the series H and J structures are plotted as a function of  $\frac{K_w}{K_c}$  in FIGURE 7.14. It should be noted that at  $\lambda = 1.00$ , no hinges had formed in any of the basic structures.

The two horizontal dashed lines appearing on these plots represent the values of F derived using the traditional moment magnifier relationship<sup>(48)</sup> given by EQUATION (7-1). The critical load, P<sub>cr</sub>, is based on a nomographic



(a) Series H Structures



(b) Series J Structures

FIGURE 7.14  
EFFECT OF RELATIVE SHEAR WALL  
STIFFNESS ON THE COLUMN MOMENT  
MAGNIFIER IN SERIES H AND J STRUCTURES

evaluation of effective length<sup>(48,49)</sup>.

$$F = \frac{1}{1 - \frac{P}{P_{cr}}} \quad (7-1)$$

The F values derived from the analysis never approach the values computed using EQUATION (7-1) assuming the frame is free to sway. Part of this discrepancy is caused by the fact that the values of the effective column lengths used were derived<sup>(50)</sup> assuming a typical interior column in an infinitely large rectangular structure. In addition, the effective lengths were derived assuming only axial loads in the column, while the frames considered here were subjected to the additional effects of both wind and uniformly distributed gravity loads.

On the other hand, for values of  $\frac{K_w}{K_c}$  greater than about 6, the moment magnifier values computed in this study do approach the F values computed by EQUATION (7-1) assuming a frame braced against sidesway. As is shown in FIGURE 7.15, similar effects were noted for the more heavily loaded leeward column in other storeys of the H and J structures.

As the loads were increased beyond the working load values, hinges developed in the structures at differing rates, depending on the shear wall stiffness. As a result of the different hinge patterns in the structures at any particular load level, irregularities in magnification values made a comparison of the type discussed above quite meaningless.

The results shown in FIGURE 7.14 and TABLE 7.1 suggest that a relatively low shear wall stiffness value is required to change the behaviour from that of an unbraced frame to that of a braced frame with respect to instability.

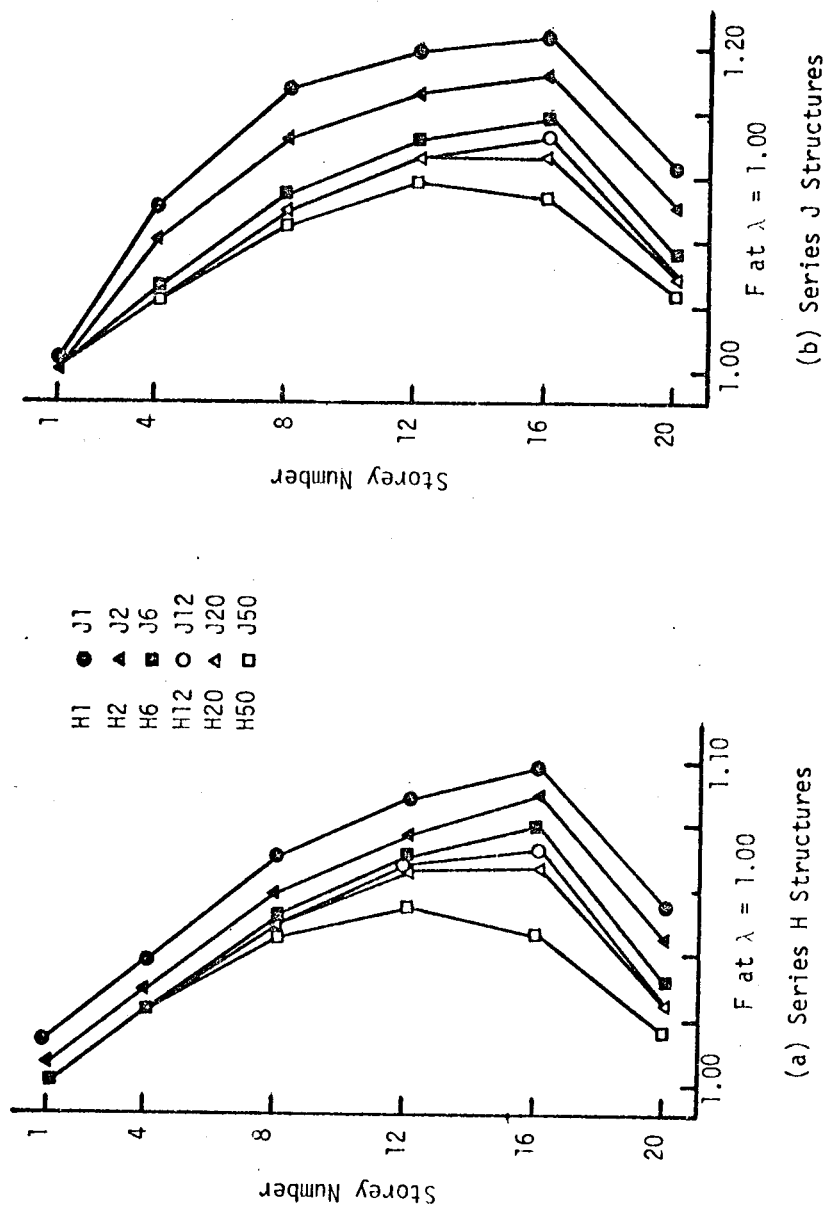


FIGURE 7.15

DISTRIBUTION OF MOMENT MAGNIFIERS IN LEeward  
COLUMN STACK AT WORKING LOADS

A comparison of FIGURES 7.14(a) and 7.14(b) indicates that the break in linearity of the plot occurs at a lower value of  $\frac{K_w}{K_c}$  in the H structures than in the more slender J structures. This suggests that the critical value of  $\frac{K_w}{K_c}$  which delineates the transition from unbraced to braced behaviour is a function of the slenderness of the structure. Before a truly dependable critical value of  $\frac{K_w}{K_c}$  could be defined, however, a number of other types of structures should be investigated, including unsymmetrical structures, structures with abrupt changes in shear wall stiffness, very low structures, and structures with different loadings.

The values of the moment magnifiers presented in FIGURE 7.14 suggest that a safe approximate design procedure for multi-storey frames of the type considered here would be to:

1. Analyze forces and moments using a conventional first order elastic analysis.
2. Amplify the column moments, and where necessary the girder moments, using a moment magnifier value given by EQUATION (7-1). The effective length factor for braced columns could be used in computing  $P_{cr}$  if  $\frac{K_w}{K_c}$  is greater than 6, and that for unbraced columns if  $\frac{K_w}{K_c}$  is less than 6.
3. Design all sections to have a plastic moment capacity equal to or greater than the moments computed in step 2.

This procedure is valid only if the wall remains elastic throughout the loading history.

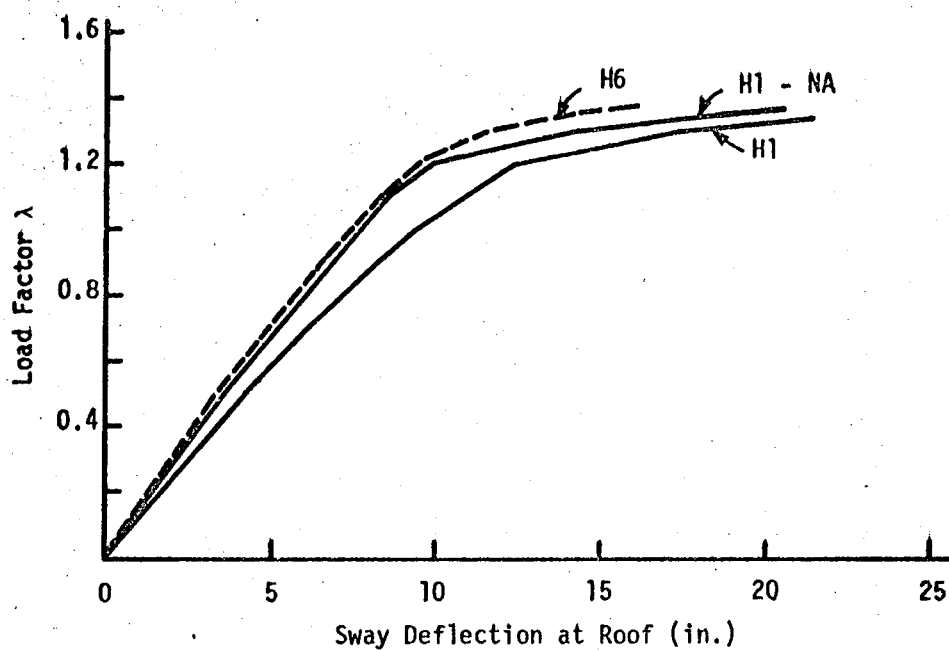
### 7.7 Significance of the Consideration of Axial Shortening and the Finite Width of the Shear Wall in the Analysis

FIGURES 7.16 and 7.17 were prepared to illustrate the significance of changes in the overall stiffness of braced and unbraced structures resulting from the neglect of axial shortening and the width of the shear wall in the analysis. These plots permit assessment of the effects of neglecting these two factors in terms of changes in the observed "effective" shear wall flexural stiffness.

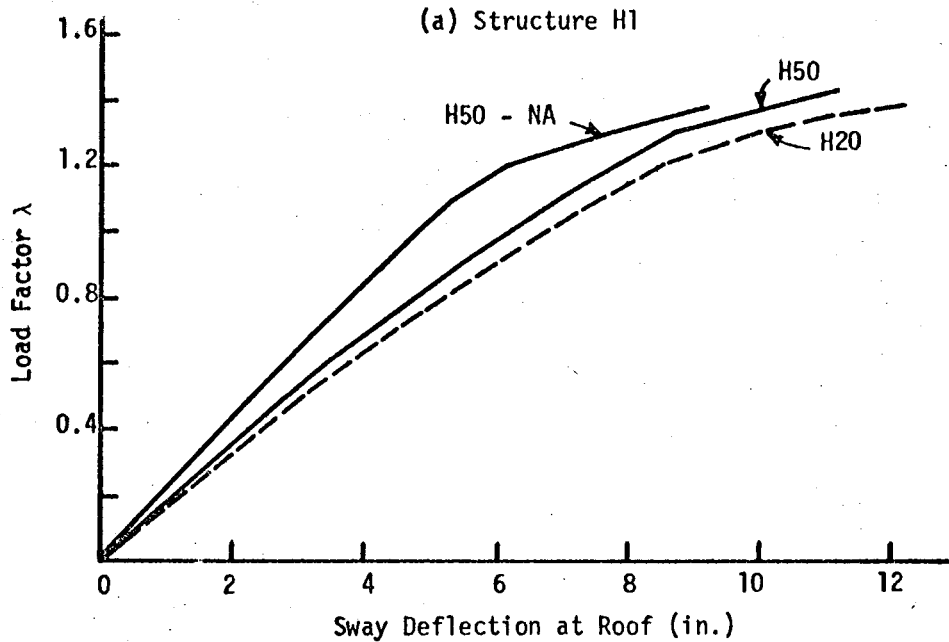
Reference to FIGURE 7.16(a) indicates that neglect of axial shortening of the shear wall and columns of the unbraced frame, H1, produces results similar to an increase in the shear wall stiffness by a factor of about five. FIGURE 7.16(b) also indicates a significant increase in the overall stiffness of H50. In this case, however, the numerical value of the increase in "effective" shear wall stiffness is impossible to gauge.

In the unbraced structure, H50, considered in FIGURE 7.17(b), the decrease in stiffness resulting from neglect of the finite width of the shear wall is approximately equivalent to a halving of the shear wall stiffness. FIGURE 7.17(a) indicates the significant decrease in "effective" shear wall stiffness resulting from the neglect of the finite width of the wall in the unbraced structure.

These results clearly indicate the necessity of considering axial shortening and finite width effects in any analysis of multi-storey reinforced concrete structures.



(a) Structure H1

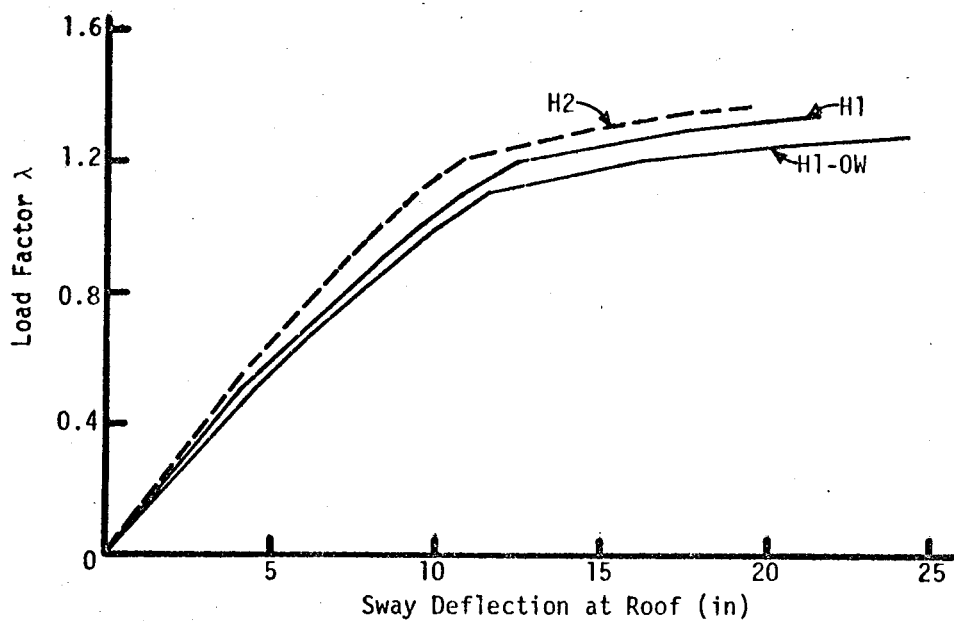


(b) Structure H50

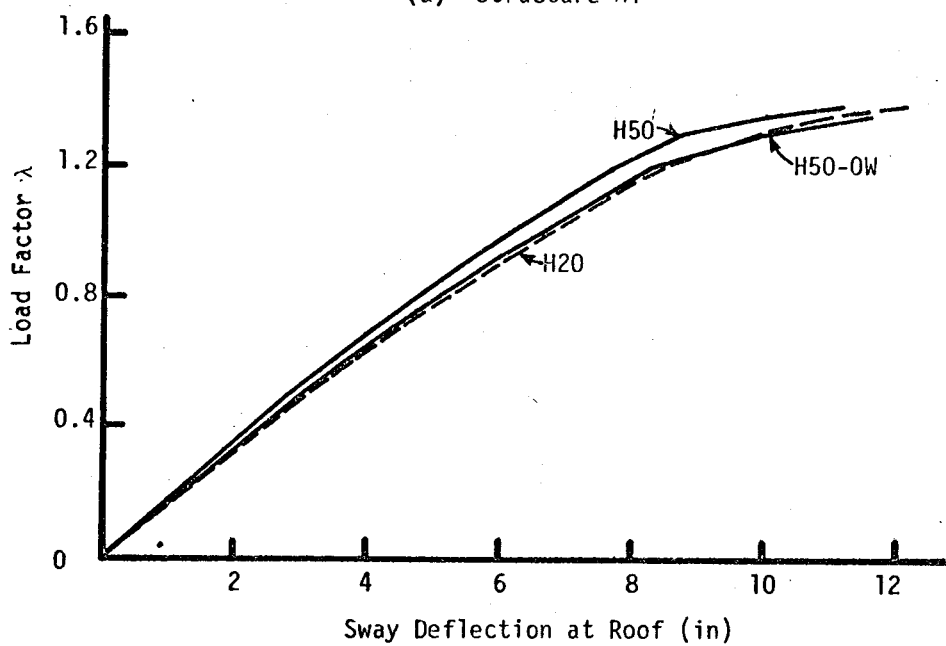
FIGURE 7.16

SIGNIFICANCE OF NEGLECT OF AXIAL  
SHORTENING IN THE ANALYSIS OF H1 AND H50





(a) Structure H1



(b) Structure H50

FIGURE 7.17

SIGNIFICANCE OF NEGLECT OF SHEAR WALL  
FINITE WIDTH IN THE ANALYSIS OF H1 AND H50

### 7.8 Limitations of the Investigation

In considering the results of this investigation, it should always be borne in mind that the basis for the results is one type of shear wall-frame structure subjected to a particular loading history. The frame portion of all structures was proportioned as an unbraced frame, and in all cases except the basic H1 structure the shear wall element possessed sufficient strength to remain elastic throughout the loading history. In view of the apparent significance of member proportions, additional studies with other structures are required.

Moreover, the studies of the effects of the variables were not particularly extensive, and were intended primarily to provide spot checks on the behaviour of these structures.

In spite of these limitations, the results of this investigation should provide meaningful trends regarding the elastic-plastic behavioural characteristics of multi-storey reinforced concrete structures.

## CHAPTER VIII

### SUMMARY, CONCLUSIONS AND RECOMMENDATIONS

#### 8.1 Summary

This thesis presents a method of analysis which traces the second order elastic-plastic response of large planar reinforced concrete structures as loading progresses to failure. In the analysis, conditions of equilibrium are formulated on the deformed members and the deformed structure to consider the secondary axial load effects in the columns and shear walls. The analysis considers axial shortening of the columns and shear walls and includes the effects of the finite width of the shear wall elements. Provided the framework is regular and rectangular, application of the analysis involves no geometrical simplification of the frame.

To formulate the solution, elastic-perfectly plastic moment-curvature relationships were used to represent the response of the member cross-sections. Rationalized methods were developed to predict elastic-plastic column section moment-thrust-curvature and girder section moment-curvature relationships. This assumption of elastic-plastic behaviour represents perhaps the most significant limitation of the analysis. In addition, time effects and shear deformations in the members and joints are neglected.

In the computer programme developed for the analysis, the solution is derived by the deformation method, using slope-deflection equations

modified to consider the presence of plastic hinges in the members. The equations of equilibrium are solved by an iterative procedure.

Using the analysis, good correlation was obtained with three other analyses and with the results of tests of sway frames reported by Ferguson and Breen.

To illustrate the application of the analysis and gain some insight into the behaviour of large reinforced concrete structures, the analysis was used to investigate the behaviour of a symmetrical, twenty storey, two bay, reinforced concrete structure designed by ultimate strength methods. The properties of the basic structure were adjusted to isolate the effects of several variables on the behaviour of the structure. Spot checks were made to assess the significance of the effects of axial shortening, the finite width of the shear wall in the structure, slenderness, and the effects of varying shear wall stiffness on the behaviour of the overall structure and individual members in the structure.

## 8.2 Conclusions

The analysis presented in this thesis represents the most comprehensive method yet developed for large planar reinforced concrete structures. The comparisons obtained with the results of the frame tests by Ferguson and Breen indicate that the method will accurately predict the behaviour of small reinforced concrete structures. The applicability and effectiveness of the analysis were demonstrated in the investigation of the behaviour of the large reinforced concrete structure.

In view of the limitations of the model studied and the extent

of the investigation, the results of the study of behaviour of braced and unbraced structures must be regarded as trends, and should only be interpreted in a qualitative manner.

The study indicates that a realistic structural analysis of a shear wall-frame structure must consider the effects of axial shortening and the finite width of the shear wall elements. In both braced and unbraced structures, the neglect of axial shortening led to a significant underestimation of the sway deflections at working loads. In the unbraced structure, axial shortening did not significantly alter the hinge pattern at failure, and the failure load was not appreciably affected. On the other hand, in the braced structure, the failure load increased somewhat with the consideration of axial shortening.

The study indicates that significant differences in the stress levels in the columns and shear wall can lead to premature hinging of the girders. In this structure, the resultant differential axial shortening produced girder hinges before the working load level was reached. This suggests that axial shortening should be considered, particularly in the design of braced structures where the shear wall area may be large relative to the axial loads it carries.

The study indicates that neglect of the finite width of the stiff shear wall elements in an analysis can lead to an underestimation of the stiffness and failure loads of the structure.

The investigation of slenderness effects suggests that instability over several storeys can arise if the structure is sufficiently slender. However, in this particular structure, this type of overall instability was found to be a problem only in lightly braced structures in which the

slenderness ratios exceeded the normal practical range of values.

The study of the effect of variations in the shear wall stiffness suggests that a relatively low value of shear wall stiffness is required to effectively brace the structure. In this type of structure, if the ratio of shear wall stiffness to total column stiffness,  $\frac{K_w}{K_c}$ , exceeded a value of about six, the structure could be considered to be essentially a braced structure. This effect was noted in the study of the amplification of frame column moments resulting from the secondary  $P\Delta$  effects.

In this structure, it was found that increasing the shear wall stiffness was not an efficient method of increasing the overall stiffness of the system. This inefficient utilization of shear wall stiffness appears to result from reversion from portal behaviour to cantilever behaviour at the base of the shear wall. As the shear wall stiffness is increased, the extent of the cantilever portion of the shear wall increases, and the shear wall element loses much of its effectiveness in stiffening the structure against lateral loads.

Moreover, increasing of the shear wall stiffness did not significantly alter the failure load. In almost all cases, failure resulted from the formation of a joint mechanism.

Even with a relatively stiff shear wall element, the frame portion of the structure carried some proportion of the lateral load, continuing to support this load as inelastic action progressed. This suggests that any economical and safe design procedure for shear wall-frame structures should consider the load-sharing nature of the interaction of the frame and the shear wall.

### 8.3 Recommendations for Future Research

The frequency of occurrence of a joint mechanism in this study suggests that this type of failure should be studied more fully and that the analysis should be modified to eliminate the consideration of an isolated joint mechanism as a mode of failure. A method of approach for this modification was outlined in SECTION 7.2, and the assumptions involved in the revision were discussed.

The effects of shear deformations in the shear wall member, neglected in this analysis, may be significant. Tests currently being conducted by the Portland Cement Association may clarify this issue.

The analysis could be extended to permit the derivation of post-instability behaviour. This would involve major revisions as mentioned in SECTION 4.7.

The study of the behaviour of reinforced concrete structures presented in this thesis was limited to one type of structure subjected to one type of loading history. The structures were consistently weak girder, strong column systems with a tapered shear wall which remained elastic throughout the loading history. Moreover, the procedures used to isolate the variables led to rather unrealistic structures, particularly in the case of the structures with stiff shear walls, since the frame portion of the structure was not changed from that of the unbraced structure. Despite these limitations, the study serves to indicate problems which require additional investigation. Much more extensive studies with other types of structures are required to substantiate the findings of this study.

The most apparent requirement, however, is for large scale laboratory tests of braced and unbraced reinforced concrete structures to assess the applicability and accuracy of the method of analysis in large reinforced concrete structures.



## LIST OF REFERENCES

## LIST OF REFERENCES

1. "Plastic Design of Multi-Story Frames", Fritz Engineering Laboratory Report No. 273.20, Lehigh University, 1965.
2. ACI Committee 318 - "Building Code Requirements for Reinforced Concrete (ACI 318-63)", American Concrete Institute, 1963.
3. Goldberg, J.E. - "On the Lateral Bracing of Multi-Story Building Frames with Shear Bracing", Final Report, Sixth Congress, International Association for Bridge and Structural Engineering, 1961, pp 231-240.
4. Ostapenko, A. - "Plastic Design of Multi-Story Frames", Lecture 13 - "Behaviour of Unbraced Frames", Fritz Engineering Laboratory Report No. 273.20, Lehigh University, 1965.
5. Bleich, F. - "Buckling Strength of Metal Structures", McGraw-Hill Book Company Inc., New York, 1952.
6. Lu, L.W. - "Plastic Design of Multi-Story Frames", Lecture 15 - "Frame Buckling", Fritz Engineering Laboratory Report No. 273.20, Lehigh University, 1965.
7. Merchant, W. - "The Failure Load of Rigidly Jointed Frameworks as Influenced by Stability", The Structural Engineer, Vol. 32, 1954, pp 185-190.
8. Horne, M.R. - "Elastic-Plastic Failure Loads of Plane Frames", Proceedings of Royal Society of Architects, Vol. 274, 1963, pp 343-364.
9. Majid, K.I. - "An Evaluation of the Elastic Critical Load and the Rankine Load of Frames", Proceedings ICE, Vol. 36, 1967, pp 579-593.

10. Wood, R.H. - "The Stability of Tall Buildings", Proceedings ICE, Vol. II, 1958, pp 69-102.
11. Jennings, A. and Majid, K. - "An Elastic-Plastic Analysis by Computer for Framed Structures Loaded up to Collapse", The Structural Engineer, Vol. 43, No. 12, 1965, pp 407-412.
12. Livesley, R.K. and Chandler, D.B. - "Stability Functions for Structural Frameworks", Manchester University Press, 1962.
13. Davies, J.M. - "The Stability of Plane Frameworks under Static and Repeated Loading", Ph.D. Thesis, Victoria University of Manchester, 1965.
14. Parikh, B.P. - "Elastic-Plastic Analysis and Design of Unbraced Multi-Story Steel Frames", Fritz Engineering Laboratory Report No. 273.44, Lehigh University, 1966.
15. Korn, A. - "The Elastic-Plastic Behaviour of Multi-Story, Unbraced, Planar Frames", Research Report No. 2, School of Engineering and Applied Science, Washington University, Saint Louis, 1967.
16. Gould, P.L. - "Interaction of Shear Wall-Frame Systems in Multistory Buildings", Proceedings ACI, Vol. 62, 1965, pp 45-69.
17. Bandel, H. - "Frames Combined with Shear Trusses under Lateral Loads", Journal of the Structural Division, ASCE, Vol. 88, No. ST6, 1962, pp 227-243.
18. Khan, F.R. and Sbarounis, J.A. - "Interaction of Shear Walls and Frames", Journal of the Structural Division, ASCE, Vol. 90, No. ST3, 1964, pp 285-335.
19. Parme, A.L. - "Design of Combined Frames and Shear Walls", "Tall Buildings", Pergamon Press, London, 1967, pp 291-317.

20. Cardan, B. - "Concrete Shear Walls Combined with Rigid Frames in Multistory Buildings Subject to Lateral Loads", Proceedings ACI, Vol. 58, 1961, pp 299-316.
21. Rosman, R. - "Laterally Loaded Systems Consisting of Walls and Frames", "Tall Buildings", Pergamon Press, London, 1967, pp. 273-290.
22. Frischmann, W.W., Prabhu, S.S., and Toppler, J.F. - "Multi-Storey Frames and Interconnected Shear-Walls Subjected to Lateral Loads", Concrete and Constructional Engineering, Vol. LVIII, No. 6, 1963, pp 227-234.
23. Rosenblueth, E. and Holtz, I. - "Elastic Analysis of Shear Walls in Tall Buildings", Proceedings ACI, Vol. 56, 1959, pp 1209-1222.
24. Clough, R.W., King, I.P. and Wilson, E.L. - "Structural Analysis of Multi-Story Buildings", Journal of the Structural Division, ASCE, Vol. 90, No. ST3, 1964, pp 19-34.
25. Guhamajumdar, S.N., Nikhed, R.P., MacGregor, J.G. and Adams, P.F. - "Approximate Analysis of Frame-Shear Wall Structures", Structural Engineering Report No. 14, Department of Civil Engineering, University of Alberta, May 1968.
26. Cranston, W.B. - "Determining the Relation Between Moment, Axial Load and Curvature for Structural Members", Technical Report, Cement and Concrete Association, London, June 1966.
27. Broms, B. and Viest, I.M. - "Ultimate Strength Analysis of Long Hinged Reinforced Concrete Columns", Journal of the Structural Division, ASCE, Vol. 84, No. ST1, 1958.

28. Pfrang, E.O., Siess, C.P. and Sozen, M.A. - "Load-Moment-Curvature Characteristics of Reinforced Concrete Cross Sections", Proceedings ACI, Vol. 61, 1964, pp 763-778.
29. Hognestad, E. - "A Study of Combined Bending and Axial Load in Reinforced Concrete Members", Bulletin No. 399, University of Illinois Engineering Experiment Station, November 1951.
30. Manuel, R.F. and MacGregor, J.G. - "The Behaviour of Restrained Reinforced Concrete Columns under Sustained Load", Investigation of Reinforced Concrete Columns in Multistory Buildings, Report No. 2, Department of Civil Engineering, University of Alberta, January 1966.
31. ACI Committee 318 - "Commentary on Building Code Requirements for Reinforced Concrete (ACI 318-63)", Publication SP-10, American Concrete Institute, 1965, p 55.
32. Quast, U. - "Berechnung des Zusatzmomentes für Stützen mit Rechteckquerschnitt", unpublished memorandum to Commission 8 - Flambement, Comité Européen du Béton, Braunschweig, April 11, 1968.
33. Blume, J.A., Newmark, N.M. and Corning, L.H. - "Design of Multistory Reinforced Concrete Buildings for Earthquake Motions", Portland Cement Association, Chicago, 1961.
34. Mattock, A.H. - "Rotational Capacity of Hinging Regions in Reinforced Concrete Beams", Proceedings of the International Symposium, Flexural Mechanics of Reinforced Concrete, ASCE, 1966, pp 143-181.
35. Corley, W.G. - "Rotational Capacity of Reinforced Concrete Beams", Journal of the Structural Division, ASCE, Vol. 92, ST5, 1966, pp 121-146.

36. Crandall, S.H. - "Engineering Analysis - A Survey of Numerical Procedures", McGraw-Hill Book Company Inc., New York, 1956.
37. Salvadori, M.G. and Baron, M.L. - "Numerical Methods in Engineering", Prentice-Hall Inc., Englewood Cliffs, N.J., 1962.
38. Neal, B.G. - "The Plastic Methods of Structural Analysis", John Wiley and Sons, New York, 1963.
39. Wright, E.W. and Gaylord, E.H. - "Analysis of Unbraced Multistory Steel Rigid Frames", Journal of the Structural Division, ASCE, Vol. 94, No. ST5, 1968, pp 1143-1163.
40. Pfrang, E.O. - "The Behavior of Columns in Reinforced Concrete Frameworks Subject to Sidesway", Technical Report No. 5, Department of Civil Engineering, University of Delaware, September 1965.
41. Ferguson, P.M. and Breen, J.E. - "Investigation of the Long Concrete Column in a Frame Subject to Lateral Loads", Symposium on Reinforced Concrete Columns, Publication SP-13, American Concrete Institute, 1966, pp 75-114.
42. MacGregor, J.G. and Barter, S.L. - "Long Eccentrically Loaded Concrete Columns Bent in Double Curvature", Symposium on Reinforced Concrete Columns, Publication SP-13, American Concrete Institute, 1966, pp 139-156.
43. Parme, A.L. - Discussion of "Investigation of the Long Concrete Column in a Frame Subject to Lateral Loads", Symposium on Reinforced Concrete Columns, Publication SP-13, American Concrete Institute, 1966, pp 115-119.

44. Everard, N.J. and Cohen, E. - "Ultimate Strength Design of Reinforced Concrete Columns", Publication SP-7, American Concrete Institute, 1964.
45. ACI Committee 340 - "Ultimate Strength Design Handbook - Volume 1", Special Publication No. 17, American Concrete Institute, 1967.
46. ACI Committee 435 - "Allowable Deflections", Proceedings ACI, Vol. 65, 1968, pp 433-444.
47. Breen, J.E. - "Report of the Subcommittee on Normal Range of Variables Encountered in Practice", unpublished memorandum to Joint ASCE-ACI Committee 441 - Reinforced Concrete Columns, Austin, Texas, August 2, 1967.
48. "Guide to Design Criteria for Metal Compression Members", Column Research Council of Engineering Foundation, 1960.
49. "Manual of Steel Construction", Sixth Edition, AISC, New York, 1963.
50. Grier, W.G. - "Essays on the Effective Length of Framed Columns", Jacklin Publications, Kingston, Canada, 1966.
51. MacGregor, J.G., Breen, J.E. and Pfrang, E.O. - "Proposed Revisions to Sections 9.15 and 9.16 of ACI 318-63", paper submitted for publication in ACI Proceedings, 1968.

APPENDIX A  
DERIVATION OF RATIONALIZED  
MOMENT - THRUST - CURVATURE  
PARAMETERS FOR THE COLUMN  
CROSS-SECTIONS



### A.1 Balanced Loading Conditions

For the symmetrically reinforced column section shown in FIGURE 3.2, the strain profile at the ultimate balanced loading condition corresponds to Case 4 of Reference (27). Using the equation provided in this reference, the "exact" value of  $P_b$  can be expressed as:

$$\frac{P_b}{f'_c b t} = \frac{A_s (f_{s2} + f_{s3})}{f'_c b t} + \frac{1}{(\epsilon_4 - \epsilon_1)} \left[ \frac{2\epsilon_0}{3} + \frac{(\epsilon_u - 0.85 \epsilon_0)(\epsilon_4 - \epsilon_0) - 0.075 (\epsilon_4^2 - \epsilon_0^2)}{\epsilon_u - \epsilon_0} \right] \quad (A-1)$$

By definition,  $\epsilon_4 - \epsilon_1 = \phi_b t$ . Moreover, at the balanced failure condition, it is safe to assume that the compression reinforcement has yielded. Hence,  $f_{s2} = -f_{s3} = -f_y$ , and the substitution yields:

$$\frac{P_b}{f'_c b t} = \frac{1}{\phi_b t} \left[ \frac{2\epsilon_0}{3} + \frac{(\epsilon_u - 0.85 \epsilon_0)(\epsilon_4 - \epsilon_0) - 0.075 (\epsilon_4^2 - \epsilon_0^2)}{\epsilon_u - \epsilon_0} \right] \quad (A-2)$$

Assuming a concrete stress-strain relationship as shown in FIGURE 3.1,  $\epsilon_0 = 0.0019$ ,  $\epsilon_u = 0.0038$  and  $f'_c = 0.85 f'_c$ . The definition of balanced failure conditions prescribes that  $\epsilon_4 = \epsilon_u$ . Substitution of these numerical values into EQUATION (A-2) yields:

$$P_b = \frac{0.00257 f'_c b}{\phi_b} \quad (3-4)$$

In a similar manner, the following relationship for  $M_b$  can be derived, again starting with the "exact" equation for  $M$  given in Reference

(27) for a Case 4 strain distribution.

$$M_b = 0.5 p_t b t f_y (d - d') + \frac{f'_c b}{\phi_b} (1285.3t - \frac{3.9635}{\phi_b})(1 \times 10^{-6}) \quad (A-3)$$

By definition,  $e_b = \frac{M_b}{P_b}$ . Substituting the relationships from EQUATIONS (3-4) and (A-3):

$$e_b = t[0.5 - \frac{1.542 \times 10^{-3}}{\phi_b t} + 195(d - d') \phi_b \frac{p_t f_y}{f'_c}] \quad (3-5)$$

#### A.2 Curvatures at the Yield Point of the Column Section

Two values of the yield curvature of a section are required to establish the rationalized relationship shown in FIGURE 3.5.  $\phi_{y0}$  represents the yield curvature in a section subjected to pure flexure.  $\phi_{yb}$  represents the yield curvature with applied axial force equal to  $P_b$ .

In deriving these values, it was assumed that the initial yielding of the tension reinforcement constituted yielding of the section. The reasoning behind this assumption is discussed in SECTION 3.2.2. In addition, it was assumed that the concrete exhibited a linear stress-strain relationship. The linear relationship can be considered representative of the initial portion of FIGURE 3.1, and it has been suggested<sup>(33)</sup> that the concrete stress-strain curve is approximately linear up to about  $0.7 f'_c$ . No attempt was made to check for violations of this extreme fibre stress condition, but the rationalized values compared favourably with the "exact" values over the range of variables investigated.

### A.2.1 Yield Curvature in Pure Flexure

The strain and stress profiles at yielding of a column section in pure flexure can be represented as shown in FIGURE A.1.

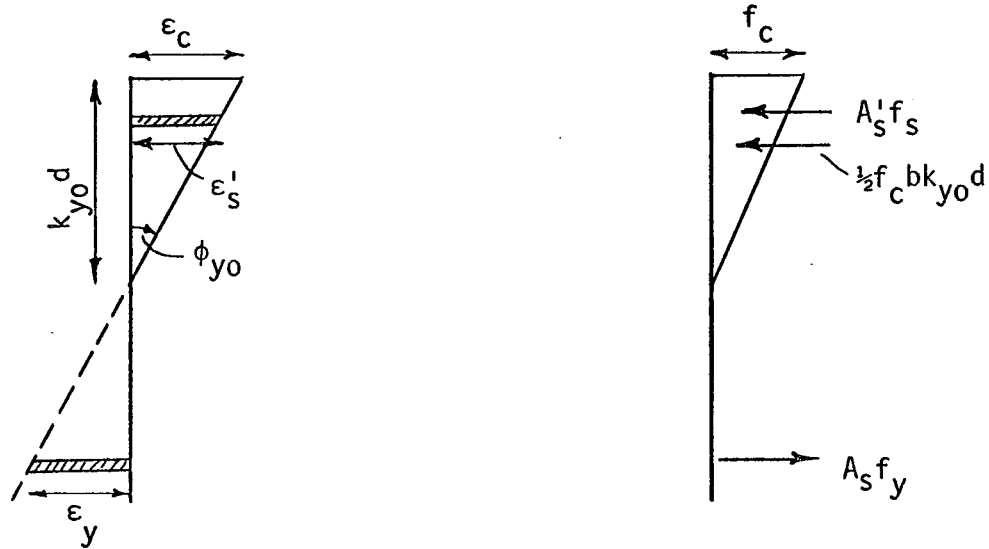


FIGURE A.1

From the linear strain profile:

$$\frac{\epsilon_c}{\epsilon_y} = \frac{k_{yo}}{1 - k_{yo}} = n \frac{f_c}{f_y}$$

$$\therefore f_c = \frac{k_{yo} f_y}{n(1 - k_{yo})}$$

Moreover:

$$\frac{\epsilon'_s}{\epsilon_y} = \frac{k_{yo} - \frac{d'}{d}}{1 - k_{yo}} = \frac{f'_s}{f_y}$$

Since the section is in pure flexure,  $\Sigma H = 0$ , and  $A_s f_y = A'_s f'_s + \frac{1}{2} f_c b k_{yo} d$ .

If  $p = \frac{A_s}{bd} = \frac{A'_s}{bd}$ , substitution of expressions for  $f_c$  and  $f'_s$  yields:

$$k_{yo}^2 + 4pnk_{yo} - 2pn(1 + \frac{d'}{d}) = 0$$

Solving the quadratic equation:

$$k_{yo} = -2pn + \sqrt{4(pn)^2 + 2pn(1 + \frac{d'}{d})} \quad (3-9)$$

From the strain profile:

$$\phi_{yo} = \frac{f_y}{E_s d (1 - k_{yo})} \quad (3-10)$$

#### A.2.2 Yield Curvature under Balanced Axial Force

The strain and stress profiles for the yield condition are shown in FIGURE A.2.

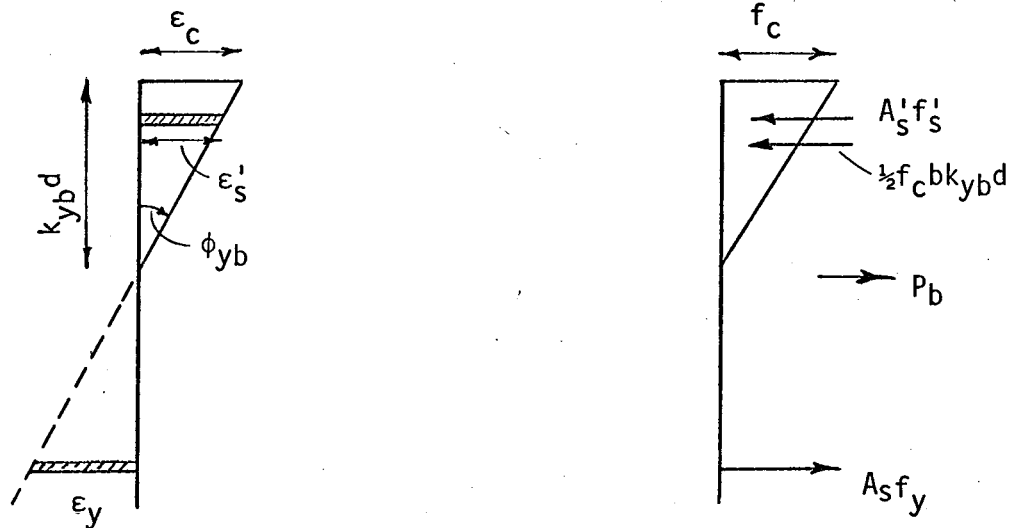


FIGURE A.2

As in SECTION A.1.2,

$$f_c = \frac{k_{yb} f_y}{n(1 - k_{yb})}$$

and

$$f'_s = \frac{k_{yb} - \frac{d'}{d}}{1 - k_{yb}} f_y$$

To satisfy the condition  $\Sigma H = 0$ :

$$A'_s f'_s + \frac{1}{2} f_c b k_{yb} d - A_s f_y = P_b$$

Substitution of expressions for  $f_c$  and  $f'_s$ , and noting that  $p = \frac{A_s}{bd} = \frac{A'_s}{bd}$  yields:

$$k_{yb}^2 \left( \frac{1}{2n} \right) + k_{yb} \left( 2p + \frac{P_b}{f_y bd} \right) - \left[ p \left( 1 + \frac{d'}{d} \right) + \frac{P_b}{f_y bd} \right] = 0$$

Solution of this quadratic equation yields EQUATION (3-11) given in CHAPTER III. From the strain profile,

$$\phi_{yb} = \frac{f_y}{E_s d (1 - k_{yb})} \quad (3-12)$$

It should be recognized that this value of  $\phi_{yb}$  is somewhat artificial since, by definition, yielding of the tension reinforcement occurs at the instant of failure in columns developing a balanced failure, while this procedure predicts a lower value of  $\phi_{yb}$ . It does serve adequately, however, to predict the curvature at which major non-linear behaviour begins to develop in the cross-section. This expression is compared to the more precise curvature values predicted by the "exact" analysis in FIGURE 3.5.

### A.3 Ultimate Curvature of a Column Section

Several assumptions were made to simplify the computation of the ultimate curvature,  $\phi_u$ , of the column section in pure flexure. An approximation of the "exact" concrete stress block shown in FIGURE 3.1 was derived by assuming that the average effective concrete strength in flexure is  $0.7 f'_c$ . Tests<sup>(29)</sup> have indicated that the average ultimate compressive stress in the stress block shown in FIGURE A.3 ranges from about  $0.8 f'_c$  to  $0.6 f'_c$ , the lower value corresponding to high values of  $f'_c$ . The average value of  $0.7 f'_c$  chosen here has been used by other investigators<sup>(33)</sup>.

The failure criterion assumed in this study specifies that the extreme concrete compression fibre is strained to  $\epsilon_u$ . In the derivation which follows, it is assumed that the tension reinforcement has reached the yield plateau, implying an under-reinforced section. To satisfy the condition of force equilibrium in the symmetrically reinforced section, the compression reinforcement must be assumed to remain elastic at failure in pure flexure.

Accordingly, the strain and stress profiles at failure are shown in FIGURE A.3.

From the linear strain profile

$$\epsilon'_{su} = \epsilon_u \left( 1 - \frac{d'}{k_u d} \right)$$

Since the compression reinforcement behaves elastically,

$$f'_{su} = E_s \epsilon'_{su}.$$

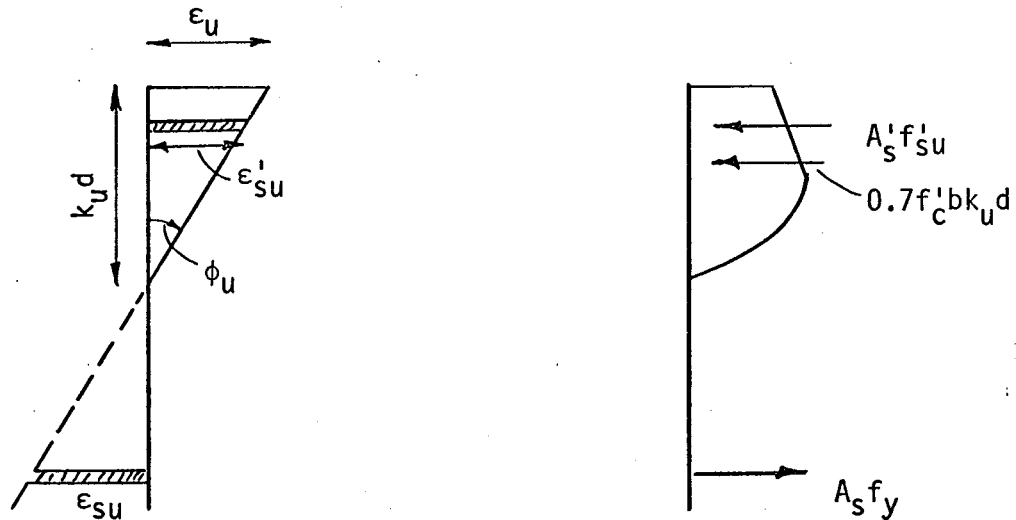


FIGURE A.3

For equilibrium of forces,  $\Sigma H = 0$ , and  $A_s f_y = A'_s f'_{su} + 0.7 f'_c b k_u d$ .

Since  $p = \frac{A_s}{bd} = \frac{A'_s}{bd}$ , substitution of the relationship for  $f'_{su}$

yields:

$$k_u^2 (0.7 f'_c) + k_u (p E_s \epsilon_u - p f_y) - p E_s \epsilon_u \frac{d'}{d} = 0$$

Solution of this quadratic equation yields EQUATION (3-15) given in CHAPTER III for evaluating  $k_u$ .

From the strain profile,

$$\phi_u = \frac{\epsilon_u}{k_u d} \quad (3-16)$$

APPENDIX B  
COMPARISON OF EXACT AND  
RATIONALIZED COLUMN AND  
GIRDER SECTION  
MOMENT-CURVATURE DIAGRAMS



### B.1 Column Section M-P- $\phi$ Relationship

To permit assessment of the inaccuracies involved in the use of the rationalized elastic-plastic column section response characteristics derived in this thesis, comparative plots of exact and rationalized M-P- $\phi$  curves for a representative column section are presented here. The rationalized relationships are discussed in SECTION 3.2.2. The exact values were derived using the approach described in Reference (28).

The section investigated was a symmetrically reinforced column section, detailed as shown in FIGURE 3.2. Although a large number of sections were checked in the course of the thesis, because of space limitations, the comparisons presented here are limited to a column having:

$$\begin{array}{ll} f'_c = 3000 \text{ psi} & \frac{d'}{t} = 0.10 \\ f_y = 45,000 \text{ psi} & b = 10 \text{ in} \\ p_t = 0.04 & t = 10 \text{ in} \end{array}$$

This is the column section shown in FIGURE 3.2 and is that considered in the study discussed in SECTION 5.2.

A comparison of the exact and rationalized values of several basic parameters for this section appears in TABLE B.1. Graphical comparisons of the ultimate interaction diagram, the yield curvature-load ( $\phi_y$ -P) relationship, and the ultimate curvature-load ( $\phi_{pc}$ -P) relationship for this section are presented in FIGURES 3.4, 3.5 and 3.6. FIGURES B.1 to B.5 present comparisons of the exact and rationalized M- $\phi$  curves with various values of axial force P on the section.

Parameter	Exact	Rationalized
$P_o$ ( $\times 10^6$ lb)	0.42480	0.42480
$P_b$ ( $\times 10^6$ lb)	0.13095	0.13092
$M_b$ ( $\times 10^6$ in.lb)	1.0319	1.0335
$M_o$ ( $\times 10^6$ in.lb)	0.73113	0.72000
$\phi_b$ ( $\times 10^{-3}$ /in)	0.58889	0.58889
$\phi_u$ ( $\times 10^{-3}$ /in)	2.7649	2.7786

TABLE B.1

## B.2 Girder Section M- $\phi$ Relationship

Comparisons of exact and rationalized M- $\phi$  relationships for a typical girder section are presented in FIGURE B.6. The rationalized relationships are discussed in SECTION 3.2.3, and the exact values were derived in a manner similar to that described in Reference (28). It should be noted that the exact analysis ignored tension in the concrete.

The girder section considered in FIGURE B.6, reinforced only in tension and detailed as shown in FIGURE 3.7, had properties as follows:

$$\begin{array}{ll}
 f'_c = 3000 \text{ psi} & d' = 1.0 \text{ in} \\
 f_y = 45,000 \text{ psi} & b = 10 \text{ in} \\
 p_b = 0.03175 & d = 10 \text{ in}
 \end{array}$$

The balanced reinforcement ratio,  $p_b$ , is that defined by the ACI Building Code<sup>(2)</sup>. Several other girder sections were considered, and yielded similar results.

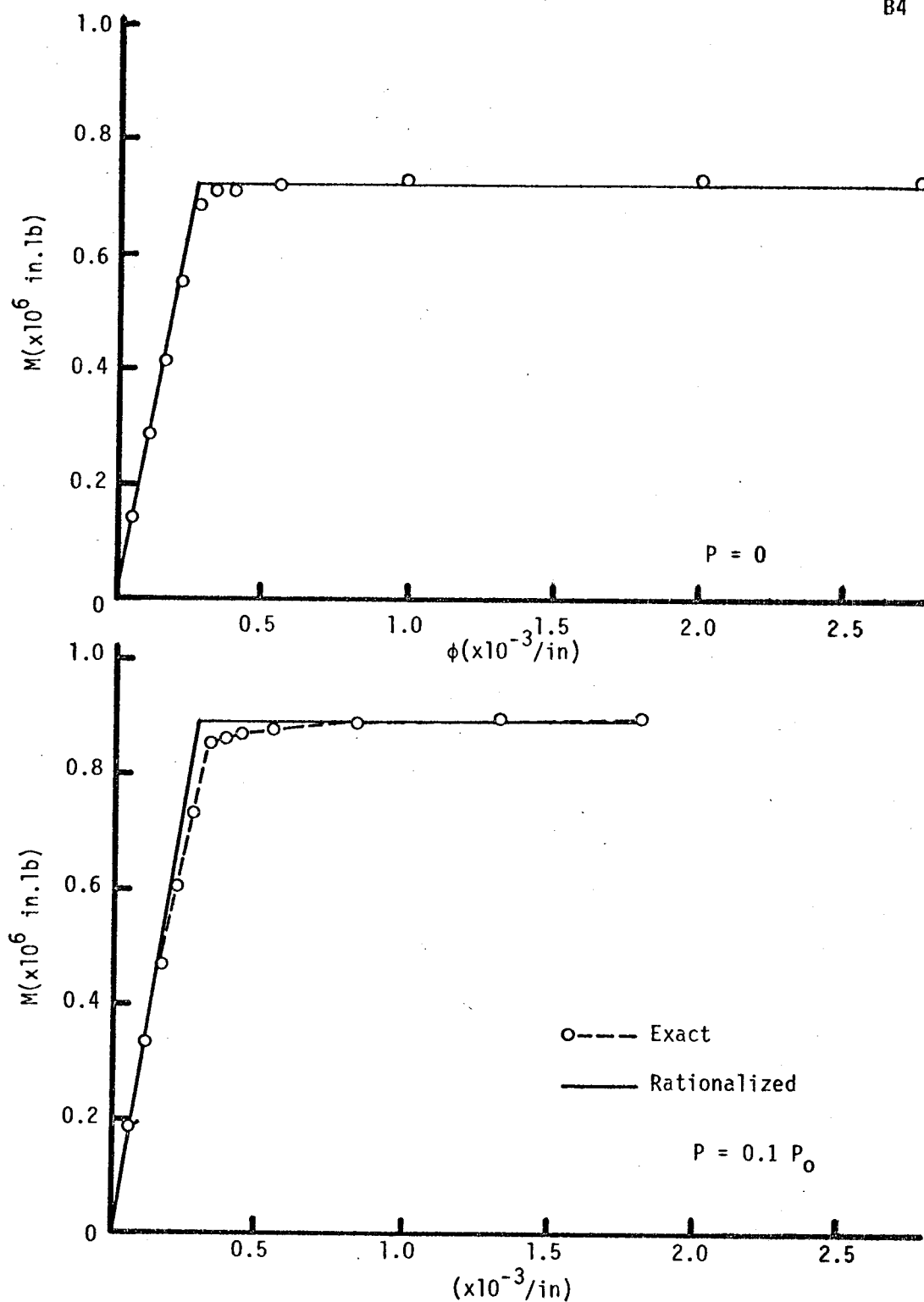


FIGURE B.1

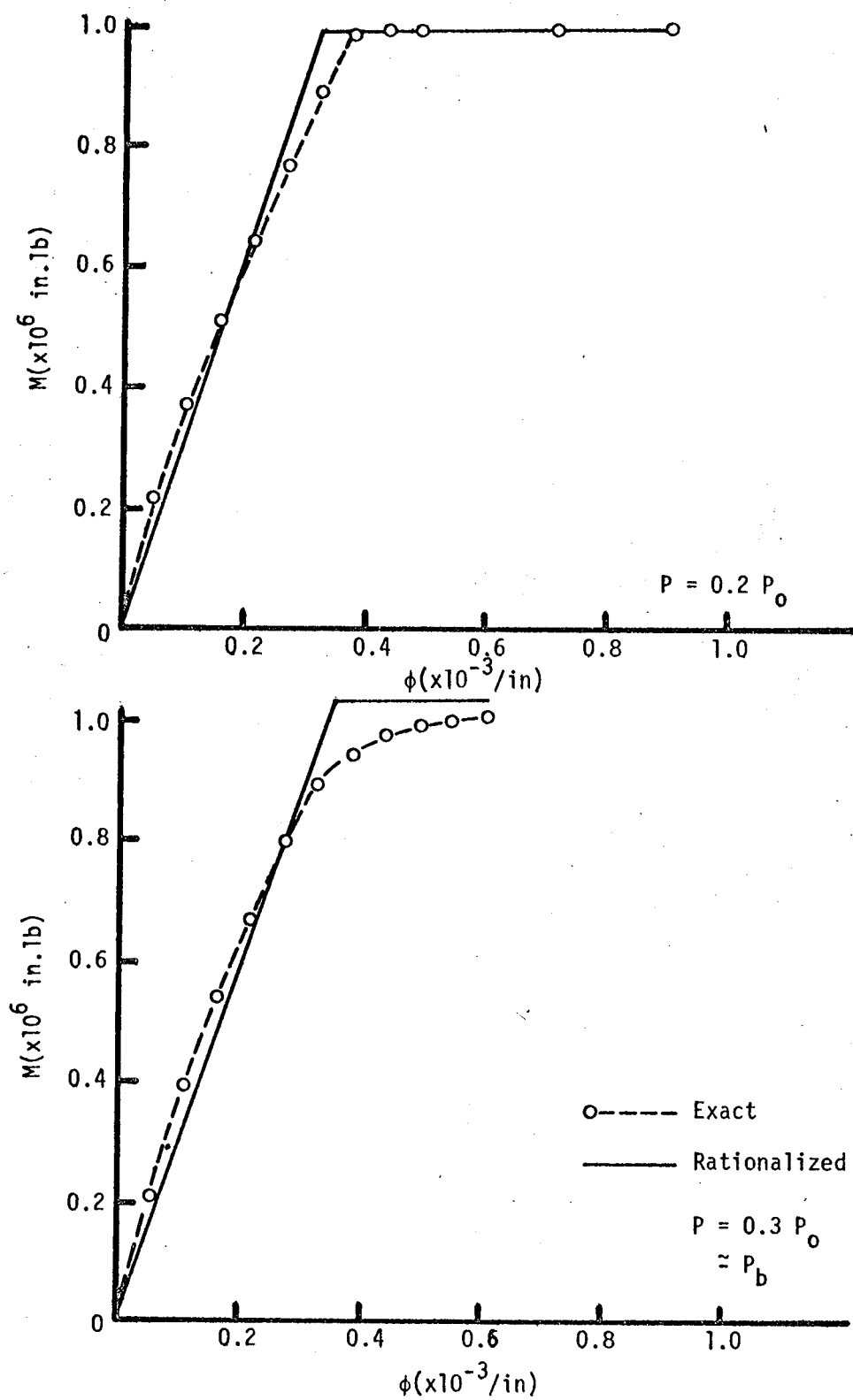


FIGURE B.2

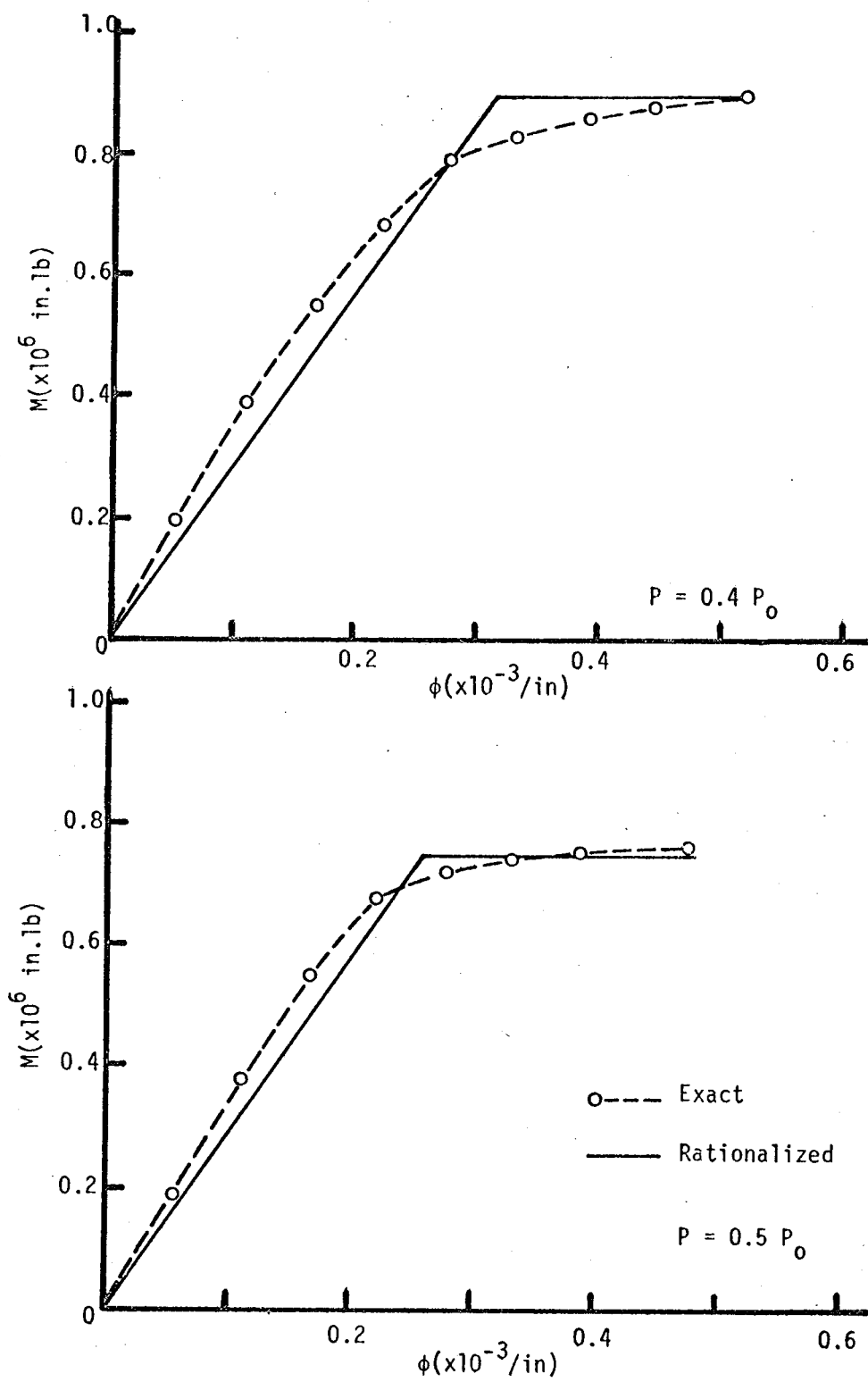


FIGURE B.3

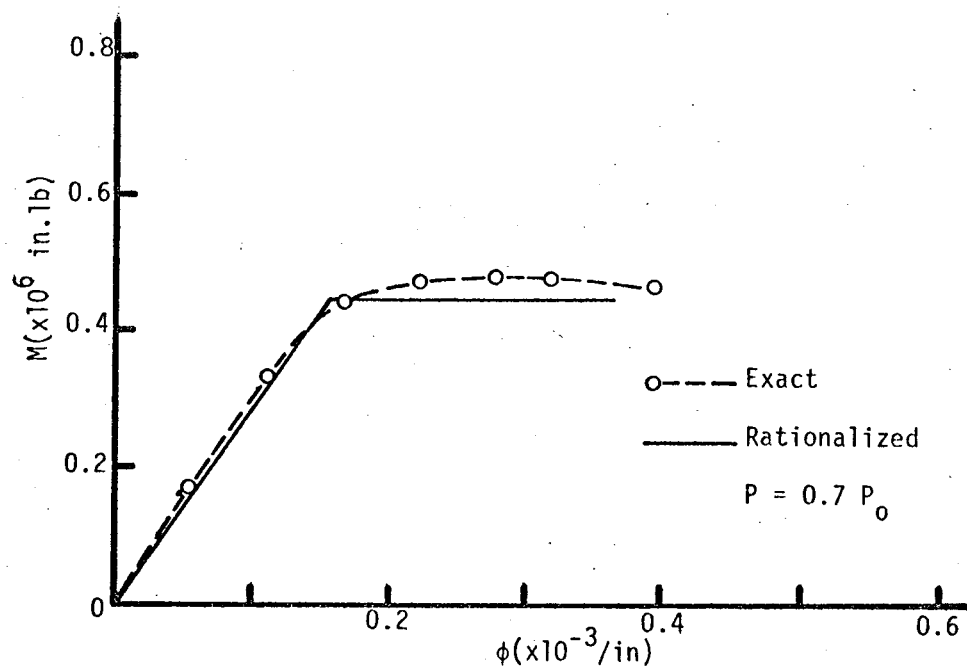
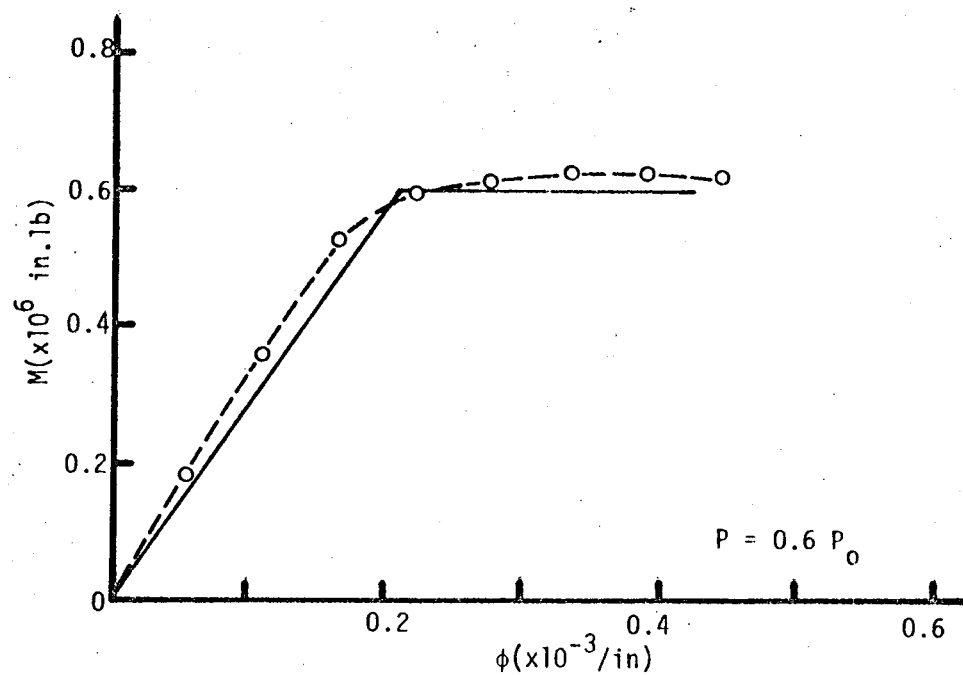


FIGURE B.4

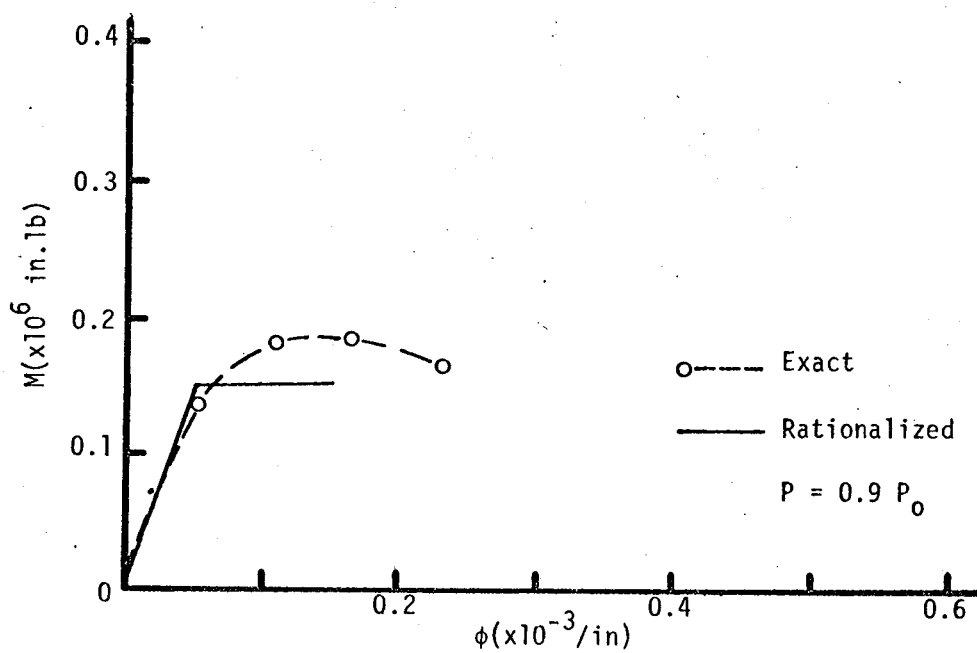
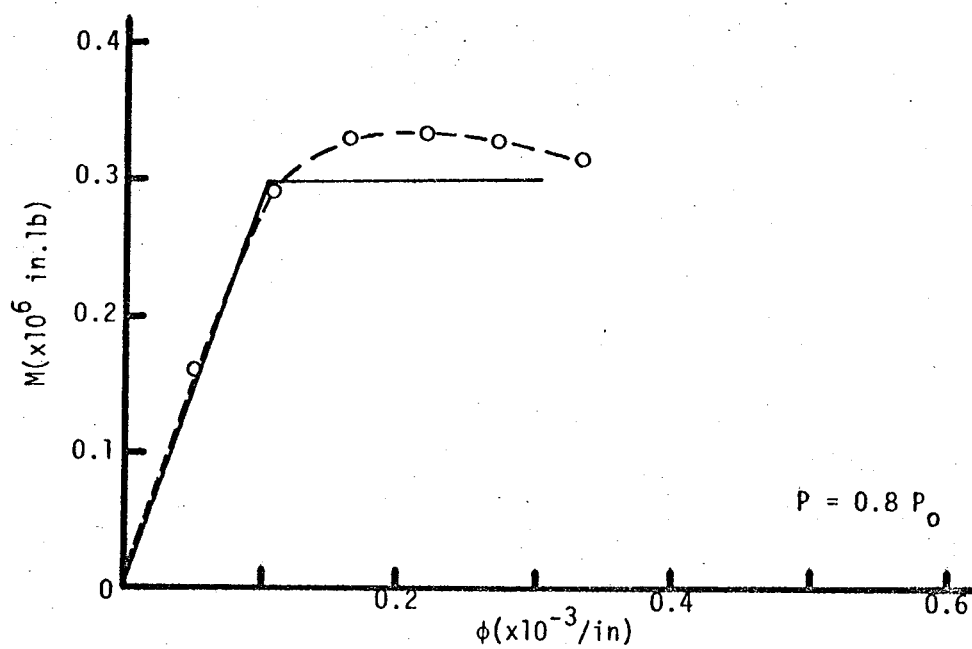


FIGURE B.5

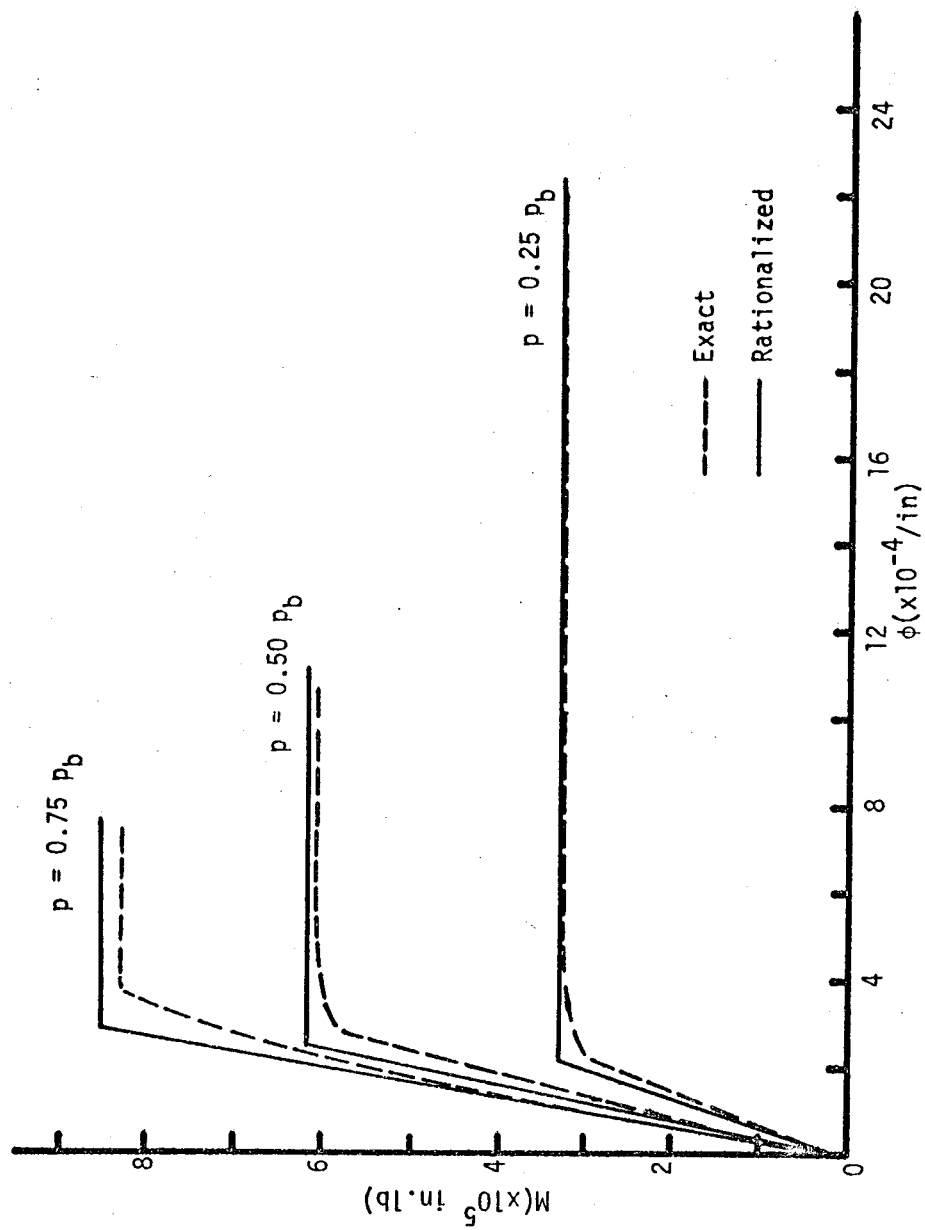


FIGURE B.6



**APPENDIX C**  
**MEMBER BEHAVIOUR**

### C.1 Location and Magnitude of Maximum Moment in a Column

Consider a typical deflected beam-column configuration in equilibrium under the action of forces as shown in FIGURE C.1. All deformations and moments are in the positive sense according to the sign conventions illustrated in FIGURE 3.9.

To check for possible plastic hinge formation along the length of member LU, it is necessary to compute the location and magnitude of the maximum bending moment in the member. In the analysis, the location of the point of maximum moment is at C, a distance  $x$  from the lower end L of the member.

To satisfy equilibrium:

$$R_U = -R_L = \frac{B_U + B_L}{h} + P\rho \quad (C-1)$$

The bending moment,  $M$ , at any point in the member can be written as:

$$M = B_L + Py - \frac{B_U + B_L}{h} x - P\rho x \quad (C-2)$$

According to small deflection theory,  $M = -EI \frac{d^2y}{dx^2}$ .

Thus,

$$EI \frac{d^2y}{dx^2} + Py = \frac{B_U + B_L}{h} x - B_L + P\rho x \quad (C-3)$$

The general solution of this differential equation yields:

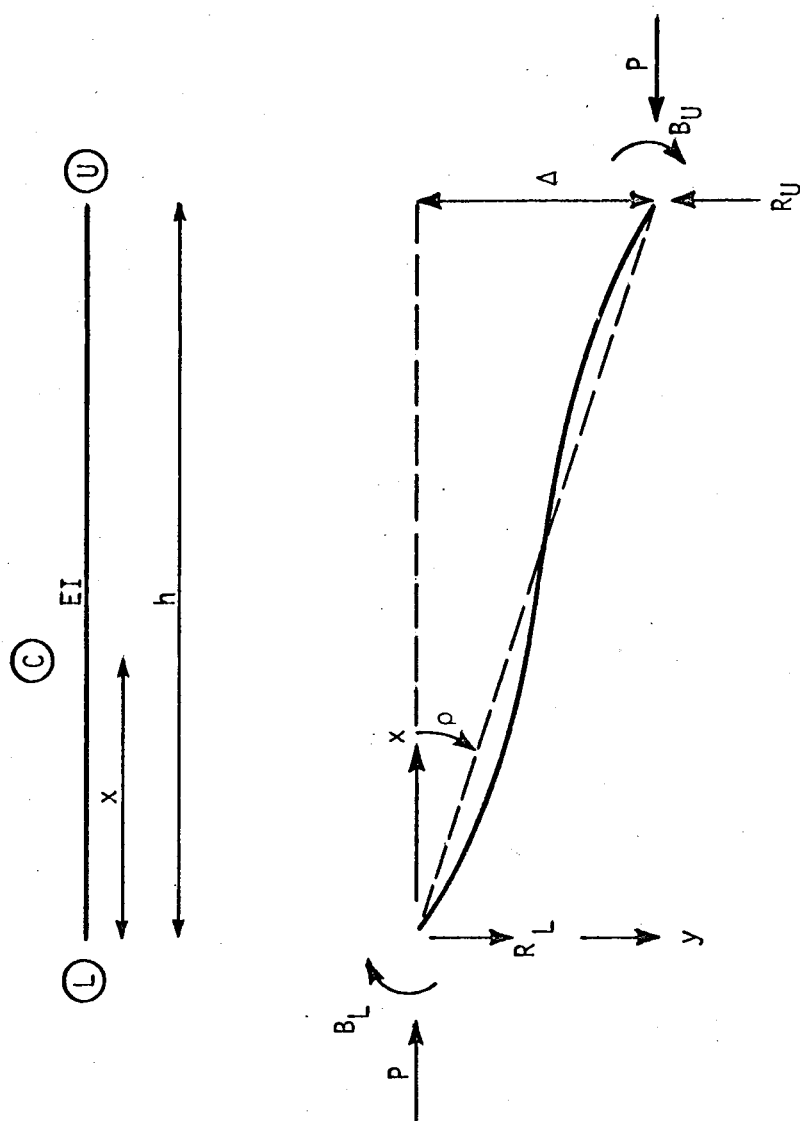


FIGURE C.1

$$y = A \sin kx + B \cos kx + \frac{1}{P} \left[ \frac{B_U + B_L}{h} x - B_L + P\rho x \right] \quad (C-4)$$

where  $k = \sqrt{\frac{P}{EI}}$ .

Applying boundary conditions to evaluate A and B, since  $y = 0$  at  $x = 0$ ,  $B = \frac{B_L}{P}$

$$y = \rho h \text{ at } x = h, A = -\frac{1}{P \sin kh} [B_L \cos kh + B_U]$$

Therefore, substituting for A and B in the general solution,

$$y = -\frac{1}{P \sin kh} (B_U + B_L \cos kh) \sin kx + \frac{B_L}{P} \cos kx + \frac{1}{P} \left( \frac{B_U + B_L}{h} x - B_L + P\rho x \right) \quad (C-5)$$

Substituting EQUATION (C-5) into EQUATION (C-2),

$$M = B_L \cos kx - (B_U + B_L \cos kh) \frac{\sin kx}{\sin kh} \quad (C-6)$$

At the point of maximum bending moment,

$$\frac{dM}{dx} = 0 \quad (C-7)$$

Differentiation of EQUATION (C-6) leads to:

$$\tan kx = -\frac{B_U + B_L \cos kh}{B_L \sin kh} \quad (C-8)$$

Thus,

$$kx = \tan^{-1} \left( - \frac{B_U + B_L \cos kh}{B_L \sin kh} \right) \quad (3-30)$$

If  $0 < kx < kh$ , point C is located along the length of the member LU, and the value of  $M_{\max}$  should be checked.

From EQUATION (C-8),

$$\sin kx = \pm \frac{B_U + B_L \cos kh}{\sqrt{B_L^2 + B_U^2 + 2B_U B_L \cos kh}} \quad (C-9)$$

$$\cos kx = \mp \frac{B_L \sin kh}{\sqrt{B_L^2 + B_U^2 + 2B_U B_L \cos kh}} \quad (C-10)$$

Substitution of the relationships in EQUATIONS (C-9) and (C-10) into EQUATION (C-6) yields:

$$M_{\max} = \mp \frac{\sqrt{B_L^2 + B_U^2 + 2B_U B_L \cos kh}}{\sin kh} \quad (3-31)$$

The problem of establishing the proper sign of  $M_{\max}$  can be approached quite logically. Examination of the sign conventions shown in FIGURE 3.9 and consideration of possible deflected shapes of the member indicates that if  $|B_L| > |B_U|$ ,  $M_{\max}$  adopts the sign of  $B_L$ , and if  $|B_U| > |B_L|$ ,  $M_{\max}$  adopts the opposite sign to  $B_U$ .

## C.2 Slope-Deflection Equations for Girders

The girder configuration considered in this thesis is shown in FIGURE 3.12. The girder is assumed to possess plastic moment capacities as shown in FIGURE 3.13.

In CHAPTER III, slope-deflection equations for this girder configuration were presented in generalized form as:

$$M_A = C_{1A}\theta_A + C_{2A}\theta_B + C_{3A}\delta_{B'} + C_{4A}\delta_{A'} + C_{5A} \quad (3-36)$$

$$M_B = C_{1B}\theta_A + C_{2B}\theta_B + C_{3B}\delta_{B'} + C_{4B}\delta_{A'} + C_{5B} \quad (3-37)$$

The coefficient values for these equations for all seven cases of girder hinging shown in FIGURE 3.14 were presented in TABLES 3.4 and 3.5.

The derivations of the slope-deflection equations for these seven hinging cases are presented in the balance of this section. Equations of this type, originally derived by Parikh<sup>(14)</sup>, are extended to include the effects of the finite width of the shear wall elements.

Throughout this presentation, the sign conventions used for moments and deformations are those shown in FIGURE 3.9.

The effects of shear wall finite width on girder deformation values can be seen in FIGURE C.2. Rotation of joint A' at the midpoint of the shear wall with finite width  $WW_L$  produces a vertical deformation of point A on the face of the shear wall. Thus,

$$\delta_A = \delta_{A'} + \theta_{A'} \frac{WW_L}{2} \quad (C-11)$$

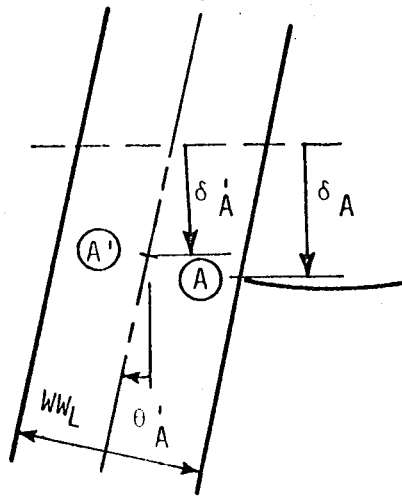


FIGURE C.2

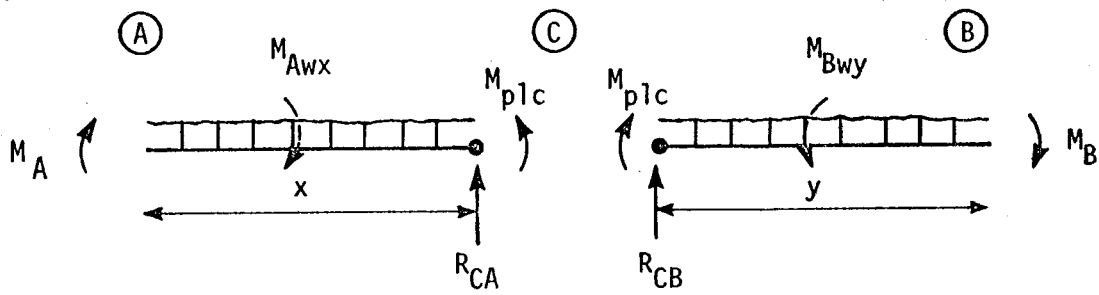


FIGURE C.3

and

$$\delta_B = \delta_{B'} - \theta_{B'} \frac{WW_R}{2} \quad (C-12)$$

The values of  $\delta_{A'}$  and  $\delta_{B'}$  are computed in considering axial shortening effects in the columns and shear walls.

Since points A and B are on the face of the shear wall,  $\theta_A = \theta_{A'}$  and  $\theta_B = \theta_{B'}$ .

To simplify the presentation of the slope-deflection equations, the following substitutions will be used:

$$K = \frac{EI}{L} \quad (C-13)$$

$$W_L = \frac{WW_L}{L} \quad (C-14)$$

$$W_R = \frac{WW_R}{L} \quad (C-15)$$

$$\Delta_L = \frac{\delta_{B'} - \delta_{A'}}{L} \quad (C-16)$$

#### Case 1:

Since there are no girder hinges present in this case, the usual slope-deflection equations apply. Therefore,

$$M_A = M_{FAB} + \frac{4EI}{L} \theta_A + \frac{2EI}{L} \theta_B - \frac{6EI}{L^2} \frac{\delta_B - \delta_A}{L} \quad (C-17)$$

Applying EQUATIONS (C-11) and (C-12) to reference the vertical deformations to points A' and B', and simplifying the expression by sub-



stituting the relationships in EQUATIONS (C-13) to (C-16);

$$M_A = M_{FAB} + (4 + 3 W_L) K \theta_A + (2 + 3 W_R) K \theta_B - 6K \Delta_L \quad (C-18)$$

In a similar manner,

$$M_B = M_{FBA} + (2 + 3 W_L) K \theta_A + (4 + 3 W_R) K \theta_B - 6K \Delta_L \quad (C-19)$$

EQUATIONS (C-18) and (C-19) provide the coefficient values for case 1 in TABLES 3.4 and 3.5 respectively.

Case 2:

With the plastic hinge at point A, the left end, in this hinging configuration,

$$M_A = T_L \quad (C-20)$$

where  $T_L$  is the plastic moment capacity and may have either sign applied to it as shown in FIGURE 3.13.

Because of the rotational discontinuity at A, it is necessary to differentiate between the rotation of the wall side of the joint,  $\theta_A$ , and that of the girder side of the joint,  $\theta_{AB}$ . In EQUATION (C-18),  $4K\theta_A$  represents the portion of  $M_A$  resulting from end rotation of the girder, and might more properly be referred to as  $4K\theta_{AB}$ , where  $\theta_{AB}$  represents the rotation on the girder side of A. On the other hand,  $3 W_L K \theta_A$  is the contribution to  $M_A$  resulting from the change in the vertical deformation of end A due to rotation of joint A'. Thus, rewriting EQUATION (C-18) and

substituting EQUATION (C-20).

$$T_L = M_{FAB} + 4K\theta_{AB} + 3W_L K\theta_A + (2 + 3 W_R) K\theta_B - 6K\Delta_L \quad (C-21)$$

Solving EQUATION (C-21) for the value of  $\theta_{AB}$ , and substituting this value in the  $2K\theta_A$  portion of EQUATION (C-19),

$$\begin{aligned} M_B = M_{FBA} - 0.5 M_{FAB} + 0.5 T_L + 1.5 W_L K\theta_A \\ + 3(1 + 0.5 W_R) K\theta_B - 3K\Delta_L \end{aligned} \quad (C-22)$$

### Case 3:

Proceeding in the same manner as for the case 2 hinging condition:

$$M_B = T_R \quad (C-23)$$

$$\begin{aligned} M_A = M_{FAB} - 0.5 M_{FBA} + 0.5 T_R + 3(1 + 0.5 W_L) K\theta_A \\ + 1.5 W_R K\theta_B - 3K\Delta_L \end{aligned} \quad (C-24)$$

### Case 4:

The girder with the case 4 hinge configuration has a hinge between its ends and can be considered to be broken into two parts, the left side portion being treated as a case 3 girder of span  $x$  with  $WW_R = 0$ , and the right side portion as a case 2 girder of span  $y$  with  $WW_L = 0$ .

In this analysis, only a positive hinge is considered at point C with resisting moments as shown in FIGURE C.3.

Thus, for the x-portion of the girder, from EQUATION (C-24):

$$M_A = M_{FAC} - 0.5 M_{FCA} - 0.5 M_{plc} + \left(1 + \frac{WW_L}{2x}\right) \frac{3EI}{x} \theta_A - \frac{3EI}{x^2} (\delta_C - \delta_A) \quad (C-25)$$

Similarly for the y-portion of the girder, from EQUATION (C-22):

$$M_B = M_{FBC} - 0.5 M_{FCB} + 0.5 M_{plc} + \left(1 + \frac{WW_R}{2y}\right) \frac{3EI}{y} \theta_B - \frac{3EI}{y^2} (\delta_B - \delta_C) \quad (C-26)$$

Consider the free-body diagram shown in FIGURE C.3, where  $M_{Awx}$  and  $M_{Bwy}$ , representing the moments due to uniformly distributed loads, are always positive in the directions shown. For equilibrium of the x portion:

$$R_{CA} = \frac{M_A - M_{plc} + M_{Awx}}{x} \quad (C-27)$$

For equilibrium of the y portion:

$$R_{CB} = - \frac{M_B + M_{plc} - M_{Bwy}}{y} \quad (C-28)$$

However, at the hinge,

$$R_{CA} + R_{CB} = 0 \quad (C-29)$$

Combining EQUATIONS (C-25) to (C-29) yields:

$$\begin{aligned} \delta_C = & \frac{1}{3EI} [x f_{xy} (M_{FAC} - 0.5 M_{FCA} - 1.5 M_{plc} + M_{Awx}) \\ & - y f_{yx} (M_{FBC} - 0.5 M_{FCB} + 1.5 M_{plc} - M_{Bwy})] \\ & + f_{xy} \left[ \left(1 + \frac{WW_L}{2x}\right) \theta_A + \frac{\delta_{A'}}{x} \right] \\ & - f_{yx} \left[ \left(1 + \frac{WW_R}{2y}\right) \theta_B - \frac{\delta_{B'}}{y} \right] \end{aligned} \quad (C-30)$$

where  $f_{xy} = \frac{1}{x^2 \left( \frac{1}{x^3} + \frac{1}{y^3} \right)}$

$$f_{yx} = \frac{1}{y^2 \left( \frac{1}{x^3} + \frac{1}{y^3} \right)}$$

Substituting EQUATION (C-30) into EQUATION (C-25):

$$\begin{aligned} M_A = & \left(1 - \frac{f_{xy}}{x}\right) (M_{FAC} - \frac{M_{FCA}}{2}) + \frac{f_{xy}}{y} (M_{FBC} - \frac{M_{FCB}}{2}) \\ & - \frac{M_{plc}}{2} \left(1 - \frac{3f_{xy}}{x} - \frac{3f_{xy}}{y}\right) - \frac{f_{xy}}{x} M_{Awx} - \frac{f_{xy}}{y} M_{Bwy} \\ & + \frac{3EI}{x} \left(1 + \frac{WW_L}{2x}\right) \left(1 - \frac{f_{xy}}{x}\right) \theta_A \end{aligned}$$

$$\begin{aligned}
& + \frac{3EI}{y} \left(1 + \frac{wR}{2y}\right) \frac{f_{xy}}{y} \theta_B \\
& + \frac{3EI}{x^2} \left(1 - \frac{f_{xy}}{x}\right) \delta_{A'} \\
& - \frac{3EI}{y^2} \frac{f_{xy}}{y} \delta_{B'}
\end{aligned} \tag{C-31}$$

Similarly, substituting EQUATION (C-30) into EQUATION (C-26):

$$\begin{aligned}
M_B = & \left(1 - \frac{f_{yx}}{y}\right) \left(M_{FBC} - \frac{M_{FCB}}{2}\right) + \frac{f_{yx}}{x} \left(M_{FAC} - \frac{M_{FCA}}{2}\right) \\
& + \frac{M_{plc}}{2} \left(1 - \frac{3f_{yx}}{x} - \frac{3f_{yx}}{y}\right) + \frac{f_{yx}}{x} M_{Awx} + \frac{f_{yx}}{y} M_{Bwy} \\
& + \frac{3EI}{x} \left(1 + \frac{wL}{2x}\right) \frac{f_{yx}}{x} \theta_A \\
& + \frac{3EI}{y} \left(1 + \frac{wR}{2y}\right) \left(1 - \frac{f_{yx}}{y}\right) \theta_B \\
& + \frac{3EI}{x^2} \frac{f_{yx}}{x} \delta_{A'} \\
& - \frac{3EI}{y^2} \left(1 - \frac{f_{yx}}{y}\right) \delta_{B'}
\end{aligned} \tag{C-32}$$

Replacement of fixed end moment terms,  $M_{Awx}$  and  $M_{Bwy}$ , in EQUATIONS (C-31) and (C-32) by actual values expressed in terms of the uniformly distributed load  $w$ , leads to the coefficient values for case 4 hinging presented in TABLES 3.4 and 3.5 respectively.

Case 5:

The formation of two plastic hinges renders the girder a statically determinate system in which the moment values are independent of rotations and stiffness values.

$$M_A = T_L \quad (C-33)$$

Using statics, it can easily be shown that:

$$M_B = (T_L - M_{plc}) \frac{y}{x} - M_{plc} + \frac{wyl}{2} \quad (C-34)$$

Case 6:

Proceeding as was done in Case 5:

$$M_A = M_{plc} + (T_R + M_{plc}) \frac{x}{y} - \frac{wxl}{2} \quad (C-35)$$

$$M_B = T_R \quad (C-36)$$

Case 7:

With plastic hinges at both ends of the girder:

$$M_A = T_L \quad (C-37)$$

$$M_B = T_R \quad (C-38)$$

These slope-deflection equations are applicable to a girder

subjected to uniformly distributed loads. The equations could easily be adapted to consider a single in-span concentrated load in place of the uniformly distributed load. Consideration of more than one in-span concentrated load, however, would necessitate extension of the number of hinging configurations considered in the analysis.

### C.3 Evaluation of Plastic Hinge Rotation

Working from the slope-deflection equations for columns and girders, it is possible to derive equations for computing plastic hinge rotations in terms of known values of moments and deformations. Only the equations are presented here.

The sign conventions for hinge rotations are shown in FIGURE 3.9.

#### Column Case 2:

$$\theta_{DL} = \frac{h}{CEI} B_L - \frac{S}{C} \theta_U + \frac{C+S}{C} \frac{\delta_U - \delta_L}{h} - \theta_L \quad (C-39)$$

#### Column Case 3:

$$\theta_{DU} = \frac{h}{CEI} B_U - \frac{S}{C} \theta_L + \frac{C+S}{C} \frac{\delta_U - \delta_L}{h} - \theta_U \quad (C-40)$$

#### Column Case 4:

$$\begin{aligned} \theta_{DH} = & \frac{x}{EI(C_x^2 - S_x^2)} (-S_x B_L - C_x B_{\max}) \\ & + \frac{y}{EI(C_y^2 - S_y^2)} (S_y B_U - C_y B_{\max}) \end{aligned}$$

$$+ \frac{\delta_C - \delta_L}{x} - \frac{\delta_U - \delta_C}{y} \quad (C-41)$$

where

$$\delta_C = \frac{y^2}{(C_y^2 - S_y^2)EI} (C_y B_U - S_y B_{\max}) - y\theta_U + \delta_U \quad (C-42)$$

Column Case 5:

$$\theta_{DU} = \frac{h}{EI(C^2 - S^2)} (CB_U - SB_L) + \frac{\delta_U - \delta_L}{h} - \theta_U \quad (C-42a)$$

$$\theta_{DL} = \frac{h}{EI(C^2 - S^2)} (CB_L - SB_U) + \frac{\delta_U - \delta_L}{h} - \theta_L \quad (C-43)$$

Girder Case 2:

$$\begin{aligned} \theta_{DA} = & - (1 + 0.75 W_L) \theta_A - (0.5 + 0.75 W_R) \theta_B \\ & + 1.5 \Delta_L + \frac{L}{4EI} (T_L - M_{FAB}) \end{aligned} \quad (C-44)$$

where  $W_L$ ,  $W_R$  and  $\Delta_L$  are defined in EQUATIONS (C-14) to (C-16).

Girder Case 3:

$$\begin{aligned} \theta_{DB} = & - (0.5 + 0.75 W_L) \theta_A - (1 + 0.75 W_R) \theta_B \\ & + 1.5 \Delta_L + \frac{L}{4EI} (T_R - M_{FBA}) \end{aligned} \quad (C-45)$$



Girder Case 4:

$$\begin{aligned}
\theta_{DC} = & \frac{x}{4EI} (-M_{plc} - M_{FCA}) - \frac{y}{4EI} (M_{plc} - M_{FCB}) \\
& - \frac{1}{2} \left(1 + \frac{3WW_L}{2x}\right) \theta_A + \frac{1}{2} \left(1 + \frac{3WW_R}{2y}\right) \theta_B \\
& + \frac{3}{2x} (\delta_C - \delta_{A'}) - \frac{3}{2y} (\delta_{B'} - \delta_C)
\end{aligned} \tag{C-46}$$

where  $\delta_C$  is given by EQUATION (C-30).

Girder Case 5:

$$\begin{aligned}
\theta_{DA} = & \frac{x}{6EI} (2T_L + M_{plc} - 2M_{FAC} + M_{FCA}) - \left(1 + \frac{WW_L}{2x}\right) \theta_A \\
& + \frac{\delta_C - \delta_{A'}}{x}
\end{aligned} \tag{C-47}$$

where

$$\begin{aligned}
\delta_C = & \frac{y^2}{3EI} \left[ T_L \frac{y}{x} - M_{plc} \left( \frac{y}{x} + \frac{3}{2} \right) + \frac{wyL}{2} - M_{FBC} + \frac{M_{FCB}}{2} \right] \\
& - (y + 0.5 WW_R) \theta_B + \delta_{B'}
\end{aligned} \tag{C-48}$$

$$\begin{aligned}
\theta_{DC} = & \frac{1}{EI} \left[ \frac{x}{6} (M_{FAC} - 2M_{FCA} - T_L - 2M_{plc}) + \frac{y}{4} (M_{FCB} - M_{plc}) \right] \\
& - \frac{WW_L}{2x} \theta_A + \left( \frac{1}{2} + \frac{3WW_R}{4y} \right) \theta_B \\
& + \frac{\delta_C - \delta_{A'}}{x} + \frac{3(\delta_{B'} - \delta_C)}{2y}
\end{aligned} \tag{C-49}$$

Girder Case 6:

$$\theta_{DB} = \frac{y}{6EI} (2T_R - M_{plc} - 2M_{FBC} + M_{FCB}) - \left(\frac{WW_R}{2y} + 1\right) \theta_B + \frac{\delta_{B'} - \delta_C}{y} \quad (C-50)$$

where

$$\delta_C = \frac{x^2}{3EI} \left[ -T_R \frac{x}{y} - M_{plc} \left( \frac{x}{y} + \frac{3}{2} \right) + \frac{wxL}{2} + M_{FAC} - \frac{M_{FCA}}{2} \right] + (x + 0.5 WW_L) \theta_A + \delta_{A'} \quad (C-51)$$

$$\theta_{DC} = \frac{1}{EI} \left[ -\frac{x}{4} (M_{plc} + M_{FCA}) + \frac{y}{6} (T_R - 2M_{plc} + 2M_{FCB} - M_{FBC}) \right] - \left( \frac{1}{2} + \frac{3WW_L}{4x} \right) \theta_A + \frac{WW_R}{2y} \theta_B + \frac{3(\delta_C - \delta_{A'})}{2x} - \frac{\delta_{B'} - \delta_C}{y} \quad (C-52)$$

Girder Case 7:

$$\theta_{DA} = \frac{L}{6EI} (2T_L - T_R - 2M_{FAB} + M_{FBA}) - (0.5W_L + 1) \theta_A - 0.5 W_R \theta_B + \Delta_L \quad (C-53)$$

$$\theta_{DB} = \frac{L}{6EI} (2T_R - T_L - 2M_{FBA} + M_{FAB}) - 0.5 W_L \theta_A - (0.5 W_R + 1) \theta_B + \Delta_L \quad (C-54)$$

APPENDIX D  
COMPUTER PROGRAMME

### D.1 Notation Used in the Computer Programme

A,B,D,F	functions used to simplify consideration of Case 4 column hinging configuration (Refer to TABLES 3.2 and 3.3)
AA,CC,DD, EE,FF,GG	dummy variables used in evaluating P(M,N) in Subroutine PCOL. The significance of each is discussed on comment cards in the programme.
V,T,Z,U	dummy variables used in computation of DH(M) in Subroutine ITER (Refer to FIGURE 4.7)
VV,TT,ZZ,UU	dummy variables used for summation of V,T,Z,U
CC,GL,AG DD,GR,AD EE,GA,AA FF,GB,AB	dummy variables used in computation of R(M,N) in Subroutine ITER (Refer to FIGURE 4.4)
ACCURD	specified required accuracy of convergence of deformation values for convergence: $(1 - \text{ACCURD}) < \frac{\text{deformation (n+1)}}{\text{deformation (n)}} < (1 + \text{ACCURD})$
ACCURP	as above, for convergence of column axial load values
AL(M,N)	sign of moment at lower end hinge in column (M,N)
AM(M,N)	sign of moment at interior hinge in column (M,N)
AU(M,N)	sign of moment at upper end hinge in column (M,N)
AUGDL	dead load incrementing fraction, as a decimal fraction of working load values
AUGE	column external load incrementing fraction
AUGL	lateral load incrementing fraction
AUGLL	live load incrementing fraction
BAS(M,N)	reinforcement area $A_s$ in girder (M,N) at interior support (sq.in.)

BB(M,N)	width of compression face b in girder (M,N) (in)
BC	maximum in-span girder moment (in.lb.)
BL	left end moment $M_A$ in girder (in.lb.) or lower end moment $B_L$ in column
BMAX	maximum interior moment in column (in.lb.)
BR	right end moment $M_B$ in girder (in.lb.)
BT(M,N)	total depth of section t in girder (M,N) - (in.)
BU	upper end moment $B_U$ in column (in.lb.)
C(M,N)	stability function C for column (M,N)
CAS(M,N)	total longitudinal reinforcement area $2A_s$ in column (M,N) (sq.in.)
CB(M,N)	width of compression face b in column (M,N) (in)
CT(M,N)	total depth of section t in column (M,N)-(in.)
CX	stability function $C_x$ in x-portion of column
CXF	$\frac{C_x}{C_x^2 - S_x^2}$
CY	stability function C in y-portion of column
CYF	$\frac{C_y}{C_y^2 - S_y^2}$
D	distance, d, from extreme compression fibre to centroid of tension reinforcement in column section (in.)
DEL	dummy used for deformations
DETF	"deterioration" factor used in reducing size of load increment as hinging progresses

DH(M)	sway deflection in story (M) (in)
DHC	total sway deflection at top of structure (in)
DHCP(3)	the last three previous values of DHC related to stable configurations (in)
DHH	total sway deflection $\delta_H$ at interior hinge in column (in)
DHI(M)	the value of DH(M) for the last previous stable load stage
DHR	$\frac{DH(M) \text{ for cycle } (n)}{DH(M) \text{ for cycle } (n-1)}$
DHU	total sway deflection $\delta_U$ at top of column (in)
DPB	concrete cover $d'$ in girder section (in)
DPC	concrete cover $d'$ in column section (in)
DV(M,N)	vertical deformation of joint (M,N) (in)
DVC	vertical deformation, $\delta_C$ , at in-span hinge in girder (in.)
EB	balanced eccentricity $e_b$ for column section (in.)
EIB(M,N)	section flexural stiffness EI of girder (M,N) (lb.in <sup>2</sup> )
EIC(M,N)	section flexural stiffness EI of column (M,N) (lb.in <sup>2</sup> )
EN	modular ratio $n = \frac{E_s}{E_c} = \frac{29,000,000}{58,000 \sqrt{f'_c}} = \frac{500}{\sqrt{f'_c}}$
F	dummy for kh
FAUGDL	load factor with respect to working load values for dead loads
FAUGE	load factor with respect to working load values for external column loads
FAUGL	load factor with respect to working load values for lateral loads
FAUGLL	load factor with respect to working load values for live loads

FAUGLP(3)	the last three previous values of FAUGL which resulted in stable configurations
FC	dummy for $f'_c$
FCB	compressive strength of concrete $f'_c$ in girders (psi)
FCC	compressive strength of concrete $f'_c$ in columns (psi)
FCW	compressive strength of concrete $f'_c$ in shear walls (psi)
FX	dummy for $k_x$ or $k_y$
FXY	$f_{xy}$ (Refer to TABLE 3.4)
FY	dummy for $f_y$
FYB	yield strength of reinforcement $f_y$ in girders (psi)
FYC	yield strength of reinforcement $f_y$ in columns (psi)
FYW	yield strength of reinforcement $f_y$ in shear walls (psi)
FYX	$f_{yx}$ (Refer to TABLE 3.5)
H(M)	centre-line height of storey (M) - (in.)
I	dummy for N
INDET	degree of indeterminacy of the structure
J	counter in Subroutine ITER for number of cycles of iteration
KB(M,N)	number denoting plastic hinge configuration in girder (M,N) (Refer to FIGURE 3.14)
KBI(M,N)	plastic hinge configuration in girder (M,N) at last previous stable load stage
KC(M,N)	number denoting plastic hinge configuration in column (M,N) (Refer to FIGURE 3.11)
KCC	dummy counter in Subroutine HINGES
KCI(M,N)	plastic hinge configuration in column (M,N) at last previous stable load stage

KD	counter for number of cases of inadequate convergence of storey sway deflection values in Subroutine ITER
KH	counter for number of new plastic hinges detected in one pass through Subroutine HINGES
KHC	total number of plastic hinges in the structure
KHCI	total number of plastic hinges in the structure at the last stable load stage
KK	dummy for KB(M,N) or KC(M,N)
KP	counter for number of cycles through Subroutine PCOL at any stage of loading
KR	counter for number of cases of inadequate convergence of joint rotation values in Subroutine ITER
LIMITD	limiting number of cycles of iteration to converge on deformation values at any load stage before instability is assumed
LIMITP	limiting number of cycles through Subroutine PCOL to converge on column axial load values at any load stage before instability is assumed
M	subscript which refers to floor or storey number, working from the top of the structure
MS	total number of storeys in the structure
N	subscript which refers to column line or bay number, working from the left side of the structure
NC	total number of column lines in the structure
NN	total number of bays in the structure



NP	counter for number of load stages considered
NSW	total number of shear walls in the structure ( $0 \leq \text{NSW} \leq \text{NC}$ )
NW(N)	number of column line where a shear wall is located
P(M,N)	current value of axial load in column (M,N) (lb.)
PB	ultimate column axial load at balanced failure condition, $P_b$ (lb.)
PE(N)	current value of external load on column line (N) (lb)
PEI(N)	working load value of external load on column line (N)(lb)
PEXC	dummy counter to record cases in Subroutine COLS where $P(M,N)$ exceeds $P_o$
PP(M,N)	the value of $P(M,N)$ at the last previous stable load stage
PS	reinforcement ratio $p = \frac{A_s}{bd}$ in girder or column section
PU	ultimate axial load capacity $P_o$ of column section in absence of flexure (lb)
R(M,N)	rotation of joint (M,N) (radians)
RATIO	a dummy used in the extrapolation procedure, representing $\frac{\text{DHC (extrapolated for new FAUGL)}}{\text{DHC (previous stable configuration)}}$
RB	balanced curvature $\phi_b$ ( $\text{in}^{-1}$ )
RBP(M,N)	permissible hinge rotation of a "half-hinge" in girder (M,N) (radians)
RCP(M,N)	permissible hinge rotation of a "half-hinge" in column (M,N) (radians)
RDA	plastic hinge rotation $\theta_{DA}$ at left end of girder (radians)
RDB	plastic hinge rotation $\theta_{DB}$ at right end of girder (radians)
RDC	plastic hinge rotation $\theta_{DC}$ at in-span hinge in girder or $\theta_{DH}$ at interior hinge in column (radians)

RDL	plastic hinge rotation $\theta_{DL}$ at lower end of column (radians)
RDU	plastic hinge rotation $\theta_{DU}$ at upper end of column (radians)
RP(M,N)	value of R(M,N) at the last previous stable load stage
RPC	ultimate curvature $\phi_{pc}$ of column section ( $\text{in}^{-1}$ )
RR	$\frac{R(M,N) \text{ for cycle } (n)}{R(M,N) \text{ for cycle } (n-1)}$
RU	ultimate curvature $\phi_u$ for column section in pure flexure ( $\text{in}^{-1}$ )
RY	yield curvature $\phi_y$ for column section ( $\text{in}^{-1}$ )
RYB	yield curvature for column section under balanced axial load $\phi_{yb}$ ( $\text{in}^{-1}$ )
RYO	yield curvature for column section in pure flexure $\phi_{yo}$ ( $\text{in}^{-1}$ )
S(M,N)	stability function S for column (M,N)
SIDE	dummy used in Subroutine PCOL to denote whether left hand or right hand girder is under consideration
SP(N)	centre-line span of bay (N) (in)
SR	girder span reduced by consideration of finite shear wall widths (in)
SX	stability function $S_x$ in x-portion of column
SXF	$\frac{S_x}{c_x^2 - S_x^2}$
SY	stability function $S_y$ in y-portion of column
SYF	$\frac{S_y}{c_y^2 - S_y^2}$
TB	ultimate column moment capacity at balanced failure condition $M_b$ (in.lb)

TL(M,N)	bending moment at left end hinge of girder (M,N) (in.lb)
TPC(M,N)	ultimate bending moment capacity $M_{pc}$ of column (M,N) (in.lb)
TPL(M,N)	ultimate bending moment capacity $M_{p1}$ of girder (M,N) (in.lb)
TPRATE	$\frac{\text{girder exterior support } M_{p1}}{\text{girder interior support } M_{p1}}$
TPRATM	$\frac{\text{girder midspan } M_{p1}}{\text{girder interior support } M_{p1}}$
TR(M,N)	bending moment at right end hinge of girder (M,N) (in.lb)
TU	column ultimate bending moment capacity in pure flexure $M_o$ (in.lb)
UK	$k_u$ , the proportion of $d$ from the extreme compression fibre to the neutral axis in a girder section
W(M)	current value of lateral load at floor (M) (lb)
WD(M,N)	current value of dead load on girder (M,N) (lb/ft), neglecting girder self-weight
WDI(M,N)	working load value of WD(M,N) (lb/ft)
WI(M)	working load value of W(M) (lb)
WL(M,N)	current value of live load on girder (M,N) (lb/ft)
WLAT	total lateral load resisted by shear wall (M,N) (lb)
WLI(M,N)	working load value of WL(M,N) (lb/ft)
WPER	percentage of total lateral shear load acting on storey N carried by shear wall (M,N)
WS	dummy to compute total transverse shear load acting at floor (M)
WT	dummy to consider total uniformly distributed load on a girder
WTW	current value of exterior wall weight (lb/storey)

WTWI            working load value of WTW (lb/storey)

WWL            dummy to represent width of shear wall at left end of  
girder (in)

WWR            dummy to represent width of shear wall at right end of  
girder (in)

X,XX           used frequently as dummies

XB(M,N)       distance x from left end of girder (M,N) to an in-span  
hinge (in)

XC(M,N)       distance x from base of column (M,N) to an interior hinge (in)

XXX            a dummy used to indicate that a condition of instability  
has been detected

XXX = 0.0 indicates that the structure is stable

XXX = 1.0 indicates that the iteration procedure in Sub-  
routine ITER has failed to converge on deformation  
values to the specified accuracy ACCURD after LIMITD  
cycles

XXX = 2.0 indicates that a joint mechanism has been detected  
in Subroutine ITER

XXX = 3.0 indicates that the structure in some storey was  
unable to support the current load values at the  
equilibrium sway deflection value previously computed  
under lower loads

XXX = 4.0 indicates that a storey sway mechanism has been  
detected in Subroutine HINGES

XXX = 5.0 indicates that the solution has failed to converge  
on column axial load values to the specified accuracy  
ACCURP after LIMITP cycles

XY	a dummy used to indicate that bending moment values should be written out in Subroutine HINGES  XY = 0.0 - no moment values written XY = 1.0 - moment values written
Y	used frequently as a dummy
YBK	$k_{yb}$ , the proportion of d from the extreme compression fibre to the neutral axis with $P(M,N) = PB$
YOK	$k_{yo}$ , the proportion of d from the extreme compression fibre to the neutral axis with $P(M,N) = 0$
YYY	a counter used to indicate the number of load adjustments made after first indication of instability (when $YYY = 4.0$ , solution stopped)
Z	dummy
ZL,ZR	dummies used to consider variation of $M_{p1}$ in girders

## D.2 Functions of the Subroutines

To perform the computer analysis, nine subroutines were employed in conjunction with the main programme. A brief description of the functions of these individual subroutines will aid in the understanding of the flow charts presented in SECTION D.3.

Subroutine BEAMS computes the values of plastic moment capacity, flexural rigidity and permissible hinge rotations for all girders in the structure.

Subroutine PCOL computes the axial loads in all columns and shear walls, based on the current load and deformation values.

Subroutine AXDEF computes the vertical deformations of all

joints resulting from axial shortening of the columns and shear walls.

Subroutine COLS, using the rationalized M-P- $\phi$  relationship, computes  $M_{pc}$ , EI, C, S, and allowable hinge rotation values for all columns and shear walls, based on the current values of axial loads.

Subroutine CASE4 computes the special values of C, S, A, B, D, F necessary for consideration of a column with the case 4 hinging configuration.

Subroutine ITER, using the "operator" relationships discussed in CHAPTER IV, computes values of lateral sway deflections and joint rotations by the Gauss-Seidel iteration procedure.

Subroutine HINGES checks and revises the hinge configurations in all columns and shear walls, using the slope-deflection equations.

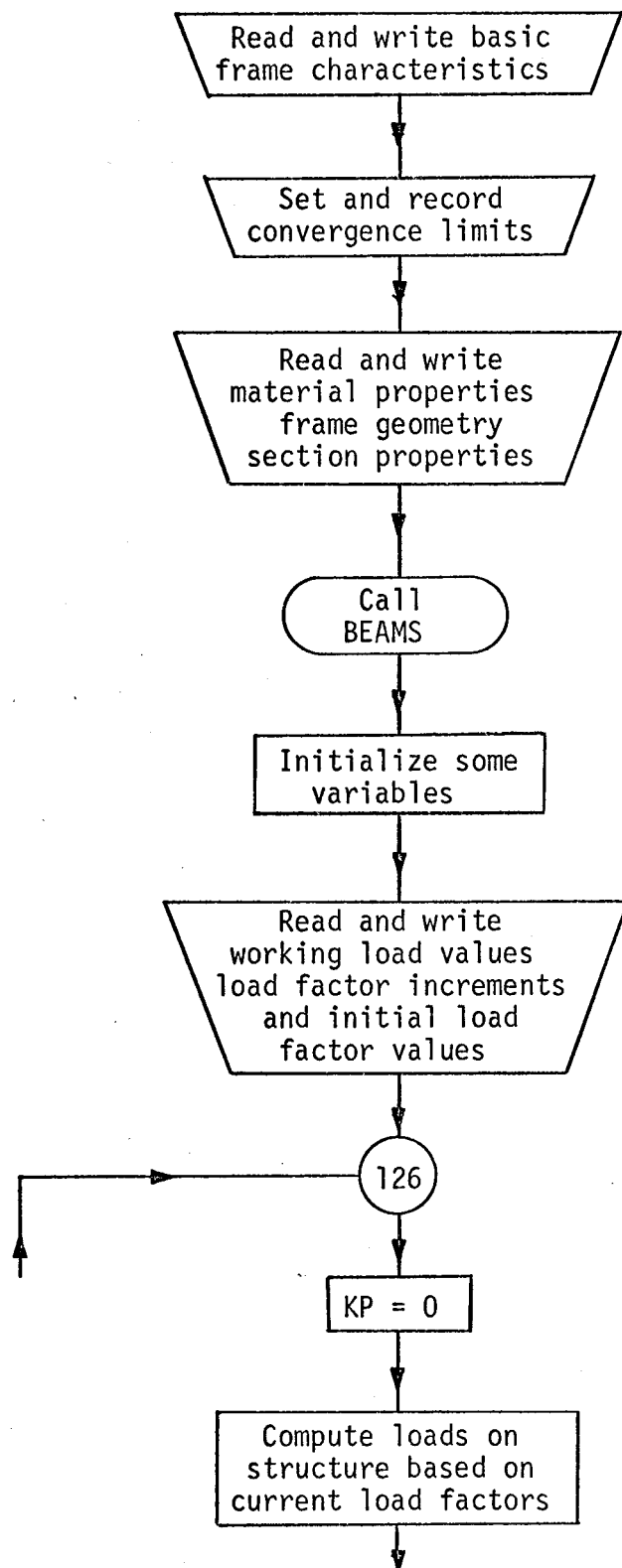
Subroutine BMHING performs the same function for the girders as Subroutine HINGES does for the columns and shear walls.

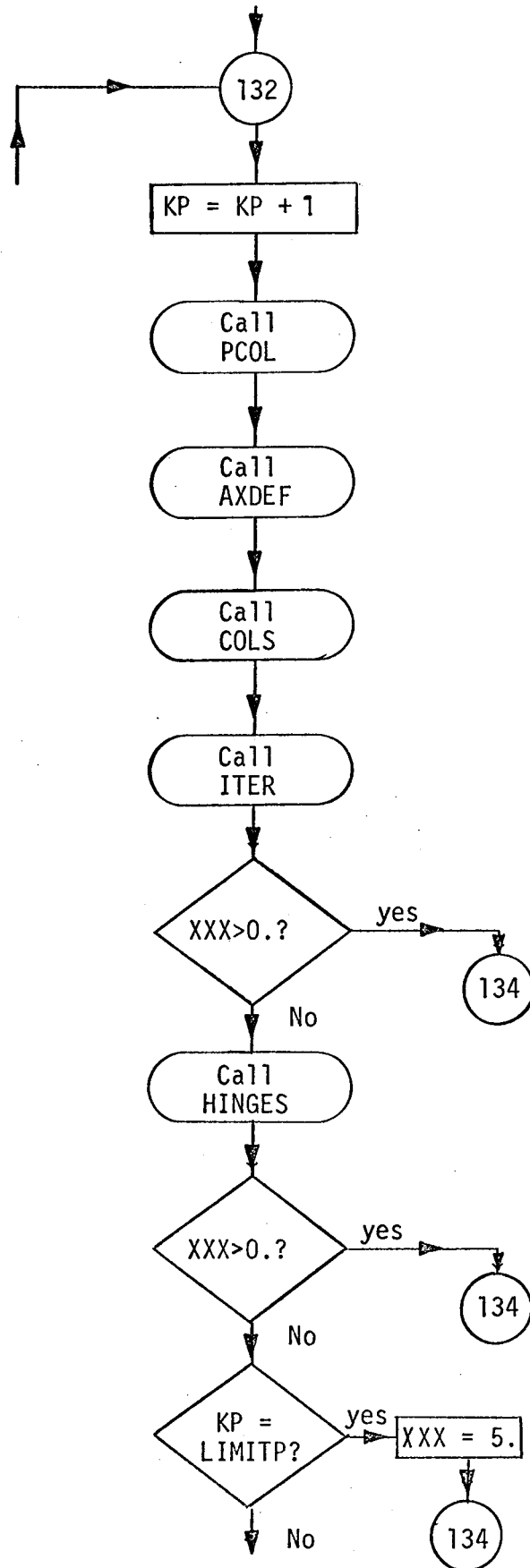
Subroutine LDPART computes the amount of lateral load resisted by the shear wall elements in every storey of the structure.

### D.3 Flow Diagrams for the Computer Programme

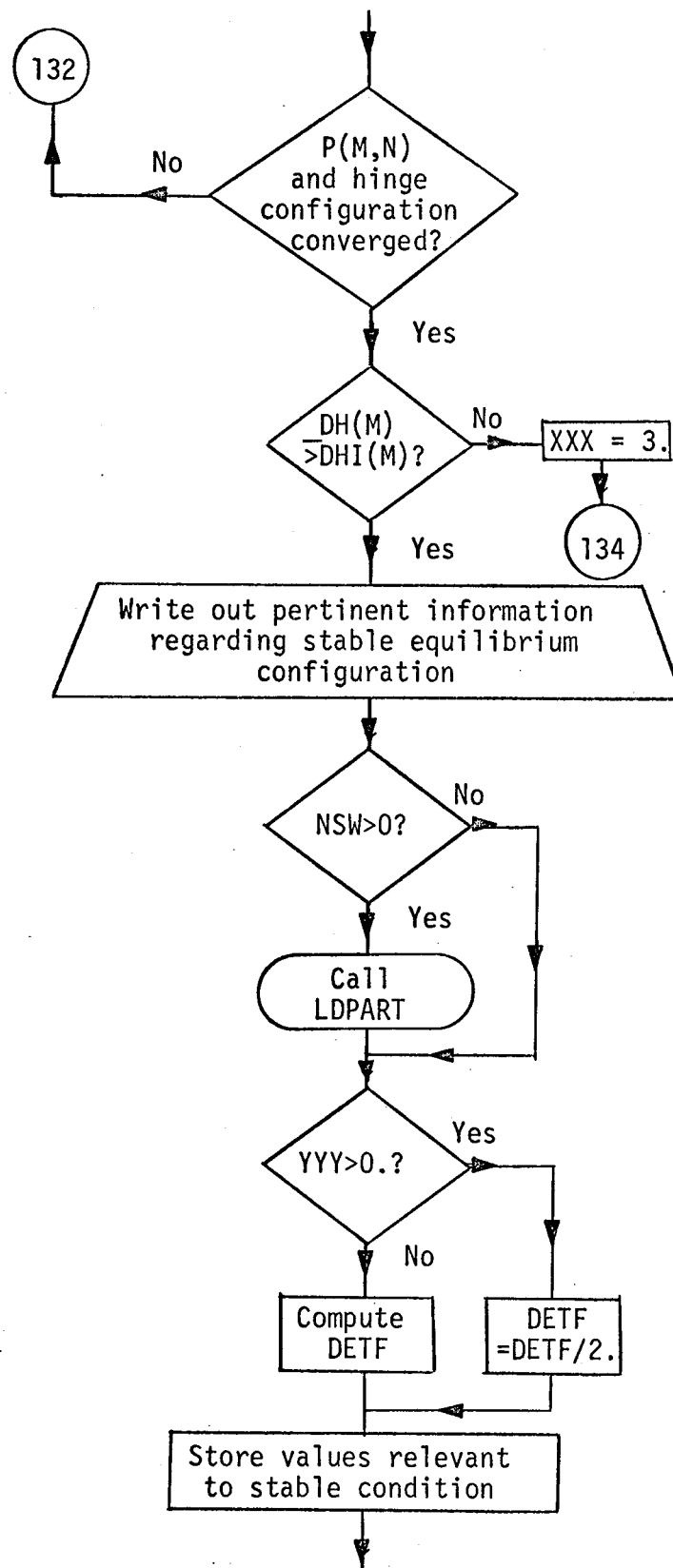
Flow diagrams for the main programme and Subroutines PCOL, ITER, HINGES and BMHING are presented in the remainder of this section. The other Subroutines are quite straightforward and their formulation can be followed in the programme listing presented in SECTION D.4.

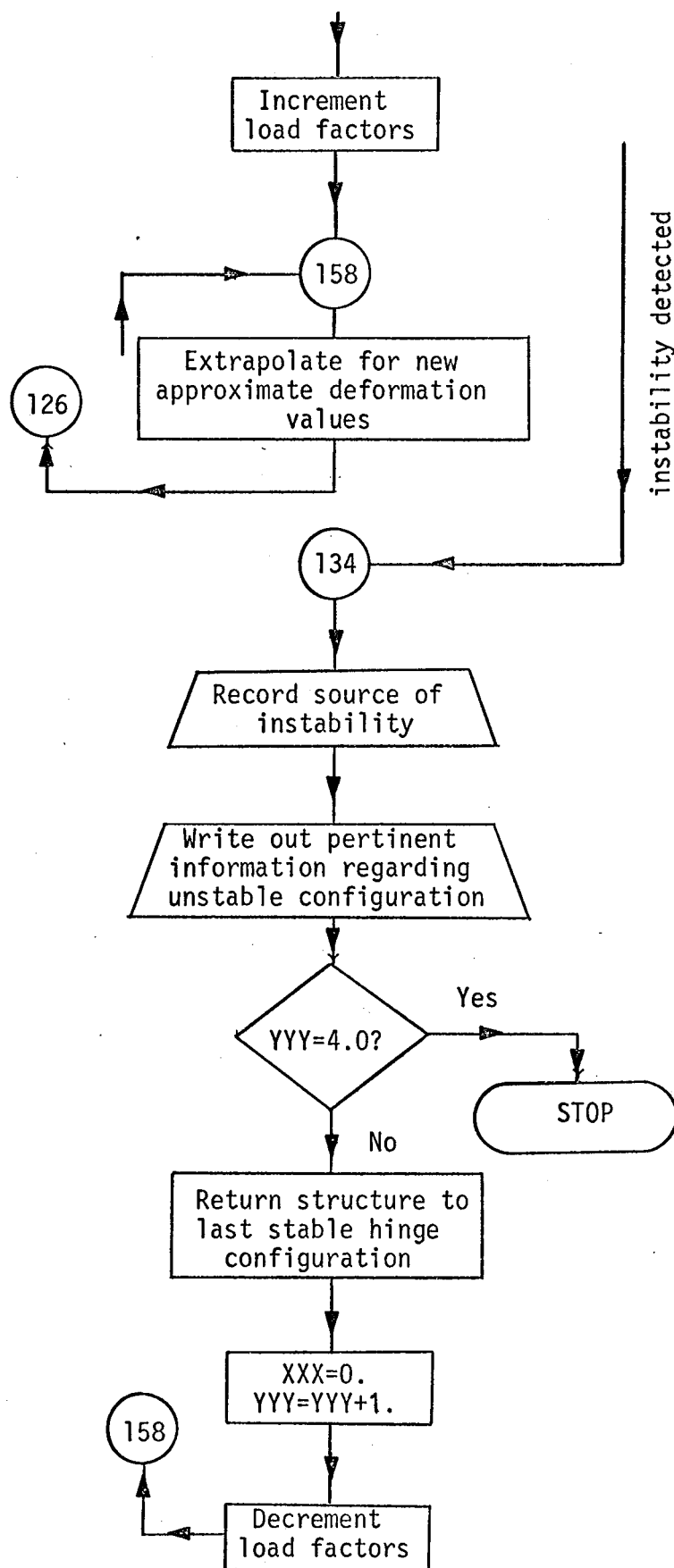
## D.3.1 Flow Diagram for the Main Programme



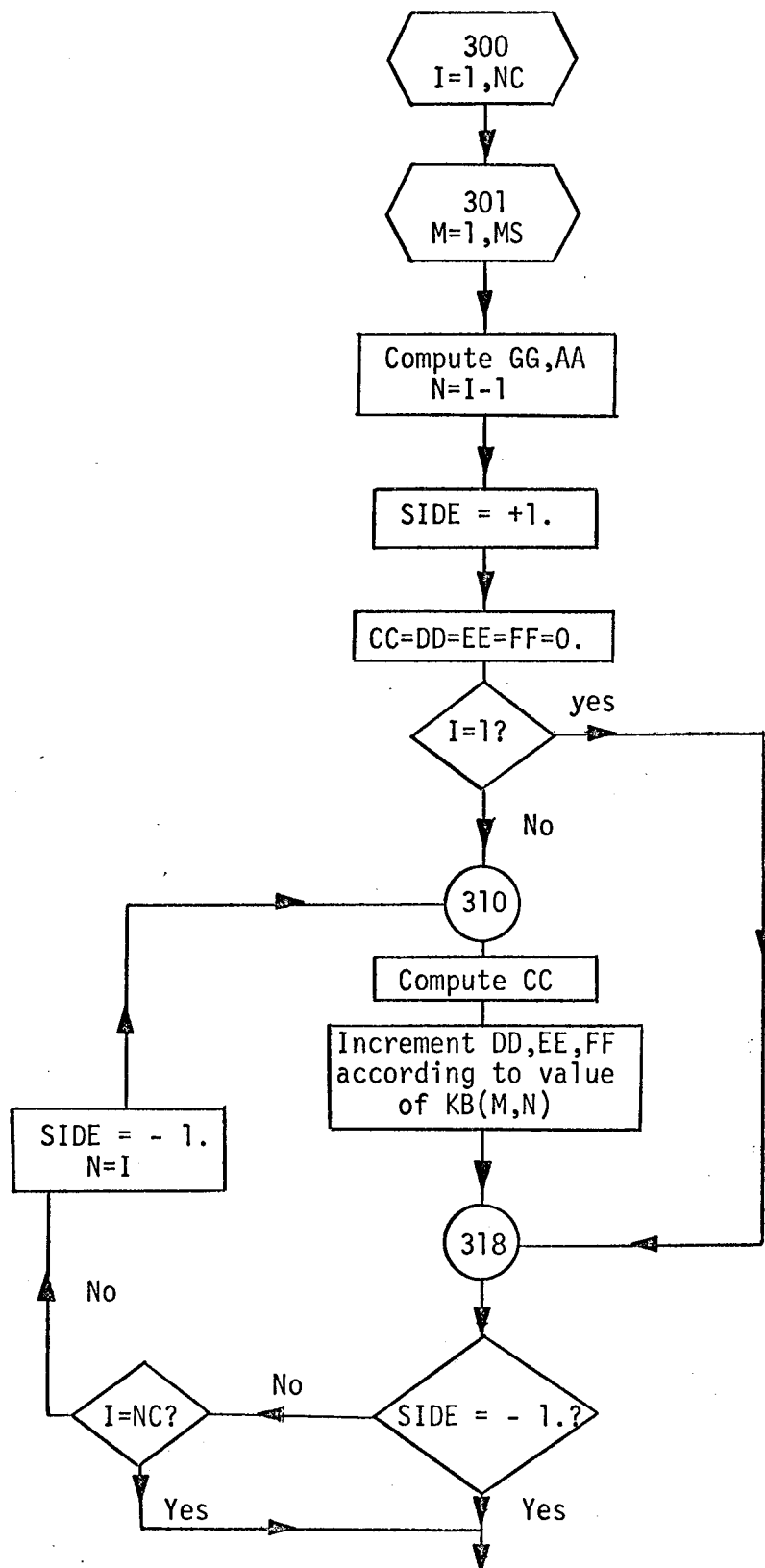


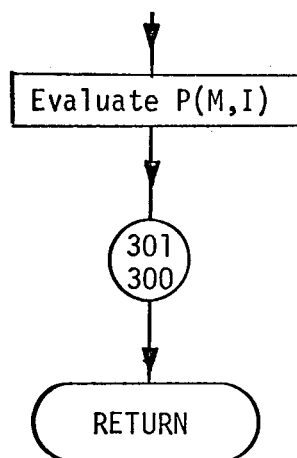




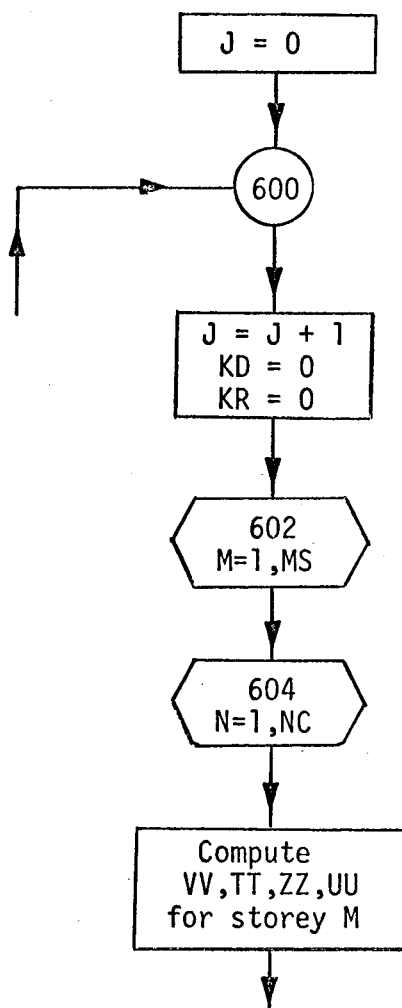


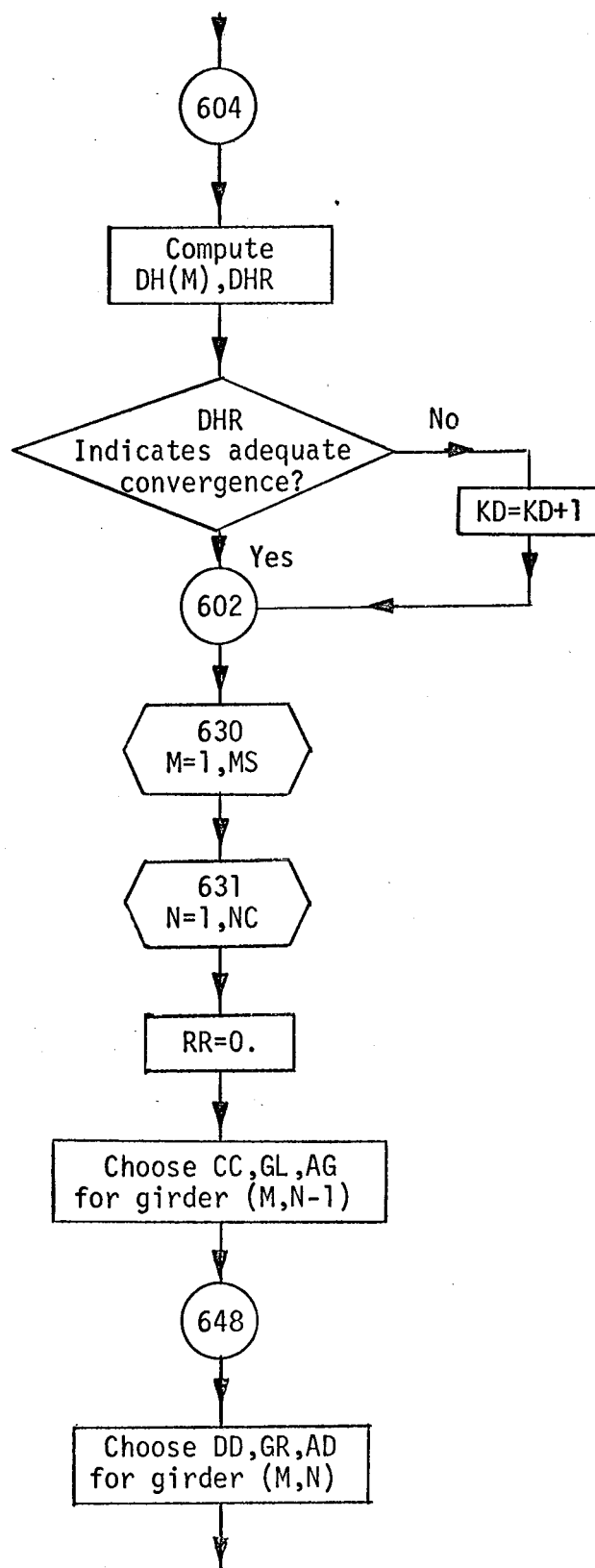
## D.3.2 Flow Diagram for Subroutine PCOL

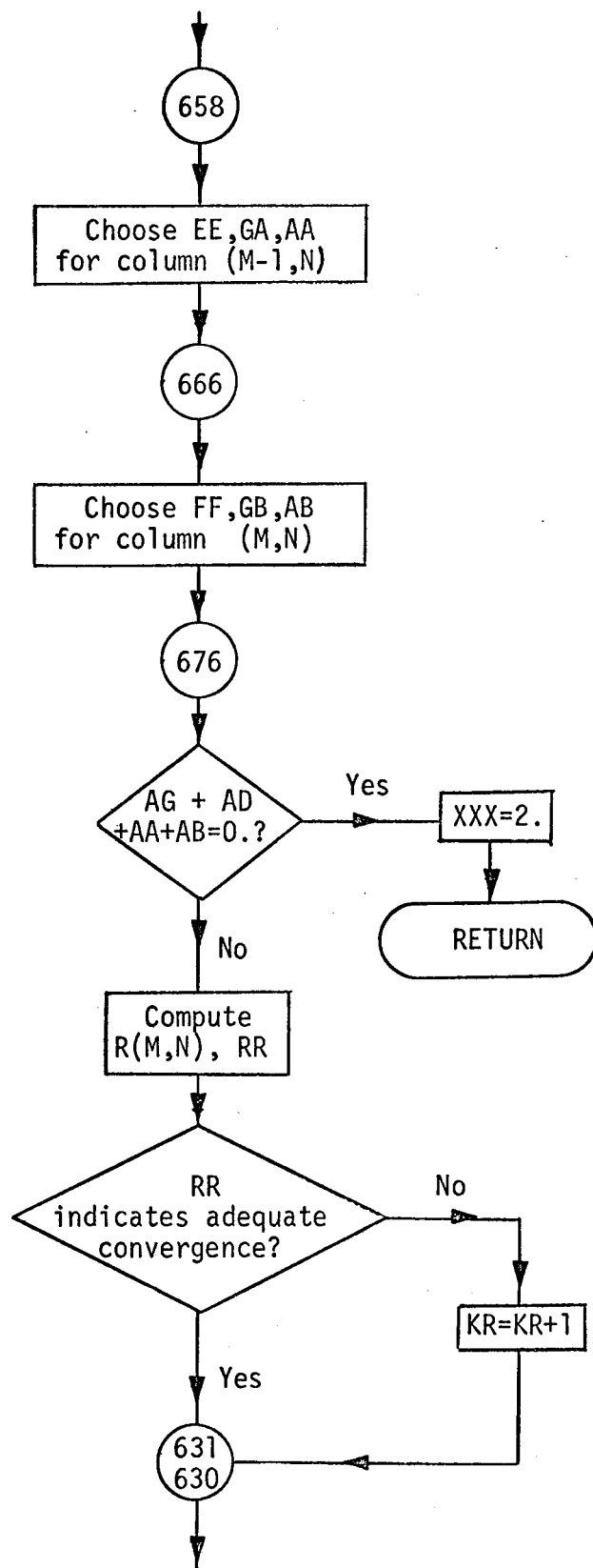


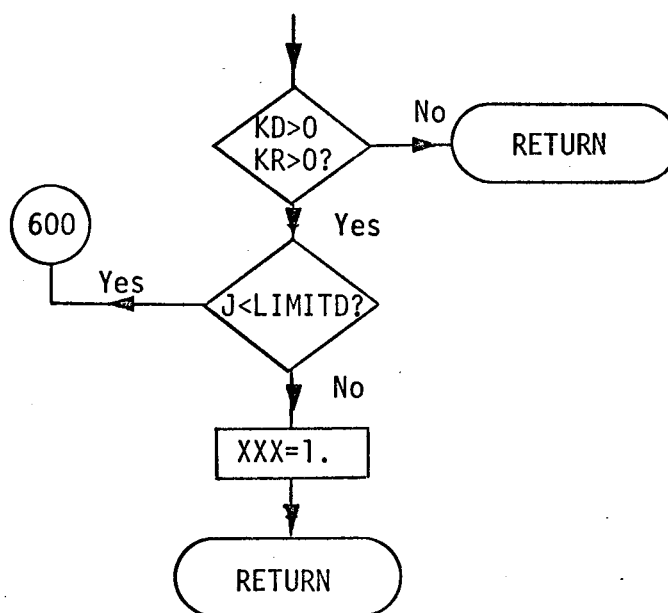


### D.3.3 Flow Diagram for Subroutine ITER

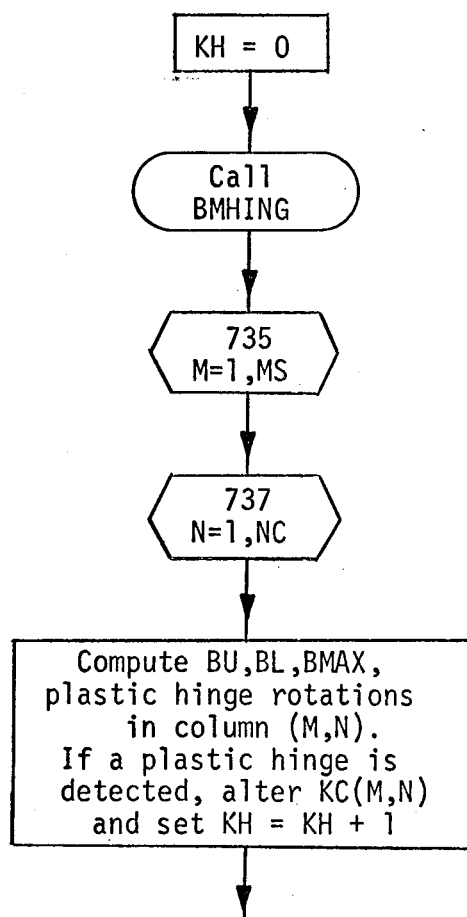


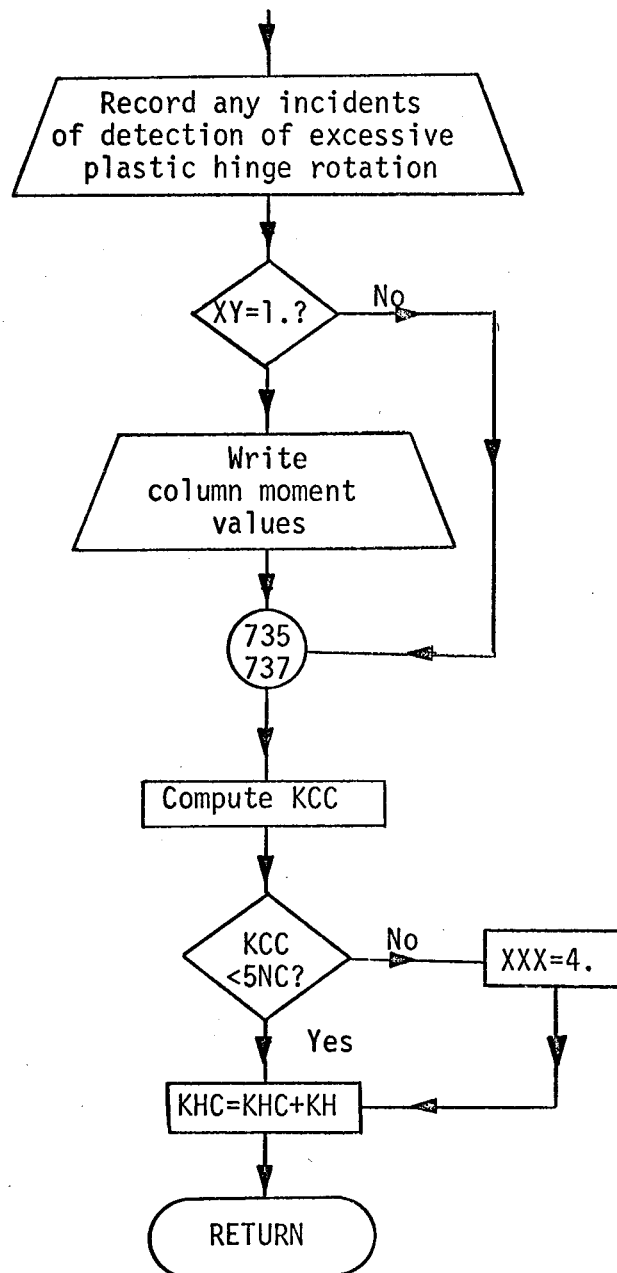




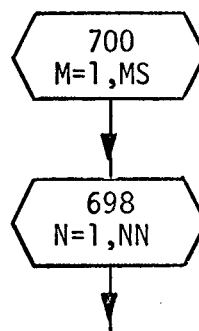


D.3.4 Flow Diagram for Subroutine HINGES

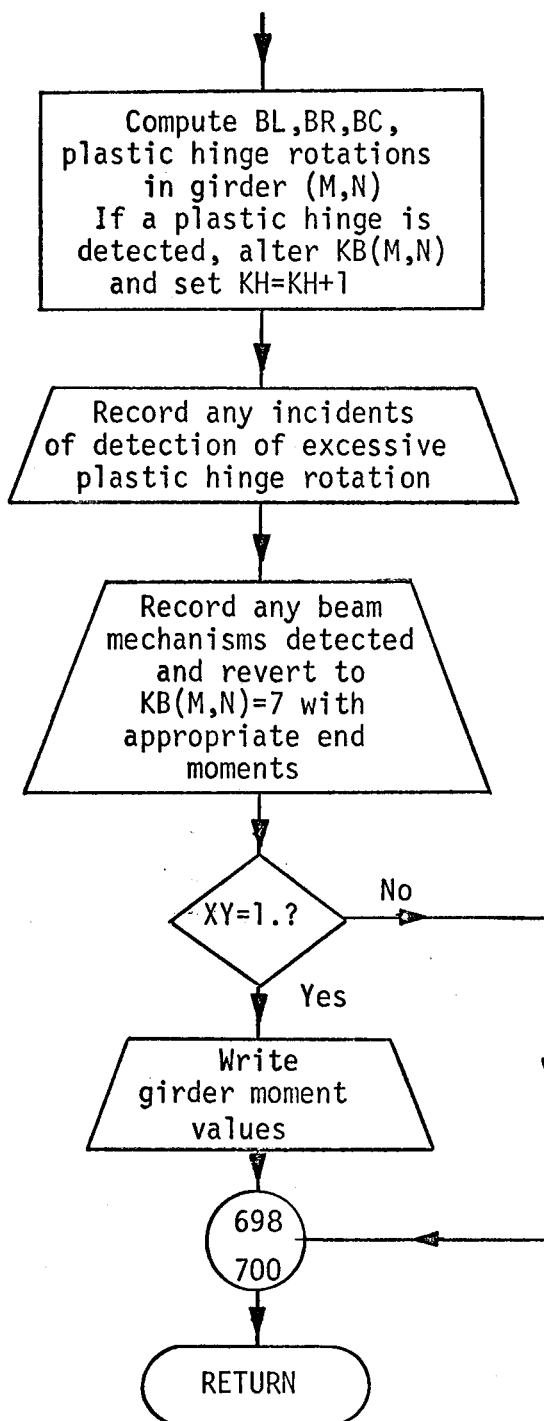




#### D.3.5 Flow Diagram for Subroutine BMHING







#### D.4 Listing of the Programme

## MAIN

```
C MAIN PROGRAMME
C -----
C SECOND ORDER ELASTIC-PLASTIC ANALYSIS OF A MULTISTOREY REINFORCED
C CONCRETE PLANE FRAME WHICH MAY BE EITHER UNBRACED I.E. NO SHEAR WALL)
C OR BRACED WITH SHEAR WALLS IN ANY OR ALL OF THE COLUMN LINES.
C THE ANALYSIS IS PERFORMED USING SLOPE-DEFLECTION EQUATIONS MODIFIED
C TO CONSIDER THE DEVELOPMENT OF 'POINT' HINGES IN BEAMS AND COLUMNS.
C THE EFFECTS OF AXIAL COLUMN LOADS ON DEFORMATIONS AND COLUMN
C STIFFNESS ARE CONSIDERED, AS IS THE FINITE SHEAR WALL WIDTH.
C
C THIS COMMON AND DIMENSION ARE SET UP FOR A 20 X 3 FRAME.
COMMON A, ACCURD, AL(20,3), AMI(20,3), AUI(20,3), BAS(20,2), BB(20,2), BI
1(20,2), C(20,3), CAS(20,3), CB(20,3), CT(20,3), CX, CF, CY, D, DH(20,1),
2DH(20,1), DPB, DPC, DV(20,3), EIB(20,2), EIC(20,3), F, FAUGDL, FCB, FCC, FCW, C
3FYB, FYC, FYM, HI(20,3), P(20,3), PE(3), R(21,3), RBP(20,2), RCP(20,2), SI(20,3),
4SI(20,2), SX, SYF, SY, T(20,2), T(20,2), TPL(20,2), TP(20,2), TP(20,2), TP(20,2),
5R(20,2), M(20,2), W(20,2), WL(20,2), WT(20,2), XB(20,2), XC(20,3), XXX, XY, Y(
6J, KB(20,2), KC(20,3), K(20,3), K(20,3), LIMITD, M, MS, NS, NC, NN, NP, NSW, NW(3)
DIMENSION OHCPI(3), FAUGL(3), PEI(3), PP(20,3), RP(20,3), WI(20), WD(20
1,2), WLI(20,2), KBI(20,2), KCI(20,3)
C
C READ IN BASIC FRAME CHARACTERISTICS.
C
READ(5,800) MS,NC,NSW
800 FORMAT(IX,3I3)
WRITE(6,802) MS,NC
802 FORMAT('1',' SECOND ORDER ELASTIC-PLASTIC ANALYSIS OF A',I3,' STOR
IEY',I3,' COLUMN LINE REINFORCED CONCRETE FRAME')
IF(NSW.EQ.0) GO TO 100
DO 102 N=1,NSW
READ(5,800) NW(N)
WRITE(6,804) NW(N)
804 FORMAT(IX,'SHEAR WALL IN COLUMN LINE',I3)
102 CONTINUE
100 READ(5,806) TPRATH,TPRATE
806 FORMAT(IX,2F9.6)
WRITE(6,808) TPRATH,TPRATE
808 FORMAT(IX,'BEAM MIDSPAN/INTERIOR SUPPORT MPL RATIO=',F9.6,' EXTERI
10R/INTERIOR SUPPORT MPL RATIO=',F9.6)
C
C SET CONVERGENCE LIMITS.
C
READ(5,810) LIMITD,ACCURD,LIMITP,ACCURP
810 FORMAT(IX,I6,F9.6,I6,F9.6)
WRITE(6,812) LIMITD,ACCURD
812 FORMAT('0',' CONVERGENCE LIMITS: FOR DEFORMATIONS-',I6,' CYCLES TO
1 A CLOSURE OF +- ',F9.6)
WRITE(6,814) LIMITP,ACCURP
814 FORMAT(IX,' FOR COLUMN LOADS-',I6,' CYCLES TO A CLOSURE OF +- ',F9
1.6)
C
C READ IN MATERIAL PROPERTIES.
C
READ(5,816) FCB,FCC,FCW
816 FORMAT(IX,3F9.1)
WRITE(6,818) FCB,FCC,FCW
818 FORMAT('0',' CONCRETE PROPERTIES:FC BEAMS=',F9.1,' FC COLUMNS=',F9
1.1,' FC WALLS=',F9.1)
READ(5,816) FYB,FYC,FYM
WRITE(6,820) FYB,FYC,FYM
820 FORMAT(IX,'STEEL PROPERTIES:FY BEAMS=',F9.1,' FY COLUMNS=',F9.1,'
IFY WALLS=',F9.1)
NN=NC-1
C
C READ IN FRAME GEOMETRY (CENTRE-LINE DIMENSIONS).
C
WRITE(6,822)
822 FORMAT('0',' FRAME DIMENSIONS (INCHES)::')
DO 104 N=1,NN
READ(5,824) SPIN)
824 FORMAT(IX,4F11.5)
WRITE(6,826) N,SPIN)
826 FORMAT(IX,'BAY WIDTH(',I3,')=',F11.5)
104 CONTINUE
DO 106 M=1,MS
READ(5,824) H(M)
WRITE(6,828) M,H(M)
828 FORMAT(IX,'STOREY HEIGHT(',I3,')=',F11.5)
106 CONTINUE
C
C READ SECTION PROPERTIES.
C
WRITE(6,830)
830 FORMAT('0',' SECTION PROPERTIES (INCHES)::')
READ(5,832) DPB,DPC
WRITE(6,832) DPB,DPC
832 FORMAT(IX,8HD,'BEAMS=F11.5,I1H D'COLUMNS=F11.5,8H D'T/I/O)
DO 108 M=1,MS
DO 109 N=1,NN
READ(5,824) BB(M,N),BT(M,N),BAS(M,N)
NOTE: BAS REFERS TO AREA OF TENSION STEEL AT AN INTERIOR SUPPORT.
109 CONTINUE
108 CONTINUE
DO 110 N=1,NC
DO 111 M=1,MS
READ(5,824) CB(M,N),CT(M,N),CAS(M,N)
111 CONTINUE
110 CONTINUE
WRITE(6,833)
833 FORMAT('1','27X,'BEAM B',6X,'BEAM T',5X,'BEAM AS',20X,'BEAM B',6X,'
1BEAM T',5X,'BEAM AS')
WRITE(6,831)
831 FORMAT(IX,'COL B',7X,'COL T',6X,'COL AST',9X,'COL B',7X,'COL T',6X,
1,'COL AST',9X,'COL B',7X,'COL T',6X,'COL AST')
DO 107 P=1,MS
WRITE(6,834) M,BB(M,1),BT(M,1),BAS(M,1),BB(M,2),BT(M,2),BAS(M,2)
834 FORMAT(IX,I4,I9X,F11.5,I4,F11.5,I4,F11.5,I4,F11.5,I4,F11.5,I4,F11.5)
1.5)
WRITE(6,836) CB(M,1),CT(M,1),CAS(M,1),CB(M,2),CT(M,2),CAS(M,2),CB(M
1,M),CT(M,M),CAS(M,M)
836 FORMAT(IX,I4,I9X,F11.5,I4,F11.5,I4,F11.5,I4,F11.5,I4,F11.5,I4,F11.5,I4,F11.5,I4,F11.5)
11.5,I4,F11.5)
107 CONTINUE
C NOW COMPUTE ALL BEAM PROPERTIES--REMAIN UNCHANGED WITH INCREASING LOAD
C
CALL BEAMS
WRITE(6,838)
838 FORMAT('0',' BEAM PROPERTIES:')
DO 112 P=1,MS
WRITE(6,840) M,TPL(M,1),EIB(M,1)
840 FORMAT(IX,'IN FLOOR',I3,' BEAMS, MPL=',F12.5,' EIB=',F12.5)
112 CONTINUE
C
C NOW INITIALIZE SOME VALUES.
C
XXX=0.
YYY=0.
XY=0.
KH=0
KHC=0
KHC1=0
NP=0
DO 114 N=1,NC
RIMS+1,N)=0.
DO 115 M=1,MS
DV(M,N)=0.
R(M,N)=0.
RP(M,N)=1.
PP(M,N)=1.
DH(M)=0.
DHI(M)=0.
115 CONTINUE
114 CONTINUE
C SET ALL BEAM AND COLUMN HINGING CONDITIONS=1 AT START.--NO HINGES
DO 116 M=1,MS
DO 117 N=1,NN
KB(M,N)=1
KBI(M,N)=1
117 CONTINUE
DO 118 N=1,NC
KC(M,N)=1
KCI(M,N)=1
118 CONTINUE
116 CONTINUE
C
C READ INITIAL EXTERNAL LOADS ON STRUCTURE AND PREPARE TO INCREMENT THEM
C
READ(5,842) AUGC,AUGL,AUGLL,AUGOL
WRITE(6,842) AUGC,AUGL,AUGLL,AUGOL
842 FORMAT('0',' INITIAL LOAD FACTOR INCREMENTS: EXT COL=',F11.5,' LAT
1='F11.5,' LL=',F11.5,' DL=',F11.5)
WRITE(6,844)
844 FORMAT('0',' WORKING LOADS ON STRUCTURE, WHICH WILL BE APPLIED AS
1SPECIFIED BY LOAD FACTORS:')
READ(5,846) WTWI
WRITE(6,847) WTWI
847 FORMAT(IX,'WORKING EXTERNAL WALL LOAD=',F13.3,' LB/STOREY')
DO 120 N=1,NC
READ(5,846) PEI(N)
846 FORMAT(IX,2F13.3)
WRITE(6,848) N,PEI(N)
848 FORMAT(IX,'WORKING EXTERNAL LOAD ON COLUMN LINE(',I3,')=',F13.3,'
1LB.')
120 CONTINUE
DO 122 M=1,MS
READ(5,846) WLMH)
WRITE(6,850) M,WLMH)
850 FORMAT(IX,'WORKING LATERAL LOAD AT FLOOR(',I3,')=',F13.3,' LB.)
122 CONTINUE
DO 124 P=1,MS
DO 125 N=1,NN
WRITE(6,846) WLI(M,N),WDI(M,N)
READ(5,852) M,N,WLI(M,N),WDI(M,N)
852 FORMAT(IX,'ON BEAM',I3,',',I3,) WORKING LIVE LOAD=',F13.3,' WOR
1KING DEAD LOAD=',F13.3,' LB/FT')
125 CONTINUE
124 CONTINUE
C NOW INITIALIZE LOAD FACTORS.
READ(5,824) FAUGE,FAUGL,FAUGLL,FAUGOL
C FROM THIS POINT ON, THE LOAD FACTORS CAN BE ADJUSTED.
C
126 KP=0
NP=NP+1
WRITE(6,854) FAUGE,FAUGL,FAUGLL,FAUGOL
854 FORMAT('1',' CURRENT LOAD FACTORS WRT WORKING LOADS: EXT COL=',F11
1.5,' LAT=',F11.5,' LL=',F11.5,' DL=',F11.5)
WRITE(6,856)
856 FORMAT(IX,'-----')
```

```

1-----*
C INCREMENT APPLIED LOADS.
  WT=FAUGDL*WTM
  DO 128 N=1,NC
    PEIN=FAUGL*PEIN
129 CONTINUE
  DO 130 M=1,MS
    WEM=FAUGL*WEM
  DO 131 K=1,NA
    WL(M,N)=FAUGLL*WL(M,N)
    WD(M,N)=FAUGDL*WD(M,N)
131 CONTINUE
130 CONTINUE

C NOW COMPUTE AXIAL LOADS IN COLUMNS.
C
132 KP=KP+1
  CALL PCOL

C NOW COMPUTE VERTICAL DISPLACEMENT OF NODAL POINTS.
C
  CALL AXDEF

C NOW COMPUTE COLUMN PROPERTIES UNDER CURRENT AXIAL LOADS.
C
  CALL COLS

C NOW COMPUTE JOINT ROTATIONS AND STOREY SWAY DEFLECTIONS.
C
  CALL ITER
  IF(XXX.GT.0.0) GO TO 134
C IF INSTABILITY HAS BEEN DETECTED IN 'ITER':
C XXX=1.0 INDICATES THAT CONVERGENCE OF DEFORMATIONS TO 'ACCUR' HAS
C NOT BEEN ACHIEVED AFTER 'LIMIT' CYCLES OF ITERATION.
C XXX=2.0 INDICATES THAT A JOINT MECHANISM HAS BEEN DETECTED
C SKIP TO END OF PROGRAMME AND DECREASE LOADS.
C
C NOW CHECK FOR EMERGENCE OF NEW HINGES IN THE STRUCTURE.
C
  CALL HINGES
  IF(XXX.GT.0.0) GO TO 134
C IF INSTABILITY HAS BEEN DETECTED IN 'HINGES':
C XXX=0.0 INDICATES A STOREY SWAY MECHANISM
C SKIP TO END OF PROGRAMME AND DECREASE LOADS.
C
C NOW CHECK FOR CONVERGENCE OF COLUMN AXIAL LOADS AND HINGING
C CONFIGURATION.
C
  IF(KP.GE.LIMITP) XXX=5.
C XXX=5.0 INDICATES THAT CONVERGENCE OF COLUMN AXIAL LOADS TO
C 'ACCURP' HAS NOT BEEN ACHIEVED AFTER 'LIMITP' CYCLES.
  IF(KP.GE.LIMITP) GO TO 134
  X=0.
  DO 138 N=1,NC
    IF((P(M,N)/PP(M,N)).GT.(1.+ACCURP).OR.(P(M,N)/PP(M,N)).LT.(1.-ACCU
    RP)) X=X+1
    PP(M,N)=P(M,N)
138 CONTINUE
139 CONTINUE
  IF(X.GT.0.0.OR.KH.GT.0) GO TO 132
C IF THE VALUES OF COLUMN AXIAL LOADS AND THE HINGING CONFIGURATION
C HAVE NOT CONVERGED, REITERATE UNLESS KP=LIMITP, IN WHICH CASE A
C CONDITION OF INSTABILITY WILL BE ASSUMED.
C
  DO 141 M=1,MS
    IF(DH(M).GE.DH(M)) GO TO 141
    XXX=3.
C XXX=3.0 INDICATES THAT STOREY SWAY INSTABILITY HAS BEEN DETECTED.
C IF DH(M), THE NEW EQUILIBRIUM VALUE OF SWAY DEFLECTION FOR STOREY M,
C IS LESS THAN DH(M), THE VALUE FOR THE LAST LOAD STAGE WHICH LED TO
C A STABLE CONFIGURATION, WE HAVE ENCOUNTERED A CONDITION OF
C INSTABILITY, SINCE THE STRUCTURE CANNOT SUPPORT THE INCREMENTED
C LOADS AT ANYTHING BUT A REDUCED DEFLECTION.
  WRITE(6,861) M,DH(M),DH(M)
  861 FORMAT('0',' STRUCTURE AT STOREY',I3,' UNABLE TO SUPPORT LOADS AT
  PREVIOUS SWAY DEFLECTION=',E12.5,'.NEW EQUILIBRIUM DEFLECTION=',E1
  22.5)
141 CONTINUE
  IF(XXX.GT.0.0) GO TO 134
C SKIP TO END OF PROGRAMME AND DECREASE LOADS.
C
C IF THIS POINT IN THE PROGRAMME IS REACHED WITHOUT A DETOUR TO
C STATEMENTS #132 OR #134, THE CURRENT DEFORMATION VALUES
C REPRESENT A DEFLECTED STRUCTURE IN EQUILIBRIUM UNDER THE CURRENT
C EXTERNAL LOADS.
C WRITE OUT THE PERTINENT VALUES.
C
  WRITE(6,862) KHC
  862 FORMAT('0',' A STABLE CONFIGURATION WITH',I4,' HINGES IS INDICATED
  1')
  WRITE(6,864) KP
  864 FORMAT('0',' NUMBER OF PASSES THROUGH SUBROUTINE PCOL=',I5)
  DHC=0.
  WRITE(6,866)
  866 FORMAT('0')
  WRITE(6,868)
  868 FORMAT('3X','M',5X,'JT ROT',6X,'KB',5X,'JT ROT',6X,'KB',5X,'JT ROT')
  WRITE(6,870)
  870 FORMAT('11X','KC',17X,'KC',17X,'KC',6X,'STOREY SWAY')
  WRITE(6,871)
  871 FORMAT('9X','PCOL',15X,'PCOL',15X,'PCOL')
  WRITE(6,873)
  873 FORMAT('9X','VDEF',15X,'VDEF',15X,'VDEF')
  DO 140 M=1,MS
    WRITE(6,872) M,R(M,1),KB(M,1),R(M,2),KB(M,2),R(M,3)
  872 FORMAT('1X,I3,2X,E12.5,14,14,2X,E12.5,1X,I4,2X,E12.5)
  WRITE(6,874) KC(M,1),KC(M,2),KC(M,3),DH(M)
  874 FORMAT('9X,I4,15X,I4,15X,I4,5X,E12.5)
  WRITE(6,875) P(M,1),P(M,2),P(M,3)
  875 FORMAT('5X,E12.5,7X,E12.5,7X,E12.5)
  WRITE(6,875) DV(M,1),DV(M,2),DV(M,3)
  DHC=DHC+DH(M)
140 CONTINUE
  WRITE(6,876) DHC
  876 FORMAT('0',' TOTAL SWAY DEFLECTION AT TOP OF FRAME=',E12.5,' IN.')
C RETURN TO 'HINGES' TO DERIVE MOMENT VALUES.
  XY=1.0
  WRITE(6,866)
  CALL HINGES
  XY=0.
C COMPUTE LATERAL LOADS CARRIED BY SHEAR WALL(S).
  IF(NSW.GT.0) CALL LDAPT
C
C NOW PROCEED TO INCREASE LOADS FOR NEXT PASS THROUGH THE PROGRAMME.
C
  IF(VVV.GT.0.0) GO TO 148
C VVV GT 0.0 INDICATES THAT INSTABILITY HAS BEEN ENCOUNTERED AT SOME
C PREVIOUS LOADING STAGE, AND WE WILL DESIRE TO AUGMENT THE LOADS
C ACCORDINGLY.
  INDET=3*P5*(NC-1)
C NOW LET US SET THE SIZE OF LOAD INCREMENT AS A FUNCTION OF THE DEGREE
C OF 'DETERIORATION' OF THE FRAME.
  IF((KHC).LT.(KHC)) DETF=1.0
  IF(INDET.LE.(4*KHC).AND.(2*KHC).LT.INDET) DETF=0.5
  IF(INDET.LE.(2*KHC).AND.(4*KHC).LT.(3*INDET)) DETF=0.25
  IF((3*INDET).LE.(4*KHC)) DETF=0.125
  GO TO 150
148 IF(VVV.GE.4.0) GO TO 152
C IE. STOP PROGRAMME 4 LOAD ADJUSTMENTS BEYOND THE FIRST EVIDENCE OF
C INSTABILITY.
  VVV=VVV+1.
  DETF=DETF/2.
C NOW LET US CONSERVE SOME OF THE CURRENT VALUES, SHOULD THE REVISED
C LOADS LEAD TO EVIDENCE OF INSTABILITY, THE STRUCTURE CAN THEN BE
C RETURNED TO ITS CURRENT STABLE STATE.
150 KHC=KHC
  DO 154 M=1,MS
    DH(M)=DH(M)
    DO 155 N=1,NC
      KC(M,N)=KC(M,N)
      RP(M,N)=RP(M,N)
155 CONTINUE
    DO 156 N=1,NN
      KB(M,N)=KB(M,N)
156 CONTINUE
154 CONTINUE
C NOW, TO SPEED UP THE CONVERGENCE IN 'PCOL' AND 'ITER', EXTRAPOLATE FOR
C NEW APPROXIMATE VALUES OF DH(M)S AND RP(M)S, USING THE RELATIONSHIP
C OF 'FAUGL' VS 'DHC' (THE TOTAL SWAY DEFLECTION OF THE TOP OF THE
C STRUCTURE) AS THE FUNCTION FOR EXTRAPOLATION.
C FOR THE FIRST 2 LOAD INCREMENTS BEYOND INITIAL LOADS, LINEAR
C EXTRAPOLATION WILL BE USED. IF, HOWEVER, AT LEAST 3 POINTS OF THIS PLOT
C HAVE BEEN OBTAINED, LAGRANGE'S EXTRAPOLATION PROCEDURE, FITTING THE
C LAST 3 POINTS TO A QUADRATIC EQUATION, WILL BE USED.
C FIRST STORE PREVIOUS VALUES OF 'FAUGL' AND 'DHC' FOR LATER USE.
  FAUGLP(3)=FAUGL(2)
  FAUGLP(2)=FAUGL(1)
  FAUGLP(1)=FAUGL
  DHCP(3)=DHC(2)
  DHCP(2)=DHC(1)
  DHCP(1)=DHC
C NOW ALTER LOAD FACTORS
  FAUGE=FAUGE+DETF*AUGE
  FAUGL=FAUGL+DETF*FAUGL
  FAUGLL=FAUGLL+DETF*FAUGLL
  FAUGDL=FAUGDL+DETF*FAUGDL
158 IF(MP.GE.3) GO TO 160
  RATIO=FAUGL/FAUGLP(1)
  GO TO 162
160 RATIO=((FAUGL-FAUGLP(2))*((FAUGL-FAUGLP(3))*DHCP(1))/((FAUGLP(1)-FAU
  GLP(2))*((FAUGLP(1)-FAUGLP(3))*((FAUGL-FAUGLP(1))*((FAUGL-FAUGLP(3))
  2*DHCP(2))/((FAUGLP(2)-FAUGLP(1))*((FAUGLP(2)-FAUGLP(3))*((FAUGL-FAUG
  3LP(1))*((FAUGL-FAUGLP(2))*DHCP(3))/((FAUGLP(3)-FAUGLP(1))*((FAUGLP(3)
  4-FAUGLP(2))))/DHC
C 'RATIO' REPRESENTS DHC(NEW EXTRAPOLATED)/DHC(PREVIOUS CYCLE)
162 DO 164 M=1,MS
  164 DO 165 N=1,NC
    R(M,N)=RATIO*RP(M,N)
165 CONTINUE
164 CONTINUE
  GO TO 126
C
C IE. RETURN WITH REVISED LOAD FACTORS AND EXTRAPOLATED DEFORMATION
C VALUES, FOR ANOTHER PASS THROUGH THE PROGRAMME.
C
C NOW CONSIDER THE CASE WHEN EVIDENCE OF INSTABILITY WAS ENCOUNTERED IN
C SUBROUTINE 'ITER' OR 'HINGES', OR IN SLOW CONVERGENCE OF COLUMN P'S.
C
134 WRITE(6,878)
  878 FORMAT('0',' ****- INSTABILITY INDICATED WITH THESE LOAD FACTORS')
  IF(XXX.EQ.1.0) GO TO 171
  IF(XXX.EQ.2.0) GO TO 172
  IF(XXX.EQ.3.0) GO TO 173
  IF(XXX.EQ.4.0) GO TO 174
  IF(XXX.EQ.5.0) GO TO 175
171 WRITE(6,880) LIMIT
  880 FORMAT('0',' ITERATION PROCEDURE FOR DEFORMATIONS FAILED TO CONVER
  GE AFTER',I6,' CYCLES')
  GO TO 177
172 WRITE(6,882) M,N
  882 FORMAT('0',' JOINT MECHANISM DETECTED AT JOINT(',I3,',',I3,')')
  GO TO 177
173 WRITE(6,884)
  884 FORMAT('0',' INSTABILITY OF SOME STOREY IS INDICATED')
  GO TO 177
174 WRITE(6,886) M
  886 FORMAT('0',' SWAY MECHANISM DETECTED IN STOREY',I3)

```

```

GO TO 177
175 WRITE(6,994) ACCURD,LIMITP
176 FORMAT('0',* ** COLUMN LOADS FAILED TO CONVERGE TO A CLOSURE OF *,
177 'IF 4.0 AFTER 16 CYCLES.')
177 WRITE(6,996)
178 WRITE(6,993) KHC
179 FORMAT(1X,* UNSTABLE STRUCTURE CONTAINS*,14,* HINGES*)
180 WRITE(6,994) KP
181 WRITE(6,996)
182 WRITE(6,997)
183 WRITE(6,998)
184 WRITE(6,999)
185 DHC=0.
DO 176 P=1,MS
WRITE(6,872) M,R(M,1),KB(M,1),R(M,2),KB(M,2),R(M,3)
WRITE(6,874) KC(M,1),KC(M,2),KC(M,3),DH(M)
WRITE(6,875) PC(M,1),PC(M,2),PC(M,3)
WRITE(6,876) DV(M,1),DV(M,2),DV(M,3)
DHC=DHC+DH(M)
176 CONTINUE
WRITE(6,876) DHC
WRITE(6,888)
888 FORMAT('0',* PROCEED TO REDUCE LOADS FOR NEXT CYCLE.*)
IF(YYY.GE.4.0) GO TO 152
YYY=YYY+1.
C NOW RETURN THE STRUCTURE TO ITS LAST STABLE CONFIGURATION.
KHC=KHCI
DO 180 P=1,MS
DO 181 N=1,NC
KC(M,N)=KCI(M,N)
181 CONTINUE
DO 182 N=1,NN
KB(M,N)=KBI(M,N)
182 CONTINUE
180 CONTINUE
XX=0.
C NOW CUT THE PREVIOUS LOAD INCREMENT, WHICH RESULTED IN EVIDENCE OF
C INSTABILITY, IN HALF, AND DERIVE NEW REDUCED LOAD FACTORS TO
C 'ZERO IN' ON THE ACTUAL INSTABILITY LOAD FACTORS.
DETF=DETF/2.
FAUG=FAUG-DETF*FAUG
FAUGL=FAUGL-DETF*FAUGL
FAUGLL=FAUGLL-DETF*FAUGLL
FAUGDL=FAUGDL-DETF*FAUGDL
C NOW RETURN TO OBTAIN EXTRAPOLATED VALUES OF DH(M)S AND R(M)S FOR THE
C REVISED LOAD FACTORS.
GO TO 158
C UNLESS YYY=4.0, IN WHICH CASE, THE LAST STABLE CONFIGURATION, AND ITS
C ACCOMPANYING LOAD FACTORS CAN BE TAKEN, WITH JUSTIFIABLE ACCURACY
C AS THE FAILURE CONDITION.
152 WRITE(6,890)
890 FORMAT('0',* PROGRAMME STOPPED AFTER 4 LOAD ADJUSTMENTS BEYOND FIFTH
1ST EVIDENCE OF INSTABILITY*)
WRITE(6,892)
892 FORMAT('0',* TAKE LOAD FACTORS AND DEFORMATIONS OF LAST STABLE CON-
FIGURATION AS FAILURE CONDITIONS*)
STOP
END

```

## BEAMS

```

SUBROUTINE BEAMS
C COMPUTES PLASTIC MOMENT CAPACITY AND EI FOR ALL BEAMS, BASED ON
C INTERIOR SUPPORT TENSION REINFORCEMENT, ASSUMING ONLY TENSION STEEL.
C A PERMISSIBLE HINGE ROTATION VALUE IS DERIVED BASED ON PCA LAB TESTS.
COMMON A,ACCURD,AL(20,3),AM(20,3),AU(20,3),B,BAS(20,2),BB(20,2),BT
1(20,2),C(20,3),CAS(20,3),CB(20,3),CT(20,3),CX,CXF,CY,CYF,D,DH(20,2),
2DH(20,2),DPB,DPC,DV(20,3),EIB(20,2),EIC(20,3),F,FAUGDL,FGB,FCC,FCH,
3FYB,FYC,FYM,H(20,3),P(20,3),PE(3),R(2,3),RBP(20,2),RCP(20,3),S(20,3),
4)SP(2),SX,SXF,SY,SXF,TL(20,2),TPC(20,3),TPL(20,2),TPRATH,TPRATH,
5R(20,2),W(20,2),WD(20,2),WL(20,2),WTW,X,XB(20,2),XC(20,3),XX,X,Y,Y,
6,J,KB(20,2),KC(20,3),KH,KHC,LIMITD,M,MS,N,NC,NN,NP,NSW,NW(3)
EN=500./SQRT(FGB)
DO 200 P=1,MS
DO 201 N=1,NN
PS=BAS(M,N)/(BB(M,N)*BT(M,N)-DPB)
C NOTE: 'BAS' HERE REFERS ONLY TO SUPPORT REGION TENSION STEEL.
YOK=-PS*EN*SQRT(PS*PS*EN*EN+2*PS*EN)
RYO=FYB/30.06*(BT(M,N)-DPB)*(1.-YOK)
TPL(M,N)=BAS(M,N)*FYB*(1.-YOK/3.)*(BT(M,N)-UPB)
EIB(M,N)=TPL(M,N)/RYO
UK=PS*FYB/10.7*FGB
RBP(M,N)=0.0038/(2.*UK)
201 CONTINUE
200 CONTINUE
C STRICTLY SPEAKING, THESE BEAM CHARACTERISTICS REFER ONLY TO THE BEAM
C SECTION AT AN INTERIOR SUPPORT. THE EFFECTS OF VARIATION IN
C REINFORCEMENT AREA ALONG THE BEAM HAVE BEEN NEGLECTED IN DERIVING
C VALUES OF RBP AND EIB. IT WILL BE ASSUMED, HOWEVER, THAT THESE VALUES
C ARE APPLICABLE TO THE ENTIRE BEAM LENGTH. WE WILL, HOWEVER, CORRECT
C THE MPL VALUES AT EXTERIOR SUPPORTS AND AT MIDSPAN BY MULTIPLYING
C THIS VALUE OF TPL(M,N) BY 'TPRATH' AND 'TPRATH' RESPECTIVELY, WHERE
C APPLICABLE.
RETURN
END

```

## PCOL

```

SUBROUTINE PCOL
C COMPUTES AXIAL LOADS IN ALL COLUMNS
COMMON A,ACCURD,AL(20,3),AM(20,3),AU(20,3),B,BAS(20,2),BB(20,2),BT
1(20,2),C(20,3),CAS(20,3),CB(20,3),CT(20,3),CX,CXF,CY,CYF,D,DH(20,2),
2DH(20,2),DPB,DPC,DV(20,3),EIB(20,2),EIC(20,3),F,FAUGDL,FGB,FCC,FCH,
3FYB,FYC,FYM,H(20,3),P(20,3),PE(3),R(2,3),RBP(20,2),RCP(20,3),S(20,3),
4)SP(2),SX,SXF,SY,SXF,TL(20,2),TPC(20,3),TPL(20,2),TPRATH,TPRATH,
5R(20,2),W(20,2),WD(20,2),WL(20,2),WTW,X,XB(20,2),XC(20,3),XX,X,Y,Y,
6,J,KB(20,2),KC(20,3),KH,KHC,LIMITD,M,MS,N,NC,NN,NP,NSW,NW(3)
DO 300 I=1,NC
DO 301 P=1,MS
GG=FAUGDL*CB(M,1)*CT(M,1)*H(M)/12.
C GG REPRESENTS SELF-WEIGHT OF COLUMN
IF(M.GT.1) GO TO 304
AA=PE(1)
GO TO 306
304 AA=P(M-1,1)
C AA REPRESENTS LOAD TRANSFERRED FROM COLUMN ABOVE
306 N=I-1
C IE. THE LEFT-HAND BEAM CONTRIBUTIONS WILL BE DEALT WITH FIRST.
SIDE=1.
C IF SIDE=1., LHS BEAM IS BEING CONSIDERED. SIDE=-1. MEANS RHS BEAM.
C THUS WE TAKE ADVANTAGE OF THE ANTISYMMETRY OF COEFFICIENTS.
CC=0.
DD=0.
EE=0.
FF=0.
C CG REPRESENTS CONTRIBUTIONS OF BEAM SELF-WEIGHT AND LIVE LOAD.
C DD REPRESENTS CONTRIBUTIONS OF BEAM LEFT HAND END ROTATION.
C EE REPRESENTS CONTRIBUTIONS OF BEAM RIGHT HAND END ROTATION.
C FF REPRESENTS CONTRIBUTIONS OF FEM'S & VERTICAL JOINT TRANSLATIONS.
IF(IE.EQ.1) GO TO 318
C IE. SKIP LHS MEMBER CONSIDERATION--NO LHS MEMBER.
310 DEL=DV(M,N+1)-DV(M,N)
WT=(WL(M,N)+WD(M,N)+FAUGDL*BB(M,N)*BT(M,N))/12.
NWL=0.
NWR=0.
IF(NSW.EQ.0) GO TO 307
DO 309 K=1,NSW
IF(SIDE.EQ.1.0.AND.1.EQ.NW(K)) NWR=CT(M,1)
IF(SIDE.EQ.1.0.AND.(1-1).EQ.NW(K)) NWL=CT(M,1-1)
IF(SIDE.EQ.-1.01.AND.1.EQ.NW(K)) NWL=CT(M,1)
IF(SIDE.EQ.-1.01.AND.(1+1).EQ.NW(K)) NWR=CT(M,1+1)
309 CONTINUE
SR=SP(N)-NWL*NWR/2.
CC=CC+(WL(M,N)+WD(M,N)+FAUGDL*BB(M,N)*BT(M,N)*SR)/24.
KK=KB(M,N)
GO TO (311,312,313,314,315,316,317),KK
1 WRITE(6,900)
900 FORMAT(1X,***-BEAM COUNTER OUT OF RANGE IN SUBROUTINE PCOL*)
311 DD=DD+SIDE*0.5*EIB(M,N)*R(M,N)*(1.+NWL/SR)/(SR*SR)
EE=EE+SIDE*0.5*EIB(M,N)*R(M,N)*(1.+NWR/SR)/(SR*SR)
FF=FF+SIDE*12.*EIB(M,N)*DEL/(SR*SR*SR)
GO TO 318
312 DD=DD+SIDE*1.5*EIB(M,N)*R(M,N)*NWL/(SR*SR*SR)
EE=EE+SIDE*3.*EIB(M,N)*(1.+0.5*NWR/SR)*R(M,N)/(SR*SR)
FF=FF+SIDE*3.*EIB(M,N)*DEL/(SR*SR*SR)-1.5*TL(M,N)/SR-WT*SR/8.
GO TO 318
313 DD=DD+SIDE*3.*EIB(M,N)*R(M,N)*(1.+0.5*NWL/SR)/(SR*SR)
EE=EE+SIDE*1.5*EIB(M,N)*R(M,N)*NWR/(SR*SR*SR)
FF=FF+SIDE*3.*EIB(M,N)*DEL/(SR*SR*SR)-1.5*TR(M,N)/SR-WT*SR/8.
GO TO 318
314 X=XB(M,N)
Y=SR-X
FXY=1./((X*X*(1./((X*X*X)+1.)/(Y*Y*Y)))
FYX=1./((Y*Y*(1./((X*X*X)+1.)/(Y*Y*Y)))
Z=FYX-FXY
DD=DD+SIDE*3.*EIB(M,N)*R(M,N)*(1.+0.5*NWL/X)*(1.+Z/X)/(X*SR)
EE=EE+SIDE*3.*EIB(M,N)*R(M,N)*(1.+0.5*NWR/Y)*(1.-Z/Y)/(Y*SR)
FF=FF+SIDE*3.*EIB(M,N)*(1.+Z/X)*DV(M,N)/(X*X*(1.-Z/Y)*DV(M,N)+1)
1/(Y*Y)+0.125*WT*(Y*Y*(1.-Z/Y)-X*X*(1.+Z/X)+4.*SR*Z)-1.5*TPRATH*TP
ZL(M,N)/(X+1./Y)/SR
GO TO 318
315 X=XB(M,N)
Y=SR-X
FF=FF+SIDE*(ITL(M,N)-TPRATH*TPL(M,N))/X+0.5*WT*Y
GO TO 318
316 X=XB(M,N)
Y=SR-X
FF=FF+SIDE*(ITR(M,N)+TPRATH*TPL(M,N))/Y+0.5*WT*X
GO TO 318
317 FF=FF+SIDE*(ITR(M,N)+TL(M,N))/SR
318 IF(SIDE.EQ.(1-1.0)) GO TO 320
C IE. BOTH LHS AND RHS BEAMS HAVE BEEN CONSIDERED.
IF(1.EQ.NC) GO TO 320
C IE. THERE IS NO RHS BEAM.
C THE RHS BEAM WILL NOW BE CONSIDERED.
SIDE=-1.0
N=1
GO TO 310
320 P(M,1)=AA+CC+DD+EE+FF+GG
IF(1.EQ.1.OR.1.EQ.NC) P(M,1)=P(M,1)+WTW
301 CONTINUE
300 CONTINUE
RETURN
END

```

## AXDEF

```

C
SUBROUTINE AXDEF
C
C COMPUTES VERTICAL DEFLECTION OF ALL NODAL POINTS USING HOGNESTAD'S
C CONCRETE STRESS-STRAIN CURVE IN A COMPOSITE SYMMETRICALLY-REINFORCED
C COLUMN SECTION
C
COMMON A, ACCURD, AL(20,3), AM(20,3), AU(20,3), B, BAS(20,2), BB(20,2), BT
1(20,2), C(20,3), CAS(20,3), CB(20,3), CT(20,3), CX, CFX, CY, CYF, D, DH(20,2),
2DH(20,2), DPB, DPC, DV(20,3), EIB(20,2), EIC(20,3), F, FAUGDL, FCB, FCC, FCM,
3FYB, FYC, FYW, HI(20,3), P(20,3), PE(3), RI(2,3), RBP(20,2), RCP(20,3), S(20,3),
4SP(2), SX, SXF, SY, SYF, TL(20,2), TPC(20,3), TPL(20,2), TPATE, TPATM, T
5SR(20,2), W(20,2), WD(20,2), WL(20,2), WTW, X, XB(20,2), XC(20,3), XXX, XY, Y, I
6J, KB(20,2), KC(20,3), KH, KHC, LIMITD, M, MS, N, NC, NN, NP, NSW, NW(3)
DO 400 N=1, NC
FC=FCC
IF(NSW.EQ.0) GO TO 399
DO 401 K=1, NSW
IF(N.EQ.NW(K)) FC=FCW
401 CONTINUE
399 CONTINUE
DO 402 JJ=1, MS
M=MS-JJ+1
C 1E. WORK UPWARD FROM BASE.
IF(P(M,N).LE.0.0) GO TO 404
C 1E. NEGLECT LENGTHENING DUE TO TENSION IN COLUMNS.
X=0.85*FC*(CB(M,N)*CT(M,N)-CAS(M,N))/(0.0019*0.0019)
Y=1.7*FC*(CAS(M,N)-CB(M,N)*CT(M,N))/0.0019-(CAS(M,N)*30.0E6
Z=P(M,N)
IF((Y-4.*X*Z).LE.0.0) GO TO 406
DEL=H(M)*(-Y-SQRT(Y-4.*X*Z))/(2.*X)
GO TO 405
406 DEL=H(M)*Y/(2.*X)
GO TO 405
404 DEL=0.
405 IF(IJJ.EQ.1) DV(M,N)=DEL
IF(IJJ.GT.1) DV(M,N)=DV(M+1,N)+DEL
402 CONTINUE
400 CONTINUE
RETURN
END

```

## COLS

```

C
SUBROUTINE COLS
C
C FROM BASIC COLUMN SECTION PROPERTIES, USING CURRENT P VALUE, COMPUTES
C MPC, ETC, ALLOWABLE HINGE ROTATION, C&S FOR ALL COLUMNS, USING A
C RATIONALIZED MOMENT-CURVATURE-THRUST RELATIONSHIP.
C

```

```

COMMON A, ACCURD, AL(20,3), AM(20,3), AU(20,3), B, BAS(20,2), BB(20,2), BT
1(20,2), C(20,3), CAS(20,3), CB(20,3), CT(20,3), CX, CFX, CY, CYF, D, DH(20,2),
2DH(20,2), DPB, DPC, DV(20,3), EIB(20,2), EIC(20,3), F, FAUGDL, FCB, FCC, FCM,
3FYB, FYC, FYW, HI(20,3), P(20,3), PE(3), RI(2,3), RBP(20,2), RCP(20,3), S(20,3),
4SP(2), SX, SXF, SY, SYF, TL(20,2), TPC(20,3), TPL(20,2), TPATE, TPATM, T
5SR(20,2), W(20,2), WD(20,2), WL(20,2), WTW, X, XB(20,2), XC(20,3), XXX, XY, Y, I
6J, KB(20,2), KC(20,3), KH, KHC, LIMITD, M, MS, N, NC, NN, NP, NSW, NW(3)
PEX=0.
DO 500 N=1, NC
FC=FCC
FY=FYC
IF(NSW.EQ.0) GO TO 498
DO 499 K=1, NSW
IF(N.EQ.NW(K)) FC=FCW
IF(N.EQ.NW(K)) FY=FYW
499 CONTINUE
498 EN=500./SQRT(FC)
DO 501 I=1, MS
IF(CT(M,N).LE.20.0) DPC=2.0
IF(CT(M,N).GT.20.0) DPC=0.1*CT(M,N)
D=CT(M,N)-DPC
RB=(0.0038*FY/30.0E6)/D
PS=CAS(M,N)/(2.*CB(M,N)*D)
X=0.7*FC
Y=PS*(30.0E6*0.0038-FY)
Z=-PS*30.0E6*0.0038*DPC/D
YY=Y-4.*X*Z
IF(YY.LT.0.0) GO TO 510
UK=(-Y+SQRT(YY))/(2.*X)
RU=0.0038/(UK*D)
GO TO 512
510 RU=0.0
WRITE(6,900) M,N
900 FORMAT('0', ' ***RU OF COLUMN(13,*,*,13,*) CANNOT BE COMPUTED IN
SUBROUTINE COLS, SINCE IMAGINARY ROOT PRESENT')
512 YUK=-2.*PS*EN+SQRT(4.*PS*PS*EN*EN+2.*PS*EN*(1.+DPC/D))
RYO=FY/(30.0E6*D*(1.-YBK))
PB=C.00257*FC*CB(M,N)/RB
X=1./(2.*EN)
Y=2.*PS*PB/(FY*CB(M,N)*D)
Z=-PS*(1.+DPC/D)-PB/(FY*CB(M,N)*D)
YKB=-Y+SQRT(Y-4.*X*Z)/(2.*X)
RYB=FY/(30.0E6*D*(1.-YBK))
PU=0.85*FC*CB(M,N)*(CT(M,N)-2.*PS*D)+2.*PS*CB(M,N)*D*FY
EH=CT(M,N)*(1.95+0.8*BD-(D-DPC)*CAS(M,N)*FY/(CB(M,N)*CT(M,N)*FC)+0.5-
11.542E-3/(RB*CT(M,N)))
TB=PB*EB
TU=0.5*CAS(M,N)*FY*(D-DPC)
C HAVE NOW COMPUTED BASIC COLUMN SECTION BEHAVIOURAL CHARACTERISTIC
C VALUES
C NOW APPLY P AND DERIVE MPC, ETC, RCP, C&S.
PAPPL=P(M,N)

```

```

IF(P(M,N).GE.PUI) PEXC=PEXC+1.0
IF(P(M,N).GE.PUI) PAPPL=0.9*PU
C 1E. TO COMPUTE MPC, PHIV, C PHIPC FOR CASE WHERE P GT PULT, USE A
C P VALUE=0.9*PULT. THIS YIELDS UNCONSERVATIVE RESULTS.***
IF(P(M,N).GE.PUI) AND PEXC.EQ.1.0) WRITE(6,901) M,N,P(M,N),PU
C 1E. NOTE ONLY THE FIRST OCCURRENCE IN EACH PASS THROUGH *COLS*.
901 FORMAT('0', ' *** P IN COLUMN(13,13,*,*,E12.5,*, PULT=*,E12.5,*,
1*CRUSHING FAILURE*COULD BE OTHERS*)
IF(P(M,N).LE.0.0) GO TO 505
IF(P(M,N).GT.PB) GO TO 502
RY=RYO+(RYB-RYO)*P(M,N)/PB
TPC(M,N)=TU+2.*(TH-TU)*P(M,N)/PB-(TB-TU)*P(M,N)/(PB*PB)
RPC=RH*PB/P(M,N)
IF(RPC.GT.(RU*(1.-0.6*P(M,N)/PB))) RPC=RU*(1.-0.6*P(M,N)/PB)
GO TO 504
505 RY=RYO
TPC(M,N)=TU
RPC=RU
GO TO 504
C THE EFFECT OF AXIAL TENSION IN COLUMNS IS NEGLECTED.
502 RY=RYB*(PU-PAPPL)/(PU-PB)
TPC(M,N)=TB*(PU-PAPPL)/(PU-PB)
RPC=RB+(IDPC/CT(M,N)+0.01)*RU*(PB-PB)/(PAPPL-PB)/(0.8*PU-PB)
IF(P(M,N).GT.(0.8*PU)) RPC=5.*RU*(IDPC/CT(M,N)+0.01)/(1.-PAPPL/PU)
504 EIC(M,N)=TPC(M,N)/RY
RCP(M,N)=RPC/D/2.
C THIS VALUE OF PERMISSIBLE HINGE ROTATION (DISCONTINUITY AT A *POINT*
C HINGE) IS BASED ON BEAM TESTS CARRIED OUT BY MATTOCK AT PCA, AND
C EXTENDED HERE FOR CONSIDERATION OF COLUMNS. AS COMPUTED, IT APPLIES
C TO HALF A HINGE (IE. AN END HINGE).
C NOW COMPUTE C & S.
IF(P(M,N).LE.0.0) GO TO 506
F=SQRT(P(M,N)/EIC(M,N))*H(M)
IF(F.LE.0.1) GO TO 506
XX=2.-2.*COS(F)-F*SIN(F)
C(M,N)=F*(SIN(F)-F*COS(F))/X
S(M,N)=F*(F-SIN(F))/X
GO TO 501
506 C(M,N)=4.0
S(M,N)=2.0
C ANY POSSIBLE STIFFENING DUE TO COLUMN AXIAL TENSILE LOAD HAS BEEN
C NEGLECTED. MOREOVER, FOR SMALL P VALUES, C & S VALUES HAVE BEEN
C SET, SINCE THE TRIGONOMETRIC EXPRESSIONS FOR THESE VALUES DO NOT
C CONVERGE FOR SMALL P VALUES.
501 CONTINUE
500 CONTINUE
RETURN
END

```

## CASE4

```

SUBROUTINE CASE4
C
C COMPUTES X,Y,CX,SX,CY,SY,CFX,SXF,CYF,SYF,A,B,D,F FOR COLUMN(I,N) WITH
C CASE 4 HINGING CONDITION.
C

```

```

COMMON A, ACCURD, AL(20,3), AM(20,3), AU(20,3), B, BAS(20,2), BB(20,2), BT
1(20,2), C(20,3), CAS(20,3), CB(20,3), CT(20,3), CX, CFX, CY, CYF, D, DH(20,2),
2DH(20,2), DPB, DPC, DV(20,3), EIB(20,2), EIC(20,3), F, FAUGDL, FCB, FCC, FCM,
3FYB, FYC, FYW, HI(20,3), P(20,3), PE(3), RI(2,3), RBP(20,2), RCP(20,3), S(20,3),
4SP(2), SX, SXF, SY, SYF, TL(20,2), TPC(20,3), TPL(20,2), TPATE, TPATM, T
5SR(20,2), W(20,2), WD(20,2), WL(20,2), WTW, X, XB(20,2), XC(20,3), XXX, XY, Y, I
6J, KB(20,2), KC(20,3), KH, KHC, LIMITD, M, MS, N, NC, NN, NP, NSW, NW(3)
X=XCI(1,N)
Y=H(1)-X
IF(P(I,N).LE.0.0) GO TO 550
FX=SQRT(P(I,N)/EIC(1,N))*X
IF(FX.LE.0.1) GO TO 552
XX=2.-2.*COS(FX)-FX*SIN(FX)
CY=FX*(SIN(FX)-FX*COS(FX))/XX
SY=FX*(FX-SIN(FX))/XX
GO TO 556
552 CX=4.0
SX=2.0
554 FX=FX*Y/X
IF(FX.LE.0.1) GO TO 556
XX=2.-2.*COS(FX)-FX*SIN(FX)
CY=FX*(SIN(FX)-FX*COS(FX))/XX
SY=FX*(FX-SIN(FX))/XX
GO TO 558
556 CY=4.0
SY=2.0
GO TO 558
550 CX=4.0
CY=4.0
SX=2.0
SY=2.0
558 CFX=CX/ICX*CX-SX*SX
SXF=SX/ICX*CX-SX*SX
CYF=CY/ICY*CY-SY*SY
SYF=SY/ICY*CY-SY*SY
B=X/H(1)-P(I,N)*Y*CYF/EIC(1,N)
A=P(I,N)*Y*Y*CYF/(B*H(1))+X*CXF/EIC(1,N)
D=Y/H(1)-P(I,N)*X*CXF/EIC(1,N)
F=-P(I,N)*(X*XX*CXF/(D*H(1))+Y*Y*CYF)/EIC(1,N)
RETURN
END

```

## ITER

```

SUBROUTINE ITER
C COMPUTES STOREY LATERAL SWAY DEFLECTIONS AND JOINT ROTATIONS BY THE
C GAUSS-SEIDEL ITERATION PROCEDURE TO A CLOSURE OF +-ACCURD, WITH
C INSTABILITY ASSUMED AFTER 'LIMITD' CYCLES OF ITERATION
C
COMMON A, ACCURD, AL(20,3), AM(20,3), AU(20,3), B, BASI(20,2), BB(20,2), BT
(120,2), C(20,3), CAS(20,3), CB(20,3), CC(20,3), CFX, CFY, CY, D, DH(20),
2DH(20), DPF, DPL, DV(20,3), EIB(20,2), EIC(20,3), F, FAUGDL, FCD, FCL, FCM,
3FYB, FYC, FYM, H(20), P(20,3), PF(3), R(20,3), RBP(20,2), RCP(20,3), S(20,3),
4S(20,2), SA, SXF, SY, SYF, TL(20,2), TPC(20,3), TPL(20,2), TPRATE, TPRATH, T
SR(20,2), W(20), WD(20,2), WL(20,2), WTM, X, XB(20,2), XC(20,3), XXX, XY, Y, I
6J, J, KB(20,2), KC(20,3), KH, KHC, LIMITD, M, MS, N, NC, NN, NP, NSW, NW(3)
J=0
600 J=J+1
RD=0
KR=0
C FIRST COMPUTE STOREY LATERAL SWAY DEFLECTIONS TO AVOID UNDERFLOW IN
C ROTATION COMPUTATIONS WHEN J=1.
C
DO 602 M=1, MS
DHR=0.
VV=0.
TT=0.
ZZ=0.
UU=0.
DO 604 N=1, NC
KK=KC(M,N)
GO TO (611,612,613,614,615), KK
1 WRITE(6,802)
802 FORMAT('0', ' *** COLUMN COUNTER OUT OF RANGE IN SUBROUTINE ITER')
611 V=IC(M,N)*C(M,N)*EIC(M,N)*R(M,N)/H(M)
T=IS(M,N)*C(M,N)*EIC(M,N)*R(M,N)/H(M)
Z=-2.*IS(M,N)*C(M,N)*EIC(M,N)/H(M)*H(M)+P(M,N)
U=0.
GO TO 616
612 V=IC(M,N)*C(M,N)*S(M,N)*S(M,N)*EIC(M,N)*R(M,N)/IC(M,N)*H(M)
T=0.
Z=IS(M,N)*S(M,N)*C(M,N)*C(M,N)*EIC(M,N)/IC(M,N)*H(M)*H(M)+P(M,N)
U=AL(M,N)*TPC(M,N)*IS(M,N)/C(M,N)+1.
GO TO 616
613 V=0.
T=IC(M,N)*C(M,N)*S(M,N)*S(M,N)*EIC(M,N)*R(M,N)/IC(M,N)*H(M)
Z=IS(M,N)*S(M,N)*C(M,N)*C(M,N)*EIC(M,N)/IC(M,N)*H(M)*H(M)+P(M,N)
U=AU(M,N)*TPC(M,N)*IS(M,N)/C(M,N)+1.
GO TO 616
614 I=M
CALL CASE4
V=PI(M,N)*Y*(H(M)*A+1.)/F1*(R(M,N)
T=PI(M,N)*X*(H(M)*F+1.)/F1*(R(M,N)
Z=P(M,N)*(Y*(1.+X*(H(M)*D))/H(M)*F+X*(1.+Y*(H(M)*B))/H(M)*A)+1.
U=AP(M,N)*P(M,N)/EIC(M,N)*(X*X*(SXF/A+CXF/F+D))-Y*Y*(SYF/F+CYF/
1(A+B))+X*Y*(X*SXF/(F+D)-Y*SYF/(A+B))/H(M)
GO TO 616
615 V=0.
T=0.
Z=P(M,N)
U=AL(M,N)+AU(M,N)*TPC(M,N)
616 VV=VV+V
TT=TT+T
ZZ=ZZ+Z
UU=UU+U
604 CONTINUE
C HAVE NOW COMPUTED AND COMBINED V,T,Z,U FOR ALL COLUMNS IN STOREY M.
C NOW COMPUTE TOTAL TRANSVERSE SHEAR LOAD AT FLOOR M.
WS=0.
DO 618 I=1, M
WS=WS+W(I)
618 CONTINUE
IF (J.EQ.1) GO TO 620
DHR=-(WS*H(M)+VV+TT+UU)/ZZ*DH(M)
620 DH(M)=-(WS*H(M)+VV+TT+UU)/ZZ
IF (DHR.LE.(1.-ACCURD).AND.DHR.GE.(1.-ACCURD)) GO TO 602
KD=KD+1
IF (J.EQ.LIMITD) WRITE(6,1160) M,LIMITD,DH(M)
1160 FORMAT('X', 'SWAY DEFLECTION VALUE IN STOREY', I4, ' WOULD NOT CONVERG
1E AFTER', I6, ' CYCLES. CURRENT VALUE=', E12,5)
C IF KD IS AUGMENTED, THE NEW VALUE OF DH(M) HAS NOT CONVERGED CLOSE
C ENOUGH (IE. +-ACCURD) TO THE OLD VALUE.
602 CONTINUE
C
C NOW PROCEED TO EVALUATE ALL NGDAL POINT ROTATIONS.
C
DO 630 P=1, MS
DO 631 A=1, NC
RK=0.
C FIRST CONSIDER LEFT HAND BEAM AT JOINT(M,N)--CC, GL, AG
C
IF (N.EQ.1) GO TO 634
C IF. THERE IS NO LEFT HAND BEAM IN THIS CASE.
I=N-1
DEL=DV(M,N)-DV(M,I)
WT=(WL(M,I)+WD(M,I)+FAUGDL*DB(M,I)+BT(M,I))/12.
WNL=0.
WNR=0.
IF (NSW.EQ.0) GO TO 623
DO 622 K=1, NSW
IF (1.EQ.NW(K)) WNL=CT(M,I)
IF (N.EQ.NW(K)) WNR=CT(M,N)
622 CONTINUE
623 SR=SP(I)-(WNL+WNR)/2.
KK=KB(M,I)
GO TO (641,642,643,644,645,646,647), KK
2 WRITE(6,804)
804 FORMAT('0', ' *** BEAM COUNTER OUT OF RANGE IN SUBROUTINE ITER')
641 CC=EIB(M,I)*R(M,I)*(1.+3.*WNL/SR)*(1.+4.*WNR/SR)/SR
GL=-6.*EIB(M,I)*DEL*(1.+WNL/SR)/(SR*SR)-WT*SR*(1.+3.*WNL/SR)/12
1.
AG=EIB(M,I)*(1.+3.*WNR*(2.*WNR/SR)/SR)
GO TO 648
642 CC=1.5*EIB(M,I)*WNL*(1.+0.5*WNR/SR)*R(M,I)/(SR*SR)
GL=-3.*EIB(M,I)*DEL*(1.+0.5*WNR/SR)/(SR*SR)+WT*SR*(1.+2.5*WNR/S
1R)/R*(1.+0.5*WNL/SR)*(1.+1.5*WNR/SR)
AG=3.*EIB(M,I)*(1.+0.5*WNR/SR)/(SR*SR)
GO TO 648
643 CC=1.5*EIB(M,I)*WNR*(1.+0.5*WNL/SR)/(SR*SR)
GL=-1.5*EIB(M,I)*DEL*WNR/(SR*SR*SR)+TR(M,I)*(1.+0.75*WNR/SR)+3.*WT
1*WNR*SR/16.
AG=0.75*EIB(M,I)*WNR*WNR/(SR*SR*SR)
GO TO 648
644 X=XB(M,I)
Y=SR-X
FX=1./X*(X*(1./X*(X*X)+1.)/(Y*Y+Y))
FY=1./Y*(Y*(1./X*(X*X)+1.)/(Y*Y+Y))
Z=FYX-FXY
CC=3.*EIB(M,I)*R(M,I)*(1.+0.5*WNL/X)*(FYX/X+0.5*(1.+Z/X)*WNR/SR)/X
GL=3.*EIB(M,I)*(DV(M,I)*(FYX/X+0.5*WNR*(1.+Z/X)/SR)/(X*X)-DV(M,N)
111.-FYX/Y+0.5*WNR*(1.-Z/Y)/SR)/(Y*Y)+WT*(Y*Y*SR*(3.*FYX+2.*WNR)
2.5*WNR*(Y-X+3.*Z)/8.+0.5*TPRATH*TPL(M,I)*(1.-1.*FYX+0.5*WNR/Z/SR
3)*1./X+1./Y)
AG=3.*EIB(M,I)*(1.+0.5*WNR/Y)*(1.-Z/Y)*WNR/(2.*SR)+1.-FYX/Y
GO TO 648
645 CC=C.
GL=(TL(M,I)-TPRATH*TPL(M,I))/X+0.5*WT*Y*(SR+0.5*WNR)-TL(M,I)+0.2
15*WT*SR*WNR
AG=0.
GO TO 648
646 CC=0.
GL=TR(M,I)+0.5*WNR*(TPRATH*TPL(M,I)+TR(M,I))/Y+0.5*WT*Y
AG=0.
GO TO 648
647 CC=C.
GL=TR(M,I)+0.5*WNR*(TR(M,I)+TL(M,I))+0.5*WT*SR*SR/SR
AG=0.
GO TO 648
648 CONTINUE
C
C NOW CONSIDER THE RIGHT HAND BEAM AT JOINT(M,N)--DD, GR, AD
C
IF (N.EQ.NC) GO TO 650
C IE. THERE IS NO RIGHT HAND BEAM IN THIS CASE.
DEL=DV(M,N+1)-DV(M,N)
WT=(WL(M,N)+WD(M,N)+FAUGDL*DB(M,N)+BT(M,N))/12.
WNL=0.
WNR=0.
IF (NSW.EQ.0) GO TO 626
DO 625 K=1, NSW
IF (N.EQ.NW(K)) WNL=CT(M,N)
IF (N+1.EQ.NW(K)) WNR=CT(M,N+1)
625 CONTINUE
626 SR=SP(N)-(WNL+WNR)/2.
KK=KB(M,N)
GO TO (651,652,653,654,655,656,657), KK
3 WRITE(6,804)
804 FORMAT('0', ' *** BEAM COUNTER OUT OF RANGE IN SUBROUTINE ITER')
651 DD=EIB(M,N)*R(M,N+1)*(2.+3.*WNR/SR+3.*WNL*(1.+WNR/SR)/SR)
GR=-6.*EIB(M,N)*DEL*(1.+WNL/SR)/(SR*SR)-WT*SR*(1.+3.*WNL/SR)/12
1.
AD=EIB(M,N)*(2.+3.*WNL/SR)*(2.*WNL/SR)-2.*WNL/SR/SR
GO TO 658
652 DD=1.5*EIB(M,N)*WNR*(1.+0.5*WNR/SR)/(SR*SR)
GR=-1.5*EIB(M,N)*DEL*WNR/(SR*SR*SR)+TL(M,N)+0.75*WNL*(TL(M,N)-0.25
1*WT*SR*SR)/SR
AD=0.75*EIB(M,N)*WNL*WNL/(SR*SR*SR)
GO TO 658
653 DD=1.5*EIB(M,N)*R(M,N+1)*WNR*(1.+0.5*WNL/SR)/(SR*SR)
GR=-3.*EIB(M,N)*DEL*(1.+0.5*WNL/SR)/(SR*SR)+0.5*TR(M,N)-WT*SR*SR/B
1.0+0.25*WNL*(3.*TR(M,N)-1.25*WT*SR*SR)/SR
AD=3.*EIB(M,N)*(1.+0.5*WNL/SR)*(1.+0.5*WNL/SR)/SR
GO TO 658
654 X=XB(M,N)
Y=SR-X
FX=1./X*(X*(1./X*(X*X)+1.)/(Y*Y+Y))
FY=1./Y*(Y*(1./X*(X*X)+1.)/(Y*Y+Y))
Z=FYX-FXY
DD=3.*EIB(M,N)*R(M,N+1)*(1.+0.5*WNR/Y)*(1.-Z/Y)*WNL/(2.*SR)+FYX/Y
1/Y
GR=3.*EIB(M,N)*(1.-FYX/X*(1.+Z/X)*WNL/(2.*SR)+DV(M,N)/(X*X)-FYX
1/Y*(1.-Z/Y)*WNL/(2.*SR)+DV(M,N+1)/(Y*Y)+WT*(0.5*WNL*(3.*Z+Y-X+
2*SR)-X*X-3.*SR*FYX)/8.+0.5*TPRATH*TPL(M,N)*(3.*FYX*(1./X+1./Y)-1.
31.5*WNL*Z*(1./X+1./Y))
AD=3.*EIB(M,N)*(1.+0.5*WNL/X)*(0.5*WNL*(1.+Z/X)/SR+1.-FYX/X)
GO TO 658
655 DD=C.
GR=TL(M,N)+0.5*WNL*(TL(M,N)-TPRATH*TPL(M,N))/SR+X-WT*SR/2./SR
AD=0.
GO TO 658
656 DD=0.
GR=TPRATH*TPL(M,N)+TR(M,N)+TPRATH*TPL(M,N)*X/Y+0.5*WT*SR*SR+0.5*W
1NL*(TR(M,N)+TPRATH*TPL(M,N))/SR/Y+0.5*WT*SR*(X*SR)/SR
AD=0.
GO TO 658
657 DD=0.
GR=TL(M,N)+0.5*WNL*(TL(M,N)+TP(M,N)-0.5*WT*SR*SR)/SR
AD=C.
GO TO 658
658 CONTINUE

```

## HINGES

```

C
C NOW CONSIDER COLUMN ABOVE JOINT(M,N)-- EE,GA,AA
C
      IF(P.EQ.1) GO TO 659
C IE. THERE IS NO COLUMN ABOVE (M,N) IN THIS CASE
      KK=KC(M-1,N)
      I=M-1
      GO TO (661,662,663,664,665),KK
4 WRITE(6,802)
661 EE=S(I,N)*EIC(I,N)*R(I,N)/H(I)
      GA=-(C(I,N)+S(I,N))*EIC(I,N)*DH(I)/(H(I)*H(I))
      AA=C(I,N)*EIC(I,N)/H(I)
      GO TO 666
662 EE=0.
      GA=AL(I,N)*TPC(I,N)
      AA=0.
      GO TO 666
663 EE=0.
      GA=AU(I,N)*TPC(I,N)*S(I,N)/C(I,N)-(C(I,N)*C(I,N)-S(I,N)*S(I,N))*E
      IC(I,N)*DH(I)/(C(I,N)*H(I))*H(I)
      AA=-(C(I,N)*C(I,N)-S(I,N)*S(I,N))*EIC(I,N)/(C(I,N)*H(I))
      GO TO 666
664 CALL CASE4
      EE=-P(I,N)*X*Y*R(I,N)/(H(I)*A*B)
      GA=(AM(I,N)*P(I,N)/(A*EIC(I,N)))+(X*X*SYF-Y*Y*CYF/B-X*Y*Y*SYF/(B*H
      I(I)))+(P(I,N)*X*(1.+Y/(B*H(I)))*DH(I)/(A*H(I))
      AA=-P(I,N)*X/A
      GO TO 666
665 EE=0.
      GA=AL(I,N)*TPC(I,N)
      AA=0.
      GO TO 666
659 EE=0.
      GA=0.
      AA=0.
666 CONTINUE
C
C NOW CONSIDER COLUMN BELOW JOINT(M,N)--FF,GB,AB
C
      KK=KC(M,N)
      I=M
      GO TO (671,672,673,674,675),KK
5 WRITE(6,802)
671 FF=S(I,N)*EIC(I,N)*R(I+1,N)/H(I)
      GB=-(C(I,N)+S(I,N))*EIC(I,N)*DH(I)/(H(I)*H(I))
      AB=C(I,N)*EIC(I,N)/H(I)
      GO TO 676
672 FF=0.
      GB=AL(I,N)*TPC(I,N)*S(I,N)/C(I,N)-(C(I,N)*C(I,N)-S(I,N)*S(I,N))*E
      IC(I,N)*DH(I)/(C(I,N)*H(I))*H(I)
      AB=-(C(I,N)*C(I,N)-S(I,N)*S(I,N))*EIC(I,N)/(C(I,N)*H(I))
      GO TO 676
673 FF=0.
      GB=AU(I,N)*TPC(I,N)
      AB=0.
      GO TO 676
674 CALL CASE4
      FF=-P(I,N)*X*Y*R(I+1,N)/(H(I)*F*D)
      GB=(AM(I,N)*P(I,N)/(F*EIC(I,N)*F)))+(Y*Y*SYF+X*X*CYF/D+X*Y*Y*SYF/(H
      I(I)*D)))+(P(I,N)*Y*(1.+X/(H(I)*D))*DH(I)/(F*H(I))
      AB=-P(I,N)*Y/F
      GO TO 676
675 FF=0.
      GB=AU(I,N)*TPC(I,N)
      AB=0.
676 CONTINUE
C
C NOW CHECK FOR A POSSIBLE JOINT MECHANISM.
C
      IF((AG+AD+AA+AB).EQ.0.0) GO TO 686
C
C NOW EVALUATE R(M,N) & RR.
C
      IF(J.EQ.1) GO TO 688
C IE. WOULD GET OVERFLOW SINCE R(M,N) ORIGINAL=0.
      RR=-(GL+GR+GA+GB+CC+DD+EE+FF)/(AG+AD+AA+AB)*R(M,N)
688 R(M,N)=-(GL+GR+GA+GB+CC+DD+EE+FF)/(AG+AD+AA+AB)
      IF(RR.LE.(1.+ACCURD).AND.RR.GE.(1.-ACCURD)) GO TO 631
      KR=KR+1
      TPE(J.EQ.LIMITD) WRITE(6,1162) M,N,LIMITD,R(M,N)
1162 FORMAT(1X,'JOINT ROTATION AT',I4,',',I4,',') WOULD NOT CONVERGE AFT
      ER',I6,' CYCLES. CURRENT VALUE=',E12.5)
631 CONTINUE
630 CONTINUE
C
C AT THIS STAGE, ONE COMPLETE CYCLE OF ITERATION HAS BEEN COMPLETED, AND
C VALUES OF DH(M),KD,R(M,N),AND KR HAVE BEEN COMPUTED.
C
C NOW CHECK FOR CONVERGENCE OF DEFORMATION VALUES.
C
      IF(KD.GT.0.0R.KR.GT.0) GO TO 692
C IE. REITERATE UNLESS J=LIMITD
      GO TO 698
C
C IF WE ARRIVE AT STATEMENT#698 BY THIS ROUTE, ALL IS OKAY. THE
C DEFORMATION VALUES HAVE CONVERGED TO +-ACCURD IN LESS THAN 'LIMITD'
C CYCLES.
C
692 IF(J.LT.LIMITD) GO TO 600
C IE. REITERATE FOR CONVERGENCE.
      XXX=1.
      GO TO 698
C
C XXX=1. INDICATES INSUFFICIENT CONVERGENCE AFTER 'LIMITD' CYCLES.
C
698 XXX=2.
C
C XXX=2. INDICATES THE FORMATION OF A JOINT MECHANISM.
C
698 CONTINUE
      RETURN
      END

```

## SUBROUTINE HINGES

```

C
C CHECKS AND REVISES HINGE CONFIGURATION IN ALL BEAMS AND COLUMNS.
C
      COMMON A,ACCURD,AL(20,3),AM(20,3),AU(20,3),B,DAS(20,2),BB(20,2),BT
      I(20,2),C(20,3),CAS(20,3),CB(20,3),CT(20,3),CX,CY,CYF,D,DH(20),
      DH(20),DPB,DPC,DV(20,3),EIB(20,2),EIC(20,3),F,FAUGDL,FCB,FCC,FCW,
      FFW,FYC,FYM,H(20),P(20,3),PE(3),R(21,3),RBP(20,2),RCP(20,3),S(20,3),
      SP(21,3),SX,SXF,S,YF,TL(20,2),TPC(20,3),TPL(20,2),TPRAT,TPRATH,T
      SR(20,2),W(20),WD(20,2),WL(20,2),WM,X,XB(20,2),XC(20,3),XX,X,Y,Y,I
      6,J,KB(20,2),KC(20,3),KH,KHC,LIMITD,M,MS,N,NC,NN,NP,NSW,NW(3)
      KH=0
C KH REPRESENTS THE TOTAL NUMBER OF NEW HINGES DETECTED IN THE CURRENT
C PASS THROUGH THIS SUBROUTINE.
C
C FIRST CHECK ALL BEAMS FOR NEW HINGES.
C
      IF(XY.GT.0.0) WRITE(6,900)
900 FORMAT('0',' * MOMENT VALUES:')
      CALL BMHING
C
C ALL BEAMS HAVE NOW HAD POSSIBLE HINGE CONFIGURATION ADJUSTMENTS MADE,
C ACCORDING TO THE NEW LOADING AND DEFORMATION CONDITIONS. THE CURRENT
C KH VALUE REPRESENTS THE NUMBER OF NEW HINGES DETECTED. THE OCCURREN
C OF ANY BEAM MECHANISMS WAS NOTED, AND THE BEAM WILL HENCEFORTH BE
C ASSUMED TO ACT AS A BEAM WITH KB=7 AND APPROPRIATE END MOMENTS.
C
C NOW CHECK ALL COLUMNS FOR NEW HINGES.
C
      DO 735 P=1,PS
      DO 737 N=1,NC
      BMAX=0.
      DEL=DH(KI)/H(M)
      KK=KC(M,N)
      GO TO (741,742,743,744,745),KK
2 WRITE(6,926)
926 FORMAT('0',' * **COLUMN COUNTER OUT OF RANGE IN SUBROUTINE HINGES')
741 BU=EIC(M,N)/H(M))*EIC(M,N)*R(M,N)+S(M,N)*R(H+1,N)-(C(M,N)+S(M,N))*
      IDEL)
C NOTE: THE C,S,EIC,MPC & P VALUES USED HERE ARE STILL THOSE
C CORRESPONDING TO DEFORMATIONS PRIOR TO THE LAST PASS THROUGH
C SUBROUTINE 'ITER'. WE HAVE NOT AS YET RECYCLED THROUGH SUBROUTINE
C 'PDL' WITH THESE REVISED DEFORMATIONS. BUT WE WILL CHECK FOR
C CONVERGENCE OF AXIAL COLUMN LOADS TO MINIMIZE ANY ERROR.
      BL=EIC(M,N)/H(M))*EIC(M,N)*R(H+1,N)+S(M,N)*R(M,N)-(C(M,N)+S(M,N))*
      IDEL)
      IF(P(M,N).LE.0.0) GO TO 750
      F=SQRT(P(M,N)/EIC(M,N))*H(M)
      FX=ATANI(-BU*BL*COS(F))/(BL*SIN(F))
      IF(FX.LT.C.0) FX=FX+3.141593
      IF(FX.LE.0.0R.FX.GE.F) GO TO 750
      BMAX=SQRT(BL*BL*OU*BU*2.*BU*BL*COS(F))/SIN(F)
      IF(ABS(BU).LT.ABS(BL)) BMAX=BL*BMAX/ABS(BL)
      IF(ABS(BL).LE.ABS(BU)) BMAX=-BU*BMAX/ABS(BU)
      GO TO 752
750 BMAX=0.
752 IF(ABS(BU).GT.ABS(BL)) GO TO 754
      IF(ABS(BMAX).GT.ABS(BL)) GO TO 756
      IF(ABS(BL).LT.TPC(M,N)) GO TO 746
      KC(M,N)=2
      KH=KH+1
      AL(M,N)=BL/ABS(BL)
      GO TO 742
754 IF(ABS(BMAX).GT.ABS(BU)) GO TO 756
      IF(ABS(BU).LT.TPC(M,N)) GO TO 746
      KC(M,N)=3
      KH=KH+1
      AU(M,N)=BU/ABS(BU)
      GO TO 743
756 IF(ABS(BMAX).LT.TPC(M,N)) GO TO 746
      KC(M,N)=4
      KH=KH+1
      XC(M,N)=FX*H(M)/F
      AM(M,N)=BMAX/ABS(BMAX)
      GO TO 744
742 BL=AL(M,N)*TPC(M,N)
      BU=S(M,N)*BL*(C(M,N)*C(M,N)-S(M,N)*S(M,N))*EIC(M,N)/H(M))*R(M,N)
      IDEL)/C(M,N)
      IF(ABS(BU).LT.TPC(M,N)) GO TO 758
      KC(M,N)=5
      KH=KH+1
      AU(M,N)=BU/ABS(BU)
      GO TO 745
758 RDL=(H(M)*BL/EIC(M,N)-S(M,N)*R(M,N)+C(M,N)*S(M,N))*DEL/C(M,N)-R
      I(M+1,N)
      IF(ABS(RDL).GT.RCP(M,N).AND.XY.GT.0.0) WRITE(6,928) M,N,RDL,RCP(M,
      N)
928 FORMAT(1X,' * - EXCESSIVE ROTATION AT BOTTOM HINGE OF COLUMN',I3,
      ',I3,') ROTATION=',E12.5,' PERMISSIBLE=',E12.5)
      GO TO 746
743 BU=AU(M,N)*TPC(M,N)
      BL=S(M,N)*BU*(C(M,N)*C(M,N)-S(M,N)*S(M,N))*EIC(M,N)/H(M))*R(M,N)
      IDEL)/C(M,N)
      IF(ABS(BL).LT.TPC(M,N)) GO TO 760
      KC(M,N)=5
      KH=KH+1
      AL(M,N)=BL/ABS(BL)
      GO TO 745
760 RDU=(H(M)*BU/EIC(M,N)-S(M,N)*R(M+1,N)+C(M,N)*S(M,N))*DEL/C(M,N)-
      R(M,N)
      IF(ABS(RDU).GT.RCP(M,N).AND.XY.GT.0.0) WRITE(6,930) M,N,RDU,RCP(M,
      N)
930 FORMAT(1X,' * - EXCESSIVE ROTATION AT TOP HINGE OF COLUMN',I3,
      ',I3,') ROTATION=',E12.5,' PERMISSIBLE=',E12.5)
      GO TO 746

```

```

744 I=M
CALL CASE4
BMX=BM(M,N)*TPC(M,N)
BU=TPC(M,N)/F1*(BMX/EIC(M,N))*IX**X*(CAF+Y*SYF/H(M))/U-Y*Y*SYF-Y*Y
RIM(N)=R*Y*BM(M,N)/F1*(BMX/EIC(M,N))*Y*Y*Y*(H(M)/U)*DEL1
BL=TPC(M,N)/A1*(BMX/EIC(M,N))*Y*Y*Y*(CAF+Y*SYF/H(M))/H*X*Y*SYF-X
RIP(N)=X*Y*TPC(M,N)/H(M)*U*(X*Y*Y*(H(M)/U)*DEL1)
IF (ABS(BU).GT.TPC(M,N)) WRITE(6,932) M,N,BU,TPC(M,N)
932 FORMAT(IX,' BLAST*** IN COLUMN',I3,'*',I3,'') BU EXCEEDS MPC WITH
ICASE 4 HINGING. BU=E12.5,' MPC=E12.5)
IF (ABS(BU).GT.TPC(M,N)) WRITE(6,934) M,N,BU,TPC(M,N)
934 FORMAT(IX,' BLAST*** IN COLUMN',I3,'*',I3,'') BL EXCEEDS MPC WITH
ICASE 4 HINGING. BU=E12.5,' MPC=E12.5)
C COMPUTE LATERAL SWAY DEFLECTION OF FLOOR M (DHU)
DHU=0.
DO 762 I=P,M5
DHU=DHU+DH(I)
762 CONTINUE
DHU=(Y*Y/EIC(M,N))*ICF*BU-SYF*BMX+Y*(M,N)*DHU
RDC=IX/EIC(M,N)*I-SXF*UL-CXF*BMX+Y*(M,N)*I*(SYF*BU-CYF*BMX)
I*(DHU-DHU+DH(M))/X-I*(DHU-DHU)/Y
IF (ABS(RDC).GT.(2.*PCP(M,N)).AND.XY.GT.0.0) WRITE(6,936) M,N,RDC,R
ICP(M,N)
936 FORMAT(IX,' --EXCESSIVE ROTATION AT INTERIOR HINGE IN COLUMN',I3
I3,'*',I3,'') ROTATION=E12.5,' PERMISSIBLE=E12.5)
GO TO 746
745 BU=AU(M,N)*TPC(M,N)
BL=AL(M,N)*TPC(M,N)
RDU=(H(M)/EIC(M,N))*IC(M,N)*BU-S(M,N)*BL/(IC(M,N)*C(M,N)-S(M,N)*S
I(M,N))*DEL-R(M,N)
RDL=(H(M)/EIC(M,N))*IC(M,N)*BL-S(M,N)*BU/(IC(M,N)*C(M,N)-S(M,N)*S
I(M,N))*DEL-R(M,N)
IF (ABS(RDU).GT.RCP(M,N).AND.XY.GT.0.0) WRITE(6,930) M,N,RDU,RCP(M
,N)
IF (ABS(RDL).GT.RCP(M,N).AND.XY.GT.0.0) WRITE(6,928) M,N,RDL,RCP(M
,N)
746 IF (XY.EQ.0.0) GO TO 737
WRITE(6,938) M,N,BU,BL,TPC(M,N),EIC(M,N)
938 FORMAT(IX,' COLUMN',I3,'*',I3,'') MU=E12.5,' MMX=E12.5,' ML=E
12.5,' MPC=E12.5,' EI=E12.5)
737 CONTINUE
735 CONTINUE
C
C ALL COLUMNS HAVE NOW HAD POSSIBLE HINGE CONFIGURATION ADJUSTMENTS
C MADE, ACCORDING TO THE NEW LOADING AND DEFORMATION CONDITIONS. THE
C CURRENT KH VALUE REPRESENTS THE NUMBER OF NEW BEAM AND COLUMN HINGES
C DETECTED.
C
C NOW CHECK FOR A POSSIBLE STOREY SWAY MECHANISM, RATHER THAN RETURNING
C TO SUBROUTINE ITER*, WHERE THIS CONDITION WOULD QUICKLY BE PICKED
C UP AS A FORM OF INSTABILITY.
C
DO 764 P=1,M5
KCC=0
DO 765 N=1,NC
KCC=KCC+K(C,M,N)
765 CONTINUE
IF (KCC.LT.(5*NC)) GO TO 764
XXX=4.
C XXX=4. INDICATES A SWAY MECHANISM IN SOME STOREY OF THE STRUCTURE.
GO TO 766
764 CONTINUE
C NOW COMPUTE CUMULATIVE NUMBER OF HINGES IN THE STRUCTURE.
766 KHC=KHC+KH
RETURN
END

SUBROUTINE BMHING
C
C CHECKS AND REVISES HINGE CONFIGURATION IN ALL BEAMS.
C
COMMON A,ACCRD,AL(20,3),AM(20,3),AU(20,3),B,BAS(20,2),BH(20,2),BT
1(20,2),C(20,3),CAS(20,3),CB(20,3),CT(20,3),CX,CXF,CY,CYF,D,DH(20,
2),DHI(20),DPB,DPC,DV(20,3),EIB(20,2),EIC(20,3),F,FAUGL,FCB,FCC,FCM,
3FYB,FYC,FYM,HI(20),P(20,3),PE(3),RI(2,3),RBP(20,2),RCP(20,3),S(20,3
4),SP(2),SX,SXF,SY,SYF,TL(20,2),TPC(20,3),TPL(20,2),TPRATE,TPRATH,T
SR(20,2),M(20),MD(20,2),ML(20,2),WTH,X,XB(20,2),XC(20,3),XX,XY,Y,I
6,J,KB(20,2),KC(20,3),KH,KHC,LIMITD,M,MS,N,NC,NN,NP,NSW,NW(3)
DO 700 M=1,M5
DO 698 N=1,NN
ZL=1.
ZR=1.
WML=0.
WNR=0.
IF (NSW.EQ.0) GO TO 697
DO 699 K=1,NSW
IF (N.EQ.NW(K)) WML=CT(M,N)
IF (IN=1).EQ.NW(K)) WNR=CT(M,N+1)
699 CONTINUE
697 SR=SP(N)-WML+WNR)/2.
IF (N.EQ.1.AND.WML.EQ.0.0) ZL=TPRATE
IF (N.EQ.NN.AND.WNR.EQ.0.0) ZR=TPRATE
WT=(WML,N)+WCM(N)+FAUGL*DB(M,N)+BT(M,N))/12.
DEL=(DV(M,N+1)-DV(M,N))/SR
KH=KB(M,N)
GO TO (701,702,703,704,705,706,707),KH
1 WRITE(6,702)
902 FORMAT(IX,' ***BEAM COUNTER OUT OF RANGE IN SUBROUTINE HINGES**
701 BL=WT*SR*SK/12.+EIB(M,N)*RIM(N)*(4.+3.*WML/SR)*R(M,N+1)*(2.+3.*W
NR/SR)-6.*DEL1/SR
BR=WT*SR*SK/12.+EIB(M,N)*RIM(N)*(2.+3.*WML/SR)*R(M,N+1)*(4.+3.*W
NR/SR)-6.*DEL1/SR
X=SR/2.-(BL+BR)/(WT*SR)
BC=0.
IF (X.GT.0.0.AND.X.LT.SR) BC=BL+WT*SR*SR/8.-0.5*(BL+BR)*(1.-(BL+BR
1)/(WT*SR*SR))
IF (ABS(BL/ZL).LT.TPL(M,N)) GO TO 710
IF (ABS(BL/ZL).LT.TPL(M,N)) GO TO 712
IF (ABS(BL/ZL).LT.ABS(BC/TPRATH)) GO TO 714
KH=KH+1
NH=KH+1
IF (BL/ZL).GE.TPL(M,N) TLM(M,N)=ZL*TPL(M,N)
IF (BL/ZL).LE.(-TPL(M,N)) TLM(M,N)=-ZL*TPL(M,N)
GO TO 702
710 IF (ABS(BR/ZR).LT.TPL(M,N)) GO TO 712
IF (ABS(BR/ZR).LT.ABS(BC/TPRATH)) GO TO 714
KH=KH+1
NH=KH+1
IF (BR/ZR).GE.TPL(M,N) TRM(M,N)=ZR*TPL(M,N)
IF (BR/ZR).LE.(-TPL(M,N)) TRM(M,N)=-ZR*TPL(M,N)
GO TO 703
712 IF (BC/TPRATH).LT.TPL(M,N) GO TO 708
C IE. NO NEW HINGE IN BEAM(M,N)
714 KH=KH+1
KH=KH+1
XB(M,N)=X
GO TO 704
702 BL=TL(M,N)
BR=WT*SR*SR/8.+0.5*BR+3.*EIB(M,N)*(0.5*WML*RI(M,N)/SR+R(M,N+1)*(1.+
10.5*WNR/SR)-DEL1)/SR
X=SR/2.-(BL+BR)/(WT*SR)
BC=0.
IF (X.GT.0.0.AND.X.LT.SR) BC=BL+WT*SR*SR/8.-0.5*(BL+BR)*(1.-(BL+BR
1)/(WT*SR*SR))
IF (ABS(BR/ZR).LT.TPL(M,N)) GO TO 716
IF (ABS(BR/ZR).LT.TPL(M,N)) GO TO 718
KH=KH+1
NH=KH+1
IF (BR/ZR).GE.TPL(M,N) TRM(M,N)=ZR*TPL(M,N)
IF (BR/ZR).LE.(-TPL(M,N)) TRM(M,N)=-ZR*TPL(M,N)
GO TO 707
716 IF (BC/TPRATH).LT.TPL(M,N) GO TO 720
C IE. NO NEW HINGE IN BEAM(M,N)
718 KH=KH+1
KH=KH+1
XB(M,N)=X
GO TO 705
720 RDB=-R(M,N)*(1.+0.75*WML/SR)-R(M,N+1)*(1.0+0.75*WNR/SR)+1.5*DEL+0.
125*SR*(TL(M,N)+WT*SR/12.)/EIB(M,N)
IF (ABS(RDB).GT.RBP(M,N).AND.XY.GT.0.0) WRITE(6,904) M,N,RDB,RBP(M
,N)
904 FORMAT(IX,' --EXCESSIVE ROTATION AT LEFT HINGE OF BEAM',I3,'*',I
13,'') ROTATION=E12.5,' PERMISSIBLE=E12.5)
GO TO 708
703 BR=TR(M,N)
BL=WT*SR*SR/8.+0.5*BR+3.*EIB(M,N)*(0.5*WML/SR)+0.5*RIM
1(N+1)*WNR/SR-DEL1/SR
X=SR/2.-(BL+BR)/(WT*SR)
BC=0.
IF (X.GT.0.0.AND.X.LT.SR) BC=BL+WT*SR*SR/8.-0.5*(BL+BR)*(1.-(BL+BR
1)/(WT*SR*SR))
IF (ABS(BL/ZL).LT.TPL(M,N)) GO TO 722
IF (ABS(BL/ZL).LT.TPL(M,N)) GO TO 724
KH=KH+1
NH=KH+1
IF (BL/ZL).GE.TPL(M,N) TLM(M,N)=ZL*TPL(M,N)
IF (BL/ZL).LE.(-TPL(M,N)) TLM(M,N)=-ZL*TPL(M,N)
GO TO 707
722 IF (BC/TPRATH).LT.TPL(M,N) GO TO 726
C IE. NO NEW HINGE IN BEAM(M,N)
724 KH=KH+1
KH=KH+1
XB(M,N)=X
GO TO 706
726 RDB=-R(M,N)*(1.+0.75*WML/SR)-R(M,N+1)*(1.0+0.75*WNR/SR)+1.5*DEL+0.
125*SR*(TR(M,N)+WT*SR/12.)/EIB(M,N)
IF (ABS(RDB).GT.RBP(M,N).AND.XY.GT.0.0) WRITE(6,906) M,N,RDB,RBP(M
,N)
906 FORMAT(IX,' --EXCESSIVE ROTATION AT RIGHT HINGE OF BEAM',I3,'*',I
13,'') ROTATION=E12.5,' PERMISSIBLE=E12.5)
GO TO 708
704 X=XE(M,N)
Y=SR-X
FXY=1./(X*X*(1./X*X+1./Y*Y))
TX=1./(Y*Y*(1./X*X+1./Y*Y))
BL=WT*(X*X+3.*SR*FXY)/8.-0.5*TPRATH*TPL(M,N)*(1.-3.*FXY*(1./X+1./
Y))+3.*EIB(M,N)*(1.-FXY/X)*R(M,N)*(1.0+0.5*WML/X)+DV(M,N)/X)+X*3.*
2EIB(M,N)*FXY*(R(M,N+1)*(1.0+0.5*WNR/Y)-DV(M,N+1)/Y)/(Y*Y)
BR=WT*(Y*Y+3.*SR*FXY)/8.-0.5*TPRATH*TPL(M,N)*(1.-3.*FXY*(1./X+1./Y
1)+3.*EIB(M,N)*FXY*(R(M,N+1)*(1.0+0.5*WML/X)+DV(M,N)/X)+X*3.*EIB
2(M,N)*(1.-FXY/Y)*R(M,N+1)*(1.0+0.5*WNR/Y)-DV(M,N+1)/Y)/(Y*Y)
IF (ABS(BL/ZL).LT.TPL(M,N)) GO TO 728
IF (ABS(BL/ZL).LT.TPL(M,N)) GO TO 728
KH=KH+1
NH=KH+1
IF (BL/ZL).GE.TPL(M,N) TLM(M,N)=ZL*TPL(M,N)
IF (BL/ZL).LE.(-TPL(M,N)) TLM(M,N)=-ZL*TPL(M,N)
GO TO 707
908 FORMAT(IX,' --- WITH CASE 4 HINGING, LEFT END MOMENT IN BEAM',I3
I3,'*',I3,'') IS GT. -MPL)
IF (BL/ZL).GT.(-TPL(M,N)) GO TO 730
KH=KH+1
NH=KH+1
TLM(M,N)=-ZL*TPL(M,N)
GO TO 705
728 IF (ABS(ZR).LE.(-TPL(M,N))) WRITE(6,910) M,N
910 FORMAT(IX,' --- WITH CASE 4 HINGING, RIGHT END MOMENT IN BEAM',I
13,'*',I3,'') IS LT. -MPL)
IF (BR/ZR).LT.TPL(M,N) GO TO 730
KH=KH+1
NH=KH+1
TRM(M,N)=ZR*TPL(M,N)
GO TO 706
730 DVL=0.5*(0.25*WT*(X*X+3.*FXY)+Y*Y*FXY)-TPRATH*TPL(M,N)*(X*FXY+Y*F
Y1)/EIB(M,N)+FXY*(R(M,N+1)*(1.0+0.5*WML/X)+DV(M,N)/X)-FXY*(R(M,N+1)*
21.+0.5*WNR/Y)-DV(M,N+1)/Y)
KDC=-0.25*(SR*TPRATH*TPL(M,N)+WT*(X*X+3.*FXY)/12.)/EIB(M,N)-0.5*(
1R(M,N+1)*(1.0+0.5*WML/X)-R(M,N+1)*(1.0+0.5*WNR/Y))+1.5*(DV(M,N)/
2X-(DV(M,N+1)-DV(M,N))/Y)

```

## BMHING



## LDPART

```

      IF(ABS(RDC).GT.(2.*RBP(M,N)).AND.XY.GT.0.0) WRITE(6,912) M,N,RDC,R
      RBP(M,N)
912 FORMAT(1X,'--EXCESSIVE ROTATION AT INTERIOR HINGE OF BEAM',I3,'
      1.,I3,') ROTATION=*,E12.5,' PERMISSIBLE=2*,E12.5)
      GO TO 708
705 X=XB(M,N)
      Y=SR-X
      BL=TL(M,N)
      BR=(BL+TPRATH*TPL(M,N))*Y/X-TPRATH*TPL(M,N)+0.5*WT*Y*SR
      IF((BR/ZR).LT.(TPL(M,N))) GO TO 732
C IF BR,GT,MPL A BEAM MECHANISM HAS BEEN DETECTED. HOWEVER, THIS IS A
C LOCALIZED FAILURE, AND CANNOT REALLY BE CONSIDERED TO CONSTITUTE
C FAILURE OF THE OVERALL STRUCTURE. THE BEAM COULD POSSIBLY CONTINUE
C DEFORMING TO A CATENARY SHAPE. HENCE, REVERT TO CASE 7 HINGING WITH
C TR(M,N)=PPL, AND CONTINUE THE STUDY OF OVERALL FRAME BEHAVIOUR.
C NOTE THE DETECTION OF THE BEAM MECHANISM.
      WRITE(6,914) M,N,RBP(M,N)
914 FORMAT(1X,'***BEAM MECHANISM DETECTED IN BEAM',I3,'',I3,') WIT
      KH=KH+1
      TR(M,N)=ZR*TPL(M,N)
      KB(M,N)=7
      GO TO 708
732 DVC=Y*Y*(BL*Y/X-TPRATH*TPL(M,N))*(Y/X+1.5)+WT*Y*(4.*SR-Y)/8./I3.*
      I1B(M,N)-R(M,N+1)*(Y+0.5*WNR)+DV(M,N+1)
      RDB=SR*(2.*BL+TPRATH*TPL(M,N)+0.25*WT*X)/I6.*E1B(M,N)-R(M,N+1)*
      1+0.5*WNL/X)+DVC-DV(M,N))/X
      IF(ABS(RDB).GT.(2.*RBP(M,N)).AND.XY.GT.0.0) WRITE(6,904) M,N,RDB,RBP(M,
      N)
      RUC=(X*(-0.25*WT*X+X*BL-2.*TPRATH*TPL(M,N))/6.+0.25*Y*(-WT*Y*Y/12.
      1-TPRATH*TPL(M,N))/E1B(M,N)-0.5*WNL*R(M,N)+X*R(M,N+1)*(0.5+0.75*WNR
      2R/Y)+DVC-DV(M,N))/X+1.5*(DV(M,N+1)-DVC)/Y
      IF(ABS(RUC).GT.(2.*RBP(M,N)).AND.XY.GT.0.0) WRITE(6,912) M,N,RDC,R
      RBP(M,N)
      GO TO 708
706 X=XB(M,N)
      Y=SR-X
      BR=TR(M,N)
      BL=TPRATH*TPL(M,N)+(BR+TPRATH*TPL(M,N))*X/Y-0.5*WT*X*SR
      IF((BL/ZL).GT.(-TPL(M,N))) GO TO 734
      WRITE(6,914) M,N,RBP(M,N)
      KH=KH+1
      TL(M,N)=-ZL*TPL(M,N)
      KB(M,N)=7
      GO TO 708
734 DVC=X*X*(-BR*X/Y-TPRATH*TPL(M,N)*(X/Y+1.5)+WT*X*(4.*SR-X)/8./I3.*
      I1B(M,N)+K(M,N)*(X+0.5*WNL)+DV(M,N)
      RDB=Y*(2.*BR+TPRATH*TPL(M,N)+0.25*WT*Y)/I6.*E1B(M,N)-R(M,N+1)*
      1+0.5*WNR/Y)+DV(M,N+1)-DVC)/Y
      RDC=(0.25*X*(TPRATH*TPL(M,N)+WT*X/12.)+Y*(BR-2.*TPRATH*TPL(M,N)
      1-0.25*WT*Y)/6./E1B(M,N)-R(M,N+1)*(0.5+0.75*WNL/X)+0.5*R(M,N+1)*WNR
      2R/Y+1.5*(DVC-DV(M,N))/X-(DV(M,N+1)-DVC)/Y
      IF(ABS(RDB).GT.(2.*RBP(M,N)).AND.XY.GT.0.0) WRITE(6,906) M,N,RDB,RBP(M,
      N)
      IF(ABS(RDC).GT.(2.*RBP(M,N)).AND.XY.GT.0.0) WRITE(6,912) M,N,RDC,R
      RBP(M,N)
      GO TO 708
707 BL=TL(M,N)
      BR=TR(M,N)
      X=SR/2.-(BL+BR)/(WT*SR)
      BC=0.
      IF(X.GT.0.0.AND.X.LT.SR) BC=BL*WT*SR*SR/8.-0.5*(BL+BR)*(1.-(BL+BR)
      1/(WT*SR*SR))
      IF(BC.LT.(TPRATH*TPL(M,N))) GO TO 736
      WRITE(6,916) M,N,X
916 FORMAT(1X,'***BEAM MECHANISM ENCOUNTERED IN BEAM',I3,'',I3,') W
      ITH KB=7. X=*,E12.5,*. RETAIN KB=7 AND CONTINUE')
      KH=KH+1
      GO TO 708
736 RDB=SR*(2.*BL+BR+0.25*WT*SR*SR)/I6.*E1B(M,N)-R(M,N+1)*1+0.5*WNL/S
      1R)-0.5*R(M,N+1)*WNR/SR+DEL
      RDB=SR*(2.*BR+BL+0.25*WT*SR*SR)/I6.*E1B(M,N)-C.5*R(M,N)*WNL/SR-R(
      1M,N+1)*1+0.5*WNR/SR+DEL
      IF(ABS(RDB).GT.(2.*RBP(M,N)).AND.XY.GT.0.0) WRITE(6,904) M,N,RDB,RBP(M,
      N)
      IF(ABS(RDB).GT.(2.*RBP(M,N)).AND.XY.GT.0.0) WRITE(6,906) M,N,RDB,RBP(M,
      N)
      GO TO 708
708 IF(BL.GT.0.0.AND.XY.GT.0.0) WRITE(6,918) M,N,BL
      IF(BR.LT.0.0.AND.XY.GT.0.0) WRITE(6,920) M,N,BR
      IF(BC.LT.0.0.AND.XY.GT.0.0) WRITE(6,922) M,N,BC
918 FORMAT(1X,'***IN BEAM',I3,'',I3,') ML IS +VE AND=*,E12.5)
920 FORMAT(1X,'***IN BEAM',I3,'',I3,') MR IS -VE AND=*,E12.5)
922 FORMAT(1X,'***IN BEAM',I3,'',I3,') INSPAN M IS -VE AND=*,E12.5)
      IF(XY.EQ.0.0) GO TO 698
      WRITE(6,924) M,N,JL,BC,BR,TPL(M,N)
924 FORMAT(1X,'BEAM',I3,'',I3,') ML=*,E12.5,*. MMAX=*,E12.5,*. MR=*,E
      12.5,*. MPL=*,E12.5)
698 CONTINUE
700 CONTINUE
      RETURN
      END

```

## SUBROUTINE LDPART

```

C COMPUTES AMOUNT OF LATERAL LOAD AT EVERY FLOOR RESISTED BY THE SHEAR
C WALL(S) AS A RESULT OF THE SHEAR WALL-FRAME INTERACTION.
C
      COMMON A,ACCURD,AL(20,3),AM(20,3),AU(20,3),B,UAS(20,2),BR(20,2),BT
      1(20,2),L(20,3),CAS(20,3),CB(20,3),CT(20,3),CX,CXF,CY,CYF,D,DH(20),
      2DHT(20),DPB,UPC,DV(20,3),E1B(20,2),E1C(20,3),F,FAUGUL,FCB,FCC,FCW,
      3FYH,FYC,FYM,H(20),P(20,3),PE(3),R(2,3),RBP(20,2),RCP(20,3),SI(20,3
      4),SP(2),SR,SXF,SY,SXF,TL(20,2),TPL(20,3),TPL(20,2),TPRATH,TPRATH,T
      5R(20,2),M(20),M(20,2),ML(20,2),MTW,X,XB(20,2),XC(20,3),XXX,XY,Y,I
      6,J,KBI(2,2),KC(20,3),KH,KHC,LIMITD,M,MS,N,NC,NN,NP,NSW,NW(3)
      DO 1000 N=1,NC
      DO 1002 K=1,NSW
      IF(N.EQ.NW(K)) GO TO 1004
1002 CONTINUE
      GO TO 1006
1004 WRITE(6,1050) N
1000 FORMAT('0',* LATERAL LOADS RESISTED BY SHEAR WALL IN COLUMN LINE*,
      1I4,* *)
      DO 1008 M=1,MS
      KK=KC(M,N)
      GO TO (1011,1012,1013,1014,1015),KK
1009 WRITE(6,1052)
1052 FORMAT(1X,'***COLUMN COUNTER OUT OF RANGE IN SUBROUTINE LDPART')
1011 V=(S(M,N)+C(M,N))*E1C(M,N)*R(M,N)/H(M)
      T=(S(M,N)+C(M,N))*E1C(M,N)*R(M,N)/H(M)
      Z=(2.*E1C(M,N)+S(M,N))*E1C(M,N)/(H(M)+H(M))*P(M,N)+DH(M)
      U=0.
      GO TO 1016
1012 V=(C(M,N)+C(M,N)-S(M,N))*E1C(M,N)*R(M,N)/(C(M,N)+H(M))
      T=0.
      Z=(S(M,N)+C(M,N)-C(M,N)*C(M,N))*E1C(M,N)/(C(M,N)+H(M)+H(M))+P(M,N
      1)*DH(M)
      U=AL(M,N)*TPC(M,N)*(S(M,N)/C(M,N)+1.)
      GO TO 1016
1013 V=0.
      T=(C(M,N)+C(M,N)-S(M,N))*E1C(M,N)*R(M,N)/(C(M,N)+H(M))
      Z=(S(M,N)+C(M,N)-C(M,N)*C(M,N))*E1C(M,N)/(C(M,N)+H(M)+H(M))+P(M,N
      1)*DH(M)
      U=AU(M,N)*TPC(M,N)*(S(M,N)/L(H,M)+1.)
      GO TO 1016
1014 I=M
      CALL CASE4
      V=-P(M,N)*Y*(X/H(M)+A*B)/L./F)*R(M,N)
      T=-P(M,N)*X*(Y/H(M)+F*D)/L./A)*R(M,N+1)
      Z=P(M,N)*DH(M)*(Y*(1.+X/H(M)+D)/H(M)+X*(1.+Y/H(M)+B)/H(M)
      1+A)+1.)
      U=AP(M,N)*(P(M,N)/E1C(M,N))*(X*X*(SXF/A+CXF/(F*D))-Y*Y*(SYF/F+CYF/
      1(A*B))+X*Y*(X*SXF/(F*D)-Y*SYF/(A*B))/H(M))
      GO TO 1016
1015 V=C.
      T=0.
      Z=P(P,M,N)*DH(M)
      U=(AL(M,N)+AU(M,N))*TPC(M,N)
C NOW COMPUTE TOTAL LATERAL SHEAR LOAD AT FLOOR M.
1016 WS=0.
      DO 1018 I=1,M
      WS=WS+(I)
1018 CONTINUE
C NOW COMPUTE TOTAL LATERAL LOAD AND PERCENTAGE OF TOTAL LATERAL LOAD
C CARRIED BY SHEAR WALL AT FLOOR M.
      WLAT=(-V+T+Z)/H(M)
      WPER=100.*WLAT/WS
      WRITE(6,1054) M,WLAT,WPER
1054 FORMAT(1X,'AT FLOOR',I4,' LOAD RESISTED=*,E12.5,*. LB. PERCENTAGE=*,
      1E12.5)
1008 CONTINUE
1006 CONTINUE
1000 RETURN
      END

```

APPENDIX E

BEHAVIOR OF REINFORCED CONCRETE  
SHEAR WALL-FRAME STRUCTURES  
ASSUMING THE JOINT MECHANISM IS NOT  
A VALID MODE OF FAILURE

BEHAVIOR OF REINFORCED CONCRETE SHEAR WALL-FRAME STRUCTURES  
ASSUMING THE JOINT MECHANISM IS NOT A VALID MODE OF FAILURE

The analysis presented in the body of this report assumed that failure occurred when one of several conditions occurred. Twelve of the 20 frames considered in Chapter 7 failed due to the formation of a joint mechanism. As discussed in Section 7.2, however, the joint mechanism generally will not be a valid mode of failure for the type of frames considered. For this reason, the basic program was modified to bypass the joint mechanism failure provided that the entire structure remained stable.

Seven of the frames listed in Tables 7.1 and 7.2 were re-analyzed using the modified program. The results of these analyses are presented in Table E1 which corresponds to Tables 7.1 and 7.2 on Pages 146 and 147. Load-roof sway deflection curves are presented in Figures E1 and E2 which resemble Figure 7.5 on Page 153 and Figure 7.10 on Page 166, respectively. In these figures the dashed lines refer to the behavior of the frame after some hinge had exceeded its rotation capacity. The order of hinge formation in Frames H50 and H50-4A is shown in Figure E3 assuming joint mechanisms are not primary mode of failure. This figure is similar to Figure 7.6 on Page 157.

Figures E1 and E3 compare the behavior of frames H50 and H50-4A. The latter had an increased wall area to simulate the case in which the axial stresses in the wall are less than those in the columns. The

resulting differential shortening of the wall and columns in this structure resulted in earlier hinging and earlier excessive hinge rotations in this frame. However, if it is assumed that both of these failure modes can be neglected, it can be seen that both structures will fail at essentially the same failure loads and deflections. In structure H50, overall instability occurred after hinges had reduced the structure to one column and a wall, each restrained by beams hinged at the far end. Structure H50-4A failed by sway instability of the top storey after the loss of the rotational restraint of the wall by beams in the top two storeys.

Structure	Failure Load $\lambda$ interval	Number of plastic hinges detected at these $\lambda$ values	Roof sway deflection at last stable $\lambda$ value (in.)	$\lambda$ value at which excessive hinge rotation first noted	Beams	Columns	Mode of Failure
H1	1.338 - 1.348	34 - 38	21.53	1.30	-		drop in equilibrium sway deflection in storeys 2 to 6 and 15 to 20
H2	1.409 - 1.413	46 - 49	23.79	1.35	1.40		drop in equilibrium sway deflection in storeys 15 to 19
H6	1.472 - 1.475	60 - 139	24.77	1.35	1.40		sway mechanism in storey 10
H12	1.500 - 1.502	61 - 66	25.81	1.45	1.40		drop in equilibrium sway deflection in all storeys
H20	1.500 - 1.503	58 - 177	20.91	1.45	1.40		sway mechanism in storey 4
H50	1.625 - 1.628	65 - 71	24.23	1.55	1.50		drop in equilibrium sway deflection in all storeys
H50-4A	1.622 - 1.624	52 - 58	24.53	1.20	1.55		sway mechanism in storey 1

\*Storeys are numbered from the roof. Coordinates refer to storey and column number, respectively, column 3 being on the leeward side.

TABLE E1

## FAILURE CONDITIONS OF BASIC SERIES H STRUCTURES - IGNORING JOINT MECHANISMS

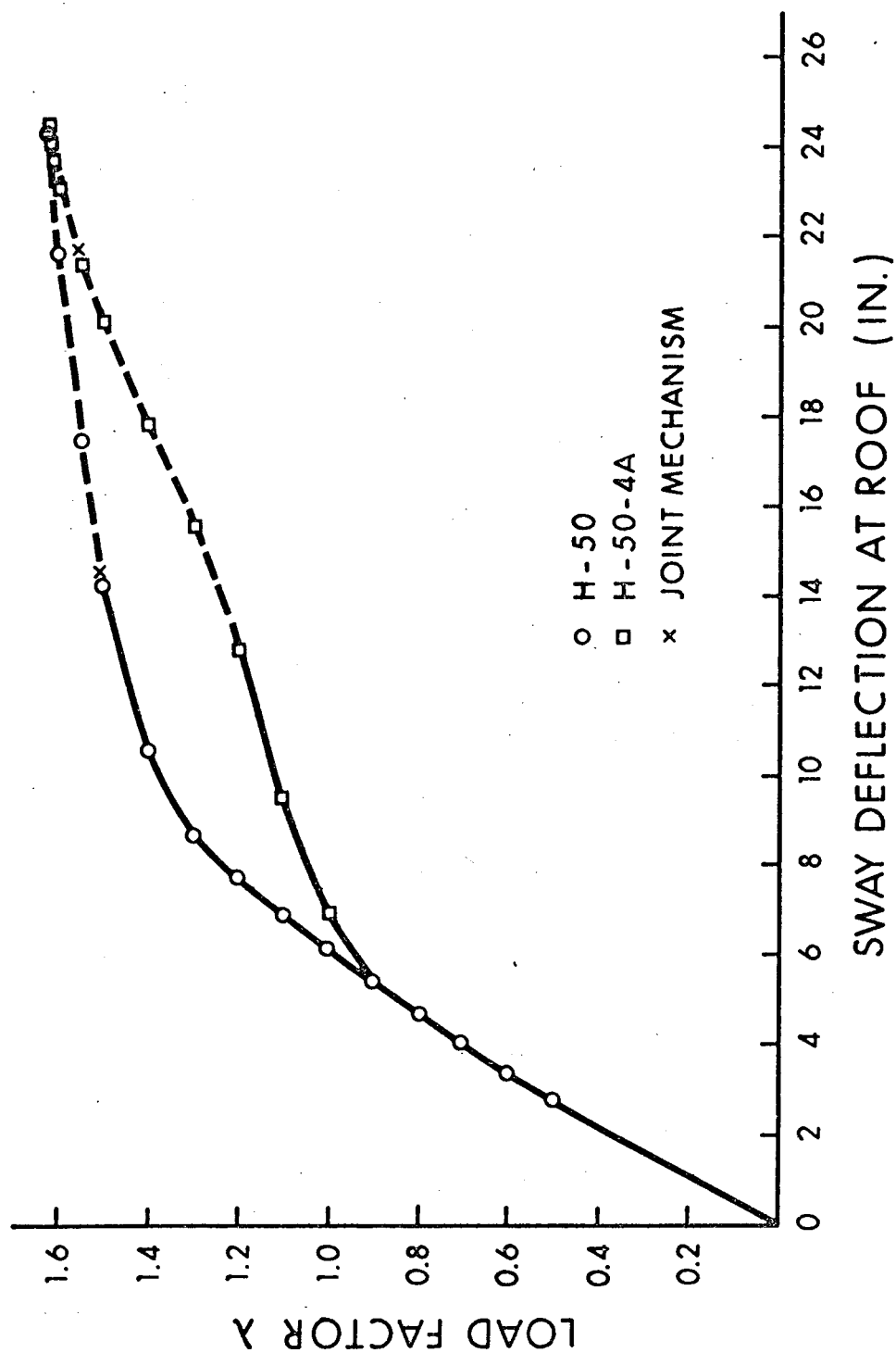


FIGURE E1 EFFECT OF AXIAL SHORTENING ON STRUCTURES H50

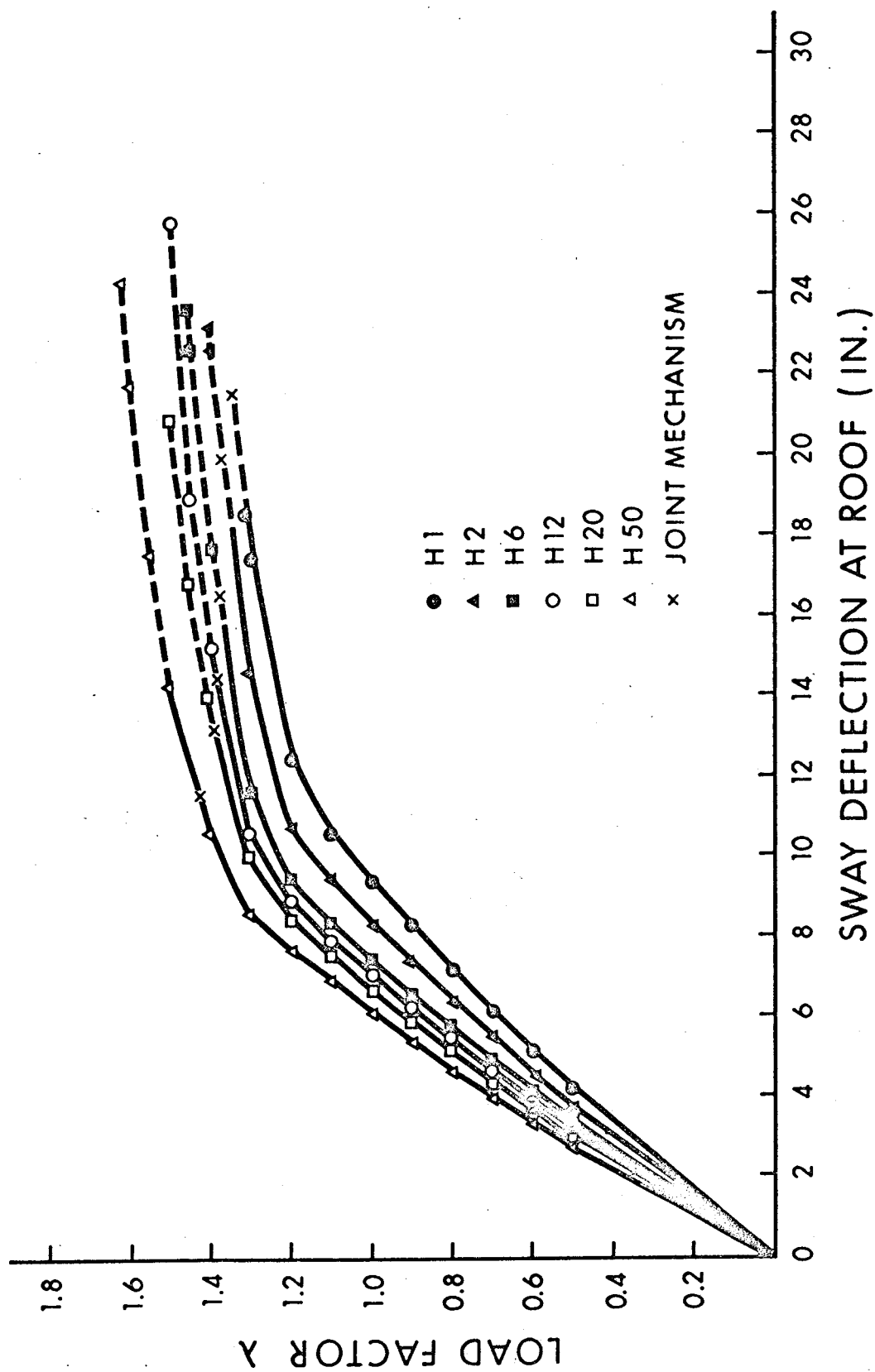
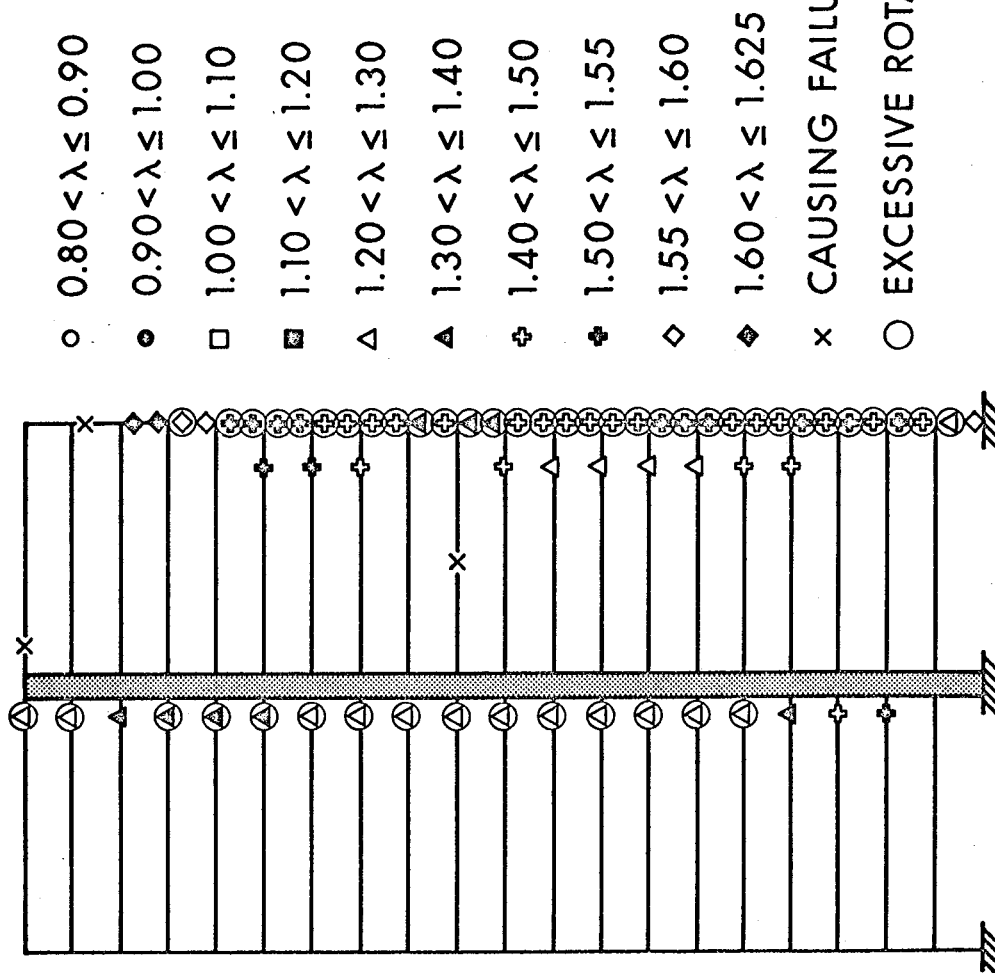
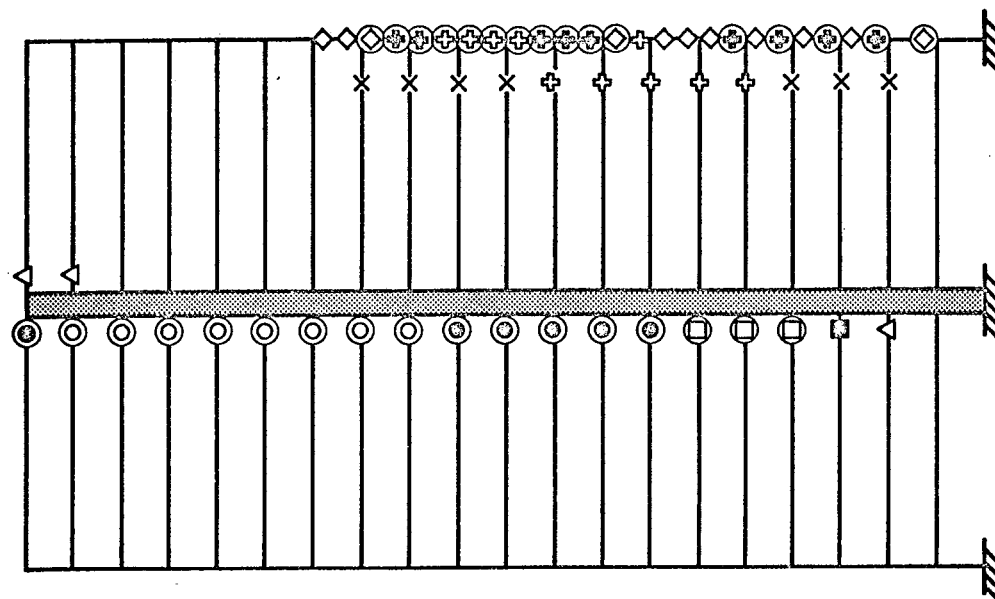


FIGURE E2. EFFECT OF WALL STIFFNESS ON LOAD DEFLECTION RESPONSE FOR SERIES H STRUCTURES.



(a) H - 50



(b) H - 50 - 4A

FIGURE 3: EFFECT OF AXIAL SHORTENING ON HINGE PROPAGATION IN H50.